

**Late Pleistocene - Early Holocene glacial dynamics, Asian
palaeomonsoon variability and landscape change at Lake
Shudu, Yunnan Province, southwestern China**

Submitted by Charlotte Cook, to the University of Exeter as a thesis for the degree of Doctor of Philosophy in Geography, September 2009.

This thesis is available for library use on the understanding that it is copyright material and that no quotation from the thesis may be published without proper acknowledgement.

I certify that all material in this thesis which is not my own work has been identified and that no material has previously been submitted and approved for the award of a degree by this or any other University.

(signature).....Charlotte G Cook.....

Abstract

A lack of well-distributed, high-resolution records of Late Quaternary Asian palaeomonsoon variability remains an outstanding issue for palaeoclimatologists, and is especially marked in remote regions such as the mountains of southwestern China (Wang et al., 2005). Characterising the nature, timing and magnitude of climate variability in southwestern China is essential for understanding the regional climate as a whole, and the potential social, economic and environmental impacts that may result from Asian monsoon system changes.

The NERC-funded research presented in this thesis focuses on a high altitude lake sediment record obtained from Lake Shudu, Yunnan Province, China. The lake is located on the southeastern edge of the Tibetan Plateau. The primary aims of this research were to identify and examine key environmental and climatic shifts which occurred in southwestern China during the Late Pleistocene (Dali) - Early Holocene Period; to examine the possible drivers of these changes; and to compare the findings with other regional proxy records in order to better understand climate dynamics in southwestern China. These aims were chosen in order to test the hypothesis that Late Quaternary millennial to centennial scale climatic and environmental changes in southwestern China were driven by changes in solar insolation and / or glacial climate boundary conditions, characterised by stepwise increases in palaeomonsoon intensity.

AMS ^{14}C radiocarbon dates obtained from bulk sediment samples and pollen concentrations indicated that the seven metre core (06SD) that forms the focus of this research spans the last c. 22.6 ka cal. yr BP, making it one of the longest high-resolution Late Quaternary records available for southwestern China. 06SD was examined using a multi-proxy approach incorporating physical, organic and palaeoecological analyses.

The record captures the shift from colder, drier Pleistocene (Dali) conditions to warmer, wetter Holocene conditions and is punctuated by two events. The first event, centred at c. 17.3 ka cal. yr BP, possibly represents a phase of warmer and / or wetter conditions in response to rising solar insolation during the deglacial period. The second event, commencing at c. 11.7 ka cal. yr BP, possibly denotes the Pleistocene - Holocene Boundary.

Overall, the findings of this research support the view that during the Late Pleistocene, Asian summer monsoon strengthening was non-linear and driven by changes in glacial dynamics and / or solar insolation.

Table of contents

Abstract	2
Table of contents	3
List of figures	6
List of tables	8
List of equations	9
List of appendices	10
Acknowledgements	11
1 Introduction	12
1.1 Research context	12
1.2 Research methods	13
1.3 Research hypothesis, aims and objectives	13
1.4 Geographical context	14
1.4.1 Site selection	16
1.5 Project partners	16
1.6 Thesis structure	17
2 Asian palaeoclimatic variability during the Late Pleistocene - Early Holocene Period	18
2.1 Introduction	18
2.2 The Asian monsoon	19
2.2.1 Seasonal climatology	22
2.3 Monsoon China	26
2.4 Chinese Quaternary terminology	31
2.5 Millennial to centennial scale proxy records of Late Pleistocene - Early Holocene palaeomonsoon variability obtained from sites in China	32
2.5.1 Drivers of palaeomonsoon variability	34
2.5.2 Environmental and climatic trends during the Late Pleistocene - Early Holocene Period	39
2.5.3 The timing of the Last Glacial Maximum (LGM) in China	41
2.5.4 Post-LGM climatic conditions	42
2.5.5 Lateglacial climate events	43
2.5.6 The Pleistocene - Holocene (P-H) Transition	53
2.5.7 The Pleistocene - Holocene (P-H) Boundary	53
2.6 Concluding remarks	55
2.7 Research questions	56
3 Methods	57
3.1 Introduction	57
3.2 Multi-proxy analysis	57
3.3 Physical properties	59
3.3.1 Particle size	59
3.3.2 Magnetic susceptibility (χ_{lf})	59
3.4 Organic analysis	61
3.4.1 Loss on Ignition (%LOI)	61
3.4.2 Total Organic Carbon (%TOC) and Total Nitrogen (%TN)	62
3.4.3 Carbon and Nitrogen (C/N) ratios	64
3.4.4 $\delta^{13}\text{C}$ analysis	64

3.4.5	Organic sample preparation and analysis	66
3.5	Palaeoecological analysis	67
3.5.1	Principles of pollen analysis	67
3.5.2	Approaches	68
3.5.3	Pollen productivity and dispersal	68
3.5.4	Pollen source area	69
3.5.5	Modern Chinese vegetation analogues	71
3.5.6	Driver - response lag	85
3.5.7	Pollen extraction	85
3.5.8	Pollen counting	86
3.5.9	Pollen identification	86
3.5.10	Statistical methods	89
3.5.10.1	Pollen percentages	89
3.5.10.2	Pollen concentrations	90
3.5.10.3	DCA / PCA	90
3.5.10.4	Ratios and indicative pollen types	90
3.5.11	Charcoal analysis	92
3.6	Dating methods	93
3.6.1	AMS ¹⁴ C radiocarbon dating of bulk sediments	94
3.6.2	AMS ¹⁴ C radiocarbon dating of coniferous pollen concentrations	94
3.7	Concluding remarks	97
4	Results	98
4.1	Introduction	98
4.2	Site investigation	98
4.2.1	Geology / geomorphology	103
4.2.2	Climate	112
4.2.2.1	Temperature	112
4.2.2.2	Precipitation	115
4.2.3	Vegetation	117
4.3	Core recovery	130
4.3.1	Selection of samples for dating	132
4.3.2	AMS ¹⁴ C radiocarbon dating of bulk sediments and pollen concentrations	134
4.3.2.1	Pollen assessment	134
4.3.2.2	Pilot test 1	135
4.3.2.3	Pilot test 2	136
4.3.2.4	A new method for extracting pollen concentrates from lake sediments for AMS ¹⁴ C radiocarbon dating	137
4.3.3	Chronology construction	139
4.4	Physical properties	149
4.4.1	Particle size	149
4.4.2	Magnetic susceptibility (χ_{lf})	151
4.5	Organic analysis	153
4.5.1	Modern values	153
4.5.2	Loss on Ignition (%LOI)	156
4.5.3	Total Organic Carbon (%TOC)	158
4.5.4	Total Nitrogen (%TN)	160
4.5.5	Carbon and Nitrogen (C/N) ratios	162
4.5.6	$\delta^{13}\text{C}$ analysis	164
4.5.7	Combined results of C/N and $\delta^{13}\text{C}$ analysis	166
4.6	Palaeoecological analysis	168
4.6.1	Pollen analysis	168
4.6.1.1	Pollen zones	173
4.6.2	Charcoal analysis	177
4.7	Construction of 06SD multi-proxy zones	179
4.8	Concluding remarks	179

5	Late Pleistocene - Early Holocene environmental changes in southwestern China	181
5.1	Introduction	181
5.2	Zone MS-SD1 (c. 22.6 - 20.3 ka cal. yr BP)	187
5.2.1	Zone MS-SD1 summary	196
5.3	Zone MS-SD2 (c. 20.3 - 17.5 ka cal. yr BP)	197
5.3.1	Zone MS-SD2 summary	200
5.4	Zone MS-SD3 (c. 17.5 - 13.5 ka cal. yr BP)	201
5.4.1	Subzone MS-SD3a (c. 17.5 - 17.0 ka cal. yr BP)	201
5.4.2	Subzone MS-SD3b (c. 17.0 - 13.5 ka cal. yr BP)	205
5.4.3	Zone MS-SD3 summary	208
5.5	Zone MS-SD4 (c. 13.5 - 11.1 ka cal. yr BP)	209
5.5.1	Subzone MS-SD4a (c. 13.5 - 12.3 ka cal. yr BP)	211
5.5.2	Subzone MS-SD4b (c. 12.3 - 11.1 ka cal. yr BP)	211
5.5.3	Zone MS-SD4 summary	212
5.6	Concluding remarks	213
6	Late Pleistocene - Early Holocene glacial dynamics and Asian palaeomonsoon variability in southwestern China	214
6.1	Introduction	214
6.2	The timing of the LGM	214
6.3	Post-LGM climatic conditions	215
6.3.1	Evidence for an abrupt climate amelioration from c. 17.5 - 17.2 ka cal. yr BP	223
6.3.2	Evidence for rising lake levels at c. 16 ka cal. yr BP	230
6.4	The Pleistocene - Holocene Transition	231
6.5	The Pleistocene - Holocene Boundary	231
6.6	Comparisons with events in other regional proxy records	232
6.7	The influence of glacial - interglacial boundary conditions upon palaeomonsoon intensity during the deglacial period	233
6.8	Concluding remarks	236
7	Main conclusions and suggestions for further work	237
7.1	Main conclusions	237
7.2	Suggestions for further work	238
7.2.1	The timing of the LGM	238
7.2.2	The timing of the response to warming	238
7.2.3	Abrupt shifts from c. 17.5 - 17.2 ka cal. yr BP	238
7.2.4	Quantification of the forest ecosystem response to climate change	239
7.2.5	The P-H Transition and Boundary	239
7.2.6	Human - landscape - climate interactions	239
	Appendices	240
	References	251

List of figures

Figure 1-1:	Map showing the location of Yunnan Province, China, the provincial capital, Kunming, and Lake Shudu (study site).	15
Figure 2-1:	The global climate system.	20
Figure 2-2:	Global atmospheric circulation.	21
Figure 2-3:	Contemporary pressure and surface wind patterns over Asia.	23
Figure 2-4:	Map showing the altitudinal zones of China.	27
Figure 2-5:	Elevation profile, Zhongdian - Jinghong, Yunnan Province, China.	28
Figure 2-6:	Map showing the climate subsystems influencing China.	30
Figure 2-7:	Map showing the locations of key speleothem and ice core records in China and their proximity to Lake Shudu.	33
Figure 2-8:	Correlations between southwestern monsoon intensity and solar insolation during the last deglaciation.	37
Figure 2-9:	Graph showing the estimated age offsets between the Hulu Cave speleothems and the Greenland Ice Core Records (GISP2 and GRIP).	46
Figure 2-10:	Graph showing the Lateglacial section of the Hulu Cave $\delta^{18}\text{O}$ speleothem records compared with the GISP2 $\delta^{18}\text{O}$ ice core record.	47
Figure 2-11:	Graph showing the Lateglacial changes in the Dongge Cave $\delta^{18}\text{O}$ speleothem record.	49
Figure 2-12:	Graph comparing the $\delta^{18}\text{O}$ and $\delta^{13}\text{C}$ values obtained from key high and mid latitude ice core and speleothem records, 20 - 10 ka BP.	52
Figure 2-13:	Suite of graphs showing 1000-year averages of dust concentrations and $\delta^{18}\text{O}$ values obtained from Core D-3, Dunde Ice Cap, 40 - 0 ka BP.	54
Figure 3-1:	Diagram showing the pathways of carbon and nitrogen for a lake located at the treeline.	63
Figure 3-2:	Graph showing theoretical $\delta^{13}\text{C}$ values plotted against C/N ratios.	65
Figure 3-3:	Relationship between lake size and pollen source area.	70
Figure 3-4:	Altitudinal gradient of key modern arboreal taxa, Yulongshan Mountains, northwestern Yunnan.	77
Figure 3-5:	Simplified idealised vegetation map for Yunnan Province, showing the most common types prior to disturbance by human activity.	79
Figure 3-6:	Selected altitudinal zonations in Yunnan Province.	80
Figure 4-1:	Lake Shudu, Yunnan Province, China, looking northeast.	101
Figure 4-2:	Map of the Lake Shudu catchment, Yunnan Province.	102
Figure 4-3:	Map showing the key geomorphological and geological features in the Lake Shudu catchment.	104
Figure 4-4:	Limestone outcrop, southeastern shore of Lake Shudu.	105
Figure 4-5:	Exposed facies with limestone bedrock covered fluvial deposits and thick topsoil, northwestern shore of Lake Shudu.	105
Figure 4-6:	Lateral moraine, southeastern shore of Lake Shudu.	106
Figure 4-7:	Landform located just after the lake outflow, to the southwest of Lake Shudu.	107
Figure 4-8:	Closer view of landform located just after the lake outflow to the southwest of Lake Shudu.	108
Figure 4-9:	Angular, unsorted fluvio-glacial deposits located on the western shoreline of Lake Shudu.	109
Figure 4-10:	Laminated fluvial deposits located on primary inflow, eastern shoreline of Lake Shudu.	110
Figure 4-11:	Palaeoshoreline running parallel to the present day western shoreline.	111
Figure 4-12:	Mean monthly temperatures for Dali, Yunnan Province, 1939 - 1988.	114
Figure 4-13:	Mean monthly precipitation rates and maximum / minimum monthly precipitation (in mm) for Zhongdian, Yunnan Province, 1972 - 2002.	116

Figure 4-14:	Mixed subalpine coniferous forest stand including <i>Abies Georgei</i> , southern slope of Lake Shudu.	119
Figure 4-15:	Coniferous trees, southern slope of Lake Shudu.	120
Figure 4-16:	A member of the Ericaceae family growing at Lake Shudu.	121
Figure 4-17:	Evergreen <i>Quercus</i> stand, western slope of Lake Shudu.	122
Figure 4-18:	Evergreen <i>Quercus</i> leaves, Lake Shudu.	123
Figure 4-19:	<i>Betula</i> stand growing on the western slope of Lake Shudu.	124
Figure 4-20:	<i>Salix purpurea</i> stand growing adjacent to a large outflow, northwestern valley floor, Lake Shudu.	125
Figure 4-21:	Grassland and peatbog areas, eastern shoreline of Lake Shudu.	127
Figure 4-22:	Herder hut, eastern lowlands of Lake Shudu.	128
Figure 4-23:	Yaks grazing, western shoreline of Lake Shudu.	129
Figure 4-24:	Loss on Ignition (%LOI) for cores 06SD 1,2,3 and 4 and core overlaps.	131
Figure 4-25:	06SD Composite core stratigraphy and zones.	133
Figure 4-26:	Age-depth curve based on the 06SD calibrated dates.	141
Figure 4-27:	06SD Age-depth curve.	144
Figure 4-28:	06SD composite core stratigraphy and sedimentation rates.	148
Figure 4-29:	06SD particle size record.	150
Figure 4-30:	06SD low frequency magnetic susceptibility record.	152
Figure 4-31:	06SD modern C/N ratios plotted against $\delta^{13}\text{C}$ values.	155
Figure 4-32:	06SD Loss on Ignition (%LOI) organic material.	157
Figure 4-33:	06SD Total Organic Carbon (%TOC) record.	159
Figure 4-34:	06SD Total Nitrogen (%TN) record.	161
Figure 4-35:	06SD C/N ratios.	163
Figure 4-36:	06SD $\delta^{13}\text{C}$ values.	165
Figure 4-37:	06SD C/N ratios plotted against $\delta^{13}\text{C}$ values.	167
Figure 4-38:	06SD pollen percentage record.	169
Figure 4-39:	06SD arboreal pollen concentrations.	170
Figure 4-40:	06SD shrub, grass and sedge pollen concentrations.	171
Figure 4-41:	06SD herb pollen concentrations.	172
Figure 4-42:	06SD charcoal concentrations.	178
Figure 4-43:	Composite diagram showing the zonal boundaries for each 06SD proxy.	180
Figure 5-1:	Lake Shudu multi-proxy zones.	182
Figure 5-2:	Lake Shudu summary pollen percentage diagram.	183
Figure 5-3:	Lake Shudu summary pollen percentage diagram excluding <i>Pinus</i> from the pollen sum.	184
Figure 5-4:	Combined percentages of <i>Picea</i> / <i>Abies</i> in the Lake Shudu pollen record.	185
Figure 5-5:	Lake Shudu proxy record, Zone MS-SD1 (c. 22.5 - 20.3 ka cal. yr BP).	188
Figure 5-6:	Lake Shudu proxy record, Zone MS-SD2 (c. 20.3 - 17.5 ka cal. yr BP).	198
Figure 5-7:	Lake Shudu proxy record, Zone MS-SD3 (c. 17.5 - 13.5 ka cal. yr BP).	202
Figure 5-8:	Lake Shudu proxy record, Zone MS-SD4 (c. 13.5 - 11.1 ka cal. yr BP).	210
Figure 6-1:	Solar insolation during June at 30°N spanning the last ~25 ka BP.	216
Figure 6-2:	AP/NAP ratios in the Lake Shudu pollen record.	218
Figure 6-3:	PCA scattergraph showing outlier samples.	220
Figure 6-4:	A/C and A/Cy ratios in the Lake Shudu pollen record.	222
Figure 6-5:	PCA scattergraph showing the clustering of samples in the Lake Shudu pollen record.	224
Figure 6-6:	PCA species biplot showing inter-species correlations between Lake Shudu pollen taxa.	225
Figure 6-7:	PCA species / samples scattergraph derived from the Lake Shudu pollen record.	227
Figure 6-8:	Percentages of <i>Quercus</i> and <i>Betula</i> in the Lake Shudu pollen record.	229
Figure 6-9:	Lake Shudu pollen percentages showing taxa with >1% abundances and inferred vegetation assemblages.	234
Figure 6-10:	Conceptualised climate trajectory.	235

List of tables

Table 2-1:	Chinese terminology for the Late Pleistocene (Dali) - Holocene Period.	31
Table 3-1:	Biome classifications for China.	72
Table 3-2:	Idealised vegetation regions, Yunnan Province, China.	74
Table 3-3:	The altitudinal belts (excluding base and mid - low mountain belts) found in the high mountainous zones of China.	75
Table 3-4:	Climatic correlations of selected vegetation types, Yunnan Province, China.	81
Table 3-5:	Climatic correlations of selected vegetation types, Tibetan Plateau.	84
Table 4-1:	Lake Shudu site investigation tasks.	99
Table 4-2:	Conventional and calibrated AMS ^{14}C radiocarbon dates for the 06SD core.	140
Table 4-3:	06SD final core chronology.	143
Table 4-4:	06SD core resolution and annual sedimentation rates.	145
Table 4-5:	Ages of 06SD stratigraphic zones ST1 - 5.	147
Table 4-6:	Modern %TOC, %TN, C/N ratios and $\delta^{13}\text{C}$ values derived from plant and sediment samples obtained from Lake Shudu.	154
Table 5-1:	Lake Shudu proxies, zones and environmental inferences.	186

List of equations

Equation 1: Calculation of Loss on Ignition percentages.	66
Equation 2: Pollen concentration calculation.	90

List of appendices

A1:	Additional information for Chapter 3 (Methods)	241
A.1.1:	Assignments of pollen taxa from China to selected Plant Functional Types (PFTs).	241
A.1.2:	Vegetation types, Yunnan Province, China.	242
A.1.3:	Pollen preparation method for Chinese sediment samples.	246
A.1.4:	Canoco DCA / PCA metadata.	247
A.2:	Additional information for Chapter 4 (Results)	250
A.2.1.	¹⁴ C AMS radiocarbon dating of coniferous pollen concentrations extraction method.	250

Acknowledgements

I would like to thank the following people for their help with various aspects of this research;

- My PhD Supervisor, Dr Richard Jones (University of Exeter), for his unfailing support, enthusiasm and superior baking skills;
- Dr Enlou Zhang and colleagues at the Nanjing Institute of Geography and Limnology (NIGL China) for providing me with a lake sediment core to work on, and for advice and logistical support whilst on fieldwork in China;
- Dr Pete Langdon (University of Southampton) and Prof. Melanie Leng (NERC Geosciences Isotope Laboratory (NIGL Keyworth) for providing expert guidance;
- Angela Elliot, Jackie Hatton and technical staff at the University of Exeter for advice and assistance in the lab;
- The Natural Environment Research Council (NERC), who funded this research under studentship NER/S/A/2005/13320;
- Staff at NIGL (Keyworth), for providing expert advice and laboratory space;
- The NERC Radiocarbon Laboratory (NERC RCL), East Kilbride and the Oxford Radiocarbon Accelerator Unit (ORAU) for help with AMS ^{14}C radiocarbon dating;
- Prof. Rewi Newnham (University of Plymouth) and Dr Leanne Franklin-Smith (University of Southampton) for pollen concentration dating advice;
- The Quaternary Research Association (QRA) and the University of Exeter for providing additional funding to attend conferences in the UK and abroad.

Special thanks goes to;

- Andrew Cook, for reasons too numerous to mention here, and for being possibly the best husband anyone could ask for;
- Family and friends, for supporting and encouraging my academic endeavours.

1 Introduction

1.1 Research context

Approximately 60% of the world's population live in the regions adjacent to the Himalayas and Tibet (Population Reference Bureau, 2010). Economic activity in the region is strongly influenced by the Asian monsoon, which produces high rainfall and temperatures (Benn et al., 1998; Zhao, 1986). Of particular importance is the rainy season, which provides a vital source of water for domestic use and agro-economic activities (Benn et al., 1998).

The nature of monsoon rainfall patterns (intense periods of rainfall followed by comparatively dry spells) can give rise to serious floods or droughts (Wang, 2006). The Fourth Assessment Report of the Intergovernmental Panel on Climate Change (IPCC AR4) suggests that parts of Asia could become either much wetter or drier (i.e. different areas are likely to be affected differently) because of changes in the Asian monsoon. This could have serious social, economic and environmental implications. Additionally, Wang et al. (1999) contend that the monsoon system controls the atmospheric heat budget in the Northern Hemisphere and therefore changes in monsoon activity could have a controlling influence on the wider global climate. The repercussions of monsoon variability are therefore potentially far-reaching.

Better characterisation, modelling and understanding of these issues is critical to our assessment of future climate change (Liu et al., 2009). Evidence of past variability can be used to help us understand and predict future climate change, enabling policy makers to develop more targeted and timely mitigation and adaptation strategies to cope with future scenarios resulting from changes in the Asian monsoon and the wider global climate system (Shukla, 2007).

Palaeorecords of climate captured in archives such as lake sediments, offer a long-term view of climate change. In recent years, palaeomonsoon researchers have been debating what drives Asian climate dynamics over centennial - millennial timescales or longer (Wang et al., 2005), and in particular whether changes in insolation or changes in glacial - interglacial climate boundary conditions (i.e. changes in ice volume, sea surface temperature, albedo) influence palaeomonsoon dynamics (Herzschuh, 2006b). Further insight into these issues can be achieved by analysing palaeorecords spanning the transition from glacial to interglacial conditions during the last deglaciation, enabling inferences to be made about the nature and dynamics of palaeomonsoon behaviour operating under differing climate regimes (Hodell et al., 1999).

1.2 Research methods

Palaeolimnology and lake sediment analysis are at the heart of this research. A multi-proxy approach is used to gain insight into past environmental and climatic conditions and includes;

- a detailed **site investigation / desktop study** to characterise modern catchment conditions;
- analysis of the **physical properties** of the sediments, based on an assessment of particle sizes and magnetic susceptibility;
- analysis of the **organic content** of the sediments based on measurements of Loss on Ignition (%LOI), Total Organic Carbon (%TOC), Total Nitrogen (%TN), C/N ratios and $\delta^{13}\text{C}$ values;
- **palaeoecological analysis** of fossil pollen grains and charcoal fragments;
- **AMS ^{14}C radiocarbon dating** of bulk sediments and coniferous pollen concentrations.

Collectively these proxies provide an insight into changes in effective moisture, temperature and weathering and / or pedogenesis processes over time (Wang et al., 2005; An, 2000).

1.3 Research hypothesis, aims and objectives

This research tests the hypothesis that Late Pleistocene - Early Holocene millennial to centennial scale environmental and climatic changes in southwestern China were driven by changes in solar insolation and / or glacial - interglacial climate boundary conditions, characterised by stepwise increases in palaeomonsoon intensity.

The research aims are to;

1. identify and examine key environmental and climatic shifts which occurred in southwestern China during the Late Pleistocene - Early Holocene Period;
2. examine the possible drivers of the observed climatic and environmental shifts;
3. compare the research findings with other regional records to better understand regional climate dynamics.

The research objectives are to;

- a. conduct a literature review to define the literature and issues underpinning this research (Chapters 1 and 2);
- b. select a suitable lake to act as the primary study site (Chapters 1, 2 and 4);
- c. collect and examine a lake sediment core from a site in southwestern China using appropriate methods (Chapter 3);
- d. subject the core sediments to multi-proxy analysis and dating (Chapter 4);
- e. produce a chronology for the core (Chapter 4);

- f. use the findings to reconstruct the Late Pleistocene - Early Holocene climatic and environmental history of the chosen study site (Chapter 5);
- g. compare and contrast the results with other proxy records in order to assess climatic trends in the dataset, and possible drivers (Chapter 6).

1.4 Geographical context

Southwestern China encompasses the municipality of Chongqing, the provinces of Sichuan, Yunnan and Guizhou and the Tibet Autonomous Region (including the Tibetan Plateau). A limited number of high-resolution Late Pleistocene - Early Holocene records are available for this region. This region is climatically important because it is located at the heart of Monsoon Asia (Yu et al., 2006). Tectonic activity, most notably the uplift of the Himalayan mountain belt and the Tibetan Plateau, has exerted a strong influence upon regional climate dynamics, triggering the development of the Asian monsoon during the Late Pliocene Epoch and producing an elevational gradient running northwest to southeast, which has resulted in locally distinct microclimates.

Located on the Tropic of Cancer, between 24 - 28°N and 98 - 105°E, Yunnan Province is one of China's largest Provinces, covering over 300,000 km². The modern provincial climate is subtropical. A cool and dry climate prevails from September to April, whilst warmer, wetter conditions persist from May to October. Average annual precipitation ranges from 1000 to 1500 mm and average annual temperature is 16 - 19°C. The mean temperature of the warmest month is 21 - 23°C, while the coldest month is 10 - 12°C (Xu et al., 2004). However, climatic variations occur on a local scale, triggered by changes in elevation. For example, the Tibetan Plateau is cool and dry whereas the central valleys are warmer and wetter in comparison. The climate therefore ranges from subtropical in the southern lowlands to temperate / alpine in the high northwest (Fan et al., 2009). As a consequence, monsoon mechanisms vary spatially, making investigation of regional climate patterns even more important (Herzschuh, 2006a).

The Yunnan landscape ranges from steep valley gorges to high mountains. Three geomorphological zones are evident; the eastern Yunnan Karst Plateau, the central Yunnan Plateau and lake basins and Hengduan Mountains (Zhao, 1986). The Yangtze, Yellow, Salween and Mekong Rivers flow from the mountains in the west to the east and south east coast (Figure 1-1). These rivers initially follow a pronounced north-south trend through Yunnan Province, dictated by the underlying fault zones. The diverse landscapes and microclimates of Yunnan Province are capable of supporting an extremely rich flora. For example, there are over 15,000 species of higher plants growing in Yunnan Province (Wong, 2005), comprised of 2076 genera and 274 families, which equates to over half (56%) of China's seed plants (Mansfield, 2001).

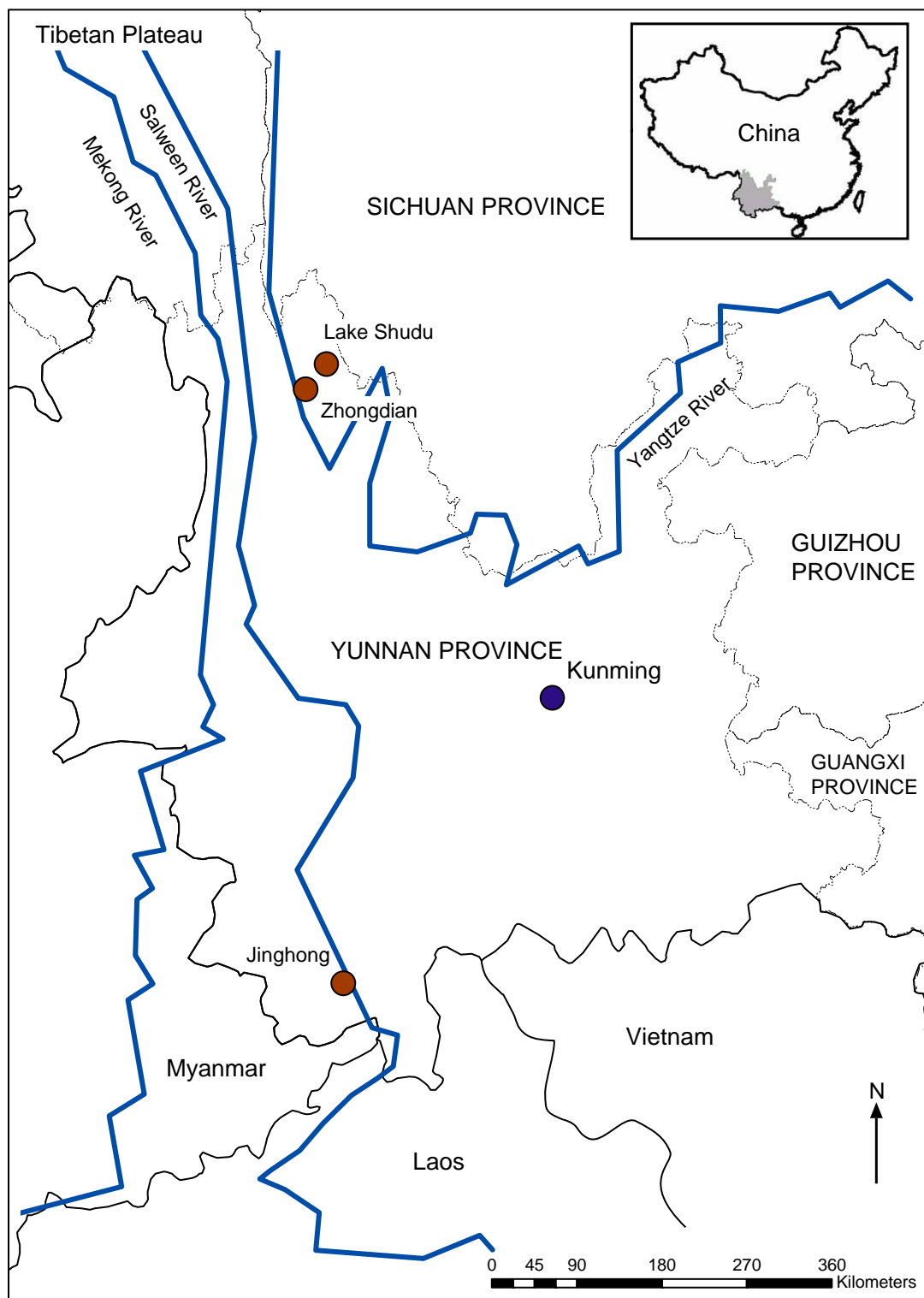


Figure 1-1: Map showing the location of Yunnan Province, China, the provincial capital, Kunming, and Lake Shudu (study site).

1.4.1 Site selection

China is home to more than 2800 naturally occurring lakes (Zhao, 1986). The chosen study site for this research is Lake Shudu, also known as Shudu Hai ($27^{\circ}54.616^{\circ}\text{N}$; $99^{\circ}56.974^{\circ}\text{E}$), located in Zhongdian County, northwestern Yunnan Province (Figure 1-1). It is a medium sized, high altitude, subalpine lake, located ~3680 m asl on the southeastern edge of the Tibetan Plateau. The high altitude mountain location gives rise to strong altitudinal / environmental gradients that exist over relatively short distances, which means that the catchment is highly sensitive to climatic changes (Bunting, 2008; Shen et al., 2005a).

Extreme environments including high altitude, mountainous regions and deserts are likely to be one of the first places to exhibit a response to future climate change, because they are particularly sensitive to changes in precipitation and / or temperature (Tinner pers comm.; Bunting, 2008). Analysing past trends in these sensitive regions may therefore provide insight into the likely sequences of future climate change, and possibly presenting us with an opportunity to try to mitigate or adapt to the forewarned changes.

A lake sediment core measuring approximately seven metres in length and spanning the Late Pleistocene - Early Holocene Period was extracted from Lake Shudu. In the absence of human impact, the long term changes in environmental conditions at Lake Shudu captured in the proxies reflect changes in weathering and / or pedogenesis, organic productivity and vegetation and inferred shifts in effective moisture (Wang et al., 2005). It was assumed that anthropogenic forces were not a significant influencing factor upon the Lake Shudu record during the Period, based on the findings of previous studies which suggest that humans inhabited sites in northwestern Yunnan from the Early Holocene at the earliest (Dearing et al., 2008).

1.5 Project partners

The University of Exeter is a joint partner in a project involving researchers based at Nanjing Institute of Geography and Limnology (NIGL China), NERC Isotope Geosciences Laboratory (NIGL Keyworth) and the University of Liverpool. The project aims to explore the relationship between climate and environment in Yunnan Province, primarily using evidence derived from lake sediments. This PhD research is a part of this partnership and is focused on climatic and environmental changes during the Late Pleistocene - Early Holocene Period. This study provides one of the longest records of climate change for this region, and contributes to the growing body of evidence underpinning our understanding of the nature and dynamics of the regional climate and environment of southwestern China.

1.6 Thesis structure

This thesis is organised into seven chapters;

- **Chapter 1** briefly outlines the primary research hypothesis, aims and objectives and discusses some important issues relating to research Objectives a and b outlined in Section 1.4, including site selection.
- Previous research focusing on the environmental and climatic changes in China during the Late Quaternary is reviewed in **Chapter 2**, in relation to Objective a.
- **Chapter 3** discusses the principles and multi-proxy methods employed in this study, with a view to addressing Objective c.
- The results of laboratory analysis and a site investigation are presented in **Chapter 4**, which deals with Objectives d and e of this research.
- Aims 1 and 2 and Objective f are dealt with in **Chapter 5**, which deals with the results of this research, interpreting them in relation to the environmental shifts which occurred at the study site, and highlighting the potential drivers of change.
- **Chapter 6** focuses on Aim 3 and Objective g, comparing and contrasting the Lake Shudu record with other regional proxy records and examining whether these shifts provide evidence of Late Pleistocene - Early Holocene climatic changes in southwestern China.
- The issues highlighted in Chapters 1 - 6 are drawn together in **Chapter 7**, which provides an overview of the main findings of this research and summarises how these address the primary research hypothesis. Ideas for further work are presented.

2 Asian palaeoclimatic variability during the Late Pleistocene - Early Holocene Period

2.1 Introduction

The aim of this review is to provide a detailed account of Asian palaeoclimatic research undertaken to date, with particular reference to Late Quaternary proxy records from China. This chapter addresses Objective a identified in Chapter 1.

Asian palaeoclimatology is a diverse and rapidly developing research field, which is reflected in the scope and nature of the research published on this topic. Three papers have been published which provide an overview of research undertaken to date (Wang et al., 2005; Yihui et al., 2005; An, 2000). Four primary research themes are evident;

1. Monsoon evolution
2. Monsoon variability over orbital to intraseasonal timescales and identification of potential forcing mechanisms
3. Global teleconnections (the relationship of the monsoon system with other climate events, including unique and recurring phenomena)
4. Modelling and prediction of the onset of summer monsoon rains on interannual timescales

This review primarily focuses on the key scientific advances made under Theme 2 because this underpins the work presented in this thesis. Whilst acknowledging the possible teleconnections between the Asian monsoon and other global phenomena such as the African monsoon and the North Atlantic climate, these issues are considered outside the scope of this review, primarily because they represent significant research fields in their own right. Consequently, this review focuses on the high-resolution, millennial scale proxy records obtained from sites in Southeast Asia (e.g. Dykoski et al., 2005; Wang et al., 2001; Thompson et al., 1989).

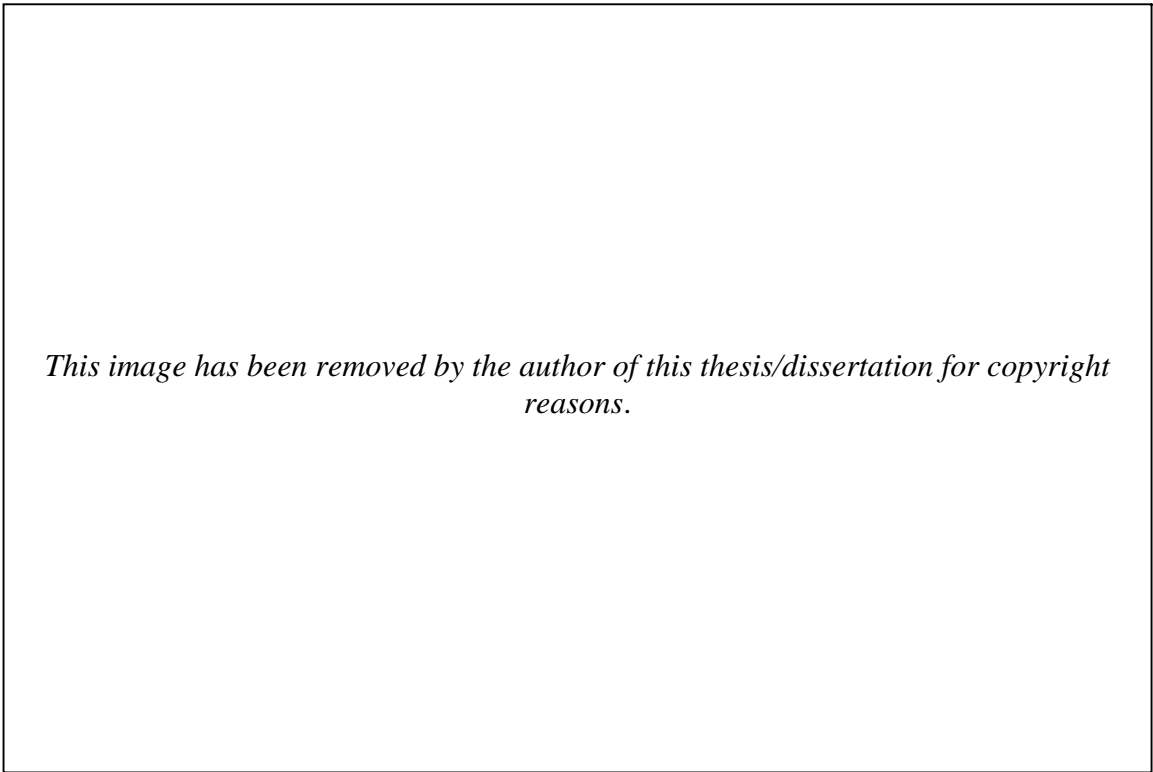
Significant advances have been made in this field. However, there are gaps in our knowledge of Asian palaeoclimate variability during the Late Pleistocene - Early Holocene Period, which have arisen as a direct consequence of a lack of well-distributed, robust proxy records, particularly in certain regions of China (Yihui et al., 2005) and a consequent lack of sufficiently detailed climate models for this region (Shukla, 2007). This research project seeks to address this gap by producing a high-resolution record of palaeoclimatic variability for southwestern China, which is one of the regions that currently lack a network of good quality proxy records.

2.2 The Asian monsoon

The influence of the contemporary Asian monsoon system is wide-ranging, extending from the western Arabian Sea through to East Asia and North Australia. According to Barry et al. (1995), the word ‘monsoon’ is derived from the Arabic word ‘*mausim*’, which means season, owing to its strong seasonal gradients. Many different definitions are used in the literature to describe the monsoon. For example, the IPCC defines a monsoon as a tropical and subtropical seasonal reversal in both the surface winds and associated precipitation (IPCC, 2007b). This is a useful but over-simplified definition, for in reality, monsoons are the result of a complex interplay of factors, including solar activity and land - ocean interactions.

Set within the context of the global climate system (Figure 2-1), atmospheric circulation is driven by changes in precipitation and evaporation, and the activity of vertical and horizontal convective cells covering the globe (Figure 2-2). Warm air rises in the Intertropical Convergence Zone (ITCZ). This is located on the equator at 0° and delineates the zone of convergence of the trade wind systems over the ocean. This air circulates to the subtropics, resulting in movement of heat away from the equator. More warm air is transported poleward from the mid and high latitudes. Conversely, cold air sinks and moves towards the equator. The movement of warm and cold air in this way triggers the global circulation of air masses from the equator to the poles and back. The rising warm air in the tropics is also moist, which results in a net excess of precipitation over evaporation, whilst the cooler sinking air in the subtropics causes an excess of evaporation over precipitation. Ruddiman (2001) concludes that the varying spatial relationship between precipitation and evaporation and global convection patterns produce climatic phenomena such as monsoons. However, atmospheric circulation is not the only factor responsible for the development of monsoons. In Asia, the unique configuration of land (the vast and orogenically distinct Eurasian Continent) and water (the Pacific Ocean) that occurs in this region modifies the regional climate, giving rise to the Asian monsoon.

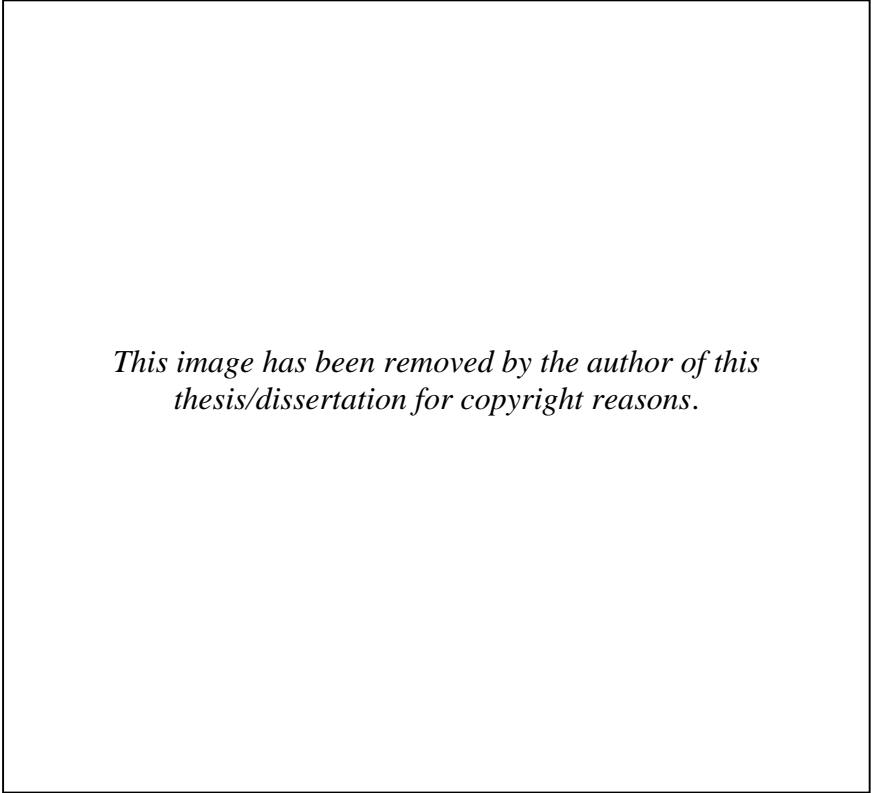
The Asian monsoon began to evolve during the Late Pliocene Epoch, when the Qinghai / Tibetan Plateau was uplifted to 1000 m asl. At the end of the Tertiary, the Plateau was abruptly uplifted to 3000 m asl, then uplifted again to its current altitude of 4000 m asl during the Late Quaternary (Wang et al., 2005; Zhao, 1986). During the Miocene Epoch, the Himalayan Arc Mountain folding belt was formed and uplifted to 9000 m asl, which when coupled with changes in global ice volume and wind strength, most likely triggered the onset of Asian monsoon patterns similar to the present (Harris, 2006). The monsoon is therefore a coupled system, because the interaction between the atmosphere and ocean, combined with the influence of the land surface features (including orogeny, geomorphology and geology), are important components of this self-regulating system (Webster, 2006).



This image has been removed by the author of this thesis/dissertation for copyright reasons.

Figure 2-1: The global climate system.

This is a simplified representation. Positive and negative feedback loops exist between different parts of this system. See Ruddiman (2001).



This image has been removed by the author of this thesis/dissertation for copyright reasons.

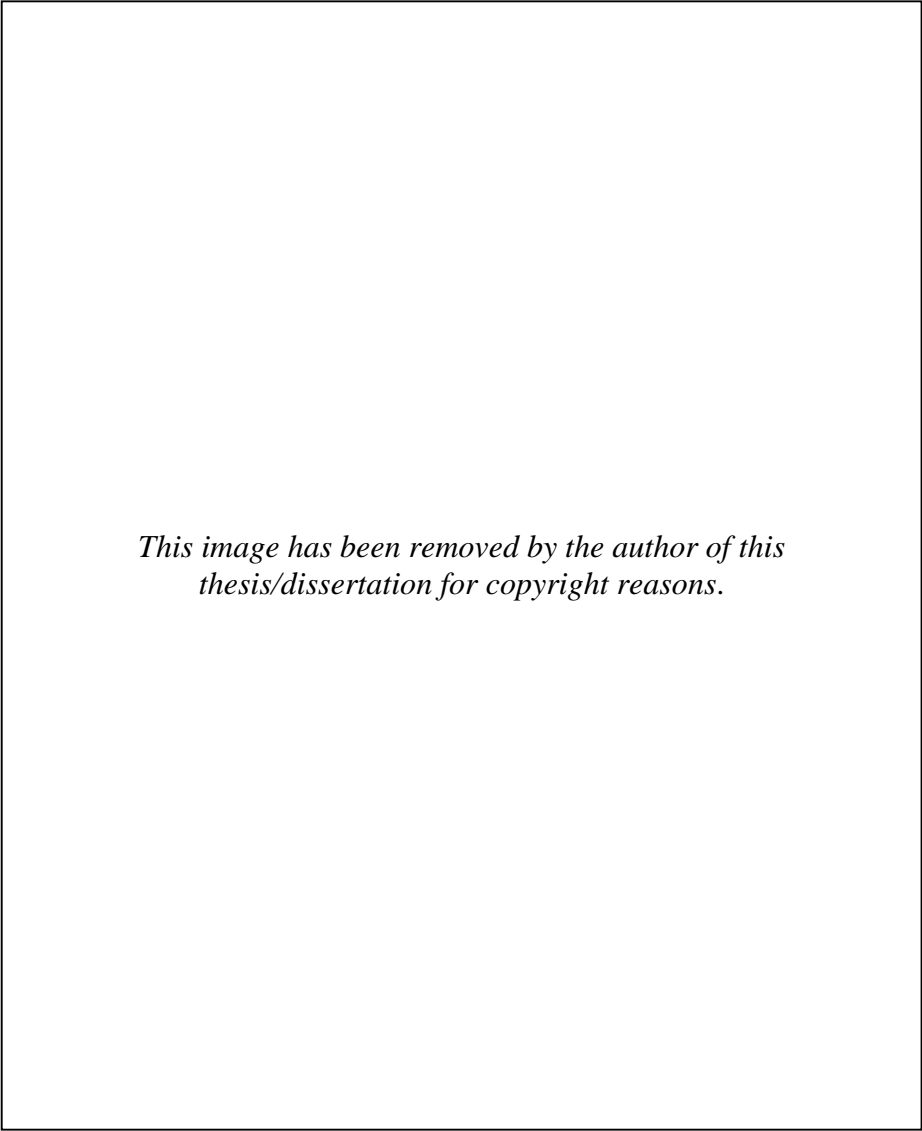
Figure 2-2: Global atmospheric circulation.

The diagram shows how air masses circulate vertically and horizontally.

From Short (2008).

2.2.1 Seasonal climatology

Seasonal monsoon patterns are triggered by a reversal in large - scale, meridional, tropospheric overturning of Hadley circulation, coupled with overturning in three transverse cells (the Pacific and Atlantic Cells and an Asia - Africa transverse cell that overturns towards the west) and precipitation changes (Trenberth et al., 2006). These phenomena are caused by reversals in heating and temperature gradients between the continental land mass and the ocean. The Pacific Ocean has a large capacity to absorb and retain heat and responds more slowly to seasonal changes in solar intensity than the continental landmass (Ruddiman, 2001). This disequilibrium, coupled with the orogenic influence of the Himalayas and the Tibetan Plateau produces distinct seasonal precipitation and temperature patterns manifesting as warm, humid (the rainy season) and cold dry phases (Trenberth et al., 2006). These broadly equate to the summer and winter seasons (Figure 2-3). The timing and duration of these seasons varies across the Asian monsoon region according to local climate regime and the level of influence of the Asian monsoon (Ding et al., 2006). However, it is possible to make some general observations relating to the onset and characteristics of the Asian monsoon.



This image has been removed by the author of this thesis/dissertation for copyright reasons.

Figure 2-3: Contemporary pressure and surface wind patterns over Asia.

Diagram B shows the winter patterns and Diagram C shows the summer patterns.

From Wang et al. (2005).

During the Asian winter monsoon (December - February), levels of solar radiation are reduced, and the continental land mass cools more rapidly than the ocean. This causes continental air masses to cool and sink, creating an area of high pressure over the land surface. Generally, cool, dry conditions prevail. Westerly airflows (located between the trade wind belts) dominate above the near surface airflows (Barry et al., 1995). Because of its height (~4000 m asl) and shape (ellipsoidal and orientated in a west - east direction) (Yanai et al., 2006), the Tibetan Plateau forces the upper westerlies to flow around it, splitting into two currents (jets) flowing to the north and south of the Tibetan Plateau and reconnecting again over Northern China and Japan. The intensity of the Siberian High can also significantly influence winter temperature variation in China (Ding et al., 2006).

During Spring, the upper westerlies migrate northwards. The northerly jet strengthens and extends across central China and into Japan, whilst the southerly jet remains south of Tibet, and weakens in intensity (Barry et al., 1995). In April, the ITCZ drives air circulation over India, centering over the Equator and moving north with the sun to the Indian Ocean. Conditions are hot, dry and squally in India because of increased solar heating (Barry et al., 1995). The pre-monsoon season is unique to India and does not occur in other parts of Asia. Low pressure zones occur most frequently over China in Spring, originating either in central Asia or in the jet convergence zone located at the lee of the Tibetan Plateau. Spring is therefore wetter than Winter. From March - May, a quarter to a third of annual rainfall occurs over central and southern China (Barry et al., 1995).

The Asian summer monsoon (wet season) commences in May - June and lasts for about six months (Ding et al., 2006). The summer monsoon is triggered when the land surface is more rapidly heated than the ocean, causing air masses over the continent to warm, expand and rise, creating an area of low pressure at the land surface (Ruddiman, 2001). During the latter half of May, the southern jet begins to break down and shifts northward over the Tibetan Plateau. The upper level flow to the south is deflected by the Coriolis Force, which produces a strengthening easterly jet at 10 - 15°N and a westerly jet at 20°S (Barry et al., 1995). The Tibetan Plateau blocks the air flow at 500 mb and below, causing the jet axis to jump from the south to the north side of the Plateau (Barry et al., 1995). Over India, the Equatorial Trough travels northward as the Westerlies weaken. Warm air containing water vapour evaporated from the ocean is drawn towards the low pressure zone located over the continent, resulting in higher rainfall rates.

In early to mid June these changes trigger the Meiyu / Baiu rainy season over the Yangtze River Basin, which coincides with the onset of the Indian rainy season (Ding et al., 2006). In early July, rainfall surges first occur over the Indo China Peninsula, which establishes a monsoon rain belt extending northward and eastwards to the Bay of Bengal, the South China Sea, mainland China, the Korean peninsula, North Japan and the Western North Pacific. North of the Tibetan Plateau, there is a weak upper westerly current with a subtropical high pressure cell over the Plateau. The Indian monsoon in southern Asia is overlain by strong upper easterlies with a pronounced jet at 150 mb (~50,000 ft), which extends westwards across South Arabia and Africa (Barry et al., 1995).

By mid July warm, moist monsoon conditions dominate conditions in South and Southeast Asia (Barry et al., 1995). From May to September, precipitation patterns alternate between 'active' (pluvial) and 'break' (drought) periods, which produces the rainy season (Ding et al., 2006). Break troughs force air to rise by the Himalayas and replace the monsoon trough, which causes rain to fall in the foothills and the Brahmaputra Valley when rainfall is generally low elsewhere (Barry et al., 1995).

In Autumn, the Equatorial Trough (a low pressure zone where the trade wind systems converge) changes course and moves southward. During October the westerly jet quickly re-establishes itself south of the Tibetan Plateau, bringing a return to cool conditions throughout southern and eastern Asia (Barry et al., 1995). The cycle then begins again.

Total annual rainfall is often used as a measure of monsoon strength (Webster, 2006), however analysis of intraseasonal rainfall patterns indicates that monsoon strength (or intensity) varies considerably on these timescales. For example, areas having the largest annual range of precipitation exceeding 17 mm day^{-1} (equivalent to a total summer precipitation $<1530 \text{ mm}$) include the Bay of Bengal, the Philippines Sea and the South China Sea (Ding et al., 2006). Regions with the largest ranges also tend to record the maximum summer rainfall. The ratio of summer to annual rainfall can be used as a measure of the relative importance of rainfalls during the wet season within the context of annual precipitation values. A large ratio indicates an intense rainy season combined with a dry winter. For example, a ratio of 85% has been recorded for northeast continental Asia (Ding et al., 2006). Generally, precipitation levels in Monsoon Asia tend to be high, and intense, with most of the annual rainfall occurring during a few months. The chances of floods or droughts occurring are higher because of this distinctive cycle (Wang, 2006).

In summary, Mayewski et al. (2004) identified the following key atmospheric characteristics of the Asian monsoon;

- Westerlies north of 30°N, NE Trade Winds and sub-tropical winds south of 30°N;
- winds migrating north during Summer and south during Winter;
- an interface between Westerlies and Easterlies (25 - 35°N);
- changing prevailing wind patterns from Westerlies in the Winter to Easterlies in the Summer.

The annual cycle of the Asian monsoon system is divided into two distinct wet and dry phases. The wet phase is defined as the rainy season during which warm, moist wind blows inland from the warm tropical oceans (Indian and Pacific), whereas the dry phase refers to the other half of the year when winds bring cool and dry winter air from the Asian continent. Generally, the wet season takes place from May to October and lasts approximately six months, whilst the dry season is from November to April. The timing and duration of the wet and dry seasons varies spatially (Ding et al., 2006) and can change over time.

2.3 Monsoon China

China is situated primarily in the mid latitudes, between 20°N and 50°N; consequently, the climate is primarily subtropical. However, periods of tectonic activity have given rise to a pronounced altitudinal gradient extending from the Himalayas in the northwest to the coastal lowlands in the southeast defined by a series of terraces (Figure 2-4). The highest terrace is located in the west (Zone 1), and includes the Himalayas, and the Tibetan Plateau and has an average elevation of 4000 m asl. The next highest terrace (Zone 2) includes the Loess Plateau and averages 1000 - 2000 m asl. The third zone incorporates the east coast and lowlands and averages 200 m asl. These factors induce marked vertical and horizontal variations in temperature and precipitation (Xu et al., 2004), producing regional distinct climatic zones. Cold conditions dominate the Tibetan Plateau and the Himalayas (Zone 1). Zone 2 is climatically divided into two subzones. Northwestern and central China (Zone 2a) are dominated by arid conditions, whilst humid conditions influence southwestern China (Zone 2b). Zone 3 is humid, and subject to increased rainfall during the summer (Zhao, 1986).

The landscape of Yunnan Province, southwestern China, follows the same elevational pattern, sloping on a northwest to southeast gradient from Zhongdian (NW) to Jhonghong (SE) as illustrated by Figure 2-5. Elevation declines gradually from the interior to the coast. Landscape elevation is highest in the northwestern zone, peaking at 6470 m asl at Meili Snow Mountain and declining to an elevation of 75 m asl at the Vietnam border. This has resulted in a ~6400 m difference in elevation between highest and lowest areas of Yunnan Province.

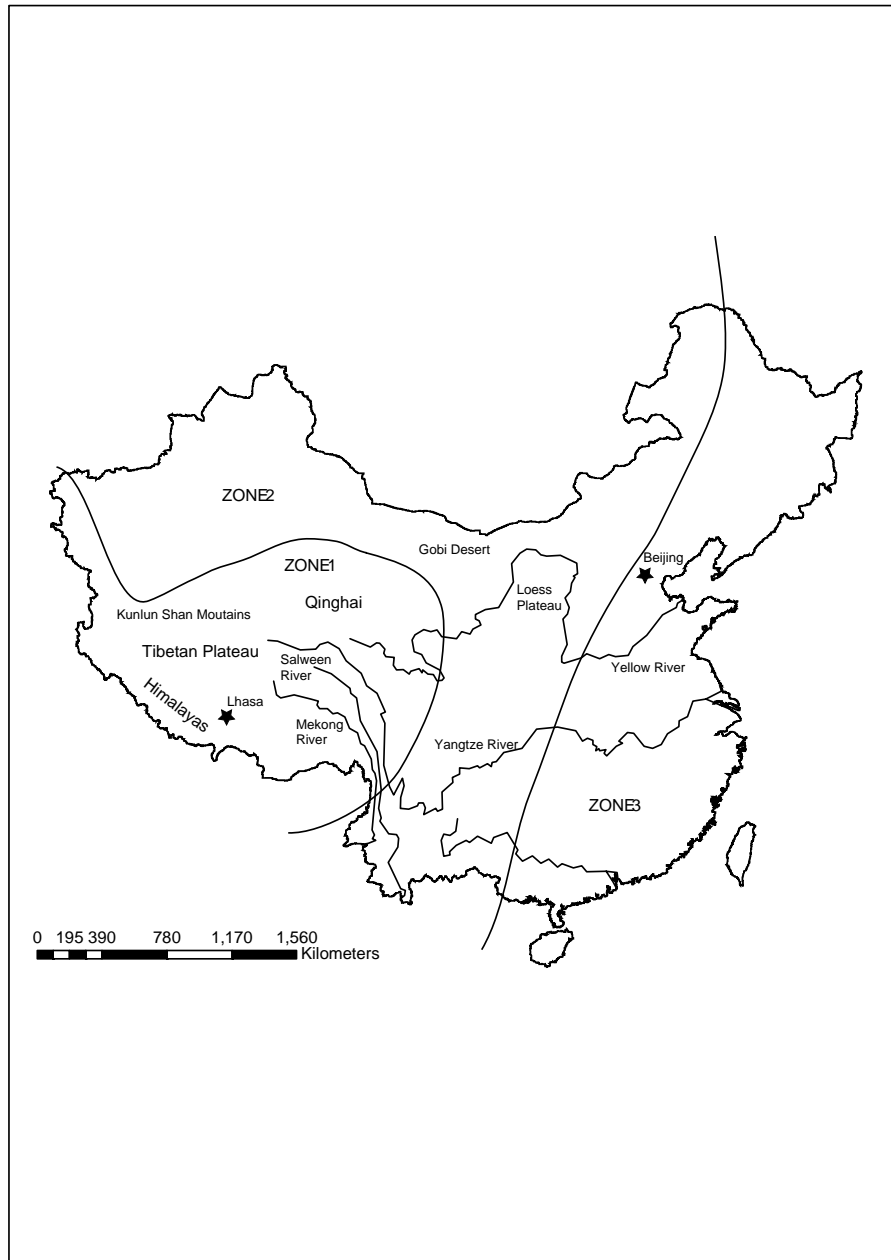


Figure 2-4: Map showing the altitudinal zones of China.

Zone 1 represents the highest terrace.

Source: China Facts and Figures (2004).

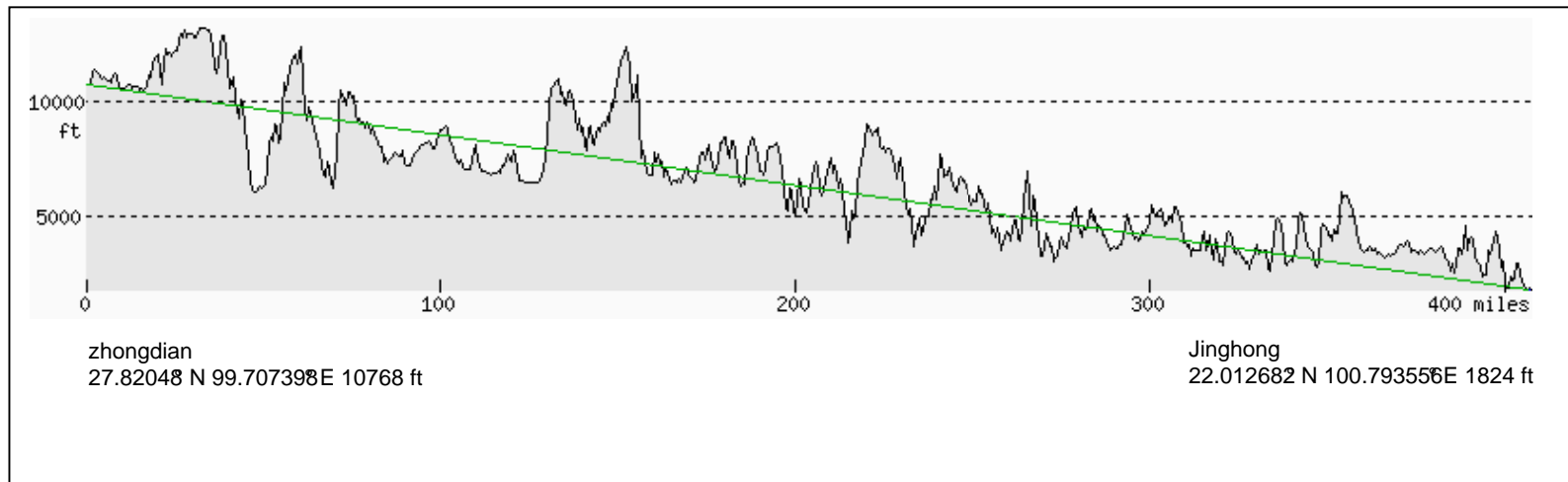


Figure 2-5: Elevation profile, Zhongdian - Jinghong, Yunnan Province, China.

Source: Google Earth (2008).

It is possible to distinguish two distinct subsystems within the Asian monsoon system, which influence the climate of southwestern China (Figure 2-6). The tropical Indian monsoon (also called the southwestern or South Asian monsoon) and the subtropical East Asian monsoon (also called the Southeast Asian monsoon) are roughly delineated by the line of 105°E longitude, which runs along the southeastern flank of the Tibetan Plateau (Wang et al., 2005; Wang et al., 2003). A convergence zone is proposed at the point at which these subsystems meet.

The main distinctions between the contemporary southwestern and East Asian monsoons are identified in a comparative study carried out by Wang et al. (2003). The authors surmise that the southwestern monsoon is dominated by a distinct clockwise gyre centred in the equatorial Indian Ocean, which is linked to the Somalia Jet and the Mascarene High. It is characterised by two seasonal wet and dry phases and two rain bands.

In contrast, the main characteristics of the East Asian monsoon are the Western North Pacific (WNP) monsoon trough (the ITCZ), the WNP subtropical ridge, the East Asian subtropical Meiyu Front (also called the Baiu, Changma and Plum Rains), blocking highs and polar anticyclones (low pressure zones). The East Asian winter monsoon results from development of a cold core high over the Siberia - Mongolian region. In East Asia, four seasons can be distinguished (Ding et al., 2006). From June to October, one rainy season occurs.

Differing views exist regarding the relative influence each of these subsystems exerts upon the climate of southwestern China (Yihui et al., 2005; Chen et al., 1999). For example, Chen et al. (1999) reconstructed palaeomonsoon variability spanning the last ~800,000 years from pollen and magnetic proxies contained in lake sediments obtained from the eastern side of the Tibetan Plateau. They conclude that the plateau region is primarily sensitive to changes in the East Asian monsoon. Conversely, Hu et al. (2005) analysed magnetic susceptibility and pollen records from the Heqing Basin and obtained a record of climate change for Yunnan Province spanning the last one million years. Cyclic patterns of temperate / arid and cold / humid conditions indicated that the southwestern monsoon predominantly drove the regional climate. Herzschuh (2006b) analysed 75 palaeomoisture records spread across central Asia and concluded that during the last ~50,000 years, the influence of the southwestern monsoon extended to the Tibetan Plateau. The Southeast Asian monsoon dominated the southeast region of China and the northwestern and central areas of China were dominated by the Westerlies.

Collectively, these studies suggest that the relative influences of the Asian monsoon subsystems vary spatially and temporally over China during the Late Pleistocene - Early Holocene Period. However, the recent studies tend to support the view that the southwestern Monsoon governed the climate of southwestern China (including Yunnan and the plateau), whilst the Southeast Asian monsoon primarily influenced the climate of southeast and central China at this time.

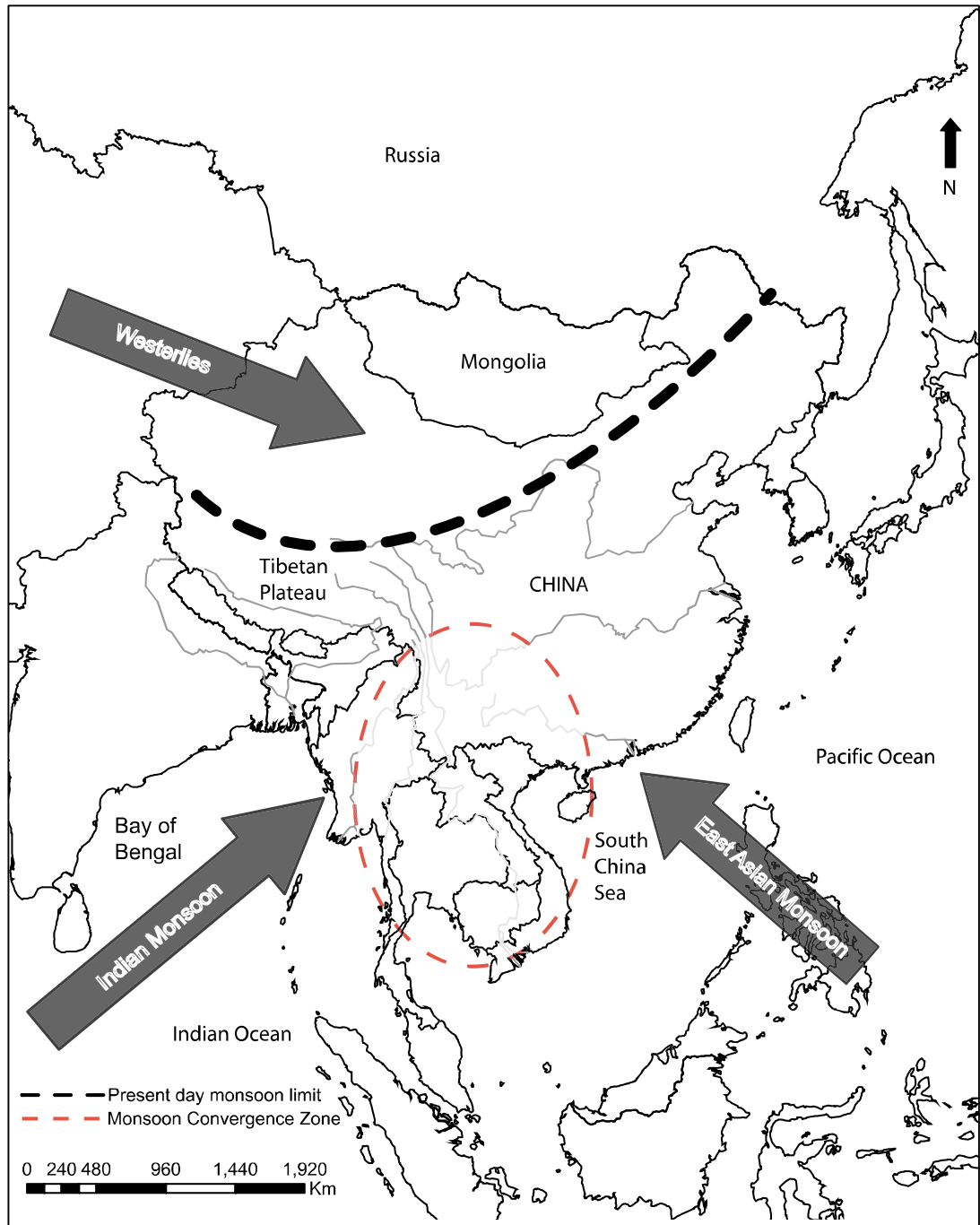


Figure 2-6: Map showing the climate subsystems influencing China.

The present day summer monsoon limit and the proposed monsoon convergence zone are also illustrated.

NB: Onshore wind directions represented by the black arrows are indicative only. The East Asian Monsoon winds head inland in a northwesterly direction before being deflected to the right by the Coriolis force (see Figure 2-3).

Adapted from Herzsuh (2006).

2.4 Chinese Quaternary terminology

Chinese terms that broadly correspond with the Late Pleistocene and Holocene periods is summarised in Table 2-1. The Dali (or Tali) Glaciation is thought to have commenced between ~70,000 and 40,000 yr BP, and ended at ~10,000 yr BP, based on changes in the snowline and estimations of the previous extent of uncalibrated ^{14}C radiocarbon dated valley glaciers found on Mount Diancang located near Dali, northwestern Yunnan Province (Shi et al., 1979). The Dali Glaciation is the last glaciation before the onset of the Holocene interglacial period. Temperatures during the Dali stage are estimated to have been 2 to 6°C lower than present day temperatures. A continuous permafrost zone extended southward to 40°N in East China and to ~30°N on the Tibetan Plateau (Shi et al., 1979). This period is divided into the Early Dali Glaciation (>40 ka BP) and the Late Dali Glaciation (25 - 10 ka BP), separated by a glacial interstadial (40 - 25 ka BP). The Late Dali Glaciation is most relevant to this study. During this stage, the climate was much drier and colder than previous stages. Temperatures are estimated to be ~7 to 8 °C lower than today, and the length of valley glaciers was 1.6 to 5.9 times greater than the present (Shi et al., 1979).

The Late Dali Glaciation encompasses the Last Glacial Maximum (LGM) and the Lateglacial. The LGM represents maximum glacial extent at the end of the last glaciation. The precise timing of the LGM remains open to debate (see Section 2.5.3). Evidence suggests that climatic conditions were much colder and drier than present. Mean annual temperatures were ~4 to 6°C lower in the south (Zheng et al., 1998). Relict glacial landforms on the Kunlun mountains of western China indicate a lowering of the snowline by 300 - 500 m. Composite analysis of pollen records indicates that forests retreated towards the equator and desert / steppe vegetation extended eastward in China (Yu et al., 2000a; Zheng et al., 1998). In northwestern Europe, the Lateglacial, (or Late Weichselian) refers to the end of the last cold stage when the glaciers and ice sheets were retreating. It is dated to c. 13 - 10 ^{14}C ka BP, although the sequence of events associated with this phase may have occurred from ~15 - 9 ka BP (Lowe et al., 1997).

Region / Time	China
Holocene	Present Neoglaciation (3 - 2 ka BP)
	Post Glaciation (10 ka BP)
Late Pleistocene	Late Dali Glaciation (25 - 10 ka BP) LGM (14.7 ka BP)
	Glacial Interstadial (40 - 25 ka BP)
	Early Dali Glaciation (>40 ka BP)

Table 2-1: Chinese terminology for the Late Pleistocene (Dali) - Holocene Period.

Quoted dates are uncalibrated. After Zhang (1992).

2.5 Millennial to centennial scale proxy records of Late Pleistocene - Early Holocene palaeomonsoon variability obtained from sites in China

The literature indicates that there are four key speleothem or ice core records covering the Late Pleistocene - Early Holocene climate of China; (Zhou et al., 2008; Dykoski et al., 2005; Wang et al., 2001; Thompson et al., 1989). These records are widely cited in the literature and are often used as 'benchmarks' within other studies. Figure 2-7 indicates their geographical locations in relation to each other and to Lake Shudu. The key trends and events captured in these records are discussed in greater depth in Section 2.5.5. and presented in Figure 2-10; Figure 2-11; Figure 2-13 and Figure 2-14.

Figure 2-11A number of other Chinese palaeorecords are available, but many are written in Chinese. Fortunately, some of these have now been translated into English and published in comparative studies seeking to synthesis, compare and contrast the results obtained (e.g. Herzschuh, 2006b; Fang, 1991). These studies are an important source of otherwise unavailable material. High-resolution palaeoecological records focusing on individual sites are also available (e.g. Shen et al., 2005a; Shen et al., 2005b). However, the collective spatial and temporal coverage of these records is patchy, particularly in southwestern China (Wang et al., 2005).

Collectively these studies provide a valuable insight into the climatic shifts that took place during the Late Pleistocene - Early Holocene Period. They also highlight key debates in the literature relating to this period, including differing views regarding the relative influences of forces driving Asian palaeomonsoon dynamics and the timing and nature of key climatic shifts, including the LGM and the transition from Pleistocene - Holocene conditions.

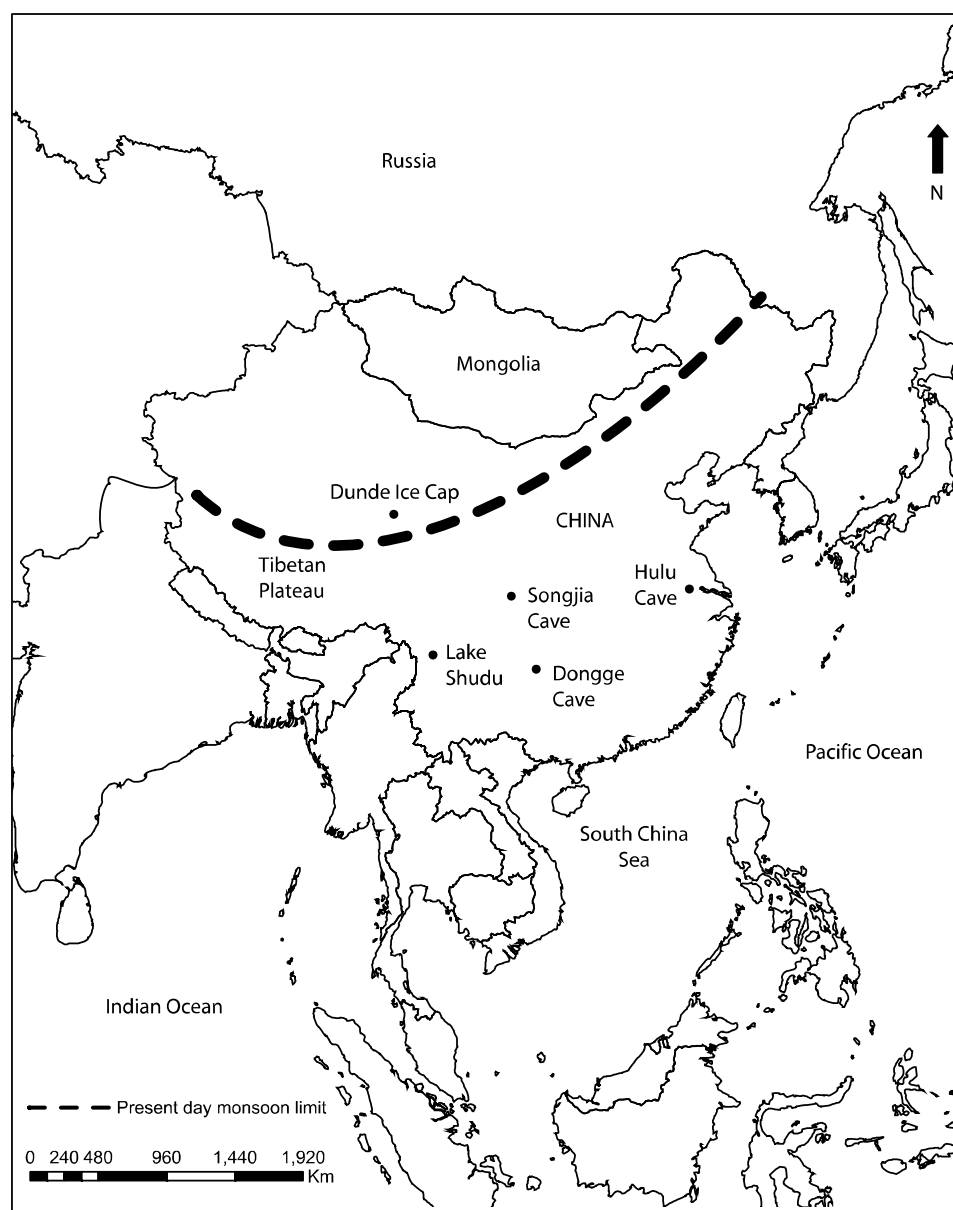


Figure 2-7: Map showing the locations of key speleothem and ice core records in China and their proximity to Lake Shudu.

2.5.1 Drivers of palaeomonsoon variability

On millennial or longer timescales, changes in the areal extent of the Asian summer and winter monsoons are driven by factors including changes in solar insolation and / or global climate excursions (such as a shift to an ice age, warmer conditions, or changes in sun-earth geometry) (Wang et al., 2005; Pant, 2003; Maslin et al., 2001; Zonneveld et al., 1997).

For example, previous studies focusing on orbital patterns of Indian palaeomonsoon variability during the Late Pleistocene based on $\delta^{18}\text{O}$ records derived from *G. Bulloides* obtained from the Arabian Sea suggest that the summer monsoon strengthened with increasing Northern Hemisphere summer insolation but weakened with increasing boundary conditions and associated ice cover dynamics (Wang et al., 2005). Stronger winter monsoons have also been observed during glacial intervals, based on evidence obtained from $\delta^{18}\text{O}$ records derived from foraminifera contained in marine cores from the Arabian Sea (Wang et al., 2005). Similar trends have been elucidated from marine cores from the South China Sea for the East Asian monsoon (Wang et al., 1999).

Analysis of the literature indicates that previous research into the drivers of the palaeomonsoon in China has primarily focused upon the influence of solar insolation upon monsoon variability. The observed trends are used as a means of correlating Chinese proxy records with those obtained from the North Atlantic, where synchronicity between observed shifts in $\delta^{18}\text{O}$ ice core records and solar insolation have been inferred (e.g. Zhou et al., 2008; Wang et al., 2001).

In the Greenland ice core records, $\delta^{18}\text{O}$ values became much lower from c. 18 ka until c. 10.5 ka and then stabilised (Galy et al., 2008). Genty et al. (2006) suggest that the peak at c. 16.5 ka represents the first signs of a warming climate. In the Chinese speleothem records, $\delta^{18}\text{O}$ values follow the same trend but the observed isotopic values are inverted (values become higher). These shifts are believed to result from colder and drier glacial conditions relative to the present, but becoming warmer and wetter in response to increased levels of solar insolation.

Spectral analysis of the $\delta^{18}\text{O}$ record obtained from Dongge Cave, China (Dykoski et al., 2005) highlights peaks at 208 and 86 yrs, which are thought to coincide with the de Vries and Gleissberg solar frequencies at 207 and 88 yrs identified in $\delta^{13}\text{C}$ / dendrochronological records, which elicits a link between solar forcing and monsoon dynamics. The authors contend that the similarity of these results and those obtained for Hulu Cave (Wang et al., 2001) and the Greenland Ice Cores (Stuvier et al., 1995) suggest that the same mechanisms were driving Late Quaternary Indian and East Asian monsoon dynamics on millennial timescales.

Correlations are also inferred between the Dongge Cave and the Hulu Cave record (Wang et al., 2001). For example, similar patterns are observed in the $\delta^{18}\text{O}$ values, which seemingly correspond to the deglacial sequences in the records at Dongge Cave (D4 stalagmite) and Hulu Cave (stalagmite H82). Dykoski et al. (2005) conclude that the changes in the $\delta^{18}\text{O}$ record reflect changes in Asian monsoon intensity, and that the observed patterns broadly mirror changes in solar insolation. Furthermore, the Dongge Cave and Dunde Ice Cap records point to monsoon strengthening at c. 10,000 years, which is suggested by other researchers (e.g. Sirocko et al., 1996).

However, the similarities between the Dongge and Hulu Cave records only extend to the deglacial sequence. As the authors themselves acknowledge, the caves are located 1200 km apart and therefore the recorded climate history may be very different. It is also argued that the observed similarities are small within the context of the overall records, and may not therefore be climatically significant (Dykoski et al., 2005).

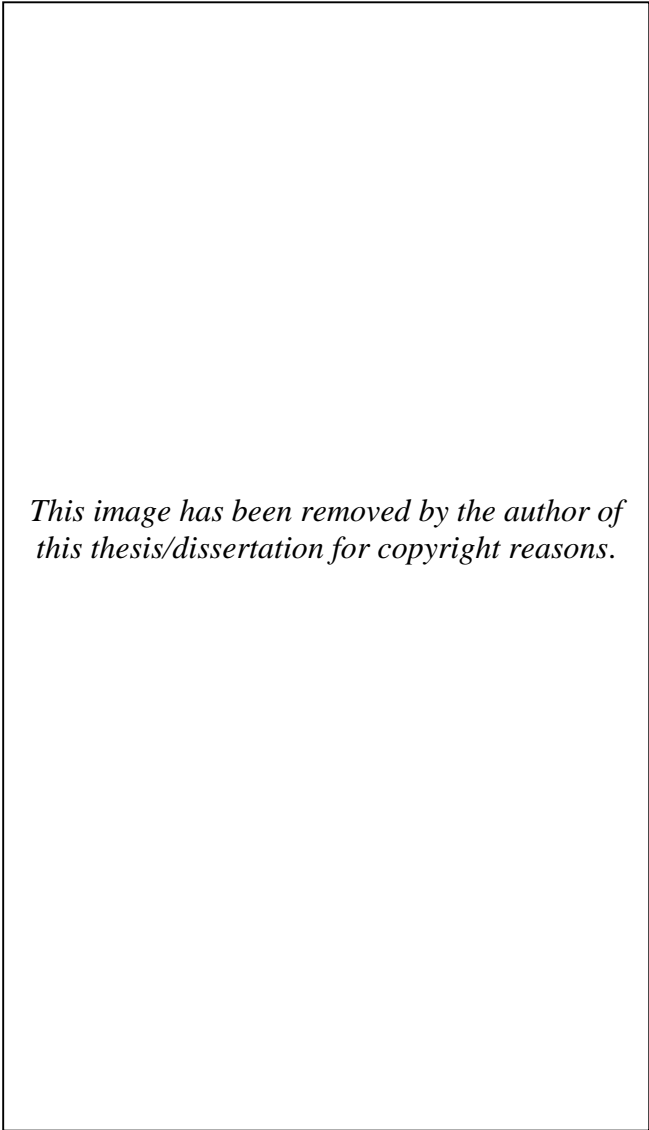
Pollen, isotopic and lithological records obtained from lake and peat bog records from sites in Tibet, Northwest and Northern China and Mongolia were used to reconstruct moisture conditions in central Asia over the last c. 50,000 cal. yr BP (Herzschuh, 2006b). The records were calibrated using tree ring and U/Th coral data from CalPal2003. Millennial-scale trends in the composite data had a similar pattern to the insolation changes for 30°N in June, with strong correlations between inferred periods of high effective moisture and high insolation (i.e. during the Early Holocene) and conversely drier conditions during periods of weaker insolation (i.e. during the LGM). However, the peaks do not match exactly. Herzschuh (2006b) concludes that it is not possible to determine whether the differences were caused by other factors driving monsoon variability, or whether this was a product of chronological inconsistencies. It is clear from these findings that the production of palaeorecords with more robust chronologies is required in order to determine whether the timings of these phenomena are truly correlated or not.

A multi-proxy study based on pollen, carbonate, TOC and $\delta^{13}\text{C}$ values in a Lateglacial lake sediment record obtained from the Lake Qinghai region indicates that the climate was very cold before c. 16.9 ka cal. yr BP (Shen et al., 2005b). After c. 14.1 ka cal. yr BP, conditions became warmer and wetter. This is identified as the point of glacial decline by An et al. (1991). The authors suggest that solar insolation changes on a millennial (10,000 year) scale are the likely drivers of the East Asian monsoon subsystem.

At c. 10,000 ^{14}C yr BP, solar insolation was at a maximum in the Northern Hemisphere, but at a minimum in the Southern Hemisphere (An, 2000). This lends support to the Kutzbach Theory that monsoon intensity is driven by Northern Hemisphere dynamics (Kutzbach, 1981). According to this theory, millennial scale monsoon dynamics are driven by solar precession cycling every 23,000 years. Precession maximum was reached approximately 10,000 years ago, with proxy records reflecting an increase in solar insolation, triggering increased Asian monsoon intensity.

However, it is proposed that solar insolation only became the dominant influence upon monsoon intensity once the ice sheets had retreated (Dykoski et al., 2005). Previous research also indicates that the nature of the response of the monsoon to solar forcing is significantly modified by glacial dynamics (Herzschuh, 2006b). For example, Zonneveld et al. (1997) used the number of dinoflagellate cysts obtained from a marine core from the Indian Ocean as a proxy for southwestern monsoon intensity during the last deglaciation. The resulting curve was correlated with mean July solar insolation levels derived from calculating variation in contrast between 30°N and 30°S insolation levels (Figure 2-8). The results suggest a lag between solar insolation contrast and monsoon intensity. Minimal monsoon intensity lags minimal contrast by ~ 7.5 ka, whereas maximal monsoon intensity lags maximal contrast by ~ 4 ka. However, more recently, high-resolution records from China (see Section 2.5.5) suggest that the lags are shorter. The lag between minimum solar insolation and minimum summer monsoon intensity is estimated to be no more than $\sim 5 - 6$ ka (e.g. Wang et al., 2001), while the lag between maximum solar insolation and maximum summer monsoon intensity is estimated to be no more than $\sim 1 - 2$ ka (e.g. Dykoski et al., 2005). The difference in lag duration highlighted in all of these studies points to a non-linear relationship between solar insolation and monsoon intensity.

The existence of snow / ice cover over central Asia is proposed as a possible explanation for this difference. On the Tibetan Plateau, increased snow / ice cover (especially during glacial times) increased the regional surface albedo, reducing or perhaps even preventing the establishment of low surface pressure zones and suppressing the effects of increasing solar insolation contrast. This would have resulted in a decreased land - sea pressure gradient, triggering a reduction in southwestern monsoon intensity (Zonneveld et al., 1997). However, there is little consensus over the extent of snow / ice cover in this region during the Lateglacial (Zonneveld et al., 1997).



This image has been removed by the author of this thesis/dissertation for copyright reasons.

Figure 2-8: Correlations between southwestern monsoon intensity and solar insolation during the last deglaciation.

The solid line shows the number of upwelling / non-upwelling dinoflagellate cysts used as a proxy for monsoon intensity. Minimal monsoon intensity lags minimal contrast by ~7.5 ka, whereas maximal monsoon intensity lags maximal contrast by ~4ka.

From Zonneveld et al. (1997).

Within the literature, there are two primary theories relating to Chinese glaciation (Shi, 2002). The first theory is that during this period, glaciation was restricted to dispersed mountain glaciers, whilst the second hypothesis proposes that there was a unified ice sheet, which covered some or all of the mountainous regions. There tends to be more support in the literature for restricted glaciers rather than an ice sheet, primarily because conditions were too dry (as evidenced from loess records). Shi (2002) suggests that field observations of glacial features in the Himalayas and the Qilian Mountains favour the mountain glacier hypothesis during the Late Pleistocene and previous Pleistocene glaciations. It is contended that on the margins of the Tibetan Plateau, the Equilibrium Line Altitude (ELA) was ~1000 m lower than today during these episodes. It is therefore theoretically possible that high altitude sites in Yunnan Province were covered by a glacier at least once during the Quaternary (Shi et al., 1979).

It is estimated that at least four glaciations took place in southwestern China during the Late Pleistocene (Yang et al., (2006)). Glacial features including tarns, cirques and moraines on Mount Gongwang, Yunnan Province (101 - 102°E and 25°N, 4344 m asl) and Mount Diancang, Yunnan Province (99 - 100°E and 25°N, 4122 m asl) were classified and dated using AMS ¹⁴C radiocarbon dating and thermoluminescence. The glacial relics found on Mount Gongwang suggested the area was glaciated at ~100, 40, 25 - 18 ka BP and during the Lateglacial period. Kuang (1997) also investigated glacial remnants (cirques, trough valleys and lateral moraines) present in the Gongwang Mountains and contended that Quaternary glaciation occurred above 3100 m asl in the Gongwang Mountains, northeast Yunnan. However, owing to a lack of evidence, it is difficult to assess the extent to which these landforms and inferred glaciations provide evidence of a strong regional precipitation / temperature gradient or regional climatic variability. Further research is required to investigate this relationship.

Analysis of glacial deposits on Mount Diancang associated with the last glaciation suggested that Mount Diancang was the southernmost area to be glaciated in continental Asia (Yang et al., 2006). This area was extensively glaciated during the Lateglacial Period. Yang et al. (2006) found evidence for the oldest glaciation of the Diancang Mountain complex in the lowest cirque at an elevation of 3800 m asl, at Yuji Peak. Conversely, at Gongwang Mountains, Holocene moraines are present as low as 2950 m asl. The penultimate and earlier glaciations were generally found to be more extensive than the LGM (Zhang et al., 2006b; Kuang, 1997), when moisture availability was more restricted (Owen et al., 2006), caused by lower insolation levels and leading to restricted glacier accumulation and advance (Li et al., 2008).

Previous research therefore indicates that glaciation was not uniform across China. For example, Yang et al. (2006) discovered that glaciation during the early part of the last glacial cycle was more extensive on Mount Gongwang than on Mount Diancang, Yunnan Province (99 - 100°E and 25°S), but during the Late Pleistocene - Early Holocene Period, this trend was reversed.

This implies that the last glaciation was more extensive in some locales than others. This research indicates regional responses to climatic events such as glaciation are non-uniform. The differing patterns of glaciation are attributable to differences in the atmospheric circulation of the two regions, being controlled by different monsoon subsystems (the Indian and Southeast Asian monsoons). Being nearest to Mount Diancang, the results of Yang's research suggest that the Late Pleistocene - Early Holocene climate of southwestern China was primarily influenced by the Indian monsoon. This is supported by other studies (e.g. Zhang et al., 2006b; Shen et al., 2005a), but remains open to debate.

Based on the results of the abovementioned speleothem, ice records and geomorphological studies, it would therefore appear that both glacial dynamics and solar insolation were important influencing factors driving Asian palaeomonsoon variability during the Late Pleistocene - Early Holocene Period. However, based on available evidence, the precise extent and mechanisms of glacial dynamics (i.e. ice sheets, glaciers, meltwater etc), and effects on the regional climate remain open to question. The relative influence of glacial dynamics appears to vary geographically, but this issue has not yet been fully explored (Zhou et al., 2008). Further research is required to confirm this hypothesis and to more gain further insight into the relationship between ice, the sun and the Asian monsoon.

2.5.2 Environmental and climatic trends during the Late Pleistocene - Early Holocene Period

Several studies suggest that conditions in southwestern China during the Late Dali Glaciation (25 - 10 ka BP) were colder and drier than the present (Hodell et al., 1999; Thompson et al., 1989). For example, in his review of the evidence for Late Pleistocene glaciation in China, Shi et al. (1979) concludes that it was much colder in the Late Dali compared to the Early Dali Glaciation, and temperatures were on average at least 7 - 8°C lower than the present. Conversely, Winkler et al. (1997) collated and reviewed evidence from glacial deposits, palaeomagnetism, pollen records from lake sediments and a study of Neolithic sites in southwestern China. Reconstructed Late Pleistocene temperatures were only 4 - 5°C lower than the present day, as suggested by the position of cirques and other glacial features.

Palaeocoastline records indicate that the Chinese coastline was also several hundred kilometres further eastwards, indicating lower sea levels compared to the present (Shi et al., 1979). Coupled with increased ice cover in the mountains, these factors would have intensified the continentality of the climate and reduced the transfer of precipitation from the ocean to the land, resulting in drier conditions (Shi et al., 1979). Evidence for weakened monsoon is provided by Benn et al. (1998), who investigated the role of the Asian monsoon in Himalayan Glaciation and concluded that during the last glacial stage (30 - 11 ka BP), the Indian Monsoon was less intense

and / or had a shorter seasonal duration compared to the present. Other researchers have provided evidence of a weaker summer monsoon and a stronger winter monsoon from 25 - 12 ka BP, during the last glaciation (e.g. Huang et al., 2004; Hodell et al., 1999). Ice core records from the Tibetan Plateau indicate that the last glaciation was also much colder and dustier than the Holocene (e.g. Hodell et al., 1999; Thompson et al., 1989).

Records of organic and inorganic carbon and magnetic susceptibility (proxies of temperature and productivity) were obtained from two lake sediment records located near Kunming, Yunnan Province, China (Hodell et al., 1999). The Xingyun Hu record spans c. 25 ka cal. yr BP and was calibrated using INTCAL98; and the Qilu Hu record spans c. 50 ka cal. yr BP. For Qilu Hu, dates younger than c. 24 ka cal. yr BP were calibrated using INTCAL98, whilst older dates were converted using a linear regression of ^{14}C dates calibrated to U/Th dated corals. Overall, the results suggest that the 50,000 yr record was punctuated with warm, moist interglacial or interstadial periods (most notably at c. 22 and 12 ka cal. yr BP), indicated by the presence of carbonate and cold dry glacial or stadial conditions, inferred from levels of coarse grain quartz ($>38\text{ }\mu\text{m}$). $\delta^{18}\text{O}$ values from calcite suggested that from c. 50 - 12 ka cal. yr BP, the Chinese summer monsoon was weaker than today, resulting in cooler conditions. From c. 12 - 8 ka cal. yr BP, summer monsoon strength increased in response to insolation forcing, resulting in warmer conditions.

A palynological reconstruction of the vegetation at Menghai, Yunnan Province from c. 36 - 20 ka BP indicated that during the transition into the LGM, the Yunnan Province climate was influenced by increased winter humidity and rainfall, but mean annual temperatures were slightly lower than at present (Liu et al., 1986). Dates were calibrated to a Chinese sugar standard. The main drawback of this research (also acknowledged by the authors) is the significant dating uncertainties. Many of the dates obtained are muddled and / or anachronistic. Consequently, the results of pollen analysis are discussed in generalised terms rather than in relation to specific periods within the overall chronological framework, which reduces the overall applicability of the results of this study to subsequent studies.

Pollen records obtained from Xi Hu and Er Yuan, Yunnan Province provided an insight into past vegetation changes from c. 17 ka BP to the present (Lin et al., 1986). Dates were calibrated to dendrochronological timescales. From c. 17 - 15 ka BP, montane conifers dominated the upper areas of the catchment, whereas *Pinus* and evergreen sclerophyllous *Quercus* dominated lower zones. From c. 15 - 14 ka BP the montane conifers were temporarily restricted. Between c. 14 - 10.5 ka BP montane conifers again dominated the upper slopes whereas evergreen and deciduous forests, *Pinus* forests and semi - arid scrub below. From c. 10.5 ka BP to the present day, the pollen record indicated the prevalence of *Pinus* forests and evergreen broadleaved trees on all slopes.

The authors interpret the pollen and sediment stratigraphy as being suggestive of a cold semi-humid phase from c. 17 - 15 ka BP, followed by a fluctuating climate with increased seasonality, becoming warmer until c. 10.5 - 0 ka BP, when the climate adjusted to the subtropical monsoon climate conditions which are in existence today. The main limitation of this record is the lack of detailed results for the period c. 10.5 ka BP to the present.

A pollen record was obtained from a site near to Kunming which spans the last c. 16 ka and was calibrated using dendrochronological records (Sun et al., 1986). Key features of this record include higher levels of aquatic taxa before c. 9.5 ka BP, thought to correspond with higher levels of precipitation compared to the Holocene. Pre-Holocene vegetation was dominated by *Pinus* forests and mixed deciduous / evergreen forests. A reduction in montane pollen taxa at c. 9.5 - 8 ka BP heralded the onset of warmer winters.

Holocene vegetation was reconstructed by Shen et al. (2005a), using pollen extracted from Lake Erhai, Yunnan Province. *Betula* and deciduous *Quercus* pollen were dominant in the record from c. 11,750 cal. yr BP, which was thought to indicate more cold and wet winter conditions. After c. 11,750 cal. yr BP, *Tsuga* and evergreen broadleaved tree pollen (including *Cyclobalanopsis*, *Lithocarpus* and *Castanopsis*) increased, which implies warmer conditions and increased summer precipitation. After c. 10,320 cal. yr BP evergreen *Quercus* increased, which was thought to reflect increased seasonal rainfall patterns, indicating a southward shift in the winter front across the region. Inferred warming and increased precipitation continued into the Mid Holocene.

Collectively these records point to a broadly synchronous response to warming after c. 12 ka BP. However, the lack of high-resolution studies currently available for southwestern China, coupled with the inherent dating uncertainties associated with some of the key proxy records precludes further detailed analysis. Further detailed investigations are needed in order to clarify regional environmental response and inferred monsoon variability on different timescales.

2.5.3 The timing of the Last Glacial Maximum (LGM) in China

There is currently little consensus in the literature on the extent and duration of the last glaciation (Herzschuh et al., 2005) and in particular, the timing of the LGM in China remains a contested issue. Estimates vary widely. For example, Otto-Bleisner et al. (2005) base their LGM climate model upon a median date of 21 ka BP. Shi et al. (1979) dated glacial relicts from China, concluding that the LGM occurred at c. 14.9 ka BP. In contrast, Owen et al. (2005) compared records of glaciation across the Himalayas and conclude that maximum glaciation occurred at different times at different locations, some between 20 - 18 ka BP, some much earlier.

Similar conclusions are drawn in the higher latitudes (Sejrup et al., 2009). Zhou et al. (2008) suggests that there are marked similarities between the Late Quaternary $\delta^{18}\text{O}$ and $\delta^{13}\text{C}$ curves obtained from Songjia Cave ($\delta^{13}\text{C}$), Hulu Cave ($\delta^{18}\text{O}$) and GISP2 ($\delta^{18}\text{O}$) records as illustrated by Figure 2-12. The authors place the LGM between 20 - 18 ka, which is in broad agreement with the Hulu Cave and GISP2 records. Other Chinese studies assume a median date of 18 ka BP for the LGM in China (e.g. Yu et al., 2000b; Yu et al., 2000a). This introduces the possibility of a local LGM, rather than a globally synchronous LGM. Alternatively the differences in timing could be the result of dating uncertainties / inconsistencies. Further research is required in order to clarify this issue.

With regard to the timing of the LGM in Yunnan Province, Yang et al. (2006) dated moraines and till from Mounts Diancang and Gongwang using AMS ^{14}C radiocarbon dating of bulk sediments and Thermoluminescence (TL) dating. The results suggest that the LGM occurred between 25 - 15 ka BP, triggering a drop in the snowline by 900 m. Zhang et al., (2005) used TL to date glacial deposits in the Gongwang Mountains. The authors conclude that the LGM occurred some time between 25 - 18 ka BP, which is less precise than other estimates. The lack of precisely dated records available for this region means that the timing of the LGM in southwestern China remains largely unconstrained.

2.5.4 *Post-LGM climatic conditions*

The LGM climate (temperature and precipitation) and vegetation cover have been reconstructed in previous studies, although contrasting conclusions have been reached. For example, a comparative study carried out by Herzschuh (2006b) and detailed in Section 2.5.1 indicates that the LGM was characterised by dry conditions. In addition, a period of slightly wetter conditions was observed following the LGM, at c. 18.5 - 17 cal. yr BP. Herzschuh (2006b) contends that this represented the onset of summer monsoon circulation after the LGM. However, it is difficult to determine whether this was a result of increased monsoon precipitation entering the Asian interior, or whether it was the result of local glacial melting. However, reduced coverage of sites in eastern and southeastern China is marked, and hence within this study, inferences relating to moisture conditions (and inferred changes in Asian monsoon variability) are spatially constrained.

Other studies have also indicated dry conditions during the LGM. For example, Fang (1991) investigated lake evolution during the last 30,000 years in China. A total of 185 radiocarbon / ^{230}Th dated proxy records covering the whole of China were analysed in conjunction with historical information. Some broad conclusions can be drawn from this study. Firstly, the results indicate that the LGM was arid, indicated by enhanced lake desiccation at c. 18 ka BP.

Secondly, the evidence suggests that the majority of lakes in southwestern China reached their highest lake levels after the LGM, at c. 15 - 12 ka BP, although this was later than the estimate provided by Herzschuh (2006b). Fang (1991) considers that higher lake levels were possibly triggered by an increase in meltwater supply following the LGM. Hence, lake water levels were closely associated with glacial fluctuations. However, because the study encompasses the findings of many studies on a coarse scale, it was not possible to undertake a detailed assessment of the processes involved.

In contrast, other studies conclude that the LGM climate of southwestern China was relatively moist compared to eastern China. For example, Yu et al. (2006b) explored lake levels derived from Chinese proxy records including palaeolake shorelines, sedimentation rates, aquatic pollen assemblages, ostracods and diatoms. The review highlights three periods (pre - 28 ka, 21 - 17 ka and 7 - 6 ka), which were characterised by high lake levels in western China (west of 95°E); said to be the result of a wetter climate.

Chinese palaeovegetation patterns during the LGM (c. 18,000 ¹⁴C ka BP) and the Mid Holocene (c. 6000 ¹⁴C yr BP) were reconstructed by Yu et al. (2000a), based on a set of 658 pollen surface samples collected from mainland China, Taiwan, Hainan and Hong Kong. During the LGM, desert steppe and cool mixed forest extended to the eastern coast of China, which contrasts with the present day temperate deciduous forest. Tundra dominated on the Tibetan Plateau. It was argued that this indicated wetter conditions during the LGM, which contrasts with the findings of Herzschuh (2006b) and Fang (1991).

Collectively these studies indicate that the LGM climate of China was cold and dry, although there remains a question mark over conditions in western China, which some proxies indicating that LGM conditions were wet. Conditions following the LGM became increasingly wetter, although again there are doubts over exactly when conditions began to change. Further work is required, particularly in southwestern China, in order to clarify these issues. Constraining the timing of the LGM is essential if we are to gain insight into how the observed events in these records relate to one another.

2.5.5 *Lateglacial climate events*

Under glacial climate boundary conditions (i.e. cold North Atlantic sea surface temperatures, European ice sheets and extensive Asian snow cover), the intensity of the summer monsoon responds non-linearly to insolation forcing (Hodell et al., 1999), resulting in abrupt changes in palaeomonsoon intensity. Abrupt events occur on faster timescales than those typically associated with internal / external forcing factors (IPCC, 2007a).

To date, research focusing on abrupt events during the Lateglacial centres on the synchronicity of abrupt climatic events across China, and possible teleconnections with the North Atlantic region. In particular, correlations are proposed between events in the Chinese proxy records and Heinrich 1 (H1), the Bolling-Allerod (BA) and the Younger Dryas (YD) events recorded in the Greenland ice cores, although dating uncertainties have hampered this process.

Five $\delta^{18}\text{O}$ records were obtained from ^{230}Th dated speleothems growing in Hulu Cave, located near Nanjing, eastern China (Wang et al., 2001). The records are calibrated to 1950 AD and provide a detailed insight into Lateglacial East Asian monsoon variability (Figure 2-10) and in particular, abrupt climate events. Key features of the section of the record spanning 20 - 10 ka BP include a 2‰ increase in $\delta^{18}\text{O}$ values at $16,073 \pm 60$ yrs BP, which takes place over <20 years. Highest values occur at $16,032 \pm 60$ yrs BP, signifying very low temperatures. This event possibly correlates with H1 in the Greenland ice core records (GRIP and GISP2). Although the causes of these events are still being debated, one hypothesis is that Heinrich events were prompted by ice-rafting in the North Atlantic, triggered by warmer conditions destabilising the Laurentide ice sheet (Adams et al., 1999; Bond et al., 1995). However, Wang et al (2001) do not discuss the precise timing and duration of this event in the Greenland record in any detail. It is therefore difficult to assess whether these events can be truly correlated.

A warm event centred at c. $14,645 \pm 60$ yrs BP is possibly correlated with the BA warm phase in GISP2 (c. $14,500 \pm 150$ yrs BP; Sirocko et al., 1996). However, the authors observe that the rapid part of the transition into the BA is more gradual in the Hulu record (180 years compared to 100 years), raising doubts over whether these are the same or different events.

An abrupt cold event - suggested to be the YD event - occurs between $12,823 \pm 60$ yrs BP and $11,473 \pm 100$ yrs BP in the Hulu record. The drivers of the YD remain open to debate, although it has been suggested that it was caused by an ice-rafting event, because its characteristics are similar to the Heinrich events (Adams et al., 1999; Bond et al., 1995). The transition into this event is <20 years, and the termination of this event is <10 years. The overall duration of this event is 1350 ± 120 years. In the GISP2 record, an event occurs between $12,880 \pm 260$ yrs BP and $11,640 \pm 250$ yrs BP, and is similar (but not identical) to the event identified in the Hulu record in terms of its transitional phases, overall event duration and timing.

Lacustrine sediments from Gucheng Lake, Jiangsu were used to investigate climate change over the last 15 ka BP (Wang et al., 1996). The main conclusion of this research is that orbital forcing primarily controlled monsoon circulation during this period. In addition, an abrupt decrease in temperature occurs from 11.3 to 11.0 ka cal. yr BP, which is possibly correlated with the YD abrupt cold event.

However, analysis of lake sediment and shoreline samples obtained from Sumxi Co, Western Tibet, spanning the past 13 ka suggests that cool, dry conditions between 11 - 10 ka BP cannot be explained by orbital variations (Gasse et al., 1991). Instead, the cooling is linked to a YD-type event. The appearance of this event in a Tibetan proxy record adds credence to the theory that the YD event was global in nature. However, the differences in timing between this record and Hulu Cave are marked.

Palaeoenvironmental changes in China during the past 130 ka recorded in dust accumulation, vegetation evolution, mountain glacier activity and sea level change are summarised in An et al. (1991). Most notably, a cool, humid event occurs at 12 ka BP, followed by an abrupt change to cold and dry conditions at c. 11 ka BP. This broadly corresponds with the YD in other studies (e.g. Dykoski et al., 2005; Shen et al., 2005b).

Correlating proxy records that have been dated using different methods poses a problem because they may have different age errors and consequently there may be an age offset when comparing records. For example, Wang et al. (2001) estimate that the offset between GISP2 and Hulu is <500 years and increases with age, with a more marked but gradual offset occurring after 15 ka BP (Figure 2-9). Consequently, the GISP2 ice core is likely to be younger than the Hulu speleothems. Conversely, the offset between the GRIP ice cores and Hulu is more pronounced and increases sharply after 15 ka BP from ~500 to ~2500 years at 30 ka BP. This implies that when correlating Asian and Greenland records, it may be better to use the GISP2 record, which has a reduced age offset (although this offset may vary when compared with other Chinese records). The dating uncertainties consequently mean that apparent correlations between events in different records - such as the Younger Dryas abrupt event - is far from certain. Further dating and evidence is required to precisely constrain these issues.

Overall, the main findings obtained from Hulu Cave are as follows. Firstly, long term trends in the Hulu speleothem record tends to follow summer insolation (illustrated by Figure 2-10), suggesting that high summer insolation increases the continent - ocean temperature difference, resulting in an enhanced summer monsoon. Secondly, the record is punctuated with a number of millennial and sub-millennial scale events, which do not follow orbital scale trends, suggesting other factors are involved. Thirdly, there are marked similarities and differences between the Hulu and Greenland ice core records (GISP2), which require further investigation.

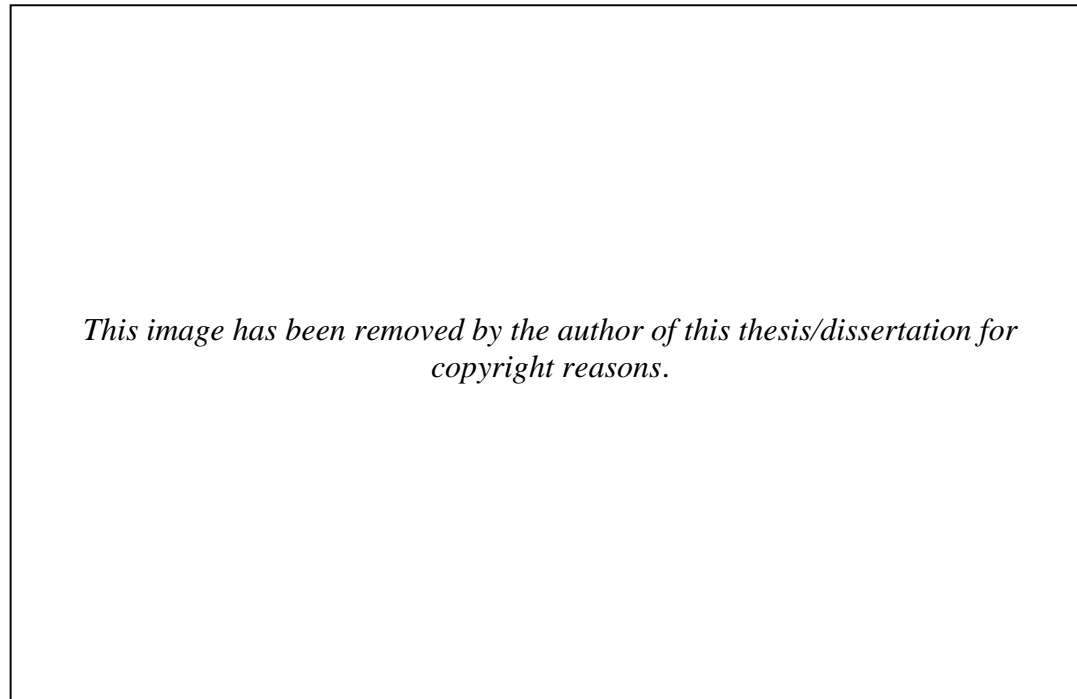


Figure 2-9: Graph showing the estimated age offsets between the Hulu Cave speleothems and the Greenland Ice Core Records (GISP2 and GRIP).

Each point is based on a correlation between GRIP or GISP2 and Hulu. Positive values are times when the ice core age is less than the Hulu age; negative values are times when the ice core age is more than the Hulu age. Typical ^{230}Th dating errors as a function of time are illustrated by the grey error envelope where the difference in age is zero. Error bars are estimates of the error in the ice core chronologies. From Wang et al. (2001).

This image has been removed by the author of this thesis/dissertation for copyright reasons.

Figure 2-10: Graph showing the Lateglacial section of the Hulu Cave $\delta^{18}\text{O}$ speleothem records compared with the GISP2 $\delta^{18}\text{O}$ ice core record.

The $\delta^{18}\text{O}$ values obtained from the Hulu speleothems (H82, YT and PD) are shown as purple, black, and blue lines. The Greenland ice core (GISP2) is shown as a dark blue line (20 year averages) and a grey line (3-year averages). Yellow bands indicate the timing and duration of the YD and the transition into the BA (t-BA). The BA is the interval between the yellow bands. ^{230}Th ages and errors are color-coded by speleothem. The chronology of YT and most of the chronology of H82 are fixed by annual banding. YT and H82 are more precisely and continuously dated than PD, therefore the timescale of PD was adjusted between 17 and 14 ka to match the major $\delta^{18}\text{O}$ features. From Wang et al. (2001).

Dongge Cave is located 680 m asl to the southeast of Libo, Guizhou Province, China and is approximately 1200 km from Hulu Cave. The $\delta^{18}\text{O}$ record obtained from speleothem from Dongge Cave is long, and extends back as far as the last interglacial. Consequently, a number of different studies are available for Dongge Cave, focused on different periods. The D4 speleothem record produced by Dykoski et al. (2005) is presented here (Figure 2-11), because it is a Lateglacial record, and is therefore directly relevant to this study (see Section 2.4). Figure 2-11 illustrates that there is good agreement between the Dongge and Hulu Cave records, suggesting that the observed climatic variations reflect regional trends.

Key features of the Dongge Cave record include a 3‰ shift to lighter isotopic values (–8‰) commencing at c. 14.7 ka. The authors link this to the start of the Bolling Allerod in the Greenland ice core records. At c. 13 ka, values began to become heavier again, peaking at –6‰ at c. 12.5 ka. This event lasted ~1500 years. The authors correlate this event with the Younger Dryas event in the Greenland records (NGRIP / GISP2). This event also broadly correlates with the Younger Dryas-type event in the Hulu Cave record.

At c. 11.5 ka, values became lighter (–8.4‰), signalling the end of the Younger Dryas-type event and the onset of Holocene conditions. A warming event occurs in the Greenland ice core records at $11,600 \pm 150$ yrs BP (Sirocko et al., 1996). Values then became progressively lighter, peaking between 9 and 8 ka. These shifts broadly accord with the Dunde Ice Cap record. However, the onset of the Holocene as recorded at Dongge Cave is later than the estimate obtained from the Dunde Ice Cap (c. 11,950 yrs BP) and the overall duration of the Holocene onset recorded in the Dongge Cave record is longer than the Dunde Ice Cap record. However, the timing of the onset of Holocene conditions and the duration of the transition phase from Late Pleistocene to Holocene conditions are not discussed in detail.

Thereafter, $\delta^{18}\text{O}$ values are lighter, but there are also periods of heavier values. The first of four events is centred at $11,225 \pm 97$ yrs BP (1.05‰) and broadly coincides with the Preboreal Oscillation in the North Atlantic, centred at $11,360 \pm 227$ yrs BP in GISP2 and $11,340 \pm 30$ yrs BP in NGRIP. However, this event is not discussed in relation to other Chinese proxy records. The second event is centred at $10,880 \pm 117$ yrs BP (1.15‰) in D4, at $10,850 \pm 217$ yrs BP in GISP2 and $10,850 \pm 30$ yrs BP in NGRIP. Other than suggesting a possible correlation between the Greenland and Dongge records, there is no further discussion on the nature or characteristics of the second event. The third and fourth events occur during the Holocene and therefore fall outside the remit of this study. Differences in the timing of these events could be attributable to age offsets (Wang et al., 2001). Because of dating uncertainties, the authors conclude that they cannot not definitively link the events in the Dongge Cave record and those observed in the Greenland ice core records.

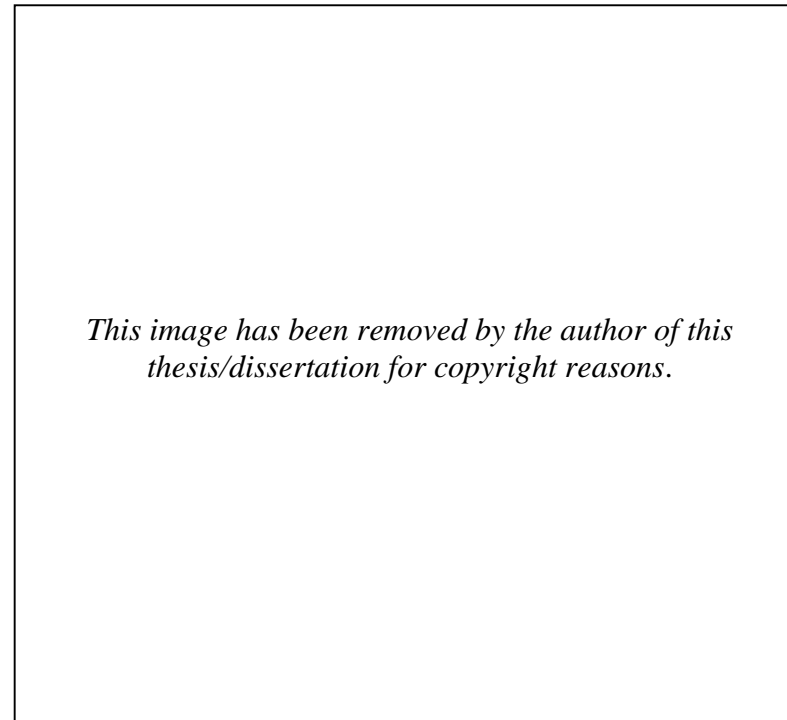


Figure 2-11: Graph showing the Lateglacial changes in the Dongge Cave $\delta^{18}\text{O}$ speleothem record.

The deglacial sequence of Dongge stalagmite D4 (black line) and Hulu stalagmite H82 (grey line) from 10 ka to 16 ka. From Dykoski et al. (2005).

It is important to note that assumptions relating to the interpretation of the $\delta^{18}\text{O}$ speleothem records are currently undergoing re-evaluation. For example, Maher (2008) suggests that the Chinese $\delta^{18}\text{O}$ speleothem records do not record changes in monsoon intensity (rainfall amount), but rather changes in the source of precipitation and air mass trajectory (and changes in the extent of the influence of each of the monsoon subsystems) across China. Hence, further research is required in order to determine more precisely what the $\delta^{18}\text{O}$ record represents and how it correlates (if at all) with other types of proxy records.

Finally, Dykoski et al. (2005) contend that Dongge Cave is located in an area governed by the Indian Monsoon and the $\delta^{18}\text{O}$ record therefore reflects changes in Indian Monsoon intensity (interpreted as temperature and $\delta^{18}\text{O}$ of meteoric precipitation). This contrasts with Hulu Cave, which is likely to reflect changes in East Asian monsoon intensity. It is therefore possible that the records reflect differing climatic conditions and / or events.

$\delta^{13}\text{C}$ and $\delta^{18}\text{O}$ records were obtained from a speleothem (SJ3) from Songjia Cave, which is located ~680 m asl, 1000 km west of Hulu Cave and 700 km north of Dongge Cave (Zhou et al., 2008). The record covers the last 10 - 20 ka and is ^{230}Th dated. The most prominent feature of this record is the coldest phase from c. 17.6 to 14.5 ka, represented by a shift to higher $\delta^{18}\text{O}$ values (Figure 2-12). Values are +2‰ heavier during this period. The authors compared this record with the Hulu, Dongge Cave and GISP2 record and concluded that the timing and duration was similar to the H1 event recorded in the Greenland ice cores (GISP2), and a cold, dry event recorded in the Hulu Cave record. The primary difference between parallel events recorded at Hulu and Songjia is the duration, which is estimated as ~3100 years at Songjia and ~1000 years at Hulu. The timing of the onset of these events is also different ($16,073 \pm 60$ yrs BP at Hulu compared to c. 17.6 ka at Songjia). This may be attributed to dating uncertainties associated with the Songjia Cave record. However this issue is not discussed in detail by Zhou et al. (2008).

Warm and humid conditions prevailed from c. 14.5 - 11.5 ka, indicated by a return to lower $\delta^{18}\text{O}$ values. This event is thought to be synonymous with a warm phase centred at 14,645 yrs BP in the Hulu $\delta^{18}\text{O}$ record, which correlates with the Bolling Allerod in the Greenland ice cores. The onset of a similar event recorded in the Dunde ice cap occurs earlier, at c. 14.7 ka. Despite the similarities between the Hulu and Songjia events, the transition from H1 to BA appears to be faster in the Songjia record (~100 years from c. 14.6 - 14.5 ka) than the Hulu record (~400 years from c. 14.9 - 14.5 ka).

A sharp H1 - BA transition also features in the GISP2 record. This was proposed as evidence that the H1 recession commenced earlier in eastern China than central China. The duration of this event is recorded as being shorter at Hulu (~2000 years) than at Songjia (~3000 years). However, the difference in event duration may result from dating uncertainties.

There is evidence of a Younger Dryas type event starting at c. 11.5 ka. Zhou et al. (2008) compared the timing and duration of this event with a similar event in the Hulu Cave record. The event recorded in the Songjia speleothem (SJ3) occurs later (c. 11.5 ka compared to c. 12.8 ka) and has a shorter duration (<1000 years compared to 1350 ± 120 years) than the event in the Hulu record. Similar conclusions are reached when comparing the Songjia and Dongge Cave records (in the latter, onset is at c. 13 ka and event duration is ~1500 years). However, the timing of the ending of the events is similar (c. 11.4 ka). The ending of this cold event is also similar at Dongge Cave. The difference between the Songjia and Dongge records is attributable to a lack of dates for SJ3. The observed similarities between the Dongge and Hulu cave events may reinforce this hypothesis. The authors concur with Dykoski et al. (2005) and Wang et al. (2001), concluding that Lateglacial climate change was broadly synchronous across China and proposing that teleconnections exist between the North Atlantic and Asian climate, as evidenced by near-concurrent shifts in $\delta^{18}\text{O}$ values captured in ice core and cave records.

In summary, high-resolution speleothem records of Lateglacial Asian palaeomonsoon dynamics (e.g. Zhou et al., 2008; Dykoski et al., 2005; Wang et al., 2001) reveal periods of pronounced variability, with abrupt amplitude shifts between warm / wet and cold / dry phases that occur on millennial, centennial and decadal timescales (Wang et al., 2005). Tentative correlations are made between the events in these cave records and those observed in the Greenland ice cores (e.g. D-O cycles, Heinrich events and the Younger Dryas). However, further research is required in order to pinpoint more precisely the timing and causes of these events and to determine whether the events are truly correlated or not (Wang et al., 2005).

*This image has been removed by the author of this thesis/dissertation
for copyright reasons.*

Figure 2-12: Graph comparing the $\delta^{18}\text{O}$ and $\delta^{13}\text{C}$ values obtained from key high and mid latitude ice core and speleothem records, 20 - 10 ka BP.

Hulu Cave speleothem = b; GISP2 ice core = c; Songjia Cave speleothem = a and d.

From Zhou et al. (2008).

2.5.6 The Pleistocene - Holocene (P-H) Transition

Ice cores obtained from the Dunde Ice Cap (located 5325 m asl, to the north of the Tibetan Plateau between the Qaidam Basin and the Gobi Desert) provide one of the first high-resolution records of climate change in this region spanning 40 - 0 ka (Thompson et al., 1989). The results for core D-3 are shown in Figure 2-13. The authors provide a broader account of the observed changes in the core, compared to more detailed descriptions provided by other authors (e.g. Wang et al., 2001). Negative $\delta^{18}\text{O}$ values, smaller ice crystals, increased dust and decreased soluble aerosol concentrations revealed that prior to the Holocene, conditions were colder, wetter and dustier. The P-H Transition was pinpointed as occurring c. 11,950 yrs BP (ice core years), based on an increase in ice crystal size (Figure 2-13). The transition was completed within ~40 years. A marked transition to more warmer, drier conditions occurred at c. 10 ka BP, delineated by marked increases in Cl^- and SO_4^{2-} , reflecting the expansion of salt and loess deposits and drying of freshwater lakes in response to increasingly warm conditions. The authors conclude that the Asian summer monsoon underwent gradual strengthening, which broadly coincided with the start of the Holocene. In other pollen records (e.g. Shen et al., 2005a; Walker, 1986), a marked rise in arboreal pollen is used to denote the transition from Pleistocene to Holocene climatic conditions.

2.5.7 The Pleistocene - Holocene (P-H) Boundary

Herzschuh (2006b) places the P-H Boundary for central Asia at c. 11.5 ka BP, denoted by enhanced effective moisture indicating significantly wetter conditions. Recently, the base of the Holocene has been formally defined using the Greenland NGRIP ice core and auxiliary records as 11,700 cal. yr b2k (before AD 2000) (Walker et al., 2009). However, Walker et al. (2009) acknowledge that there are ongoing issues associated with defining the P-H Boundary in lake sediment records, including dating uncertainties and debates over what constitutes the defining features of the boundary in palynological records. These issues need to be resolved before the boundary can be formally defined for lacustrine sequences.

Previous studies suggest that peak insolation was reached at c. 10 ka (Galy et al., 2008), prompting the onset of full Holocene climatic conditions, which included a strong Asian summer monsoon. Walker (1986) compared and synthesised Lateglacial pollen records obtained from lakes at Menghai, Er Yuan and Kunming, Yunnan Province, China. Climatic conditions comparable to the present were reached at c. $10,500 \pm 500$ yrs BP. Ren (2007) and Chen et al. (2006) suggest that the onset of full Holocene conditions was characterised by an increase in mountain forest cover.

This image has been removed by the author of this thesis/dissertation for copyright reasons.

Figure 2-13: Suite of graphs showing 1000-year averages of dust concentrations and $\delta^{18}\text{O}$ values obtained from Core D-3, Dundee Ice Cap, 40 - 0 ka BP.

From Thompson et al. (1989).

2.6 Concluding remarks

Lateglacial proxy records obtained for China collectively point to non-linear changes in monsoon intensity in response to changes in solar insolation. Glacial climate boundary conditions and associated glacial dynamics may have influenced palaeomonsoon variability during the Lateglacial. However, further research is required to clarify the role of glacial dynamics and to examine the possible drivers of palaeomonsoon variability in more detail.

The observed non-linearity in the palaeorecord appears to have resulted in a series of abrupt climatic events (e.g. H1, the BA and the YD). These events were seemingly broadly synchronous across China. However, there are also outstanding questions regarding the timing and nature of key climatic shifts across China.

Parallels are drawn between observed events in the Chinese proxy records and those contained within the ice core records obtained from Greenland. Similarities in the timing and duration of these events imply a teleconnection between the Asian monsoon and North Atlantic climates. However, there are also differences between the events recorded. Furthermore, the dating uncertainties associated with these records mean that the nature and timing of these events remains unconstrained. Consequently, any potential correlations are far from certain. Further research is required to precisely constrain these events.

Finally, Wang et al. (2005) contend that the acquisition of high-resolution records that are sufficiently geographically distributed across Asia remains an outstanding issue which needs to be addressed in order to resolve the issues identified above. In particular, few high-resolution records exist for high altitude sites in southwestern China, and thus our understanding of the regional climate as a whole is limited. This area is highly sensitive to climate change (Yu et al., 2006) and may play an important role in wider climate dynamics, which is as yet undetermined.

2.7 Research questions

This review highlights the significant advances that have been made towards understanding Asian palaeoclimatic variability on millennial to centennial timescales. However, several key questions remain unanswered;

1. What are the fundamental drivers and processes underlying millennial to centennial scale environmental and climatic changes in Monsoon Asia during the Late Pleistocene - Early Holocene Period?
2. Few high-resolution proxy records have been produced for southwestern China during this period. What are the precise climate dynamics in this region?
3. What is the timing / duration of regional climate events and do they vary from record to record?

This research engages with these questions, by examining lake sediments from a site in southwestern China in order to investigate the hypothesis that millennial to centennial scale environmental and climatic changes in southwestern China during the Late Pleistocene - Early Holocene Period were driven by shifts in Asian palaeomonsoon dynamics, which were driven by wider changes in the global climate system.

Further work in all of these areas is vital to improving our understanding of factors at the heart of Asian palaeoclimatic variability. Furthermore, this may lead to improved modelling projections and more targeted adaptation / mitigation strategies to deal with the likely social, economic and environmental impacts of potential changes in Asian monsoon intensity - including floods, droughts and increased social vulnerability in Monsoon Asia.

3 Methods

3.1 Introduction

The success of any research project largely hinges on the methods and analytical techniques employed. It is therefore important to ensure that these are appropriate to the aims and objectives of the research, effective and scientifically robust. This chapter addresses Objective c identified in Chapter 1.

A pilot study was undertaken on a short core (05SD) extracted from Lake Shudu in order to assess the suitability of the site for palaeolimnological research and to test the applicability of the multi-proxy methods used in this study and described in this chapter. Based on the results of the pilot study, a long core (06SD) was obtained from the same lake. This long core forms the focus of the present study.

3.2 Multi-proxy analysis

Multi-proxy studies enable comparison of chemical, biological and lithological evidence obtained from sediments, collectively providing independent, yet converging and mutually supportive data (Lowe et al., 1997). This helps to distinguish climatic and other influences upon each proxy, provides a means of accounting for problems associated with multiple mechanisms influencing individual proxies (Wang et al., 2005) and enables the development of an integrated assessment of environmental change.

However, factors other than climatic variables can affect the proxy record and therefore distort the emerging climate patterns. For example, pollen records are used to reconstruct vegetational changes, which are then taken to reflect (albeit indirectly), changes in climate over defined geographic and temporal scales. However, anthropogenic activities such as land clearance to make way for agricultural practices can distort the record of climate change captured in pollen records. Any observed patterns may therefore reflect factors other than climate variations. These signals need to be distinguished. This is achieved by drawing upon a range of proxies, which individually reflect these influences, and can be analysed collectively to develop an overview of catchment processes and the various influences at play.

Furthermore, the integrity of each record depends on the extent to which it is responding to changes in the monsoon, or if other influencing factors are involved, the extent to which these signals can be distinguished (Wang et al., 2005). In addition, the theory of equifinality proposes that similar results may be produced by different processes or causes not represented in the modern paradigm (Lowe et al., 1997). Conversely, different results could

be obtained from similar processes or causes. It is arguable that these uncertainties may result in misinterpretation of the past. Multi proxy analysis allows the causes of the results to be more fully explored and understood, which reduces the effects of equifinality.

If conclusions are based on well-tested methods that have been shown to provide consistent results that can be correlated with other datasets, then this further reduces the level of uncertainty associated with the data. These are the primary strengths of multi-proxy analyses when compared to a single proxy approach.

Within palaeomonsoon research, monsoon proxies can be divided into two main groups, based on the primary aspect of the monsoon that they address (Wang et al., 2005);

1. monsoon winds (strength, direction and persistence);
2. monsoon precipitation.

In this study, the proxies used are all broadly measures of monsoon precipitation, according to the categories defined by Wang et al. (2005);

- analysis of the physical properties of sediments, including particle size and magnetic susceptibility.
- organic analysis, including Loss on Ignition (%LOI), Total Organic Carbon (%TOC) and Total Nitrogen (%TN) percentages, C/N ratios and $\delta^{13}\text{C}$ values.
- palaeoecological analysis of fossil pollen grains and charcoal fragments.

Particle size and magnetic susceptibility are used to indicate changes weathering and / or pedogenesis, whereas the organic proxies and pollen are used to indicate changes in effective moisture (An, 2000). The core chronology is based on AMS ^{14}C radiocarbon dating of bulk sediments and coniferous pollen concentrations.

Pollen and organic analysis were selected because they complement each other and enable coupled analysis of the sources of organic carbon sources (i.e. terrestrial or aquatic material) and changes in catchment and / or lake vegetation (Lamb et al., 2004). Initially it was envisaged that it would be possible to produce a $\delta^{18}\text{O}$ record based on ostracods from which precipitation and / or temperature could be inferred, but an inspection of the core composition revealed that these were not present in sufficient quantities.

Analysis of the physical properties of sediments was vital for establishing basic information about the types and rates of sedimentary processes operating in the catchment and / or lake, and may be useful in helping to distinguish the various factors (such climatic shifts, human activity, natural hazards) influencing the pollen and isotope records.

3.3 Physical properties

The physical attributes of sediment grains such as particle size and magnetic susceptibility are often useful within multi-proxy studies, because they reflect changes in climate, limnology and / or human activity (Last et al., 2001).

There are two main types of Quaternary sediment. Inorganic (clastic) deposits consist of mineral detritus resulting from the disintegration of pre-existing rock, differentiated by grain size (Hakanson et al., 1983). Biogenic sediments, consist of the remains of plants or animals or mineral matter produced by living organisms (Lowe et al., 1997; Strahler et al., 1992). Regional geology, climate, vegetation, water chemistry and biological processes, such as diagenesis, control the overall composition of biogenic deposits (Wetzel, 2001).

3.3.1 Particle size

Changes in the size and size distribution (sorting) of clastic lake deposits vary with catchment erosion, transport and deposition processes, which are controlled by a variety of factors including precipitation rates and vegetation cover (Leeder, 1992; Knighton, 1984), and which vary in response to wider climatic and / or environmental changes. Analysing the particles sizes present within the lake sediment record can therefore provide an insight into catchment processes in operation, and inferred drivers.

Particle size analysis involves measuring the size (diameter) of clastic particles contained in a sample. Freeze dried samples were chemically treated in order to remove organic material, using standard techniques outlined in Last et al. (2001). The remaining sediments were analysed using a Saturn Digitiser, which measures particles ranging from 0.1 to 1000 μm in size. Sediments were categorised according to the classified according to the Udden - Wentworth scale. Smaller particles are classed as sand ($>63 \mu\text{m}$), silt (2 - 63 μm) or clay ($<2 \mu\text{m}$) (Last et al., 2001; Leeder, 1992).

3.3.2 Magnetic susceptibility (χ_f)

Magnetic minerals originate from a range of sources (Evans et al., 2003). They are formed naturally within igneous formations (particularly basalt), which break down because of erosional processes, releasing minerals into the wider environment, which may eventually become deposited as lake sediments. These sediments may also be redeposited at a later stage because of geological processes. In particularly arid environments, magnetic minerals may become entrained and deposited elsewhere. Events such as volcanic eruptions deposit material including magnetic minerals into the atmosphere, which may be transported long distances.

Chemical and biological processes also produce minerogenic particles. For example, magnetotactic bacteria create magnetic particles for navigation, which are resistant to decay (Last et al., 2001). Pedogenesis and human activities such as the burning of fossil fuels and industrial activities such as steel production can also contribute minerogenic particles to the wider environment, although this is not normally a factor in pre-industrial studies such as this one.

Minerogenic sediments are transported to the lake via rivers and streams as suspended or bedload, or via overland flow. They can also be transferred in the atmosphere as aerosols emitted from volcanoes, for example. The majority of magnetic minerals contained within lake sediments are produced from processes such as catchment erosion, and originate from bedrock, subsoil and topsoil in the lake drainage basin (Last et al., 2001). Variations in the magnetic properties of minerogenic sediments over time can therefore provide insights into the changing sediment sources and erosion rates with a catchment system (Dearing, 2008; Shen et al., 2005a). For example, previous studies highlight a link between high magnetic susceptibility and periods of deforestation and subsequent erosion of mineral soils in Holocene lake sediments obtained from Lough Neagh, Northern Ireland (Thompson et al. (1975), [quoted in Last et al., 2001]).

Low frequency susceptibility measurements provide an insight into the total concentration of ferromagnetic minerals within a sample (Walden et al., 1999). Readings are expressed as $\chi_{lf} \times 10^{-6} \text{ m}^3 \text{ kg}^{-1}$. Lower χ_{lf} values broadly reflect periods of reduced influx of magnetic minerals into the lake and low erosion rates, whilst higher χ_{lf} values represent phases of increased deposition of magnetic minerals, and correspondingly higher erosion rates (Shen et al., 2005a; Last et al., 2001). Periods denoted by marked fluctuations in the magnetic susceptibility record may suggest destabilised environmental conditions (Eriksson and Sandgren 1999 [quoted in Last et al., 2001]).

Ferromagnetic minerals tend to have higher magnetic susceptibility values than diamagnetic or paramagnetic materials (Walden et al., 1999). However, it must be noted that *in situ* processes such as chemical dissolution, biological diagenesis and the formation of high concentrations of authigenic magnetic iron sulphides in certain settings may act upon post-depositional sediments, creating new magnetic minerals, and / or disrupting the deposited magnetic phases (Last et al., 2001).

Freeze-dried samples were analysed at 2 cm intervals using mass specific low frequency magnetic susceptibility (χ_{lf}), following standard preparation techniques outlined in Walden et al. (1999). Samples were loaded into small plastic pots packed with cling film to ensure the sample remained still, and analysed at room temperature using a Bartington MS2 Dual Frequency Magnetic Susceptibility Meter. Each sample was measured a minimum of three times and the average result calculated. Measurements were calibrated using AMSWIN - BAR software and a standard (control) sample for which the magnetic properties are known (Dalan, 2008).

3.4 Organic analysis

Deposition of organic material as lake sediments is strongly influenced by climate, local environment, and plant abundances within the catchment. Modern isotope patterns suggest that changes in the organic carbon isotope values recorded within the sedimentary record may be used to indirectly infer how the climate changes over time. The composition of organic material depends on the origin and subsequent changes it undergoes in the environment. Three main groups of organic constituents have been identified;

- autochthonous material produced within the lake and primarily containing aquatic elements including algal / zooclastic material and plant macrophytes;
- allochthonous material produced outside of the lake, including terrestrial cellulose and lignin (Leng et al., 2006);
- wind-deposited material including pollen, spores and forest fire material transported to the lake via wind and water.

The amounts and types of organic material preserved within in lake sediments can be used to make inferences about past productivity within the catchment and / or lake and the factors driving deposition (Wetzel, 2001; Meyers et al., 1997). Organic productivity is driven by light availability, wind strength and local environmental factors including lake size, vegetation cover and nutrient availability. The organic record is therefore an important proxy for climate change.

3.4.1 Loss on Ignition (%LOI)

Loss on Ignition (%LOI) is used to measure the amounts of organic and inorganic material in sediments (total organic content, carbonates and silicates), expressed as a percentage. Organic material generally combusts at ~550°C, whilst carbonate minerals tend to combust at ~925 to 950°C (Santisteban et al., 2004). Silicates combust at even higher temperatures. Consequently, the relationship between combustion temperature and sediment type is used to estimate the percentage of organic and inorganic material present in a sediment core.

3.4.2 Total Organic Carbon (%TOC) and Total Nitrogen (%TN)

In aquatic systems, primary organic material is produced by phytoplankton during photosynthesis (Meyers, 1997). Light availability (intensity and amount) is therefore a primary control on organic carbon productivity. However, nutrient availability, pH and water (transporting phosphates and nitrates from the terrestrial environment) are also important influencing factors (Pendall et al., 2001; Meyers, 1997).

Most organic matter contains approximately 40% organic carbon (Leng, pers comm.). Total Organic Carbon (%TOC) measures the organic carbon content of sediments expressed as a percentage (Zhou et al., 2007). The results of LOI and %TOC analyses should therefore be very similar in terms of the results curve produced, but dissimilar with regard to the relative percentages recorded.

Total Nitrogen (%TN) reflects the amount of organic nitrogen present, expressed as a percentage. Nitrogen is derived from several sources including the atmosphere (as dissolved organic and inorganic nitrogen) or streams and groundwater (as particulates and dissolved organic nitrogen originating from plants and soils, and dissolved inorganic nitrogen as nitrate or ammonium) (Leng et al., 2005).

The relative contribution of carbon and nitrogen from these sources changes according to environmental and climatic conditions, illustrated by diagrams (a) and (b) in Figure 3-1. Lake water carbon and nitrogen balances are strongly influenced by changes in catchment hydrology, soil decomposition and vegetation (Wolfe et al., 1999). During warmer / forested intervals, higher organic productivity occurs, coupled with an increased contribution from terrestrial sources. During cooler, tundra intervals, atmospheric contributions become more influential.

*This image has been removed by the author of this thesis/dissertation
for copyright reasons.*

Figure 3-1: Diagram showing the pathways of carbon and nitrogen for a lake located at the treeline.

Diagram (a) shows the pathways associated with warmer, forested conditions, and diagram (b) shows the pathways associated with cooler tundra conditions.

From Wolfe et al. (1999).

3.4.3 Carbon and Nitrogen (C/N) ratios

C/N ratios are derived from TOC / TN (calculated by molecular weight), and is an indicator of the origin of organic material (i.e. aquatic or terrestrial). Nonvascular, aquatic plants such as phytoplankton contain higher levels of nitrogen because they contain little or no carbon rich cellulose or lignin and are protein rich. A low C/N ratio (<10) therefore suggests that material is primarily aquatic in origin. Conversely, vascular terrestrial plants such as grasses, trees and shrubs contain high amounts of carbon rich cellulose or lignin and comparatively low levels of protein (Meyers et al., 1999; Meyers, 1997). Organic material originating from terrestrial plants therefore has a higher C/N ratio (i.e. >20 and into the 100s) (Meyers et al., 1999). Ratios between 10 and 20 tend to suggest organic material from a mixture of terrestrial and aquatic sources (Meyers et al., 1999). C/N analysis is often carried out in conjunction with $\delta^{13}\text{C}$ analysis.

3.4.4 $\delta^{13}\text{C}$ analysis

Carbon has two stable isotopes of mass numbers 12 and 13 with relative abundances of 98.90 and 1.10% respectively (Fritz et al., 1986). $\delta^{13}\text{C}$ values are produced by measuring the ratio of ^{13}C to ^{12}C in organic material, relative to a standard. Plants fix carbon via one of two pathways. C_3 photosynthetic plants (including algae and certain types of land plants) use ribulose biphosphate (RuBP) to incorporate carbon dioxide using the Calvin Pathway. These plants preferentially uptake ^{12}C (Meyers et al., 1999). $\delta^{13}\text{C}$ values associated with C_3 plants are therefore typically between -20‰ and -32‰ (Leng et al., 2004). C_4 plants obtain carbon using phosphoenolpyruvate (PEP) via the Hatch - Slack Pathway. Resulting values average -14‰ . Plants growing in hot, tropical conditions (e.g. savannas) tend to use C_4 photosynthesis because PEP has a high affinity for CO_2 and tends to work more efficiently under high temperature / bright light conditions compared to RuBP. Measuring the $\delta^{13}\text{C}$ value of organic material therefore allows different plant types (and their inferred provenance) to be distinguished. In this study, analyses were undertaken on the organic carbon fraction of both modern and palaeo samples, referred to as $\delta^{13}\text{C}_{\text{palaeo}}$ or $\delta^{13}\text{C}_{\text{modern}}$, quoted in ‰ (per mille).

By plotting $\delta^{13}\text{C}$ values against C/N ratios (Figure 3-2), it is possible to detect changes in plant type abundances, lake productivity and / or carbon cycling (Leng, 2006). These processes are influenced by wider climatic and environmental shifts. Measuring C/N and $\delta^{13}\text{C}$ of organic carbon may therefore enable inferences to be made about the broader factors driving organic productivity (Meyers et al., 1997). Meyers et al. (1999) also suggest comparing the results of organic analysis with other proxies.

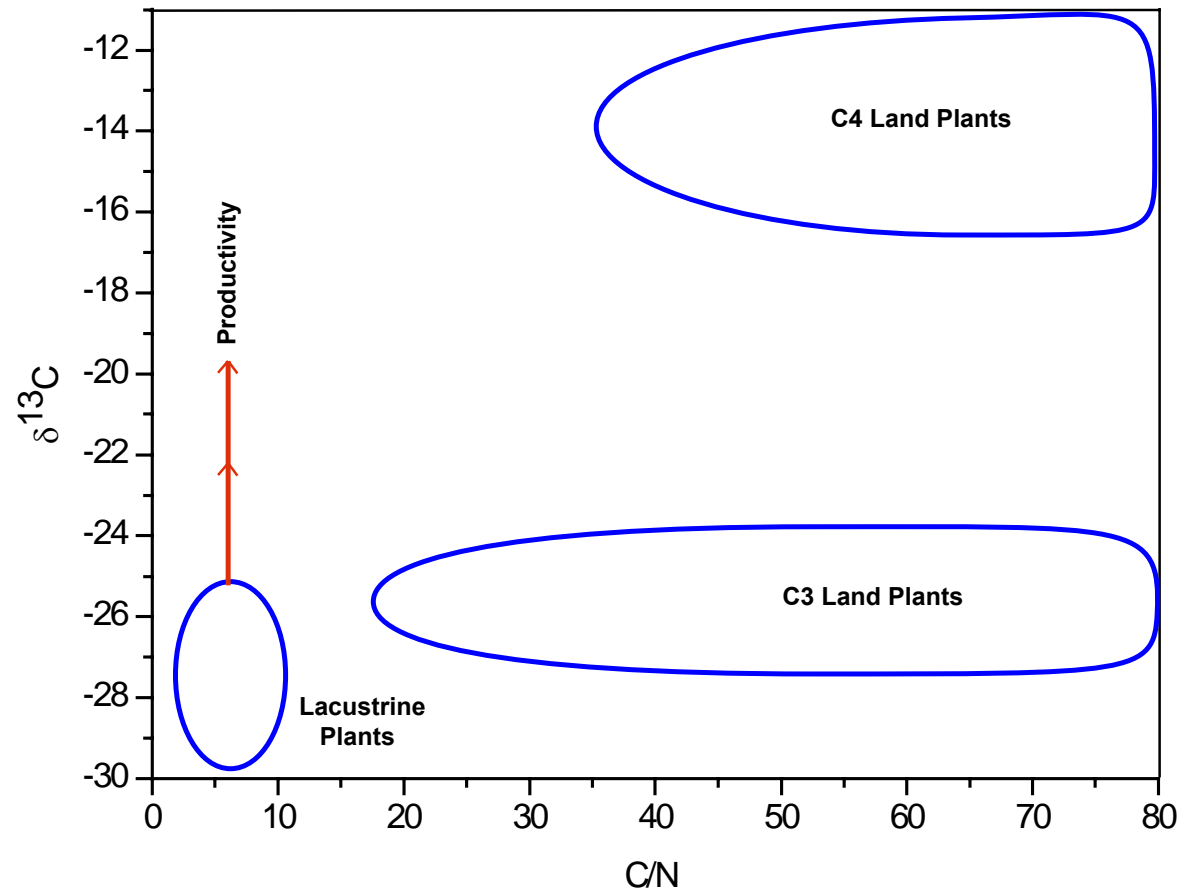


Figure 3-2: Graph showing theoretical $\delta^{13}\text{C}$ values plotted against C/N ratios.

The graph shows the generalised fields for major plant groups. Adapted from Meyers et al. (1999).

3.4.5 Organic sample preparation and analysis

Carbon isotope analysis requires characterisation of the modern catchment isotope systematics. Modern plant and soil samples were therefore collected from the shores and catchment of Lake Shudu (see Chapter 4). Samples were freeze dried, ground to a fine powder and analysed at NIGL (Keyworth) to determine modern %TOC, %TN, C/N ratios and $\delta^{13}\text{C}$ values and inferred modern isotopic systematics, establishing a baseline for exploring the palaeoisotopic record.

Organic analysis of the 06SD core (%LOI, %TOC, %TN, C/N ratios and $\delta^{13}\text{C}$ values) was undertaken at 2 cm intervals. Samples were prepared according to standard techniques referenced in the literature or provided by NIGL (Keyworth).

LOI combustion temperatures were selected in accordance with guidelines stated in Faegri et al. (1981) to ensure that material was fully combusted. The organic and carbonate (CaCO_3) content of the samples was calculated as follows;

$$\text{Calculation: Organic content} = \frac{(W_s) - (W_A)}{(W_s) - (W_C)} * 100\%$$

$$\text{Calculation: Carbonate} = \frac{(W_A) - (W_{CA})}{(W_s) - (W_C)} * 100\%$$

W_C = Weight of the crucible

W_s = Combined weight of crucible and original sample

W_A = Combined weight of the crucible and ash after burning at 550°C

W_{CA} = Combined weight of the crucible and ash after burning at 925°C

Equation 1: Calculation of Loss on Ignition percentages.

There are some limitations associated with this method. For example, organic and inorganic carbon combustion ranges are quite large. In addition, some materials such as clay can coagulate and adhere to other material, which can be difficult to disaggregate before combustion. Some carbonates also combust at lower temperatures (Santisteban et al., 2004). Distinguishing the relative signals of organic and inorganic carbon where these ranges overlap can therefore be problematic. The results of %LOI were therefore used cautiously to infer broad organic trends in the core, and %TOC analysis was used to constrain the organic carbon content of the core.

Samples subjected to %TOC, %TN, C/N and $\delta^{13}\text{C}$ analysis were prepared using the standard techniques outlined in Leng et al. (2005) and analysed using a Carlo Erba elemental analyser and VG Optima Mass Spectrometer at NIGL (Keyworth).

3.5 Palaeoecological analysis

Pollen and charcoal analysis are part of a suite of established palaeoecological techniques developed to reconstruct past environments (Moore et al., 1991). The concept of pollen analysis was first developed by Von Post in the early 1900s (Faegri et al., 1981) and involves extracting, identifying and counting pollen grains, which are abundant in most sediments and resistant to decay. The indirect relationship between pollen and climate has been used by palaeoclimatologists to reconstruct past climate change (e.g. Shen et al., 2005a; Lin et al., 1986). The changing abundance and spatial distribution of plant taxa can be a major source of climatic information on millennial to geological timescales, when species evolution and extinction rates are more stable (Webb, 1980). On sub-millennial timescales, it is important to refer to other proxies such as charcoal, which can provide insight into potential issues including human activities, which might influence the pollen record and inferred climatic conditions.

3.5.1 Principles of pollen analysis

The principles underpinning pollen analysis are described by Smol et al. (2001a). In summary;

- Plants produce pollen and spores in abundance.
- Most of these fall to the ground.
- The exine of pollen and spores are preserved in anaerobic environments, such as bogs, lakes, fens and the ocean floor.
- Pollen and spores in the atmosphere are mixed by atmospheric turbulence, resulting in a uniform 'pollen rain' over a given area.
- The amount of each species in the pollen rain depends upon the abundance of its parent plants; therefore, the composition of the pollen rain is a function of the composition of the vegetation.
- Pollen is identifiable to various taxonomic levels.
- When a sample of pollen from sediment of a known age is examined, the result is an index of the vegetation surrounding the site of deposition at that point in space and time.
- When pollen spectra are obtained from several samples through a sequence of sediment, they provide a picture of vegetation changes through time.

3.5.2 Approaches

There are two main applications of pollen analysis to climate reconstructions (Wigley et al., 1981). The floristic / indicator species approach involves analysing the modern distribution of one or two plant species and comparing this with modern climate patterns. These trends are then applied to fossil pollen assemblages. The vegetational / multivariate approach involves analysing a whole modern pollen assemblage in relation to the modern climate, and using this information to transfer fossil pollen data into a quantitative estimate of past climate. The latter approach is primarily used in this study and is preferred by palaeoclimatologists because the indicator approach is considered too narrow (Wigley et al., 1981).

However, both approaches have limitations. Firstly, it is assumed that modern day relationships between vegetation and climate are consistent with modern environmental analogues, which can be easily observed and understood (Wigley et al., 1981). Following Uniformitarian principles, it is assumed that modern conditions can be used as a basis for developing a detailed understanding of past environmental conditions. However this assumes that past and present analogues are consistent (Wigley et al., 1981).

Secondly, the pollen record could reflect issues other than climate change. For example, Ren (2000) analysed fossil pollen from several sites spanning China covering the last 6000 years. It is concluded that the millennial scale temporal and spatial patterns of forest decline cannot be explained solely by climate change. Forest decline correlates with a rise in agricultural activity and population expansion, pointing to human activity as a key influence upon the landscape. The findings of this study clearly demonstrate that when trying to reconstruct patterns of climate variability using proxy data such as pollen, it is essential to recognise that many factors may influence pollen influx and thus the distribution and abundance of pollen captured within the sedimentary record at any given site (Moore et al., 1991).

3.5.3 Pollen productivity and dispersal

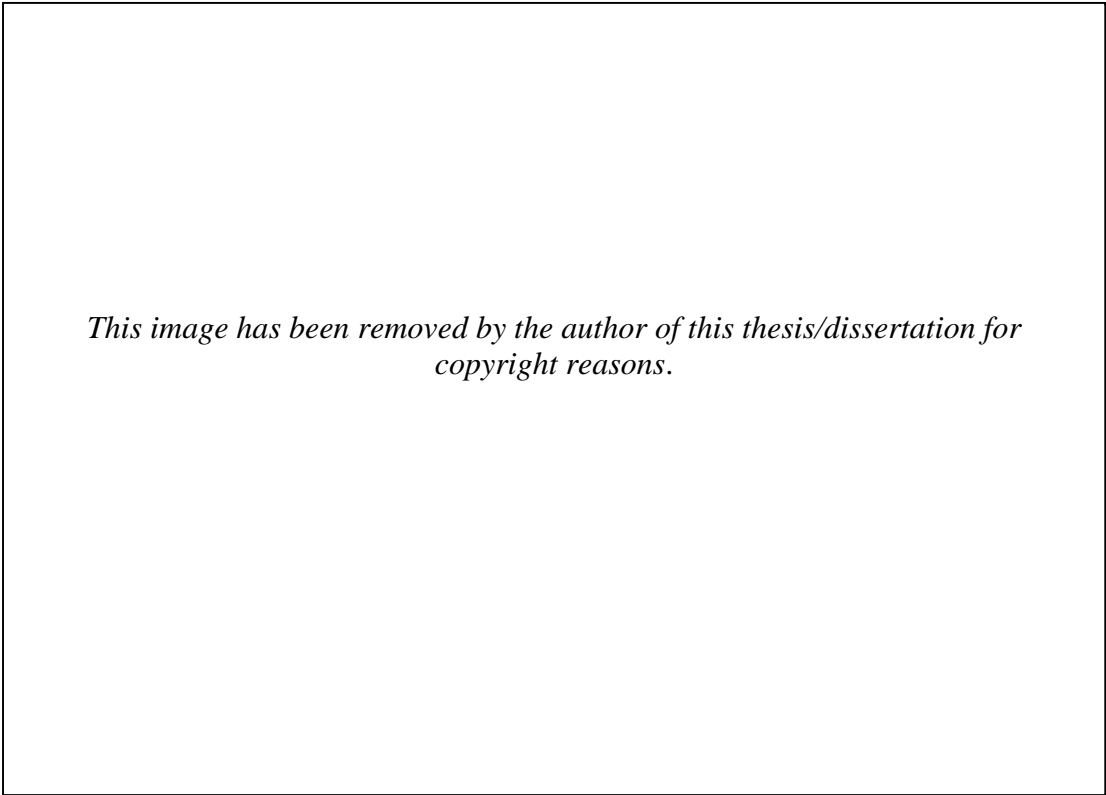
Pollen grains disperse from a point of origin to the wider environment via a number of methods including wind, soil, water, insects and birds. Up to 90% of pollen accumulated in lake sediments may be derived from inflowing streams and ground water as well as local pollen from aquatic plants (Moore et al., 1991). However, the distance a grain is transported depends on factors such as grain morphology, size and any barriers to movement (such as mountains).

Assemblages may contain grains transported long distances that are not of local or regional origin. If investigating local vegetation patterns, the influx of extra local pollen can distort any inferences made about the local assemblage based on pollen counts. For example, Van Dinter and Birks (1996), [quoted in Birks et al., 2000] studied the long distance transportation of tree pollen and concluded that the influx of *Betula* created a background signal, which confused interpretation of local pollen assemblages.

Productivity and dispersal rates vary from species to species. For example, *Pinus* pollen is an excellent disperser because the grains tend to have large air sacs attached to them, which enables them to be transported much longer distances compared to grains that do not have air sacs. Similarly, wind dispersed species are often high pollen producers. Consequently, well-dispersed and / or highly productive species tend to be more abundant (over-represented) in pollen records. This means that the numbers of pollen grains in the sediment record cannot be directly interpreted as directly reflecting species abundance (Bradley, 1999). Records therefore must be interpreted carefully and with reference to the pollen source area, catchment vegetation, and altitudinal effects on pollen deposition.

3.5.4 Pollen source area

The pollen source area describes the likely distance from which pollen is transported from the wider environment to the lake. According to Jacobson et al. (1981), there is a relationship between lake size and pollen source area (Figure 3-3). The abundance of extralocal pollen increases with lake size (Herzschuh, 2007). The regional component is defined as zones >1 km from the basin edge and the extralocal component is defined as >20 m - 1 km from the edge. The local component includes plants growing within 20 m of the edge of the basin (Jacobson et al., 1981). However, it should be noted that this model primarily applies to closed lakes (i.e. those with no inflows). For open lakes, the local component is likely to be larger than estimated by this model because of the increased influx of grains from inflowing streams and other conduits.



This image has been removed by the author of this thesis/dissertation for copyright reasons.

Figure 3-3: Relationship between lake size and pollen source area.

The study site (Lake Shudu) diameter is ~2.27 km, therefore pollen influx is likely to be on a regional scale. Key for pollen transport mechanisms; Cw = Streams/ runoff; Ct = through trunk space; Cc = from above the canopy; Cr = Via rainfall; Cg = via gravity (dry deposition of pollen, anthers, catkins etc. hanging over or near the edge of the sampling site). The graph assumes closed lake conditions. Redrawn from Jacobson et al. (1981).

3.5.5 *Modern Chinese vegetation analogues*

A number of studies have been undertaken in order to characterise the modern vegetation assemblages of China, providing a basis for palaeoenvironmental reconstructions. Detailed examples exist for the Tibetan Plateau (e.g. Zhao et al., 2009). However, recent human activity, particularly in Yunnan Province has resulted in significant ecosystem modifications. Many of the vegetation assemblages present today cannot be used as an analogue for reconstructing past vegetation assemblages driven by climate change. Fortunately, remnant vegetation patches provide insight into the types of vegetation that would have grown today in the absence of human impact. Studies based on remnant patches are used in the present study as a context for characterising palaeovegetation assemblages at Lake Shudu, and provide a context for understanding vegetational shifts over time.

Chinese pollen taxa were assigned to Plant Functional Types (PFTs) by Yu et al. (2000a). The PFTs were then grouped as biomes representing LGM / Mid Holocene vegetation assemblages. A full description of the PFTs, including the major plant type associated with each biome, is included in A.1.1., Appendix A.1. The main advantage of this study is that it includes a comprehensive list of Chinese plant types used to define each biome. The main drawback is that the system is possibly over-generalised compared to other studies and does not fully reflect the range of ecosystems previously in operation in China.

This image has been removed by the author of this thesis/dissertation for copyright reasons.

Table 3-1: Biome classifications for China.

A list of the pollen taxa assigned to each Plant Functional Type (PFT) is included in A.1.1, Appendix A.1. From Yu et al. (2000a).

▪ Yunnan Province

The vegetation of Yunnan Province was of direct relevance to this research because the study site, Lake Shudu, is located in northwestern Yunnan Province. The standard reference work for classifying the modern regional vegetation of Yunnan Province was produced by the Writing Group of Yunnan Vegetation (WGYV, 1987). It contains an idealised vegetation map based on analysis of remnant vegetation patches that distinguishes three major regions: tropical monsoon forest, subtropical evergreen broadleaved forest and alpine vegetation of Qinghai - Tibet Plateau (Song et al., 2007). Each region is subdivided into domains and subdomains that represent distinctive types of natural forest recognized by the presence of key taxa (Song et al., 2007).

This system is summarised in Table 3-2. The vegetation of southern Yunnan is primarily defined as tropical monsoon rainforest, whilst mid Yunnan is dominated by subtropical evergreen broadleaved forest, including species such as *Cyclobalanopsis glaucoides*, *Castanopsis delavayi* (Zhao, 1986). Northern Yunnan is classed as alpine. However, there are some drawbacks associated with this system. Firstly, a full list of the taxa included in each idealised zone is not available in English, so it is difficult to examine the precise configuration of each vegetation zone.

Secondly, it does not take local altitudinal effects upon vegetation into account. According to the Koppen Climate Classification System, southwestern China is located within the latitudes identified as forming the temperate / subtropical transition zone (Ohsawa, 1993) between ~20 and 35°N. However, it is possible to identify altitudinal vegetation belts, which modify these latitudinal vegetation zones. In high mountain regions, base belts correspond to the basic climatic regime at the foot of the mountain system (Faegri et al., 1981). Higher up, altitudinal belts occur in different combinations that characterise individual mountain systems, and are collectively termed 'spectra'. Zhang et al. (2006) identified 6 spectra in the mountain regions of China; monostructural, flattening structure, exposure dependent, stepwise rising, abnormal and Tibetan complex. All spectra have the same number of altitudinal belts and an identical vertical combination, but the belts vary in extent. In northwestern Yunnan, the belts in a spectra are few but wide, and are associated with the Tibetan Complex spectra.

Belts are distinguished according to vegetation assemblages and soil type (Zhang et al., 2006a). For example, the alpine and subalpine altitudinal belts associated with high altitude zones (excluding base belts) are shown in Table 3-3 (Zhang et al., 2006a). Steppe, desert, meadow and coniferous forest dominate these zones. These are all ecosystems that include taxa adapted to cope with cool temperatures, reduced seasonality, thin soils and reduced water availability associated with extreme conditions.

Region	Subregion	Domain	Subdomain	Zone	Type	Location in Yunnan
1					Tropical monsoon forest / rainforest	S / SW
	1A				Monsoon forest / rainforest	SW
				1Ai	Tropical seasonal rainforest / semi - evergreen monsoon rainforest	S / SW
		1Ai-1			Seasonal rainforest / semi - seasonal evergreen monsoon forest	Inter-montane basins, W / SW
2					Subtropical evergreen broadleaved forest	central Yunnan
	2A				Semi - humid evergreen broadleaved forest	W
				2Ai	Subtropical monsoon evergreen broadleaved forest	southern plateau
				2Aii	Subtropical evergreen broadleaved forest	Northern plateau
		Aii-1			Semi - humid evergreen broadleaved forest of <i>Pinus yunnanensis</i>	C / E
			1c		<i>Pinus yunnanensis</i> , <i>Picea</i> and <i>Abies</i> forest	NW central Yunnan
3					Alpine vegetation	Qinghai - Tibetan Plateau

Table 3-2: Idealised vegetation regions, Yunnan Province, China.

Each region is designated based on the vegetation type believed to be most common prior to human activity. Based on work undertaken by Song et al. (2007); the Writing Group of Yunnan Vegetation (1987) and Li et al. (1986).

Altitudinal Belt Group	Altitudinal Belt
Alpine Group	Nival Sub-nival Alpine meadow Alpine steppe-meadow Alpine steppe Alpine desert-steppe Alpine desert
Subalpine Group	Evergreen shrub-meadow Sub-alpine meadow Sub-alpine shrub-meadow Sub-alpine shrub Sub-alpine evergreen coniferous shrub Sub-alpine krummholz Sub-alpine coniferous forest

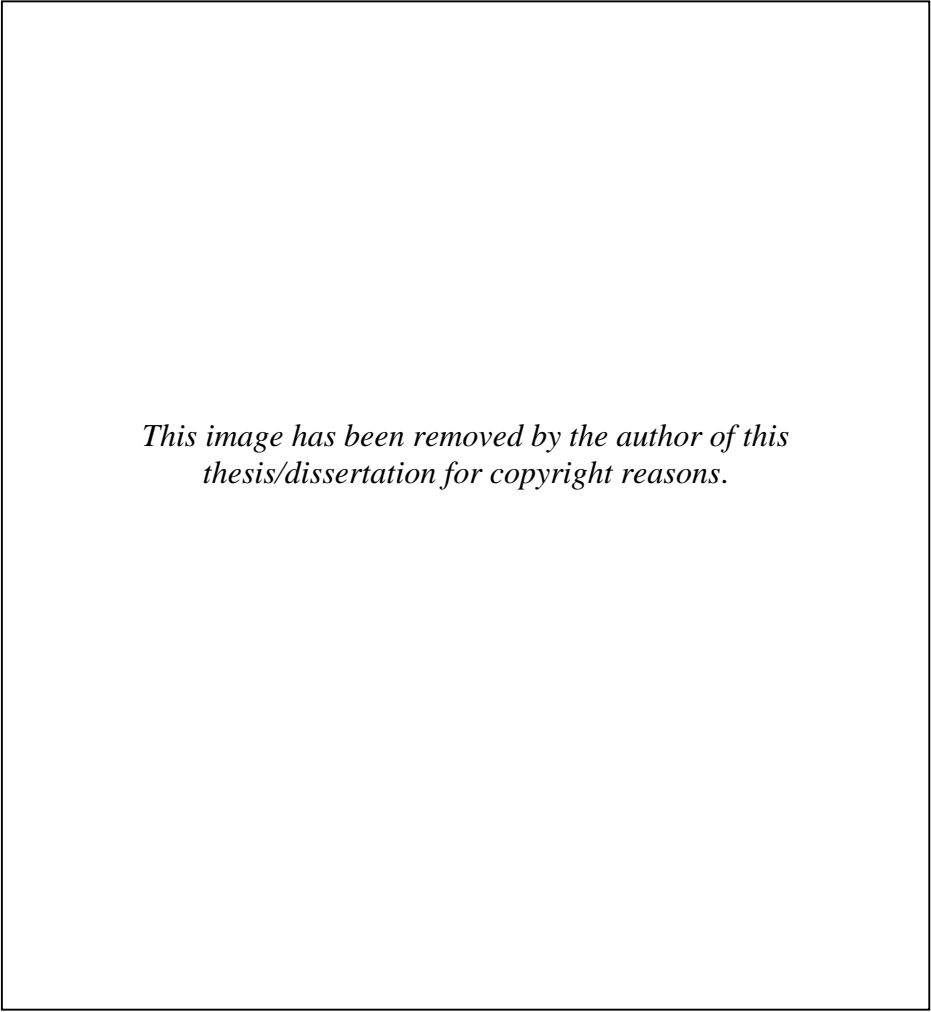
Table 3-3: The altitudinal belts (excluding base and mid - low mountain belts) found in the high mountainous zones of China.

These occur in various combinations constituting spectra with regional characteristics.

From Zhang et al. (2006a).

The relationship between altitude, vegetation distribution and climate is further highlighted in Figure 3-4, which illustrates the modern altitudinal gradients of key types of arboreal pollen in the mountains of northwestern Yunnan. From 2000 - 3200 m asl, deciduous and evergreen broadleaved trees dominate, whilst from 3000 m asl, coniferous taxa such as *Abies* and *Picea* are the dominant taxa. *Pinus* occupies a large altitudinal range. However, the other genera, particularly *Picea* and *Tsuga* occupy relatively narrow altitudinal ranges. This suggests that they are more sensitive to climatic shifts compared to other genera with wider ecological tolerances. The presence or absence of these indicator species in pollen records from high altitude sites can therefore be used to infer changing climatic conditions.

The relative position of the treeline alters in response to a change in conditions, and from this shifts in climatic conditions can be indirectly inferred. The relationship has been confirmed in a number of studies (Lu et al., 2008). For example, Tinner et al. (2005) investigated the response of high mountain vegetation to environmental changes in the Swiss Alps and discovered that tree line vegetation was in dynamic equilibrium with climate, including during abrupt climatic shifts. The vertical migration of tree species therefore occurs in response to changing climatic conditions. Lu et al. (2008) argues that understanding the relationships between modern pollen spectra, vegetation and environment are crucial for interpretation of tree line, vegetation and environment history from fossil pollen data. Lu et al. (2008) estimate that the upper treeline is presently located between 4000 and 4300 m asl in southeastern Tibet.



This image has been removed by the author of this thesis/dissertation for copyright reasons.

Figure 3-4: Altitudinal gradient of key modern arboreal taxa, Yulongshan Mountains, northwestern Yunnan.

From Shen et al. (2005a).

An alternative description of the vegetation of Yunnan Province is proposed by Li et al. (1986), which incorporates the influences of altitude and latitude, and recognises the importance of landscape heterogeneity and local differences in vegetation assemblages that is lacking in the other studies mentioned above. Further details of the scheme, which includes detailed information on the major plant types found growing in Yunnan, are provided in A.1.2., Appendix A.1. Li et al. (1986) illustrated the importance of accounting for local topographic variety and climatic and edaphic heterogeneity by comparing the idealised vegetation regions (Figure 3-5) proposed by Wu (1980), and used by the WGYV (1987), with specific altitudinal zonations (Figure 3-6). For example, vegetation assemblages associated with Zhongdian County located in northwestern Yunnan are defined as subtropical according to the vegetation map (horizontal zones) whereas the altitudinal (vertical) assemblage zones for this region are defined as dry valley, small leaved shrubland (SEBF), *Picea* and *Abies* forests (MonCF) and montane shrubland and alpine meadow (MonSh and MonMea).

The system therefore emphasises vegetation types rather than geographic zones. Types are classed according to physiognomic and ecophysiological criteria. Thirteen major vegetation types are distinguishable, based on geographical region and climate, seasonality, dominant species and leaf form. The composition of each vegetation unit was inferred from remnant patches; hence, the vegetation assemblages are idealised. Virtually none of the vegetation types identified occupies their natural zones following human activity (the exceptions being vegetation assemblages in the remote alpine and subalpine regions). It is estimated that <10% of Yunnan's forest cover is naturally occurring, because high population densities have given rise to land clearance and planting of managed coniferous stands. However, the system still offers a detailed insight into vegetation distributions in the Province prior to human intervention, which provides a useful analogue for reconstructing past vegetation assemblages. Climatic correlations are also inferred for selected vegetation types (Table 3-4).

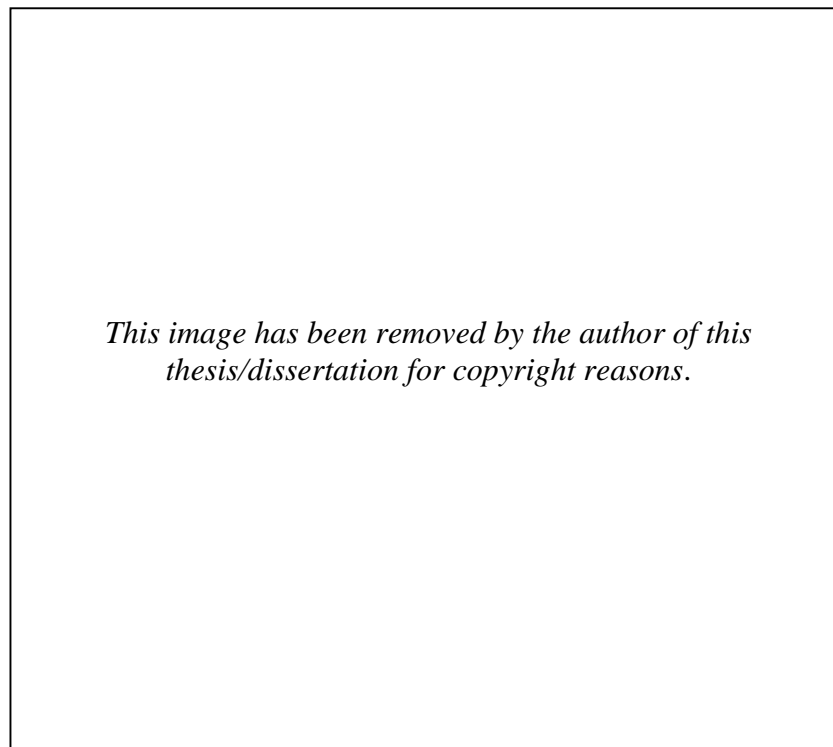


Figure 3-5: Simplified idealised vegetation map for Yunnan Province, showing the most common types prior to disturbance by human activity.

I: Tropical rainforest and monsoon forest; II: Subtropical evergreen broadleaved forest; III: Montane conifer forest. Z = Zhongdian County; W = Weixi County; J = Jindong County; M = Menghai County and Y = Jingping County. From Li et al. (1986).

This image has been removed by the author of this thesis/dissertation for copyright reasons.

Figure 3-6: Selected altitudinal zonation in Yunnan Province.

Z = Zhongdian County; W = Weixi County; J = Jindong County; M = Menghai County and Y = Jingping County. 1: Humid rainforest; 2: Seasonal rainforest; 3: Montane rainforest; 4: Dry valley shrubland and grassland; 5: Monsoonal evergreen broadleaved forest and *Pinus kesiya*; 6: Semi-humid evergreen broadleaved forest and *Pinus yunnanensis*; 7: Montane humid evergreen broadleaved forest; 8: Mixed *Tsuga* forest; 9: Montane mossy dwarf forest; 10: Dry valley small-leaved shrubland; 11: *Picea* and *Abies* forests; 12: Montane shrubland and alpine meadow. From Li et al. (1986).

This image has been removed by the author of this thesis/dissertation for copyright reasons.

Table 3-4: Climatic correlations of selected vegetation types, Yunnan Province, China.

From Li et al. (1986).

▪ Tibetan Plateau

Modern pollen assemblages and contemporary vegetation patterns in the Qaidam Basin on the Tibetan Plateau indicate that the main vegetation zones are distinguished by their modern pollen spectra (Zhao et al., 2009). The results are used in this study to help interpret the Lake Shudu fossil pollen record.

The average elevation of the Qaidam Basin is 2800 m asl, whilst Mean Annual Precipitation (MAP) varies from >530 mm to < 20 mm from east to west, with most of the rainfall occurring during the summer months. A similar east to west gradient is observed with regard to temperatures, which range from 7.8°C in the east (and highlands) compared to ~17.5°C in the west (and lowlands) in the summer time. Four major vegetation types are distinguished based on major taxa (Table 3-5) They are associated with the three treeless biomes - tundra, steppe and desert (Yu et al., 2000a).

The first vegetation type is Alpine Meadow, located on mountains above >3600 m asl. It is a subdivision of the tundra biome. Tundra primarily consists of grasses, heaths and sedges. Alpine meadow is distinguished by the presence of alpine forbs (Yu et al., 2000a). The dominant taxa are Cyperaceae and Poaceae, with contributions from Asteraceae, Ericaceae, Gentianaceae, Fabaceae, Saxifragaceae and *Polygonum*. Pollen assemblages derived from alpine meadow sites consisted of Cyperaceae (>20%) and *Artemisia* (>10%). Other pollen types include Poaceae (5 - 15%) and Fabaceae (up to 38%). Asteraceae, *Gentiana*, *Thalictrum* and *Polygonum* appear in low abundances. Although not a primary form of vegetation presently found on the Tibetan Plateau, the other main type of tundra is alpine shrubland, which is distinguished by the presence of members of the Betulaceae family, *Hippophae*, *Sabina* and *Salix* (Yu et al., 2000a). Tundra vegetation assemblages are currently found growing above ~3000 m asl in eastern and central Tibet (Yu et al., 2000a).

The second vegetation type is steppe, which is found growing on the lower mountain slopes, 3400 - 3600 m asl (~3100 m asl at Lake Qinghai). Dominant taxa include temperate plants mixed with more Poaceae and *Artemisia* than alpine meadow and accompanied by Cyperaceae and Fabaceae. Pollen assemblages include Poaceae (up to 48%) and *Artemisia* (up to 68%), with Fabaceae, Asteraceae and Cyperaceae (all < 10%).

The third vegetation type is steppe desert, found growing at 2800 - 3000 m asl, between Lake Qinghai and Chaka Salty Lake and in transitional zones. Primary taxa include *Artemisia*, Poaceae and Chenopodiaceae with *Ephedra*, Brassicaceae and other types of Asteraceae. Pollen assemblages consist of *Artemisia* (up to 65%), Chenopodiaceae (up to 23%) and Poaceae (up to 36%).

The fourth type of vegetation associated with the Tibetan Plateau is desert, found in areas <3200 m asl. Vegetation is sparse and dominated by Chenopodiaceae, *Ephedra* and Asteraceae. Chenopodiaceae (up to 97%) dominates the desert pollen assemblages, with contributions from *Artemisia* (<20%) and Poaceae (<10%).

In all cases, arboreal taxa (and associated pollen concentrations) are low. Crucially, samples obtained from lake sediments have a similar taxonomic composition to those obtained from moss polsters and topsoils, although *Artemisia* percentages are slightly higher than those obtained from soils in the desert zone. Relative to Poaceae (which appeared in all assemblages), a high relative representation value is observed for *Artemisia* and Chenopodiaceae, indicating that these taxon may be over-represented in samples, whilst Ranunculaceae, Asteraceae, *Ephedra* and Fabaceae have relatively low representation values, implying under representation. Cyperaceae and *Gentiana* are neither significantly over or under-represented.

Vegetation type	Temperature (°C)				Frost days per year	Rainfall		Other observations
	Annual Mean	Warmest Month Mean	Coldest Month Mean	Absolute coldest		Annual total (mm)	Seasonality	
Alpine Meadow	0	10	-16	-	-	>400	Strong	Cold climate, low evaporation, positive water budget
Steppe	0.5	13	-13	-	-	300 - 400	Strong	Cold climate
Steppe Desert	1	14	-13	-	-	200 - 300	Strong	Cold climate
Desert	~3	16	-12	-	-	<200	Moderate	Extremely dry climate

Table 3-5: Climatic correlations of selected vegetation types, Tibetan Plateau.

From Zhao et al. (2009).

3.5.6 *Driver - response lag*

Davis and Botkin (1985) [quoted in Moore et al., 1991] studied the response of forests to climate change and propose that there is a ~150-year lag between a change in climate and forest response. However, the precise duration of this lag is debated in the literature, and possibly varies according to vegetation type. For example, Tinner et al., 2005 suggest that the response of high mountain vegetation to environmental changes during the Late Pleistocene - Early Holocene Period was decadal, or perhaps even synchronous. A number of factors are likely to impact on the biotic response of ecosystems to change, including altitude, latitude and species composition. For the purposes of this study, a centennial lag is assumed following Davis and Botkin (1985), acknowledging the dominance of arboreal pollen types in the pollen record. However, it is apparent from the literature that further research is required to precisely constrain the relationship between forcing and response in the high altitude ecosystems of southwestern China.

Davis and Botkin (1985) [quoted in Moore et al., 1991] also suggest that forests do not respond to changes in temperature below a certain threshold. These findings indicate that care must be taken when interpreting the pollen record, because shifts in arboreal pollen may be related to an event that occurred earlier than implied by the pollen record. Also, some events may not be recorded in the pollen record if they are not of sufficient magnitude / extent to trigger a vegetational response. Thus, any low magnitude or low frequency climatic events may not be captured, which can lead to a 'smoothing' of the climatic changes recorded in the pollen record.

However, the relationship between driver and response is complicated by the fact that different taxa have different ecological tolerances, and therefore some taxa will be more or less sensitive to change than others. Therefore, the degree to which an event is recorded in the pollen record may in part be a function of the types of taxa present in the assemblage, and their ability to respond and / or adapt to change. The relationship is therefore very much a two-way process. Over longer timescales, Bradley (1999) argue that this effect is less important because vegetation maintains a dynamic equilibrium with climate change, but this hypothesis is strongly refuted by others including Birks [quoted in Wigley et al., 1981].

3.5.7 *Pollen extraction*

Pollen was extracted from freeze-dried sediment samples prepared according to the standard techniques outlined in Moore et al. (1991) and Faegri et al. (1981). Following pilot testing, the method was adapted for use on the Chinese sediments, which were rich in organic detritus (see A.1.3., Appendix A.1. for further details).

3.5.8 Pollen counting

The core was initially sampled at 24 cm intervals. In preparation for counting, pollen grains were placed in silicon oil, mounted onto slides and covered with a coverslip. Terrestrial pollen (including trees, shrubs, herbs, grass / sedge), aquatics, spores and non-Chinese pollen grains (added to act as a standard) were identified and counted by undertaking a number of traversals of the slide at regular intervals, using a light microscope set to a magnification of x400. A magnification of x1000 and immersion oil was used for critical determinations.

The pollen sum (including trees, shrubs, herbs, grasses and sedge pollen) was based on a count of 300 pollen grains per sample. Owing to time constraints and the inherent complexity associated with identifying Chinese pollen (see Section 3.5.9), it was not possible to undertake a larger count. Samples containing very low pollen concentrations were counted to 100 grains. Samples containing <100 pollen grains were re-prepped and re-counted to check for procedural errors.

3.5.9 Pollen identification

Pollen grains are identified by unique characteristics, usually to family or genus level. Pollen grains are usually spherical or elliptical and vary in diameter from 10 - 100 μm (0.01 - 0.1 mm). Identifying features on the exine include apertures (pores and furrows), surface sculpturing and deterioration markings (which may reflect the conditions of fossilisation). Spores of ferns and mosses are structurally different from pollen but are a similar size and tend to be wind dispersed. Spores also possess identifying surface characteristics and therefore are a useful palaeoenvironmental indicator.

China supports a vast range of plant taxa including rare types, and is one the most ecologically diverse countries in the world. Consequently the pollen record is very challenging to interpret because of the number and type of species represented. Preliminary counts were therefore carried out on the 05SD core and any unknown grains were photographed. Counted slides, the photographs of unidentified pollen grains and any suggested identifications were sent to palynologists at NIGL (China) for feedback. An archive of photographs of identified grains was developed for reference. A preliminary count was then undertaken on the 06SD core.

A visit to the Department of Hydrology and Environmental Geology at the Chinese Academy of Geological Science (CAS), Shijiazhuang, was undertaken in August 2007 in order to discuss the results of the preliminary count with Professor Tong. NIGL (China) carried out a parallel count on the core so that the results could be directly compared to check for any obvious differences in identification. This helped to ensure consistency between UK and Chinese approaches. Comparison of the counts confirmed that they were sufficiently similar to suggest agreement between UK and Chinese palynologists. A visit to the Australian National University (ANU), Canberra was also undertaken to access ANU's extensive collection of type slides and discuss the pollen record with Professor Geoff Hope who specialises in Southeast Asian pollen.

Following training, a full pollen count was undertaken on 06SD, with reference to training notes, type slides, photographs, pollen reference guides (e.g. E-Floras, 2006; Fujiki et al., 2005; Menitsky, 2005; Qiao, 2004 and Beug, 2004) and correspondence with Professor Tong. Standard descriptive terms developed by Punt et al. (2007) are used in this study.

Particular issues encountered included;

- Rare species
- Similarity of pollen morphology of species of Rosaceae and Fagaceae
- Difficulties in distinguishing deciduous and evergreen *Quercus*
- Difficulties distinguishing Chinese *Pinus*, *Abies* and *Picea* pollen

Chinese pollen is diverse and includes numerous rare species. Consequently, the 06SD core contains a few pollen grains that were not identifiable from the available reference material and type slides. Unknown grains were counted to monitor levels of unidentified species. Damaged grains were also counted to provide an indication of sediment reworking.

There are well-known difficulties associated with distinguishing particular Chinese pollen in ecologically or taxonomically distinct groups whose pollen is morphologically similar (Jarvis et al., 1992). For example, the pollen morphologies of some species of Fagaceae and Rosaceae are very similar, which can pose a problem when trying to distinguish pollen from these families. However, Jarvis et al. (1992) has demonstrated that with careful observation, it is possible to distinguish selected types of Rosaceae and Fagaceae pollen. The resulting pollen key and photographs of individual pollen grains in Jarvis et al. (1992) were used to guide identification in this study, in combination with guidance from Professor Tong (CAS).

Similar issues arise when attempting to distinguish the pollen types within Fagaceae. Nevertheless, Liu et al. (2007) suggests that the size, shape, aperture, and exine structure of pollen grains of the modern *Quercus* are easily distinguished from those of other fagaceous genera such as *Castanea*, *Castanopsis*, *Lithocarpus*, *Fagus*, *Trigonobalanus*, *Formanodendron*, and *Colombobalanus*. However, *Quercus* is a genus that is prone to introgressive hybridisation, producing offspring including the subgenus *Cyclobalanopsis*, which represent new species, but are morphologically very similar (Liu et al., 2007). Consequently, the main area of concern appears to be associated with distinguishing the pollen of evergreen and deciduous *Quercus* and the subgenus *Cyclobalanopsis*.

For example, Liu et al. (2007) suggest that oaks are rarely identifiable beyond genus level. This is emphasised by the fact that an infrageneric classification for the Chinese oaks is not proposed in the latest edition of the Flora of China, which is currently the definitive source of information for distinguishing living species. However, Jarvis et al. (1992) are confident that through careful examination of grain sculpturing and aperture types, it is possible to identify and assign pollen grains to genus level.

With regard to the pollen produced by these genera, the grain surface sculpturing is highly variable. Oak pollen extracted from the 06SD core exhibits this trait, with sculptural features ranging from psilate, scabrate / verrucate to rugulate. Grain size was also shown to be highly variable in both groups, in agreement with Jarvis et al. (1992). Equatorial measurements varied from <18 to 30 µm, whilst grain length measured from pole to pole varied from 18 to >30 µm. The high variability of these features indicates that criteria other than size should be considered in order to properly distinguish these genera.

A pollen key was devised under the guidance of Professor Tong and with reference to the works of Liu et al. (2007) and Jarvis et al. (1992), which enabled evergreen *Quercus* to be distinguished from deciduous *Quercus* and Rosaceous genera. Grain size is omitted as a criterion, on the basis that pollen from each genera can be the same size, so this does not aid the process of identification (in fact in many cases this would further confuse matters). Professor Tong recommended grouping evergreen *Quercus* with *Cyclobalanopsis* on the basis that it was not possible to distinguish these species using only light microscopy. Liu et al. (2007) shared this viewpoint. The evergreen *Quercus* pollen count therefore includes *Cyclobalanopsis*. This group is termed ‘evergreen *Quercus* type’ on subsequent pollen diagrams.

Chinese coniferous pollen grains including *Pinus*, *Picea* and *Abies* are saccate and range in size from 45 - 150 μm . Consequently, Chinese coniferous pollen grains cannot be distinguished primarily by grain size because there is considerable overlap across these genera. They form an important component of the Lake Shudu pollen record; therefore, Professor Tong (CAS) provided specific advice on how to distinguish these grains. A pollen key for distinguishing *Pinus*, *Abies* and *Picea* pollen grains was devised based on his advice, type slides provided by CAS and observations. Because of the inherent difficulties associated with Chinese pollen identification outlined above, grains were identified to family or genus level.

3.5.10 Statistical methods

Quantitative measurements of temperature and precipitation are commonly used to as indicators of climate variability and associated warm / cold and humid / arid conditions. Quantitative palaeoenvironmental proxies include the $\delta^{18}\text{O}$ record derived from diatoms and chironomids. It was hoped that a $\delta^{18}\text{O}$ record of temperature and / or precipitation could be derived from diatoms present in the Lake Shudu record, but this was not possible owing to financial and time constraints. Climate variability is therefore primarily described semi-quantitatively in this study.

Within semi-quantitative studies, pollen and other proxy records are subjected to statistical analysis in order to determine the relative influence of climatic and environmental variables. Palaeomonsoon variability tends to be described qualitatively, as either weak or strong, wherein warmer / wetter conditions are associated with a strong summer monsoon, and conversely colder / drier conditions are linked to a strong winter monsoon. Statistical analysis involving Detrended Correspondence Analysis (DCA), Principal Components Analysis (PCA) and pollen ratios provide semi-quantitative assessments of variables such as temperature and / or precipitation shifts (e.g. Zhao et al., 2009; Herzschuh, 2007; Van Campo et al., 1993 and Faegri et al., 1981).

3.5.10.1 Pollen percentages

Raw pollen counts of trees, shrubs, herbs, grasses and sedge were converted to percentages using Tilia v2.02 (Grimm, 2004). Pollen percentages are useful for determining the contributions of each taxon to the pollen record. However, pollen percentages assume that each type of pollen influences all others within the sum (i.e. the pollen sum must always equal 100%) (Moore et al., 1991). Hence, pollen percentage estimates do not take account of the differing rates of pollen production and dispersal, which means that some taxon may become over or under-represented in the pollen record.

3.5.10.2 Pollen concentrations

Total pollen concentrations of arboreal and non arboreal pollen (AP and NAP) provide an indication of the relative abundances of taxon over time (Smol et al., 2001a), thus overcoming some of the inherent issues associated with the interpretation of pollen percentages. In order to determine pollen concentration, two tablets containing a known concentration of *Lycopodium* spores were added to each sample prior to beginning the process of extracting the pollen. After counting the number of pollen and spores present in each sample, pollen concentrations were calculated following Stockmarr (1971);

$$\frac{\text{No. Grains counted} \times \text{No. } Lycopodium \text{ spores added}}{\text{No. } Lycopodium \text{ counted}} \times \frac{1}{\text{Sample Mass}}$$

Equation 2: Pollen concentration calculation.

3.5.10.3 DCA / PCA

Pollen taxa with abundances of >2% in one sample were subjected to numerical analysis (Zhao et al., 2009; Birks, 2007). The dataset was analysed using CANOCO v.4.5.2 (ter Braak et al., 2003). In order to determine whether trends in the pollen dataset were likely to be linear (related to environmental variables) or unimodal (related to biological variables), Detrended Correspondence Analysis (DCA) was applied to the data, using the parameters outlined in A.1.4., Appendix A.1. The results are expressed as axes and gradients (Frey et al., 1998).

If the resulting axis gradient is longer than 2 SD, then the dataset should be analysed using unimodal methods, whereas if it is less than 2 SD, linear methods are appropriate (Birks, 2006). The results indicated that numerical analyses based on a linear response model (and assuming the influence of environmental variables) were most appropriate (Birks, 2007; Frey et al., 1998). The dataset was subsequently analysed using Principal Components Analysis (PCA) using the parameters outlined in A.1.4., Appendix A.1. PCA visualises the variance in data in relation to the best fitting theoretical variables, allowing the variables that are likely to be responsible for the variation to be deduced indirectly (Birks, 2007).

3.5.10.4 Ratios and indicative pollen types

In this study, ratios and indicative pollen types are used as a semi-quantitative indicator of vegetation density, temperature and effective moisture following Zhao et al. (2009) and Van Campo et al. (1993), and with reference to the full assessment of the pollen types and abundances in the Lake Shudu record.

- **Treeline elevation**

Combined percentages of *Abies* and *Picea* are used to detect changes in the upper treeline, following Lu et al. (2008). Combined percentages of <15% have been recorded at sites within an elevation range of 800 m above the treeline in mountainous regions of the Qinghai - Tibetan Plateau, and <6% in unforested regions (Lu et al., 2008). This method is used to explore whether the treeline was located above or below Lake Shudu in the past.

- **AP/NAP ratios**

The ratio of Arboreal Pollen (AP) to Non Arboreal Pollen (NAP) is used as an indicator of vegetation density, reflecting changes in the openness of forest - steppe and subalpine environments (Herzschuh, 2007). Ratios are based on the percentages of arboreal and non-arboreal taxa (including shrubs, herbs and grasses / sedges) and calculated following the method outlined in Herzschuh (2007). An AP/NAP ratio of 8.5 reflects dense forest, whereas open woodland / grassland have a ratio of 4, whilst grassland vegetation has a ratio of ~2.5. Wholly open conditions have ratios of <0.2 (Herzschuh, 2007). In order to gain an insight into catchment vegetation, arboreal pollen taxon with high pollen percentages but low pollen concentrations (indicating that they were likely to have been derived from sources outside the catchment) were excluded from the calculation.

Where AP/NAP ratios indicate that vegetation cover is predominantly sparse / unforested, the ratios of *Artemisia* to Chenopodiaceae (A/C) and *Artemisia* to Cyperaceae (A/Cy) are used to examine the alignment of the pollen record with the unforested biomes (e.g. tundra, desert and steppe) and associated climatic conditions.

- **A/C ratios**

Artemisia is a primary component of the steppe vegetation assemblage, whilst Chenopodiaceae is a desert taxon (Zhao et al., 2009). Both biomes are dry, but steppe conditions are generally moist relative to desert conditions. Where the pollen record indicates that conditions are generally quite dry, such as on the Tibetan Plateau today (i.e. sparse vegetation, lack of forest cover and / or a low AP/NAP ratio), the ratio of *Artemisia* relative to Chenopodiaceae indicates primary alignment to the steppe or desert biome. A/C ratios were calculated using pollen percentages, following the method outlined in Herzschuh (2007). Low A/C ratios (<1) are correlated with desert areas, whilst higher ratios (~33) are correlated with steppe. Intermediate ratios correspond with tundra (Zhao et al., 2009). On the Tibetan Plateau today, A/C ratios positively correlate with mean annual precipitation (P_{ann} : 104 - 670 mm) (Herzschuh, 2007).

- **A/Cy ratios**

Artemisia is a primary component of steppe assemblages whereas Cyperaceae is associated with alpine meadow. Both biomes are associated with a cool climate, but climatic conditions associated with steppe are generally mild relative to conditions associated with alpine meadow. Where the pollen record indicates that conditions are quite cool, such as on the Tibetan Plateau today (i.e. sparse vegetation, lack of forest cover and / or a low AP/NAP ratio), and A/C ratios are >2 but <33 , the ratio of *Artemisia* relative to Cyperaceae is used to indicate whether vegetation assemblages are primarily aligned to steppe or alpine meadow (Zhao et al., 2009). Alpine meadow is a subdivision of the tundra biome, which also includes alpine shrubland (Yu et al., 2000a). In this study, A/Cy ratios were used more widely to distinguish cool tundra (alpine meadow / shrubland) from warmer steppe.

A/Cy ratios were calculated using pollen percentages, following the method outlined in Herzsuh (2007). Ratios of <1 correspond with tundra vegetation, ratios of >1 to <16 reflect steppe, and up to 26 represents steppe desert vegetation. Desert ratios are generally much higher. On the Tibetan Plateau today, A/Cy ratios are significantly correlated with mean July temperature (T_{July} : 4.0 - 17.4 °C) (Herzsuh, 2007).

- **Percentages of selected arboreal taxa**

Selected tree taxon are tentatively used to infer broad environmental and climatic conditions associated with the arboreal component of the pollen record (Shen et al., 2005a). In the present study, evergreen *Quercus* is used to infer dry (late) winters (Shen et al., 2005a). Combined percentages of *Betula* and deciduous *Quercus* are used to infer cold, dry winters.

3.5.11 Charcoal analysis

Charcoal has been successfully used as a proxy for Pleistocene and Holocene fire and / or landscape disturbance events (Beer et al., 2007; Gobet et al., 2005; Smol et al., 2001a), which are major drivers of vegetation change and / or ecosystem dynamics (Conedera et al., 2009). The contribution of charcoal to the palaeorecords can be primary (i.e. directly related to a fire event) or secondary (e.g. an indirect influx of relict charcoal stored in the catchment). Charcoal peaks representing primary events may pertain to local, extralocal or regional (in the latter case derived from adjacent upwind basins) fire events. Secondary charcoal may represent ‘noise’, resulting from changes in charcoal accumulation rates resulting from landscape disturbances, for example.

Broadly speaking, larger charcoal particles are likely to have been produced by local events in the catchment, whilst smaller particles are more likely to have been windblown from further away (Smol et al., 2001a; Faegri et al., 1981). Charcoal fragments were classified according to size. Fragments measuring >10 - 100 µm and 100 - 150 µm in length appearing on the pollen slides were counted against a fixed count of exotic *Lycopodium* grains, (Smol et al., 2001a). Macrofossil remains were checked for the presence of larger charcoal fragments. Owing to time constraints, the aim of this exercise was to elicit any long-term trends in the charcoal record to aid interpretation of the other proxy records, rather than to undertake a detailed high-resolution analysis of the charcoal record.

3.6 Dating methods

The 06SD core was dated using AMS ^{14}C radiocarbon dating of bulk sediments and pollen concentrations. Bulk dating of lake deposits involves dating the total amount of organic carbon present in sediments, whereas pollen concentration dating involves dating a single carbon fraction. These dating methods were chosen based on preliminary analysis of the core composition, which indicated the presence of organic-rich phases coupled with high concentrations of coniferous pollen grains (*Pinus*, *Abies* and *Picea*) in good condition, and a lack of other dateable fractions (i.e. macrofossils).

The carbonate content of the 06SD core was assessed in order to evaluate any potential hard water effects. In hard water lakes, rock contributes significantly to the carbonate ions in groundwater. Lake waters become enriched in older, dead ^{12}C in the form of dissolved carbonates, which are then fixed by photosynthetic algae (Hedges, 1991). Any dates produced from the lake sediment may therefore be older than expected (Jacobson et al., 1981). The results of carbonate content analysis carried out at NIGL (Keyworth) indicated that the core contained very low levels (<1%) of carbonate. This suggested that hard water effects were unlikely to influence dates obtained from the 06SD core. The low levels of carbonate coupled with the presence of organic-rich sediments and an abundance of coniferous pollen therefore confirmed that the sediments were suitable for AMS ^{14}C radiocarbon dating of bulk sediments and carbon fractions.

In addition, the core was sampled for dating using palaeomagnetism, to be carried out at the University of Liverpool. However, analysis and interpretation of the results proved to be very challenging and therefore the production of a palaeomagnetic chronology remains elusive.

3.6.1 AMS ^{14}C radiocarbon dating of bulk sediments

Bulk sediment samples prepared at the NERC Radiocarbon Laboratory, East Kilbride. Samples were digested in 2 ml HCl at 80°C for 8 hours, washed free from mineral acid with deionised water then dried and homogenised. The total carbon in a known weight of the pretreated sample was recovered as CO₂ by heating with CuO₂ in a sealed quartz tube. The gas was converted to graphite by Fe / Zn reduction and sent to the AMS facility for dating.

3.6.2 AMS ^{14}C radiocarbon dating of coniferous pollen concentrations

Obtaining dates from pollen concentrations involved separating pollen from other material and then dating the resulting pollen fraction. However, in practice extracting the grains is challenging and depends on a variety of complex and interconnecting factors and has led to the adoption of this technique on a limited scale. A number of studies have been undertaken to try to develop efficient methods for extracting pollen concentrates from sediments, but with limited success (e.g. Regnell, 1992; Brown et al., 1989). Many of these studies also compared pollen concentration dates with established chronostratigraphic markers to test for agreement between resulting dates (Wohlfarth, 1996).

One of the first methods was initially published by Brown et al. (1989), and updated in Brown et al. (1992). Brown et al. (1992) explored ways of extracting pollen concentrations from peat samples taken from a bog in Washington, USA, which are associated with the Mazama Ash layer. They began by testing whether it was possible to use standard palynological sample preparation methods outlined in Faegri et al. (1981). The resulting samples were examined under a microscope, which revealed that they contained amorphous debris and pollen. They therefore concluded that the method was not effective enough for extracting pollen concentrations for dating purposes. Instead, Brown et al. (1992) propose using chemical treatments to remove carbonates, silicates, humic acids and amorphous organic carbon, followed by sieving of samples at 88, 44 and 20 µm, to try and isolate the pollen fraction. They discovered that the 44 - 88 µm fraction treated with NaOCl (rather than standard acetolysis treatment) was composed of clearly identifiable coniferous grains including *Pinus*, *Picea*, *Pseudotsuga menziesii* and *Abies*. Previously, Brown et al. (1989) suggested that 200 - 500 *Picea* pollen grains are sufficient to obtain one AMS date, which is low compared to estimates provided by other researchers.

Brown et al. (1992) conclude that the technique is effective in producing a pollen extract. However, the approach was only partially successful in isolating the coniferous pollen grains because the pollen extracts still contained some residual non-pollen material. In addition, the authors did not quantify the purity of their samples, or discuss how pure a sample should be in order to be viable for dating. The ^{14}C dates produced from the pollen extracts are consistent with bulk sample dates obtained from the Mazama Ash layer, but it is not clear whether the resulting pollen dates are more accurate or precise than the bulk dates.

The method pioneered by Brown et al. (1989) was adapted by Regnell (1992) for use with lake sediments containing smaller deciduous pollen grains, using slightly different chemical treatments and a smaller sieve mesh. Dates obtained from bulk samples were compared to those obtained from pollen concentrates against a dateable horizon based on an *Ulmus* decline in the Holocene *Sphagnum* peat sequences in Northwestern Europe. The dates inferred from the resulting pollen concentrates are closer to the expected dates for the *Ulmus* horizon than the dates obtained from bulk sediments. Also, the pollen concentrate is ~1000 years younger than the bulk date obtained from the same interval, and closer to the expected age suggested by the *Ulmus* decline. The author reports that a 'pure' pollen sample was produced using this method.

However, the purity of the sample is not quantified, and no details are provided on the volume of the extracted pollen sample. Regnell (1992) concludes that the method should be adjusted to suit sediment composition and pollen flora contained within the samples under investigation.

Mensing et al. (1999) argue that the abovementioned methods are not selective enough to produce a datable sample. They created an alternative method which involves the same chemical treatment of the samples as outlined in Brown et al. (1989), but omits sieving in favour of hand picking of individual pollen grains using a 'bespoke mouth pipette'. They successfully extracted a sample of *Picea* pollen grains for AMS ^{14}C radiocarbon dating from lake sediments associated with the Mazama Ash layer from Sierra Nevada, California and from varved marine sediments of known age from the Barbara Basin, California. The authors contend that the technique is very effective for extracting pollen grains from other material, is inexpensive and does not require specialist equipment.

Comparison with bulk sediment dates from the same intervals and known horizons suggested the pollen concentrates extracted using a pipette produce dates that are more accurate. However, this approach is time consuming and labour intensive, because it involves the individual extraction of pollen grains from the source sample.

If only smaller pollen is available, then Mensing et al. (1999) suggest that approximately 10,000 grains (ca. 70 µg of carbon) are required in order to reduce difficulties associated with preparing very small samples for dating. This estimate differs significantly to Brown et al. (1989), by several or orders of magnitude.

In a more recent study, Vandergoes et al. (2003) sought to date Late Quaternary pollen concentrates from a peat bog in south Westland, New Zealand. The aim of the study was to produce an effective extraction method for sediments containing small pollen grains (<50 µm) and where limited sediment is available for dating. They propose using chemical treatment and sieving, followed by density separation of the inorganic material from the lighter organic matter using the heavy liquid Sodium Polytungstate (SPT).

Most tree and shrub species were found to separate off between 1.15 and 1.2 s.g., with little organic residue. However, the technique does not completely remove all of the organic residue and plant fibres from the samples. Although the authors do not quantify the purity of the pollen concentrates produced, they were unable to obtain dates from very small extracts (<0.1 mg). Dates based on pollen concentrates provided consistently older dates compared to bulk sediments, which they argue are less likely to be influenced by contamination, and therefore provide age estimates closer to the actual age of the sample.

Overall, the studies published to date indicate that it is possible to extract pollen concentrates from lake sediments for AMS ¹⁴C radiocarbon dating, using singular or combined techniques. Dates based on pollen concentrations appear to be more accurate than bulk sediment dates, based on comparison of these dates with known chronostratigraphic horizons. Coniferous pollen grains are particularly useful because the extent of damage to the air sacs can be used to assess sediment reworking, which may produce inaccurate dates.

However, presently these techniques have some significant drawbacks. Firstly, with the exception of labour intensive mouth pipetting, none of the techniques described have resulted in the production of pollen samples free of other non-pollen material, including material from mixed carbon sources. This is attributed to the resistance of non pollen material to chemical treatment or samples containing material that is the same density as the pollen grains being extracted, meaning that it is difficult to separate off the pollen grains. Currently, researchers account for these uncertainties into their assessment of dates produced from pollen concentrates using other information such as the type of sedimentary environment (and associated reservoir effects) and the results of other dating exercises on the same sediments.

Secondly, estimates of the degree of purity of pollen sample required for dating is described qualitatively rather than quantitatively. Quantitative estimates would facilitate cross comparison of dating results based on the same extraction techniques. Thirdly, the estimated volume of pollen required in order to produce a reliable date varies from study to study and is expressed in terms of absolute pollen counts (ranging from 200 - 10,000 grains) to measurements in mg (typically starting from 0.1 mg). Clearly there is a need to standardise terms and measurements to facilitate a consistent approach.

Refinement of existing methods or development of new techniques is required in order to obtain more accurate dates from pollen concentrations. Furthermore, the extraction process for lake sediments has not been fully established. For the purposes of this study, a new method of extraction was devised. The results of this exercise are presented in Chapter 4.

3.7 Concluding remarks

This chapter summarises the multi-proxy approach and dating techniques employed during completion of this research. A variety of methods are used in order to produce a detailed picture of past and present conditions at Lake Shudu. Pollen and organic analyses are underpinned by physical analysis of the sediments to characterise lake / vegetation dynamics and catchment processes, and inferred climatic conditions. The results are presented in subsequent chapters.

4 Results

4.1 Introduction

The following chapter presents the results of fieldwork carried out at Lake Shudu in March 2006. During this visit, a site investigation was undertaken and a long core (06SD) was extracted from the lake. The core was dated and analysed using the multi-proxy methods outlined in Chapter 4. The results are presented below. This chapter addresses Objectives d and e of this research, outlined in Chapter 1.

4.2 Site investigation

A detailed site investigation was undertaken (1a - k) to establish catchment extent, geology, hydrology and vegetation type (Table 4-1). Plant and sediment samples were collected from key parts of the lake catchment (2a - e). These were required in order to establish a modern baseline for palaeo-organic analysis (see Section 4.5.1). The site investigation is complemented by a detailed desktop survey of published and unpublished literature (e.g. climate data, geological reports, site surveys, etc.) pertaining to northwestern Yunnan and / or Lake Shudu. The results of both exercises are reported in this chapter.

Ref	Task	Subtask	Description	Sample Quantity	Type of analysis
1a	Site survey (3 days)	Site investigation	Sketch of lake and surrounding catchment showing major vegetational features.	N/A	Palaeoecol.
1b		Water depth	Record lake water depths from shore to primary areas of sedimentary deposition, esp at coring site.	N/A	Physical
1c		Modern plants	Visual investigation of modern vegetation growing near the lake.	N/A	Organics
1d		Inflows/outflows	Record lake inflows / outflows and mark positions on sketch map.	N/A	Organics
1e		Erosion / deposition rates	Record erosion points on sketch map and determine rate of deposition. Mineral magnetism measurements.	N/A	Physical
1f		Geology	Geological features including collection of in situ geological samples.	6 samples	Physical
1g		Slope	Catchment slope measurements.	N/A	Physical
1h		Photographs of site	Photographs of the lake and catchment.	N/A	Physical
1i		Wind patterns	Determine predominant wind speed and direction.	N/A	Physical
1j		Catchment definition	Establish catchment extent by through visual and cartographical analysis.	N/A	Physical
1k		Determine the lake water pH	Establishing the pH of the water to clarify any possible effects on radiocarbon age.	N/A	Dating
2a	Collection of modern plant samples (1 day)	Living plant samples	Collect living plant samples from major vegetation zones across the catchment.	100g per sample	Organics
2b		Soil samples	Establish main areas of vegetation in the catchment, then collect soil samples from these locations.	2-4g	Organics
2c		Stream sediment	Collection of sediment from inflowing streams.	2-4g	Organics
2d		Marginal lake vegetation	Collect plant samples from the lakeside.	50-100g	Organics
2e		Surface lake sediments	Collect samples from within the lake, at the margin and centre.	50-100g	Organics
3a	Sediment core (2 days)	Take a core from Lake Shudu	Use platform corer to extract a sediment core from the central part of the lake and sample in the field.	1 long core	All

Table 4-1: Lake Shudu site investigation tasks.

Lake Shudu, also known as Shudu Hai (Lat: 27°54.616'N; Long: 99°56.974'E) is located in Zhongdian County, northwestern Yunnan Province (Figure 1-1, Figure 4-1 and Figure 4-2). It is a high altitude lake situated ~3630 m asl, on the edge of the Tibetan Plateau. The catchment is approximately 14.3 km², whilst the lake covers an area of approximately 1.7 km². It is relatively shallow, reaching a maximum depth of 7.8 m (Figure 4-2), and has a secchi depth of approximately 1.4 m (Boyle et al., 2000). Lake Shudu is approximately 2.27 km in diameter, and therefore the pollen deposited in the lake probably reflects regional vegetation and inferred climatic conditions (Figure 3-3; Jacobson et al., 1981).

Lake Shudu is an open lake, having at least nine inflows, a spring supplying groundwater to the lake (northern shore) and one outflow (Figure 4-3). A number of heavily eroded slopes appear particularly on the eastern part of the Shudu basin. It is likely that these contribute water from the surrounding mountains as runoff. Based on the estimated pollen source area and the site altitude, it is likely that the pollen record reflects the regional as well as the local pollen component. In this case, the region is southwestern China, encompassing the municipality of Chongqing, the provinces of Sichuan, Yunnan and Guizhou and the Tibet Autonomous Region.

A dam has been built across the outflow. Boyle et al. (2000) estimate that this was built some time after 1970, in order to raise the water level by approximately 1 m. A further dam has also been constructed about 200 m downstream from the outflow, creating a new smaller lake. Boyle et al. (2000) explored the shoreline of Lake Shudu and found a strip of reed marsh running parallel, and set within the present lake shoreline; possibly evidence of a rise in water level, which resulted from the installation of the first dam. Downstream from the new lake is an ancient river terrace, flanked by a 'V' shaped valley with heavily eroded sides, possibly formed in response to rapid downcutting triggered by upstream glacial activity. A road has been constructed to allow easier access to Lake Shudu, and a guesthouse and boat hiring facilities are located near the lake outflow to accommodate tourists visiting the site.



Figure 4-1: Lake Shudu, Yunnan Province, China, looking northeast.

This image has been removed by the author of this thesis/dissertation for copyright reasons.

Figure 4-2: Map of the Lake Shudu catchment, Yunnan Province.

Outer dashed line = catchment boundary; solid line = present water line; bold line = outflow dam. Lake depths are shown in metres. Depths are shown in metres. The core extraction points are represented by two black dots; one in the centre of the lake (at 7.8 m) and one on the eastern shoreline.

Adapted from Boyle et al. (2000).

4.2.1 Geology / geomorphology

Located high up in the foothills of the Himalayas, the catchment geology includes igneous and metamorphic rock types including quartzites and mica schists, limestone and sandstone (Figure 4-4 and Figure 4-5). Glacial landforms including lateral and terminal moraines are possibly present in the catchment (Figure 4-3). What appear to be lateral moraines run parallel to the catchment sides (Figure 4-6). These landforms are composed of sharp angular rocks commonly formed by glacial activity. Just beyond the lake outflow, there is an elongated landform that resembles a terminal moraine (Figure 4-7 and Figure 4-8). However, a road has been constructed on top of the terminal moraine, which may have modified its appearance (i.e. flattening the top of the landform, or sediment movement), and hinders positive identification. Alternatively, the landform could be an ice contact delta (Fogwill, pers comm.). It is difficult to conclusively establish the identity of these features based on available evidence. Nevertheless, fluvio-glacial deposits of finely ground bedrock and brecciated quartz are present on the western shores of the lake (Figure 4-3; Figure 4-9), which suggests that the catchment was subject to glacial activity at least once in the past.

Observed fluvial features include laminated fluvial deposits located on the eastern outflow (Figure 4-10). Alluvial fans are present below all tributaries, including one that partially blocks the outflow (Boyle et al., 2000). The surface of this terrace was approximately 4 m above the present water level, positioned at the same height at the oldest downstream terrace (Boyle et al., 2000). In the absence of any sink holes in this part of the catchment, Boyle et al. (2000) conclude that the fans were formed only at the margin of the basin because the central area was filled with ice. Ice would have prevented sediment accumulation in the lake, whilst allowing fluvial transport of sediment along its margins during deglaciation and supplying sediment to the outflow areas, resulting in the development of an alluvial fan (Boyle et al., 2000).

Slopes of varying steepness surround Lake Shudu. The northern and eastern slopes are gentler than the western slopes. The change in height from the observed water line to ground level is estimated to be 1.5 m, 6 m and 8 m for the eastern, northern and western slopes respectively. It was not possible to measure the southern slope steepness because the shoreline was not accessible. Differing slope heights may be the result of glacial action transporting / depositing debris from the valley inlets in the north and east to the outlet in the west and increasing the slope angle on the western shoreline. There is also evidence that the lake level was higher in the past, indicated by the presence of a terrace on the western side of the lake (Figure 4-11). The modern mean sedimentation rate of Lake Shudu is low (~ 0.01 cm / yr) and possibly related to changes in ice cover / catchment stability. Overall, the catchment geomorphology appears to be influenced by glacial activity, which accords with other evidence for past glacial activity in this region (see Chapter 2).



Figure 4-3: Map showing the key geomorphological and geological features in the Lake Shudu catchment.



Figure 4-4: Limestone outcrop, southeastern shore of Lake Shudu.

Figure 4-5: Exposed facies with limestone bedrock covered fluvial deposits and thick topsoil, northwestern shore of Lake Shudu.



Figure 4-6: Lateral moraine, southeastern shore of Lake Shudu.



Figure 4-7: Landform located just after the lake outflow, to the southwest of Lake Shudu.

This landform could be a terminal moraine, an ice contact delta or flat lying lake sediments. A road has been constructed on top of this landform, which may have modified its appearance.



Figure 4-8: Closer view of landform located just after the lake outflow to the southwest of Lake Shudu.

The raised ground level and Lake Shudu Valley are visible in the background.



Figure 4-9: Angular, unsorted fluvio-glacial deposits located on the western shoreline of Lake Shudu.



Figure 4-10: Laminated fluvial deposits located on primary inflow, eastern shoreline of Lake Shudu.



Figure 4-11: Palaeoshoreline running parallel to the present day western shoreline.

The black line denotes the position of the visible section of palaeoshoreline.

4.2.2 Climate

Inferences about the modern climate at Lake Shudu were derived from the best available precipitation and temperature measurements obtained from the nearest gauging stations to Lake Shudu; at Dali (25°N; 100°E) and Zhongdian (27°N; 99°E), Northern Yunnan.

4.2.2.1 Temperature

Mean monthly (24 hr) temperatures were calculated for Dali, which is located ~1191 m asl (Figure 4-12). The dataset included temperature readings for 539 months, spanning the period 1939 - 1988, collated by the Global Historical Climatology Network (GHCN, 2009). The results indicated that mean monthly temperatures were generally quite low during this period, reaching >20°C in July and <9°C in December / January. The modern climate is therefore characterised by cold winters and mild summers. Mean annual temperatures were in the region of 15°C, compared to a MAT of 0°C associated with the alpine meadows of the Tibetan Plateau located at a similar altitude (Zhao et al., 2009) and <10°C in the montane sclerophyllous *Quercus* forest patches located at ~3100 m asl in the Jinsha Valley, Yunnan Province (Li et al., 1986).

Mean temperature is likely to be >21°C lower at Lake Shudu compared to sea level, due to differences in environmental lapse rate at each site, although this assumes no moisture and a constant atmospheric temperature. Adiabatic lapse rates for China were calculated using temperature records derived from 671 Chinese meteorological stations for the period 1951 - 1980 (Fang et al., 1988). Annual mean values were therefore calculated to be in the range of 3 - 6°C / 1000 m. Walker (1986) suggested a mean lapse rate of 5°C / 1000 m for Lijiang, northwestern Yunnan (3900 m asl), which is aligned to the annual mean rates identified by Fang et al. (1988). Estimated rates are low and are aligned to the estimated lapse rates for moist climates (Stull, 2000), suggesting that effective moisture is an important control upon the climate of NW Yunnan Province.

It is important to note that Dali is located at a lower altitude than Lake Shudu. As altitude increases, air pressure and temperature decrease. Lake Shudu is located 2500 m above Dali. Based on a mean moist lapse rate of 5°C / 1000 km, it is therefore assumed that mean annual temperatures are 10 - 12°C lower at Lake Shudu than at Dali. However, lapse rates also vary seasonally (Fang et al., 1988). Mean July temperatures at Lake Shudu are therefore estimated to be ~13°C, whilst mean December temperatures are estimated to be ~0°C. Consequently, the local climate at Lake Shudu is characterised by relatively warm summers and cold but mild winters compared to other parts of the Tibetan Plateau at similar altitudes (Zhao et al., 2009).

Summer temperatures are attributed to the increased levels of annual solar radiation reaching the Tibetan Plateau. This effect is particularly strong during the summer months. Also the blocking effect of the mountains to the north of the Plateau, which prevents cold Siberian air masses from reaching the Plateau (Fang et al., 1988) helps to maintain higher than expected temperatures. A summer temperature gradient extends across the Tibetan Plateau, running from east ($\sim 7.8^{\circ}\text{C}$) to west ($\sim 17.5^{\circ}\text{C}$) (Zhao et al., 2009). In addition, milder conditions at Lake Shudu are possibly a function of the lake's latitudinal position on the temperate / subtropical boundary (Fan et al., 2009).

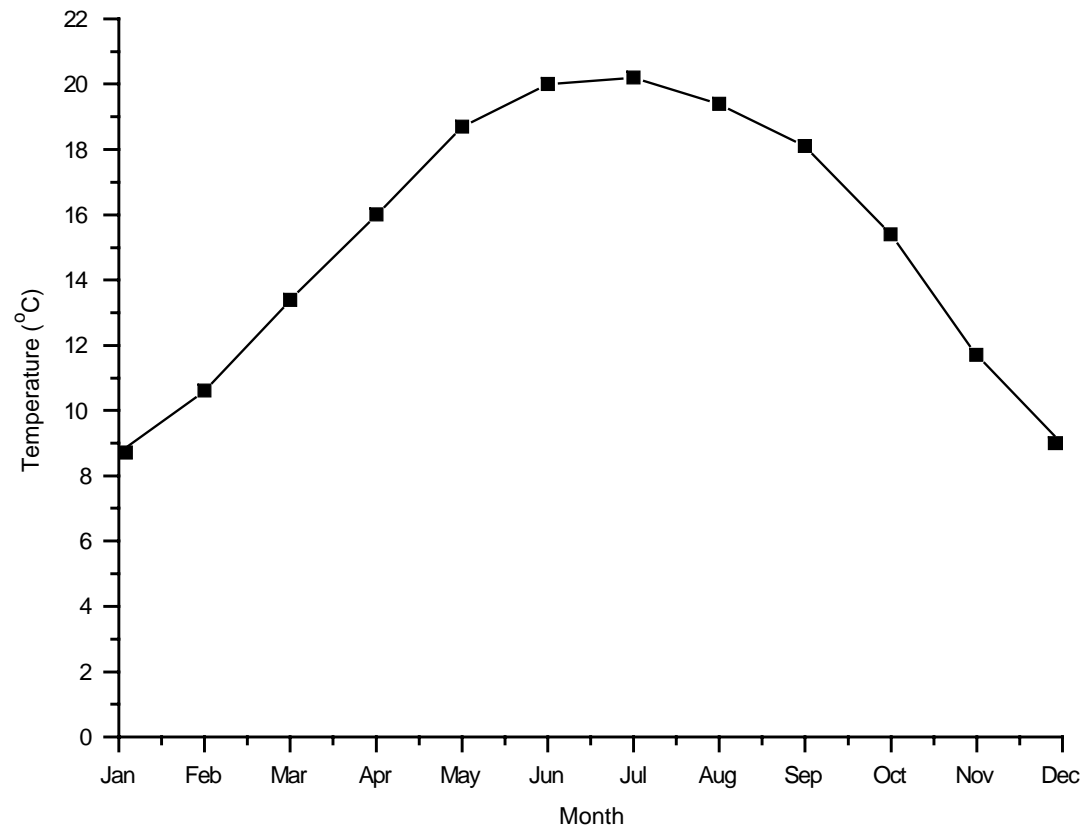


Figure 4-12: Mean monthly temperatures for Dali, Yunnan Province, 1939 - 1988.

Source: GHCN (2009)

4.2.2.2 Precipitation

Mean monthly precipitation rates, and maximum / minimum values (Figure 4-13) were calculated using data provided by NIGL (China) for Zhongdian, northwestern Yunnan Province for 360 months in the period spanning 1972 - 2002. Zhongdian is located 3160 m asl and is located at the same latitude / longitude as Lake Shudu. The results indicated that precipitation levels peaked during the months of July and August, averaging 160 and 151 mm whilst the winter months (December - February) were markedly drier, averaging just 5, 8 and 14 mm respectively. This indicates that most of the precipitation falls during the monsoon rainy season (June to October). The climate of northwestern Yunnan is therefore characterised by very dry winters and relatively humid summers.

The precipitation profile also has affinities with the Indian Monsoon profile (i.e. enhanced precipitation in spring and summer) (Shen et al., 2005a; Hodell et al., 1999). This precipitation record also demonstrates the high variability of the monsoon on the interannual scale, reflected in the wide range of measured rates, particularly in the summer months.

Mean annual precipitation rates were calculated to be ~600 mm, compared to MAP rates of >400 mm in the alpine meadows of the Tibetan Plateau located at a similar altitude (Zhao et al., 2009) and 700 - 900 mm associated with the montane sclerophyllous *Quercus* forests growing at ~2600 m asl in the Jinsha Valley, Yunnan Province (Li et al., 1986). A precipitation gradient runs from east (~530 mm) to west (<20 mm) on the Tibetan Plateau, indicating that higher rates of precipitation occur in eastern parts of the Plateau compared to the west (Zhao et al., 2009).

Together, the temperature and precipitation data indicates that at the end of the last century, the climate of northwestern Yunnan was characterised by cool humid summers and very cold dry winters associated with the Asian monsoon (Tang, 2006). Because of the effect of lowering temperatures with increasing altitude, local temperatures are comparable to the alpine meadows located at a similar altitude on the Tibetan Plateau. However, differences in precipitation are observed. Rates are higher at Lake Shudu than on the Tibetan Plateau, but lower than regions to the south such as the Jinsha Valley (Li et al., 1986). The difference is therefore likely to be the result of the lower latitude location of Lake Shudu (and associated increases in precipitation towards the tropics) coupled with its position on the southeastern corner of the Plateau, where precipitation rates are highest relative to rates observed to the west on the Plateau (Zhao et al., 2009; Fan et al., 2009).

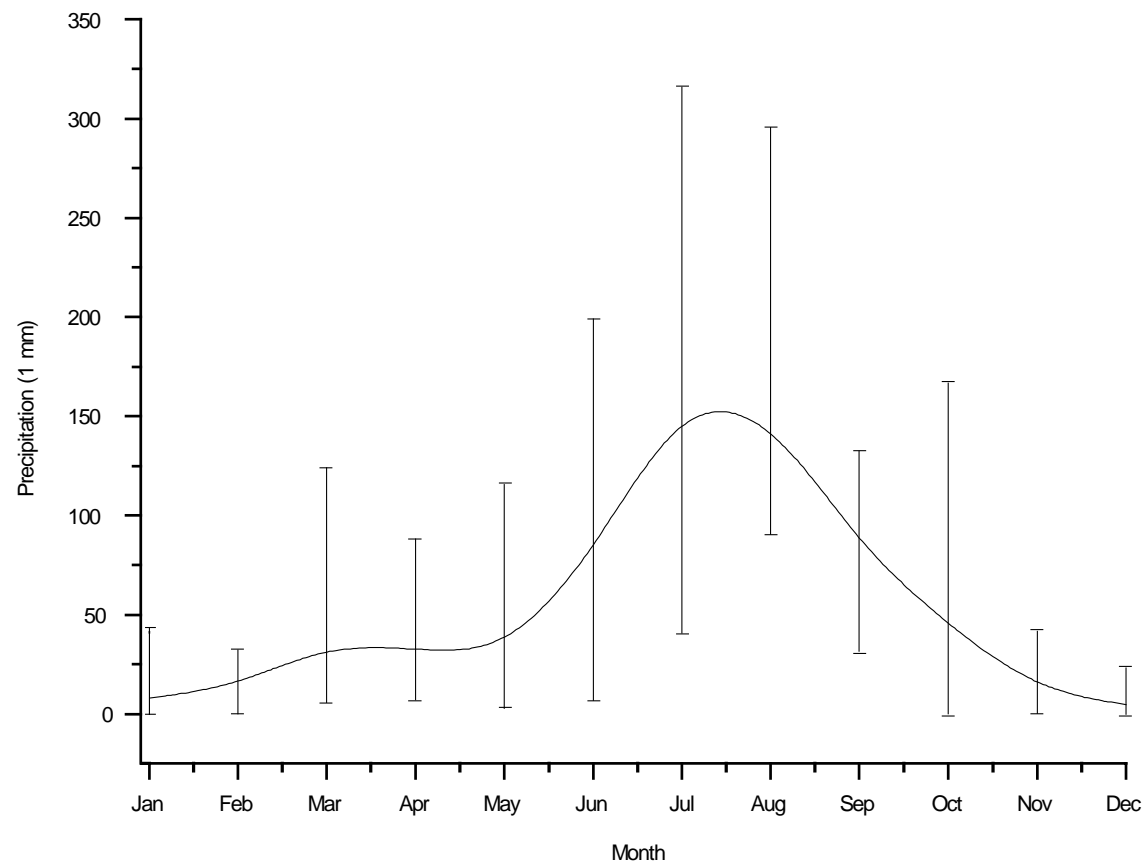


Figure 4-13: Mean monthly precipitation rates and maximum / minimum monthly precipitation (in mm) for Zhongdian, Yunnan Province, 1972 - 2002.

Source: NIGL (China).

4.2.3 Vegetation

In the Hengduan Mountains of northwestern Yunnan, the subalpine vegetational zone is located between 2800 and 3900 m asl (Fan et al., 2009), whereas the alpine zone is currently located between 3800 and 5200 m asl (Sherman et al., 2008). Lake Shudu is therefore within the subalpine zone. This suggests that it is located in an ecotone (a transition zone between the alpine and subalpine zones), and therefore supports the growth of both alpine and subalpine species (Zhang et al., 2006a; Korner et al., 2004). Its latitudinal position also means that a number of temperate and subtropical taxa (including species of Passifloraceae) are able to grow in the catchment (Fan et al., 2009).

In southwestern China today, the upper treeline for all arboreal taxa is placed at 4000 m asl (Lu et al., 2008; Peng et al., 1997). Above the treeline are shrubland, steppe and alpine meadow. Cold boreal alpine coniferous forests dominate at the treeline. Below the treeline are subalpine coniferous forest, cool mixed montane forest, semi-evergreen forest, evergreen broadleaved and then monsoon forest at lower altitudes (Thomas et al., 2007; IPCC, 2007b). The upper treeline is currently located 600 m above Lake Shudu. Catchment vegetation is likely to be sensitive to changes in the altitudinal position of the treeline, which will be reflected in changes in the presence, absence and relative abundance of arboreal taxa in the pollen record.

The site investigation revealed that Lake Shudu presently supports a range of arboreal, shrubby and herbaceous alpine and subalpine species. The current vegetation assemblage is dominated by *Picea* and *Abies* stands, which have been planted for timber (Figure 4-14 and Figure 4-15). Before the implementation of the National Forest Protection Programme in 1988, forestry activities (logging and timber) accounted for 80% of the local revenue in Yunnan Province. After 1998, the local government shifted activities to tourism, mining and hydropower (Leefers, 2005).

Grazing lands composed of grassland vegetation also dominates the landscape. Sites located at elevations above ~3000 m asl gives rise to lower temperatures and reduced moisture availability, which enables frost-tolerant species of *Pinus*, *Abies* and *Picea* to thrive (Shen et al., 2005b). Mixed montane forest stands of deciduous and coniferous species, dominated by *Picea*, *Abies*, *Betula* and evergreen *Quercus* occupy the steepest slopes surrounding Lake Shudu, whilst grassland and scrub dominate the valley floor and shoreline zones.

The southern and northern slopes are dominated by subalpine coniferous stands of *Abies* and *Picea* (Figure 4-15) and Cupressaceae including *Abies Georgei* and *Sabina squamata* (Cao, 2007). The uniform nature of these stands suggests that they are plantation stands. Some of the larger *Picea* trees are over 30 m tall and have a tree base diameter of 1 m (Boyle et al., 2000), which corresponds with historical records that suggest that these stands were planted during the 1970s. *Pinus* stands containing lone *Tsuga* trees suited to alpine conditions are confined to the ridges and dry upland south-facing slopes. Lichen and mosses grow on many of these trees. The forest understorey includes herbaceous alpine species including *Juniperus*, *Acer*, *Sorbus*, Passifloraceae and many species of the Ericaceae genus (Figure 4-16) and Rosaceous genera, such as *Rosa omeniensis*.

The north and eastern slopes are dominated by species of evergreen sclerophyllous *Quercus*, which favour the more exposed and thin soils of these slopes (Figure 4-17 and Figure 4-18). It is common for species of evergreen *Quercus* to grow as shrubs or small trees in response to the cooler, drier conditions often found in high altitude locations. It is a hardy genus, which has a wide ecological tolerance. Chinese evergreen *Quercus* is a relic of the Mediterranean subtropical vegetation evolved from sclerophyllous *Quercus* forests of the Tethys following the uplift of the Himalayas. Nine primary species of evergreen oak grow in northwestern Yunnan, including *Q. aquifolioides* Rehd. et Wils., *Q. pannosa* Hand.-Mazz., *Q. monimotricha* Hand.-Mazz., *Q. longispica* (Hand.-Mazz) A. Camus, *Q. guayavaefolia* Levl., *Q. gilliana* Rehd. et Wils., *Q. cocciferoides* Hand.-Mazz., *Q. franchetii* Skan, and *Q. pseudo-semecarpifolia* A. Camus (Tang, 2006). *Gentians* and *Polygonums* grow in the understory.

A mixture of arboreal species, which can tolerate wetter conditions, such as *Salix* and *Betula*, dominate the transition zone between shore and slope. *Betula* grows in the more sheltered conditions on the south and western slopes (Figure 4-19). *Salix purpurea* grows near to the shoreline, where conditions are moist or waterlogged (Figure 4-20). Species of *Quercus*, *Cyclobalanopsis*, *Salix* and *Betula* commonly grow across Yunnan (Li et al., 1986).

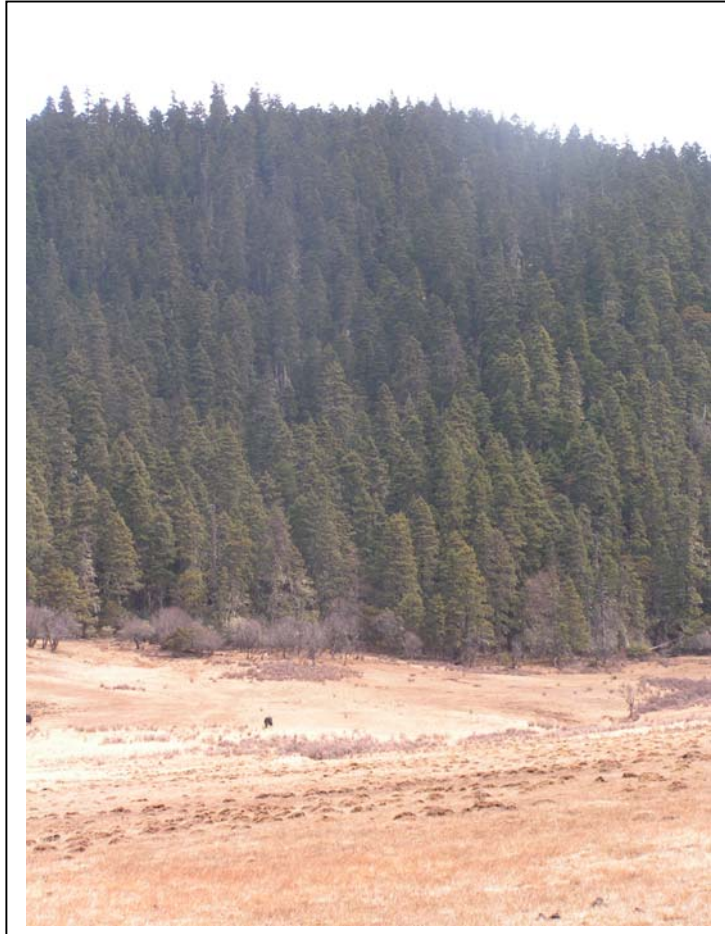


Figure 4-14: Mixed subalpine coniferous forest stand including *Abies Georgei*, southern slope of Lake Shudu.



Figure 4-15: Coniferous trees, southern slope of Lake Shudu.



Figure 4-16: A member of the Ericaceae family growing at Lake Shudu.



Figure 4-17: Evergreen *Quercus* stand, western slope of Lake Shudu.



Figure 4-18: Evergreen *Quercus* leaves, Lake Shudu.



Figure 4-19: *Betula* stand growing on the western slope of Lake Shudu.



Figure 4-20: *Salix purpurea* stand growing adjacent to a large outflow, northwestern valley floor, Lake Shudu.

Grassland and peat bogs are present on the valley floor (Figure 4-21). Species of Poaceae, Cyperaceae, Rosaceae (including *Potentilla*) and Gentianaceae, Iridaceae and Berberidaceae are abundant. The grassland areas are primarily used for grazing cattle and horses. There is a dirt track running along the shoreline on the western side of the lake, and several species of Poaceae were observed growing by the side of the track, presumably having been brought in on the wheels of carts, vehicles, or by humans and animals. The immediate shoreline is largely bog and / or peatlands, dominated by species of Poaceae and *Sphagnum*.

Macrophytes grow just below the water line near to the lakeshore. The pH of the water was measured as pH 8.7, which is alkaline. Conductivity measurements showed the lake is 23.6 mS, indicating low levels of dissolved salts. Salts leach from surrounding rocks in the catchment, so a low dissolved salt content suggests that catchment weathering rates are presently low.

Today, one or two small huts have been constructed on the eastern shoreline of Lake Shudu (Figure 4-22). Herders use them during the summer months when grazing yaks and horses on the grassland near the shores of the lake (Figure 4-23). Boyle et al. (2000) discovered that local people use drift nets to catch fish in Lake Shudu, although this remains a relatively small-scale operation.



Figure 4-21: Grassland and peatbog areas, eastern shoreline of Lake Shudu.



Figure 4-22: Herder hut, eastern lowlands of Lake Shudu.



Figure 4-23: Yaks grazing, western shoreline of Lake Shudu.

4.3 Core recovery

In March 2005, scientists from the University of Exeter and NIGL (China) participated in an expedition to Lake Shudu, Yunnan Province China to undertake a preliminary site investigation (see Chapter 3 for details) and collect a short core to be subjected to multi-proxy analysis to assess the potential of the proxy record for recording past environmental changes. A bathymetric survey was undertaken by scientists from NIGL (China) in order to guide the coring operation (Figure 4-2). A short core (05SD) measuring 120 cm in length was extracted from Lake Shudu using a tapper corer suitable for extracting cores ~1 m in length from lakes (Smol et al., 2001b). The core was subsampled in the field at 0.5 cm intervals and transported back to the UK. Samples were freeze-dried and subjected to multi-proxy analysis as part of the pilot study for this PhD project.

The results of the pilot study indicated that Lake Shudu was a viable study site, potentially able to yield a long core spanning the Late Pleistocene - Early Holocene Period, which was the primary period of interest. In March 2006, the team therefore returned to Lake Shudu to collect a suite of long and short cores. A long core (06SD) measuring ~7.2 m in length was extracted from the centre of Lake Shudu (shown at a depth of 7.8 m on Figure 4-2), using a Kullenberg Uwi-Tech Coring Platform System. The 06SD core formed the focus of this research.

The long core was extracted in four sections with 30 cm overlaps (06SD1, 2, 3 and 4) and subsampled in the field using a bespoke core fractionator designed by Dr Zhang (NIGL China). Samples were transferred to labelled plastic bags and sealed for transit back to the UK. On arrival, the samples were freeze-dried and stored in the cold room at the University of Exeter. Freeze-drying the samples reduces moisture, minimising the chances of biological activity occurring, which could affect the results of organic and dating analyses. It also enables the samples to be weighed and handled more easily, particularly if the extracted sediments are very wet, as was the case with the uppermost layers of the cores.

In order to produce a composite core sequence from 06SD1, 2, 3 and 4, LOI was used to assess the extent to which the cores overlapped. High-resolution sampling at 1 cm intervals was undertaken on the top and bottom 10 cm of each core. The organic curves obtained for each core were compared and the percentage values of each interval were assessed for similarities and differences (Figure 4-24). The results indicated that there was a ~15 cm overlap between 06SD1 and 2, no overlap between 06SD2 and 3 and a ~55 cm overlap between 06SD3 and 4. Overlapping samples were removed, enabling a composite long core profile to be created (06SD), shown in Figure 4-25.

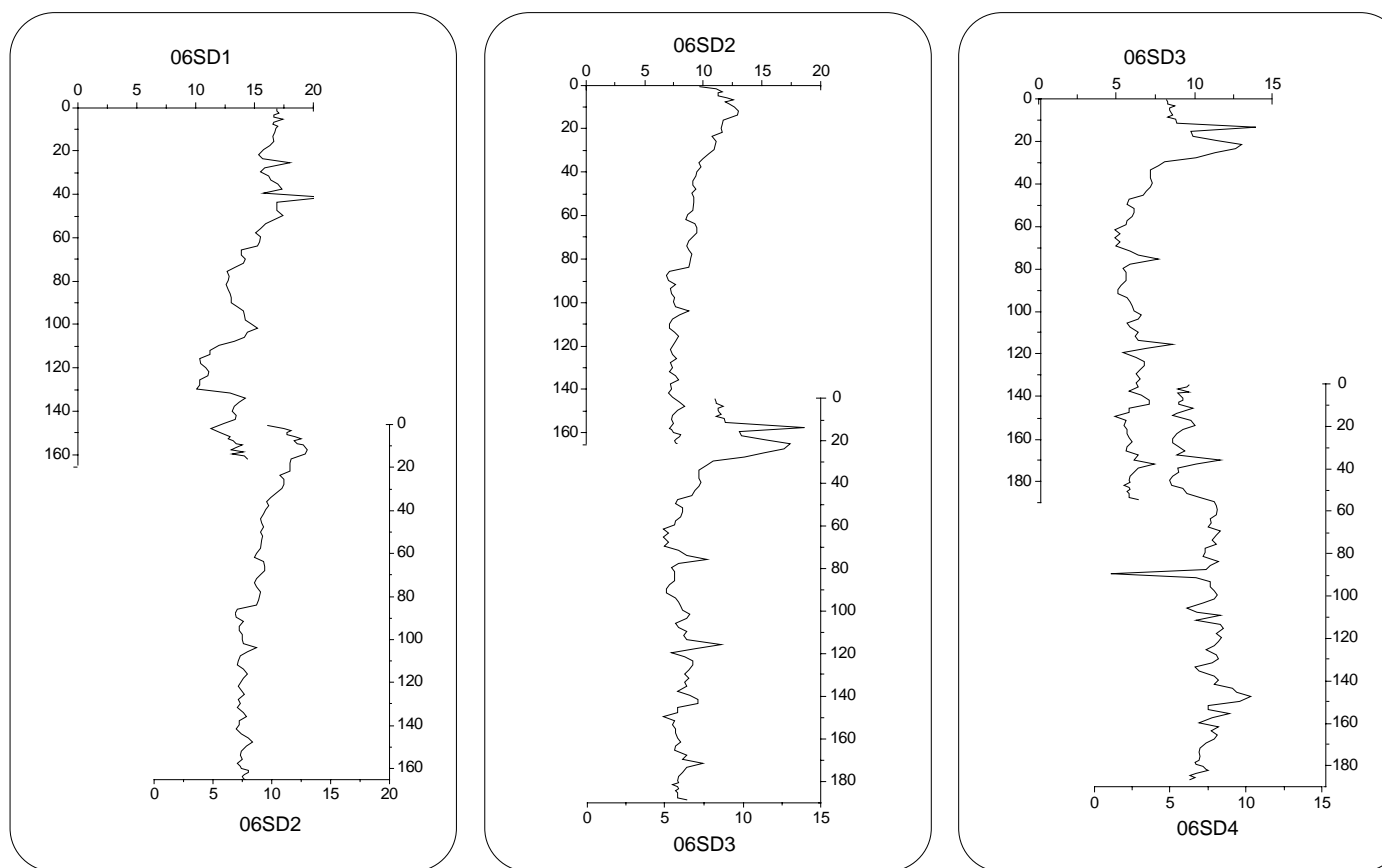


Figure 4-24: Loss on Ignition (%LOI) for cores 06SD 1,2,3 and 4 and core overlaps.

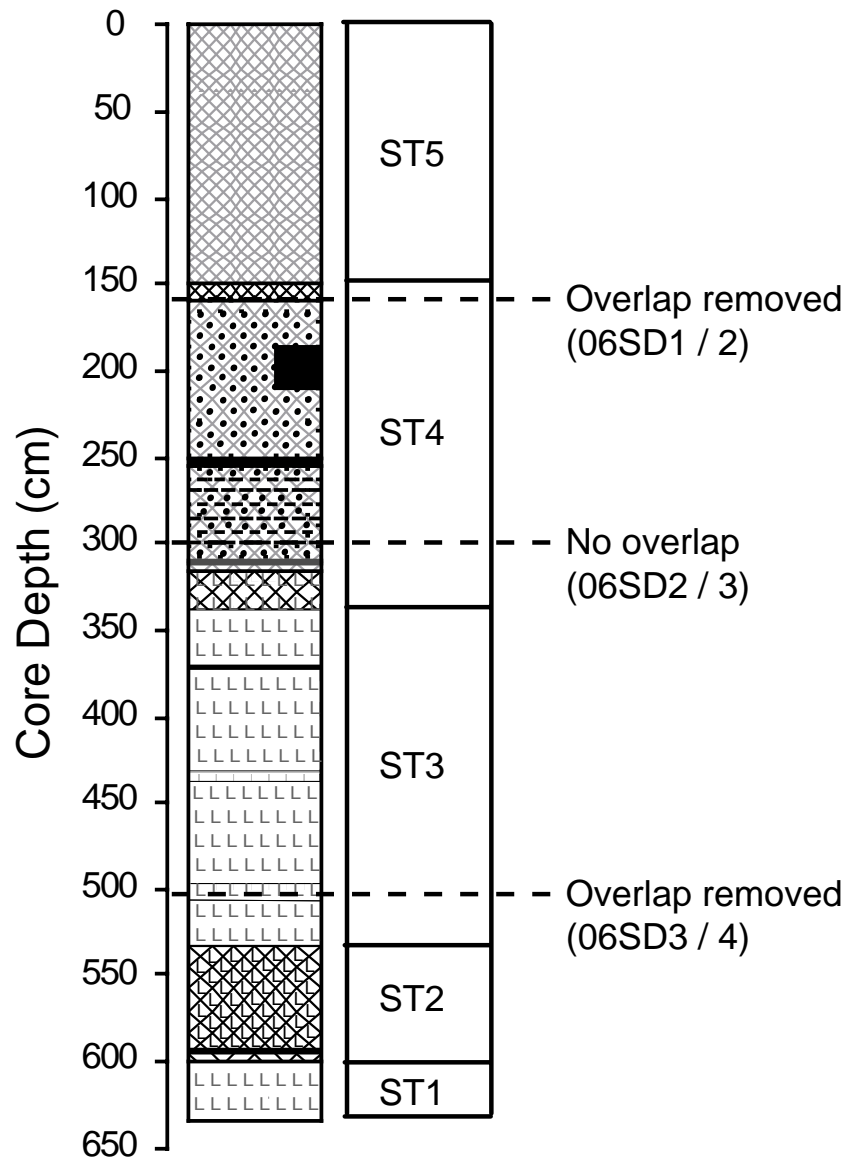
There is no obvious overlap between 06SD2 and 3

4.3.1 Selection of samples for dating

Selection of samples for dating was based upon the composite core stratigraphy, the %LOI results and the pollen record. The visual core stratigraphy revealed a number of interesting features (Figure 4-25). The lower half of the core is primarily composed of silty clay (635 - 340 cm) whereas the upper half is mainly composed of organic gyttja. The transition between each lithological phase is generally subtle. Key features include intermittent subtle banding in the middle and lower sections of the core (indicated by horizontal lines) and a period of intense banding spanning ~250 - 300 cm (dashed horizontal lines). These bands are located on major stratigraphic transition zones (594, 372, 311 and 252 cm).

Five stratigraphic zones (ST1 - 5) were determined based on the major stratigraphic shifts in the core. Zone ST1 (635 - 600 cm) is primarily composed of light grey silty clay. Zone ST2 (600 - 534 cm) is composed of organic rich sediments, which contrasts with the adjacent silt / clay rich sediments. A mixture of organic gyttja and silty clay, manifesting as subtle alternating grey-green layers was observed from 600 - 594 cm. A pronounced dark grey band was visible from 594 - 593 cm.

Mixed silty clay / gyttja sediments are replaced by light coloured silty clay at 533 cm, marking the start of Zone ST3 (534 - 340 cm). Silt / clay dominates until 503 cm. A band of darker grey silty clay is located between 503 - 500 cm. At 500 - 437 cm, the silty clay becomes lighter grey. The silty clay lightens from 437 - 433 cm, before returning to previous the colouring at 433 - 372 cm. A lighter grey sediment band was observed at 372 - 371 cm. Light silt and clay return at 371 - 339 cm. During Zone ST4 (340 - 150 cm), light silty clay is replaced by dark coloured sediment containing a mixture of organic gyttja and silt / clay (339 - 314 cm). The transition to light grey-green thick organic gyttja is completed at 314 - 311 cm. Light but subtle banding was visible between 311 - 310 cm. These shifts marked an overall transition in the 06SD core, with the stratigraphy shifting from being composed primarily of silt / clay to organic gyttja. A series of fine, light organic sediment bands occurred from ~311 - 252 cm, culminating in a darker organic band at 252 - 251 cm. Fine specks of white material were observed in the banded sediments until 160 cm. From 250 - 130 cm, the core was characterised by alternating layers of grey-green organic gyttja of varying hues. Light coloured organic gyttja occurred from 251 - 160 cm, giving rise to darker organic gyttja from 160 - 155 cm. A period of organic rich banding was observed between 155 - 150 cm, which corresponds with a 12% increase in silt. Zone ST5 (150 - 0 cm) is characterised by light grey-green organic gyttja. The top 9 cm of sediments were disturbed and therefore removed from the record.



Stratigraphy / Zones

KEY

-  Organic Gyttja
-  Silt / Clay
-  Banding

Figure 4-25: 06SD Composite core stratigraphy and zones.

Dashed lines indicate where core overlaps were removed to produce a composite core profile.

The carbon and pollen-rich sections evident in the core stratigraphy and %LOI results were assessed with reference to the pollen record (see below). These sections were preferentially selected for bulk AMS ^{14}C radiocarbon dating, to maximise the levels of dateable ^{14}C present in the samples. A limited number of bulk samples were also dated from the lower section of the core, which had a lower organic content, in order to try to obtain a chronology for the whole core. Core overlap zones were avoided. Intervals containing high levels of coniferous pollen were also selected for carbon fraction AMS ^{14}C radiocarbon dating.

4.3.2 AMS ^{14}C radiocarbon dating of bulk sediments and pollen concentrations

Coniferous pollen grains (as opposed to other pollen types) are dated where available because they offer age control, having large air sacs that are vulnerable to tearing or removal during reworking. Damage to the air sacs suggests that the grains have been re-worked and are therefore more likely to represent pollen of different ages. Samples containing grains with intact air sacs are therefore preferentially selected for dating. Overall, the error margins associated with the resulting dates are therefore likely to be less than those obtained from bulk sediments containing a mixture of carbon types and ages (Vandergoes et al., 2003).

Dates obtained from the pollen concentrates are used in this study to assess the accuracy of the bulk dates and further constrain the core chronology. NERC funding was sought for six AMS ^{14}C radiocarbon rangefinder bulk sediments dates located on (or adjacent to) stratigraphic boundaries and / or within pollen-rich phases. The objective was to establish a preliminary chronology, pinpoint the primary period under investigation and then apply for further dates (based on pollen concentrates) in order to produce a more comprehensive chronology.

A refined method for extracting pollen concentrations from lake sediment samples was developed for use in this study. This built upon previously published methods and the advice of Professor Rewi Newnham (University of Plymouth), Dr Leanne Franklin-Smith (University of Southampton) and Dr Steve Moreton (NERC Radiocarbon Laboratory).

4.3.2.1 Pollen assessment

Previous studies have indicated the importance of carrying out an initial assessment of the presence, type and amount of pollen present in order to determine suitability for pollen concentration dating (Vandergoes et al., 2003; Regnell, 1992). To avoid unnecessary wastage of 06SD sediments, two pilot tests were completed on four samples taken from the 05SD core, which was also obtained from Lake Shudu and had similar properties to 06SD.

The results of pollen analysis highlighted the zones of the core that contained high levels of coniferous pollen (i.e. several hundred grains obtained from ~0.4 g of sediment). Observed coniferous pollen grain size ranged from 50 - 120 µm. Grains were also examined in order to establish that the air sacs were generally intact, indicating that the pollen grains had not been significantly re-worked.

The method of extracting the pollen grains from sediments needed to be adapted to meet the particular characteristics of the core samples being processed (Regnell, 1992). The primary aim of the pilot testing phase was therefore to assess the efficacy of the chosen method of pollen extraction and adapt or modify the basic method to suit the 06SD core samples. Methods including chemical treatment, sieving and / or density separation were investigated on the basis that these methods had been successfully applied in previous studies. Mouth pipetting was discounted on the basis that it was too time consuming, and considered a possible health and safety risk. The conventional pollen preparation methods (e.g. Faegri et al., 1981) were also excluded for the reasons outlined in Brown et al. (1989).

4.3.2.2 Pilot test 1

The first pilot test was carried out using two samples from the 05SD core (50 - 50.5 cm and 100 - 110.5 cm), each weighing ~2 - 4 g (dry weight adapted from wet weights used in Brown et al. (1989). The choice of chemical treatments was based on those used in Regnell (1992) because this study applied to lake sediment samples, whilst sieve samples were adapted from Brown et al. (1992). The following modifications were made;

- treatment of particles smaller than 44 µm with H₂SO₄ was unnecessary because most of the coniferous pollen was >48 µm or larger (Regnell, 1992);
- 120, 80 and 48 µm nylon sieve cloths were used.

Samples were analysed under a light microscope after completion of each stage. The following issues were identified;

- treatment with Hydrofluoric acid for 20 minutes in a hot water bath did not fully remove silicate from the samples;
- treatment with NaOCl charred the samples and resulted in damage to the pollen grains;
- most of the coniferous pollen was located in the 80 - 120 µm samples. However, this fraction also unexpectedly contained large amounts of amorphous material >100 µm in size.

Overall, chemical processing and sieving of samples removed 50 - 80% of non-pollen material from the samples. The samples that contained the highest pollen concentrations (80 - 120 µm) were subjected to density separation.

The samples were separated using a Sodium Metatungstate (or SMT, which is also known as Sodium Polytungstate) solution. Density was measured using a hydrometer and then the SMT was added to the samples, beginning at a density of 2.1 s.g. following the method outlined in Vandergoes et al. (2003). Very little information is given in the literature relating to the practical aspects of density separation. It was therefore necessary to trial different techniques to determine the most effective ways of achieving separation.

The first attempt at density separation highlighted the following issues;

- the published method flow diagram is flawed. It states that if starting at a heavier density, the separated fraction is contained within the supernatant and should be decanted and stored for analysis. However, this is incorrect because the heavier material sinks whilst the lighter material floats to the surface. Consequently, the precipitate contained the separated fraction;
- no published formula exists to determine the ratio of water to powdered SMT needed to make up a solution of a given density. The amounts therefore had to be estimated, which was time-consuming. Density fluctuates with ambient temperature, therefore the density of the mixture changed frequently. This posed a significant problem when trying to accurately measure density at increments of 0.1 s.g.;
- at least five different hydrometers were needed to measure densities ranging from 2.1 - 1.12 s.g. Furthermore, the stock solution had to be of sufficient quantity to enable a hydrometer to float in it. This often meant making up significantly more than was actually required, and necessitated using a large amounts of SMT to reach the required densities;
- to minimise the chances of ambient contamination, freshly made SMT was used;
- SMT solutions are extremely sensitive to changes in the ambient temperature;
- fractions rarely separated out fully, despite repeat centrifuging;
- repeated washing / decanting lead to unacceptably high losses of pollen grains;
- the washing process increased the risk of cross contamination;
- overall, the process was very time-consuming and did not elicit satisfactory results.

4.3.2.3 *Pilot test 2*

A second pilot test was carried out on ~4 g samples taken from the 05SD core (44.5 and 85.5 cm intervals). The following modifications were made;

- testing was carried out under optimal temperature conditions for SMT;
- sample volume was increased to try and maximise the amount of pollen extracted;
- nitric acid was substituted for NaOCl;
- samples were also immersed in stronger Hydrofluoric acid (58%) for longer;
- a fourth sieve (106 μ m mesh) was added;

- fractions containing the highest levels of pollen (48 - 80 µm and 80 - 106 µm) were separated starting at a density of 2.2 s.g. and on a finer scale between 1.4 and 1.3 s.g.;
- density was measured using a precision balance instead of hydrometers;
- samples were left to stand during separation, rather than centrifuged;
- samples were sieved rather than decanted during separation.

The revised method was effective in removing more material from the samples compared to the previous method, however charring occurred after treatment with Hydroflouric acid. Furthermore, the samples still contained high levels of non-pollen material (approximately 40 - 50%). This is possibly due to using a larger volume of sediment, which may not have mixed as well with the chemical treatments. Additional sieving further facilitated the separation of pollen from larger and smaller material but samples still contained non-pollen material.

Microscopic analysis revealed that the additional separations produced much purer pollen concentrations at 1.4 and 1.35 s.g. Levels of non-pollen material were much lower (20 - 30%) in these fractions. Pollen concentrations contained less residual SMT, and grain losses were significantly reduced. This method therefore represented a significant improvement.

Based on the results of the pilot tests, it appeared that the samples either contained non-pollen material resistant to chemical treatment, or which was of a similar density as the pollen grains, making separation problematic. Ideally, samples should contain no more than 10% non-pollen material (Franklin-Smith, pers comm.), however in reality this is difficult to achieve. Hence, samples (>0.4 mg) containing 70 - 90% coniferous pollen were deemed acceptable.

4.3.2.4 *A new method for extracting pollen concentrates from lake sediments for AMS ¹⁴C radiocarbon dating*

Following further discussion of the results of pilot testing with experts at the University of Plymouth and the Chinese Academy of Geological Science, Shijiazhuang, the following modifications were introduced;

- smaller samples volumes were adopted;
- weaker Hydroflouric acid (48%) was reintroduced;
- the 120 µm sieve was replaced with a 150 µm sieve to increase the volume of coniferous pollen grains extracted.

The finalised method involved chemically treating the samples to remove inorganic and humic material, sieving the samples into fractions, and then using density separation to sort the fractions according to density, resulting in the separation of lighter pollen grains from heavier non-pollen material. Full details of the finalised method are included in A.2.1., Appendix A.2.

Samples of coniferous pollen were considered viable for dating if they were more than 70% pure pollen, based on the accuracy of dates produced from pilot samples (compared with bulk sediment samples and stratigraphic horizons identified in the pollen record). Samples <1 mg was successfully dated.

Six samples were prepared for dating. Two standard samples of bituminous coal and wood of known Holocene ages were also prepared to check for experimental inconsistencies or sample loss during chemical treatment, sieving and density separation. The samples were chemically treated and sieved according to the method in A.2.1., Appendix A.2. The 48 - 80 µm samples from 06SD1 and 2 contained the highest levels of coniferous pollen, so these samples were subjected to density separation.

The three fractions containing the highest levels of pollen concentrates were sent to the NERC Radiocarbon Laboratory (RCL), East Kilbride for dating. These were 70 - 90% pure and <1 mg in size. A bulk sediment sample was dated from the same interval as one of the pollen concentrates so that the results could be compared. Because of the lack of pollen in 06SD3 and 4, two bulk sediment samples were dated instead.

Pollen concentrates were extracted from the 06SD core in September 2006, but owing to technical issues at the NERC RCL, the samples were not processed until June 2007. The pollen concentrates and standard samples were then prepared for AMS ¹⁴C radiocarbon dating using a modified method to date very small samples, developed by the NERC RCL.

Small samples are especially vulnerable to contamination from background sources of carbon, because the potential impacts are amplified (Hedges, 1991). This can result in dating errors. Specialised processing methods were therefore employed to minimise any potential sources of contamination. This included the use of silver foil filters during sample processing. NERC RCL was confident that the modified method would be at least as good as the conventional method, which had been used successfully in the past. However, quality control tests on the 06SD samples indicated that the modified method had not produced reliable and consistent results. It was therefore not possible to obtain dates from the 06SD pollen concentrates. However, three dates were produced from the bulk sediment samples.

Following the problems encountered with the dating of the pollen concentrates and limited time left to obtain dates for the core, funding for nine AMS ¹⁴C bulk sediment dates spanning the length of the core was approved by the NERC Radiocarbon Steering Committee. A research time extension was also granted. Given the time and effort put into perfecting the technique for extracting pollen from the sediments, it was felt that it was important to complete these experiments.

Four samples from 06SD 1, 2 and 3 were therefore prepared and dated at the Oxford Radiocarbon Accelerator Unit (ORAU), with reference to the full pollen count and organic carbon content. These samples were generally >70% pure. To enable dates to be compared, two pollen-rich samples were taken from the same intervals as two of the bulk sediment dates obtained from the NERC RCL. Primary and back up samples were selected in case of sample loss.

At ORAU, the samples were weighed into pre-cleaned tin capsules with c.10 - 15 mg of ChromosorbTM to hold the liquid pollen. The ChromosorbTM was pre-combusted overnight at 350°C. It was then directly combusted in a Roboprep CHN elemental analyser interfaced with a Europe 20 - 20 IRMS operating in continuous flow mode using a helium carrier gas. The CO₂ generated was graphitised by catalytic reduction of the CO₂ onto iron in an excess hydrogen atmosphere (Dee et al., 2000). The AMS ¹⁴C radiocarbon method and instrumentation was reported by Bronk-Ramsey et al. (2004). Dates were successfully obtained from each interval.

4.3.3 Chronology construction

A total of sixteen AMS ¹⁴C radiocarbon dates (twelve bulk sediment, four pollen dates) were obtained (Table 4-2). Dates were calibrated to AD 1950 calendar years before present (cal. yr BP) using Oxcal 4.0 and IntCal04 (Reimer et al., 2004; Bronk-Ramsey, 2001 and Bronk-Ramsey, 1995). The dates indicated that the 06SD core extends to at least 18,887 ±103 ¹⁴C yrs BP (c. 22.4 ka cal. yr BP at 621 cm).

The dates were calibrated with a >95% probability that the dates fell within expected parameters, defined by a normal distribution curve based on known ages derived from dendrochronological and marine sources (Reimer et al., 2004).

Before deciding upon the final core chronology, the dates were examined for external and internal consistency. External impacts include hard water effects (Bradley, 1999). Analysis of the carbon content was undertaken at NIGL (Keyworth). The results suggested that the core contained less than 0.5% calcium carbonate, which indicated that the influence of hard water effects was minimal. Dates were checked for internal consistency (Figure 4.27), using age-depth modelling, following Tinner et al. (2005). Outlying dates (D10, D11 and D15) are not consistent with the overall chronology and were therefore rejected.

Date ref	Median core depth (cm)	Conventional Radiocarbon Age (years BP $\pm 1\sigma$)	Error (\pm)	Cal. yr BP 95% confidence limits		Median Age (cal. yr BP)	Type	Laboratory ref
D1	72.25	8027	41	9023	8727	8875	Bulk	SUERC-14155
D2	80.25	8181	41	9265	9020	9142.5	Bulk	SUERC-17149
D3	81.75	7840	45	8931	8483	8707	Pollen	ORL-22,356.00
D4	120.25	9100	65	10486	10175	10330.5	Pollen	ORL-22,357.00
D5	140.25	9475	43	11068	10581	10824.5	Bulk	SUERC-17150
D6	220.25	11880	80	13945	13500	13722.5	Pollen	ORL-22,358.00
D7	220.75	12256	54	14394	13948	14171	Bulk	SUERC-17151
D8	250.75	13071	54	15791	15152	15471.5	Bulk	SUERC-17154
D9	305.75	14063	59	17123	16353	16738	Bulk	SUERC-17155
D10	335.25	10045	45	11801	11324	11562.5	Bulk	SUERC-14156
D11	339.25	9240	70	10577	10246	10411.5	Pollen	ORL-22,359.0
D12	359.75	14690	63	18038	17312	17675	Bulk	SUERC-17156
D13	441.75	16516	78	19847	19495	19671	Bulk	SUERC-17157
D14	498.75	17773	91	21365	20621	20993	Bulk	SUERC-17158
D15	579.75	17781	89	21371	20634	21002.5	Bulk	SUERC-17159
D16	621.25	18887	103	22609	22218	22413.5	Bulk	SUERC-14157

Table 4-2: Conventional and calibrated AMS ^{14}C radiocarbon dates for the 06SD core.

Dates in bold were included in the final chronology.

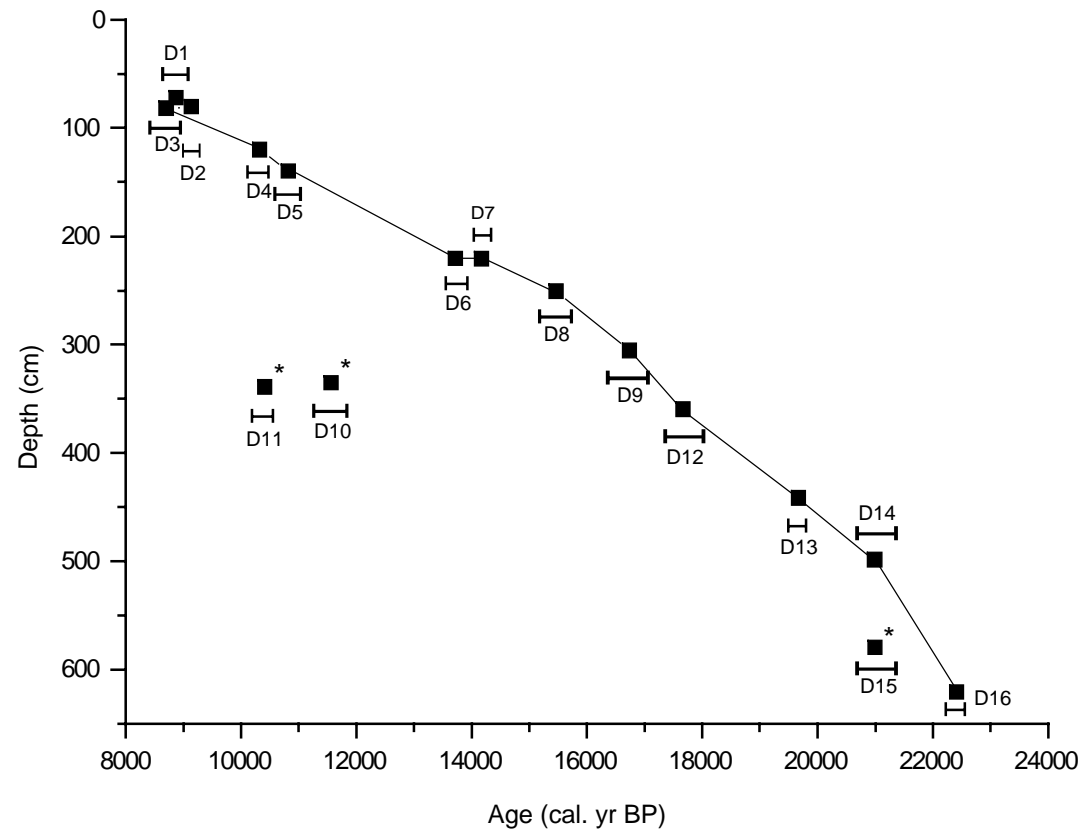


Figure 4-26: Age-depth curve based on the 06SD calibrated dates.

The age-depth model provides a means of checking the internal consistency of the core chronology and dates. The horizontal bars represent the 95% confidence intervals of the calibrated ages. Outliers (*) are not included in the final chronology. After Tinner et al. (2005).

Dates derived from samples at the same or adjacent depths (D2 / D3, D6 / D7 and D10 / D11) were compared to check for agreement. The first two pairs returned similar ages suggesting that internal consistency was high. However, the dates obtained from D10 / D11, are ~1000 years apart and showed an age reversal. Any dates that indicated an age reversal were subsequently rejected (D3, D10 and D11). D14 and D15 produced similar dates but were ~80 cm apart. These samples were originally in different cores (SD3 and 4) separated by an overlap. D14 was therefore also removed from the chronology.

Where a choice of bulk or pollen dates was available (for example, where two dates were obtained from the same or adjacent samples but have produced different radiocarbon dates), dates based on pollen concentrates were preferentially selected for inclusion in the final chronology. For example, D4 (pollen) and D5 (bulk) were obtained from samples 20 cm apart in the same core (06SD1) but produced dates that are only ~500 years apart. D6 (pollen) and D7 (bulk) were derived from adjacent samples but the calibrated dates overlapped. D5 and D7 were therefore excluded from the final chronology. In total, nine dates were accepted into the final chronology (Table 4-3). Unless otherwise stated, the 06SD dates in this study are rounded to the nearest one hundred years and quoted in ka cal. yr BP.

A continuous age depth curve was constructed by linear interpolation between dated depths (Figure 4-27). The results indicate that the dates are linear, which suggests a good fit between the dates obtained for the 06SD core and expected (modelled) values. The dates are also well spaced down the core, providing a reasonably comprehensive chronology.

Mean (smoothed) sedimentation rates were calculated for 06SD (Figure 4-28) firstly to gain insight into the shifts in rates over time and secondly to estimate the chronological resolution of the core (i.e. the number of years represented by each cm of sediment). See Table 4-4.

Date ref	Median core depth (cm)	Conventional Radiocarbon Age (years BP $\pm 1\sigma$)	Error (\pm)	Calibrated Age (cal. yr BP)	Type	Laboratory ref
D1	72.25	8027	41	8.9	Bulk	SUERC-14155
D2	80.25	8181	41	9.1	Bulk	SUERC-17149
D4	120.25	9100	65	10.3	Pollen	ORL-22,357.00
D6	220.25	11880	80	13.7	Pollen	ORL-22,358.00
D8	250.75	13071	54	15.5	Bulk	SUERC-17154
D9	305.75	14063	59	16.7	Bulk	SUERC-17155
D12	359.75	14690	63	17.7	Bulk	SUERC-17156
D13	441.75	16516	78	19.7	Bulk	SUERC-17157
D16	621.25	18887	103	22.4	Bulk	SUERC-14157

Table 4-3: 06SD final core chronology.

Calibrated ages are quoted to the nearest one hundred years.

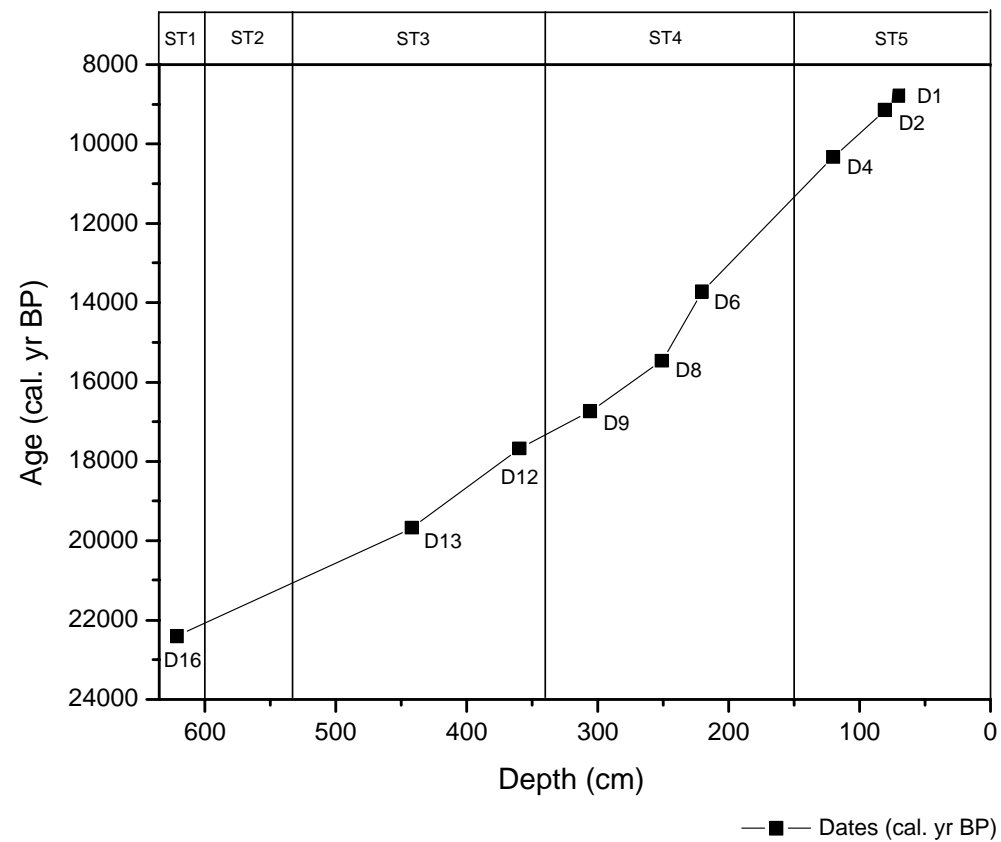


Figure 4-27: 06SD Age-depth curve.

The top axis shows the major stratigraphic zones.

06SD core ref	Interval (cm)	Median Age (cal. yr BP)	Interval (yr)	Sedimentation Rate (cm / yr)	Sedimentation Rate (yrs / cm)	Type	Zone
0	0			8.17	122.41*	-	-
72.25	72.5	8875	8875	8.17	122.41	Bulk	Dates Top - 1
80.25	8	9142.5	267.5	0.029	33.44	Bulk	Dates 1 - 2
120.25	40	10330.5	1188	0.034	29.70	Pollen	Dates 2 - 3
220.25	100	13722.5	3392	0.03	33.92	Pollen	Dates 3 - 4
250.75	30.5	15471.5	1749	0.017	57.34	Bulk	Dates 4 - 5
305.75	55	16738	1266.5	0.043	23.03	Bulk	Dates 5 - 6
359.75	54	17675	937	0.058	17.35	Bulk	Dates 6 - 7
441.75	82	19671	1996	0.041	24.34	Bulk	Dates 7 - 8
621.25	179.5	22413.5	2742.5	0.065	15.28	Bulk	Dates 8 - 9
635				0.065	15.28*	-	-

Table 4-4: 06SD core resolution and annual sedimentation rates.

An asterisk denotes estimated values based on the nearest pair of dates.

Calculation of sedimentation rates and core resolution were problematic for the top 72 cm of the core for several reasons. Firstly, the uppermost date is c. 8.9 ka cal. yr BP at 72 cm. Assuming that 0 cm represented ~AD 1950, this implies an unusually high sedimentation rate compared to the rest of the core (8.17 cm / yr compared to 0.01 cm / yr) and compared to Holocene sedimentation rates derived from parallel cores from Lake Shudu (Jones, pers comm.). Secondly, 9 cm of disturbed sediment were removed from the top of the core during extraction. The higher rate in the 06SD core may therefore be attributed to sediment removal. It is therefore likely that the sediment record spanning c. 8 - 0 ka cal. yr BP is incomplete.

Thirdly, dates obtained by NIGL (China) from the upper sediments of parallel cores extracted from Lake Shudu also returned similar ages in the region of c. 8 ka cal. yr BP (Zhang, pers comm.). This suggests that there was widespread removal of the upper sediments in the lake during the Holocene (in addition to sediment removal during extraction), although the reasons for this remain unclear.

This provided further evidence that this section of the record is incomplete, and raises questions over the reliability of calculated sedimentation rates for this section of the core, and the completeness of the section chronology. For these reasons, it was not possible to determine the resolution of this section of the core. The sediments spanning 72 - 0 cm are therefore dated to c. 8.9 ka cal. yr BP, as it is not possible to be more precise. In addition, this research focuses upon events during the Late Pleistocene - Early Holocene Period; therefore, these sediments do not play a pivotal role in this study.

The lack of organic material at the base of the core meant that it was not possible to obtain a basal date (635 cm). However, the ages of the sediments extending from the lowest date (c. 22.4 ka cal. yr BP at 621 cm) to 635 cm were extrapolated using the nearest pair of dates and associated sedimentation rates. The basal age of the core is subsequently calculated to be c. 22.6 ka cal. yr BP. Based on the 06SD core chronology, the ages of the stratigraphic zones were calculated (Table 4-5).

Zone	Depth (cm)	Age (ka cal. yr BP)
ST1	635 - 600	c. 22.6 - 22.0
ST2	600 - 534	22.0 - 21.0
ST3	534 - 340	21.0 - 17.3
ST4	340 - 150	17.3 - 11.3
ST5	150 - 0	11.3 - c. 8.9

Table 4-5: Ages of 06SD stratigraphic zones ST1 - 5.

The calculated sedimentation rates are indicative only, because they assume a constant rate of deposition between dates in order to infer key shifts in sedimentation. Furthermore, rates may have changed between dated samples, so the calculated rates are smoothed, and may actually have been more or less variable over shorter timescales.

In order to examine the possible extent of variability in the sedimentation rates, the dates and sediment accumulation rates were modelled using the Oxcal Deposition Model (P-Sequence). The P-Sequence model facilitates assessment of the degree to which the sedimentation rate was uniform or more variable down the length of the core. This is achieved by setting the k value to reflect different event spacing. The k value was set to 1 (event spacing of 1 cm), 5 (0.5 cm) and 10 (0.1 cm). The best agreement between the model and the dates occurred with the k value set to one, implying a variable sedimentation rate down the core. Hence, there was agreement between the modelled values and the calculated sedimentation rates. The Deposition Model indicates that uniform deposition was unlikely, and therefore provides an additional means of confirming variable rather than uniform sedimentation rates over time.

The mean core resolution is ~40 years per cm. However, the deposition model confirmed a variable sedimentation rate, and therefore the number of years represented by each cm of sediment is likely to vary accordingly. Figure 4-28 shows the approximate number of years represented by each cm of sediment in the 06SD core, calculated by dividing the number of years in the interval between each pair of dates by the number of cm of sediment spanning the same interval. This provides an indication of the core resolution.

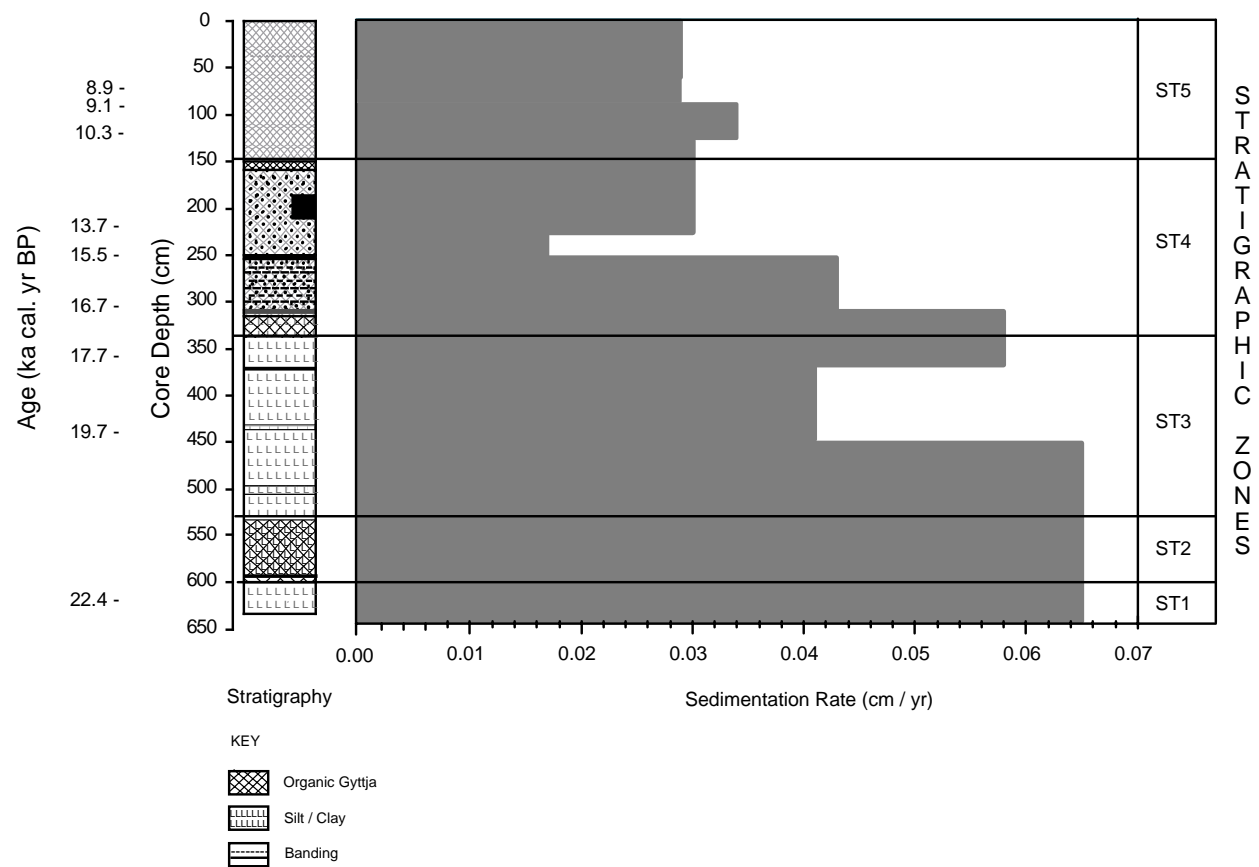


Figure 4-28: 06SD composite core stratigraphy and sedimentation rates.

4.4 Physical properties

Figure 4-29 and Figure 4-30 show the results of particle size and magnetic susceptibility measurements obtained from the 06SD sediments.

4.4.1 Particle size

Figure 4-29 highlights the relative percentages of sand, silt and clay present in the 06SD core. It is evident that the core is primarily composed of silt, which accounts for 60 - 80% of the core material. Clay values ranged from 20 - 40%. Sand content is generally low, in the range of <5 - 12%. The core is divided into three particle size zones (PS1, 2 and 3). The zone boundaries were delineated by eye, taking account of the primary shifts in the particle size record. Shifts are either gradual or abrupt and short-lived. The mean sampling resolution is ~320 years (8 cm intervals). Higher resolution sampling at 2 - 4 cm intervals was undertaken from c. 17.5 - 16.9 ka cal. yr BP (355 - 321 cm).

Zone PS1 (c. 22.6 - 16.2 ka cal. yr BP; 635 - 284 cm) is primarily composed of silt (~75%) and clay (~25%). Sand levels are low (<1%) throughout. Particle size values are relatively stable during this period, although there is a gradual trend towards increasing levels of silt (~80%). Sand values exceed 1% for the first time at c. 17.8 ka cal. yr BP (365 cm), rising to >2% at c. 17.2 ka cal. yr BP (333 cm).

Zone PS2 (c. 16.2 - 11.1 ka cal. yr BP; 284 - 143 cm) commences with a marked peak in sand values of 22.8% at c. 16.0 ka cal. yr BP (275 cm). The rest of this zone is characterised by a series of abrupt peaks and troughs in the silt and clay records. Clay values reach ~40% at c. 15.8 ka cal. yr BP (267 cm) and ~44% at c. 11.3 ka cal. yr BP (150 cm), representing the highest recorded clay contributions for the whole core.

The particle size record relating to Zone PS3 (c. 11.1 - 8.9 ka cal. yr BP; 143 - 0 cm) is characterised by increased levels of sand and a return to stable and high silt levels in the region of 80%. Overall, the sediments in Zone PS3 contain more sand than the rest of the core. At c. 10.7 ka cal. yr BP (132 cm) and c. 10.4 ka cal. yr BP (122 cm), sand content peaks at ~13%, and ~7%. However, aside from these peaks, sand content is low. At c 10.7 ka cal. yr BP (132 cm), clay content declines to 5%, which represents the lowest recorded value for clay.

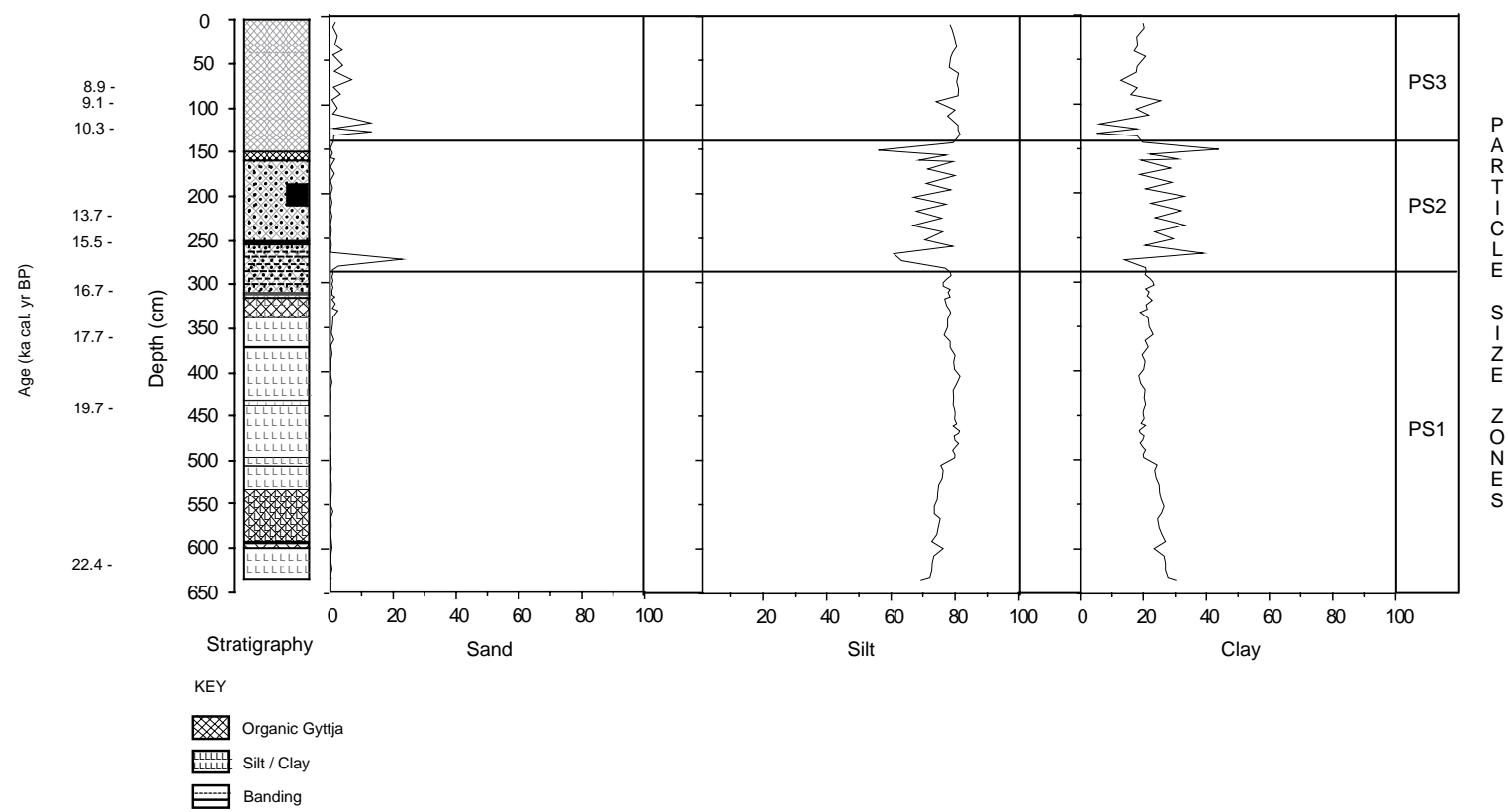


Figure 4-29: 06SD particle size record.

06SD core stratigraphy, calibrated AMS ^{14}C radiocarbon dates and particles size zones are shown for reference.

4.4.2 Magnetic susceptibility (χ_f)

Downcore magnetic susceptibility values range from ~ 6 to $31 \times 10^{-6} \text{ m}^3 \text{ kg}^{-1}$ (Figure 4-30). The mean sampling resolution is ~ 80 years (2 cm intervals). Six magnetic zones (MS1 - 6) were determined by eye, based on key shifts in the susceptibility record.

During Zone MS1 (c. 22.6 - 20.3 ka cal. yr BP; 635 - 488 cm), magnetic susceptibility ranges from 14 to $31 \times 10^{-6} \text{ m}^3 \text{ kg}^{-1}$. Values are high and variable relative to other sections of the core. Values climb to $28 \times 10^{-6} \text{ m}^3 \text{ kg}^{-1}$ at c. 22.1 ka cal. yr BP (604 cm), peaking at $31 \times 10^{-6} \text{ m}^3 \text{ kg}^{-1}$ at c. 22.0 ka cal. yr BP (596 cm). This is the highest reading within the core. Short-term (centennial) variations in magnetic susceptibility characterise this zone, although the overall trend is towards decreasing magnetic susceptibility.

In Zone MS2 (c. 20.3 - 17.5 ka cal. yr BP; 488 - 355 cm), mean magnetic susceptibility values are $16 \times 10^{-6} \text{ m}^3 \text{ kg}^{-1}$ and range from 10 to $22 \times 10^{-6} \text{ m}^3 \text{ kg}^{-1}$. The variability observed in Zone MS1 continues, but magnetic susceptibility is generally lower. Values drop sharply at c. 17.6 ka cal. yr BP (358 - 356 cm), from 19 to $10 \times 10^{-6} \text{ m}^3 \text{ kg}^{-1}$.

The magnetic susceptibility trends in Zone MS3 (c. 17.5 - 13.5 ka cal. yr BP; 355 - 215 cm) are arguably different in nature to previous zones. Firstly, magnetic susceptibility values and variability increase, averaging $19 \times 10^{-6} \text{ m}^3 \text{ kg}^{-1}$ and ranging from 12 - $28 \times 10^{-6} \text{ m}^3 \text{ kg}^{-1}$. Secondly, values rise from 19 to $28 \times 10^{-6} \text{ m}^3 \text{ kg}^{-1}$ at c. 16.9 ka cal. yr BP (321 - 320 cm), representing the second highest recorded value for the whole core. Following the sharp peak, magnetic susceptibility reverts to generally lower values. The transition from high to low values and vice versa occurred over sub-centennial timescales.

During Zone MS4 (c. 13.5 - 9.1 ka cal. yr BP; 215 - 80 cm) mean values are $19 \times 10^{-6} \text{ m}^3 \text{ kg}^{-1}$ and range from 14 to $24 \times 10^{-6} \text{ m}^3 \text{ kg}^{-1}$. Magnetic susceptibility is characterised by a series of peaks and troughs, which continues into MS5. The observed cycles initially occurs at ~ 50 cm intervals, measured from peak to peak. The interval between each peak and trough is ~ 700 - 1000 yrs. In Zone MS5 (c. 9.1 - 8.9 ka cal. yr BP; 80 - 0 cm), magnetic susceptibility continues to rise and fall on shorter intervals (< 40 cm). Mean values are $15 \times 10^{-6} \text{ m}^3 \text{ kg}^{-1}$, and range from 10 - $20 \times 10^{-6} \text{ m}^3 \text{ kg}^{-1}$. The overall trend is towards decreasing magnetic susceptibility.

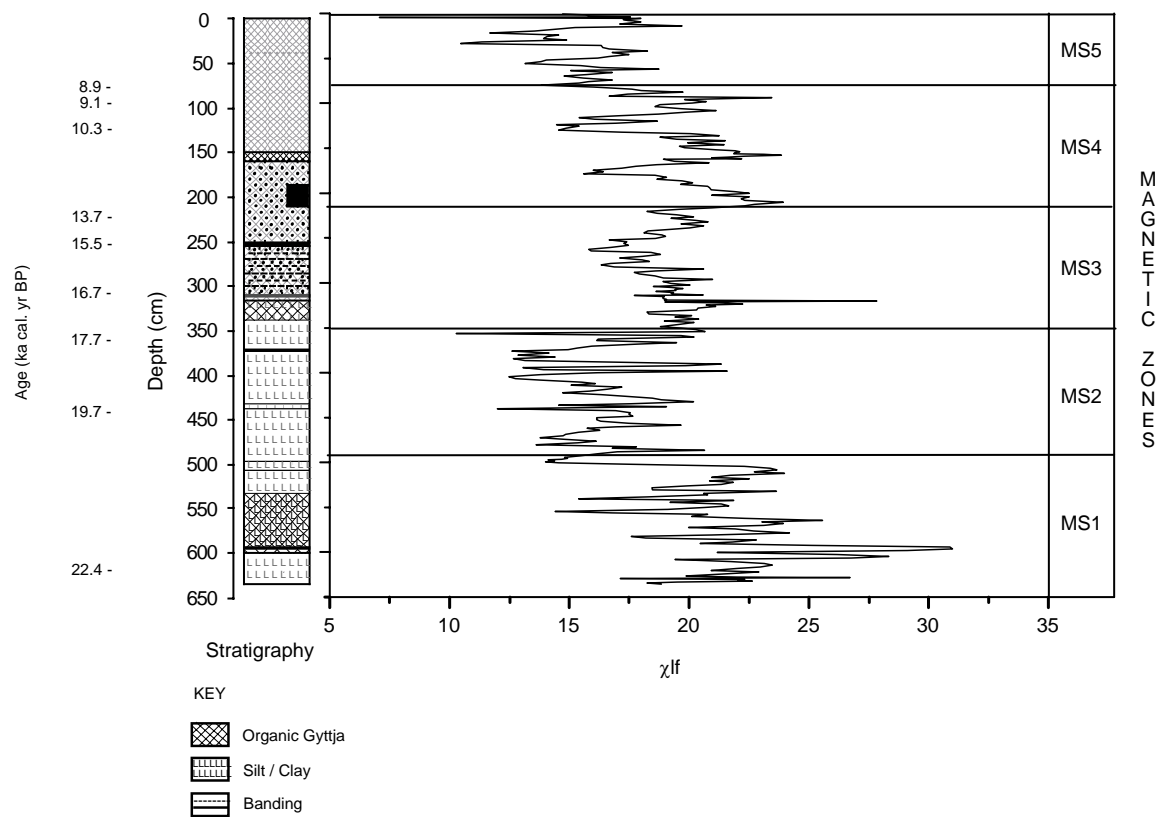


Figure 4-30: 06SD low frequency magnetic susceptibility record.

Susceptibility units are $\times 10^{-6} \text{ m}^3 \text{ kg}^{-1}$. The 06SD core stratigraphy, calibrated AMS ^{14}C radiocarbon dates and magnetic susceptibility zones are shown for reference.

4.5 Organic analysis

Results for modern and palaeo %LOI, %TOC, %TN, C/N ratios and $\delta^{13}\text{C}$ values are presented.

4.5.1 Modern values

In order to characterise the modern catchment, lake productivity and carbon cycling regime currently operating at Lake Shudu, plant and sediment samples were collected from the lake and surrounding catchment and analysed for %TOC, %TN, C/N ratios and $\delta^{13}\text{C}$ values (Table 4-6).

%TOC_{modern} values range from <1% to >53%, the highest values being associated with land plant samples, whilst the lowest values are associated with water plants. %TN_{modern} values are generally low, averaging 1 - 2%.

C/N_{modern} ratios (calculated using %TOC_{modern} and %TN_{modern}) range from 4.1 to 75.1. Higher ratios are associated with terrestrial sources of organic matter (OM), whilst lower ratios are associated with OM derived from aquatic sources. All except one of the lake inflow samples indicate the presence of mixed carbon sources, confirming that the inflows are both a source and conduit for terrestrial and aquatic OM flowing into the lake.

$\delta^{13}\text{C}_{\text{modern}}$ values are between -11.9‰ and -28.5‰. The highest values were derived from submerged and littoral macrophytes, whilst the lowest values were derived from coniferous trees and woody shrubs growing in the deciduous forest understorey.

$\delta^{13}\text{C}_{\text{modern}}$ and C/N_{modern} values were plotted against each other (Figure 4-31), in order to gain a more detailed insight into the modern sources and types of organic carbon present in the lake. The results highlight a tendency towards low C/N_{modern} ratios and low $\delta^{13}\text{C}_{\text{modern}}$ values allied to the lacustrine and C₃ plant groupings.

Of the twenty-two samples obtained, only two have a $\delta^{13}\text{C}_{\text{modern}}$ value of more than -20‰ but these samples also have C/N ratios of >11, indicating that they are allied to the lacustrine grouping rather than C₄ land plants (Herzschuh et al., 2005). This suggests that the modern catchment vegetation is primarily composed of terrestrial C₃ photosynthetic land plants utilising the Calvin pathway to preferentially obtain ¹²C, and lacustrine plants (Meyers et al., 1999). C₄ plants utilising the Hatch-Slack pathway are noticeably absent from the modern catchment samples.

Water plants	$\delta^{13}\text{C}$	%TOC	%TN	C/N
Macrophyte, SW inlet, emergent	-25.7	37.8	0.5	75.1
Macrophyte, SW inlet, submerged	-11.9	23.9	2.6	9.4
Macrophyte, SW inlet, emergent	-26.6	43.8	1.1	41.6
Macrophyte, Lake edge, water depth 0-5m	-25.7	31.3	1.6	20.2
Macrophyte, littoral zone, water depth 2.5m	-13.4	34.7	2.3	15.2
Lake sediments				
Eastern inflow	-29.2	26.4	1.8	14.3
Northern inflow	-25.9	0.4	0.1	4.1
Lake sediment, littoral zone	-22.2	26.6	2.3	11.4
Lake sediment, central zone	-24.4	19.8	1.8	11.0
Topsoil				
<i>Betula</i> stand	-26.3	9.7	0.7	14.0
<i>Picea</i> stand	-24.9	37.7	1.2	32.0
Evergreen <i>Quercus</i> stand	-24.6	3.1	0.2	12.7
Grass / shrubland	-26.5	46.9	2.5	19.1
Overgrazed area, lakeside	-26.5	38.6	2.2	17.7
Land plants				
<i>Picea</i> stand	-28.5	49.5	1.0	49.8
Coniferous stand	-28.3	49.0	0.8	58.2
<i>Betula</i> stand	-28.1	53.5	1.0	55.3
Evergreen <i>Quercus</i> stand	-26.2	48.2	1.2	41.6
Ericaceae understorey	-28.1	45.8	0.9	49.5
Broadleaved understorey	-28.3	46.2	2.9	16.2
Broadleaved understorey	-27.7	49.1	1.1	44.2
Grass / shrubland	-27.9	37.3	0.9	43.3

Table 4-6: Modern %TOC, %TN, C/N ratios and $\delta^{13}\text{C}$ values derived from plant and sediment samples obtained from Lake Shudu.

$\delta^{13}\text{C}$ values are quoted in ‰ (per mille).

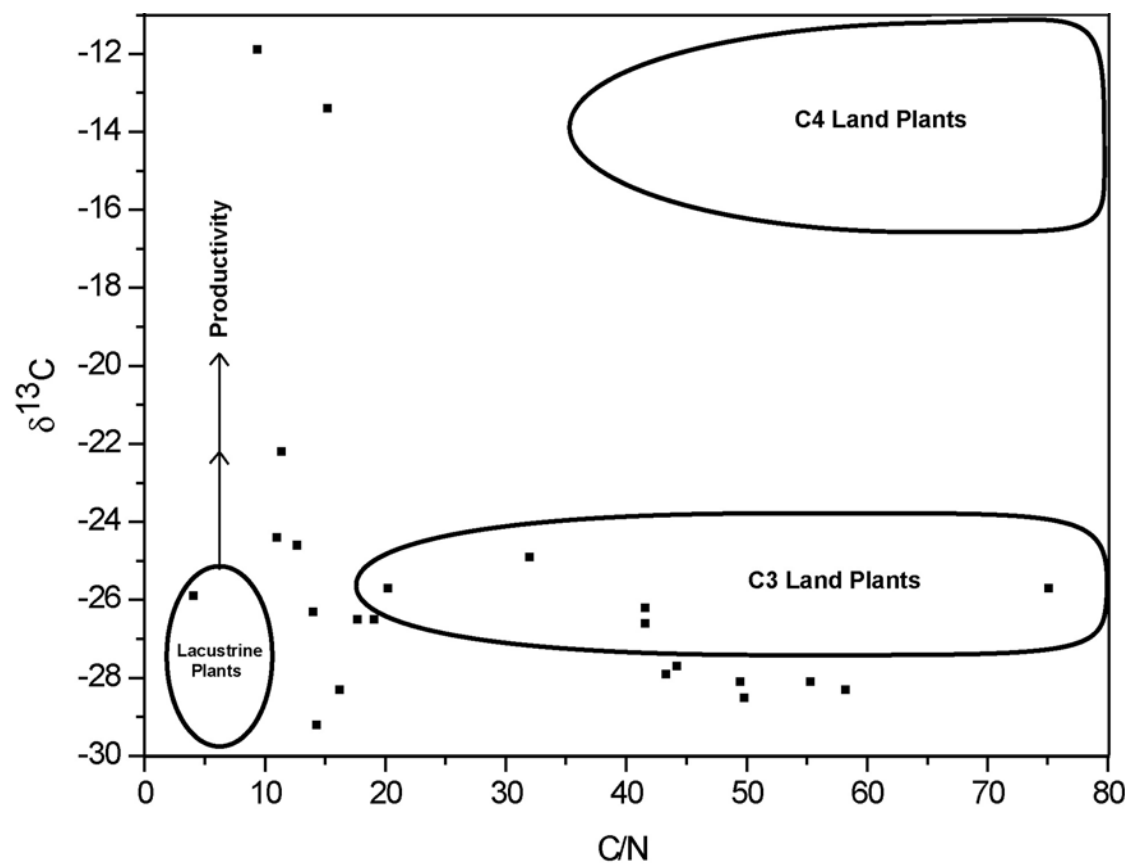


Figure 4-31: 06SD modern C/N ratios plotted against $\delta^{13}\text{C}$ values.

$\delta^{13}\text{C}$ values are quoted in ‰ (per mille). Fields for the different plant types are from Meyers et al. (1999).

4.5.2 *Loss on Ignition (%LOI)*

The 06SD core was subjected to LOI analysis (Figure 4-32) to determine the organic, calcium carbonate (CaCO_3) and silicate content of the core, at a resolution of ~80 years (2 cm intervals). The carbonate and silicate records contain some anomalies. Firstly, the CaCO_3 record indicates that some parts of the core contain up to 5% CaCO_3 . However, further analysis undertaken at NIGL (Keyworth) suggested that the core contains <1% carbonate, which is at odds with the LOI record. Low carbonate values (<1%) were also obtained from a parallel core extracted from Lake Shudu, analysed at NIGL (China). Other studies have identified similar issues and subsequently concluded that LOI is not a reliable method for quantitatively estimating the relative contributions of different types of material present in sediments at lower concentrations (i.e. <10%) (Santisteban et al., 2004).

These factors raised doubts over the reliability of the carbonate and silicate LOI records, and therefore the decision was taken not to use these data in the discussion chapter. However, the organic curve is included below (Figure 4-32), because it is in good agreement with the %TOC record, obtained independently by combustion in an elemental analyser. Five LOI zones are distinguished (LOI1 - 6).

Zone LOI1 (c. 22.6 - 22.0 ka cal. yr BP; 635 - 600 cm), mean organic content is ~10% and values range from 8 - 11%. The general trend is towards increasing organic carbon values, although the overall contribution remains low. During Zone LOI2 (c. 22.0 - 18.0 ka cal. yr BP; 600 - 376 cm), mean organic content is 9%, ranging from 6 - 13%. Values peak at c. 22.0 ka cal. yr BP (596 cm), but in contrast with the previous zone, organic carbon content then gradually declines, with the exception of an abrupt drop to ~6% at c. 21.3 ka cal. yr BP (554 cm).

In Zone LOI3 (c. 18.0 - 16.6 ka cal. yr BP; 376 - 300 cm), mean organic content is 11% and ranges from 8 - 16%. The organic profile of this zone is defined by an abrupt rise in values to >16%, which contrasts with surrounding zones. Organic content generally increases throughout this phase. In Zone LOI4 (c. 16.6 - 13.2 ka cal. yr BP; 300 - 204 cm), mean values are 10%, with a range of 9 - 11%, and overall steadily increasing organic carbon values in contrast to Zone LOI3. During Zone LOI5 (c. 13.2 - 8.9 ka cal. yr BP; 204 - 0 cm), mean values are 16%, and range from 11 - 23%. The trend towards higher contribution of organic material to the sediments continues, but in a markedly different fashion to previous zones. The increases occur as a series of stepwise centennial scale shifts in organic content. Each stage is characterised by notable peaks and troughs. Organic content is highest in this zone.

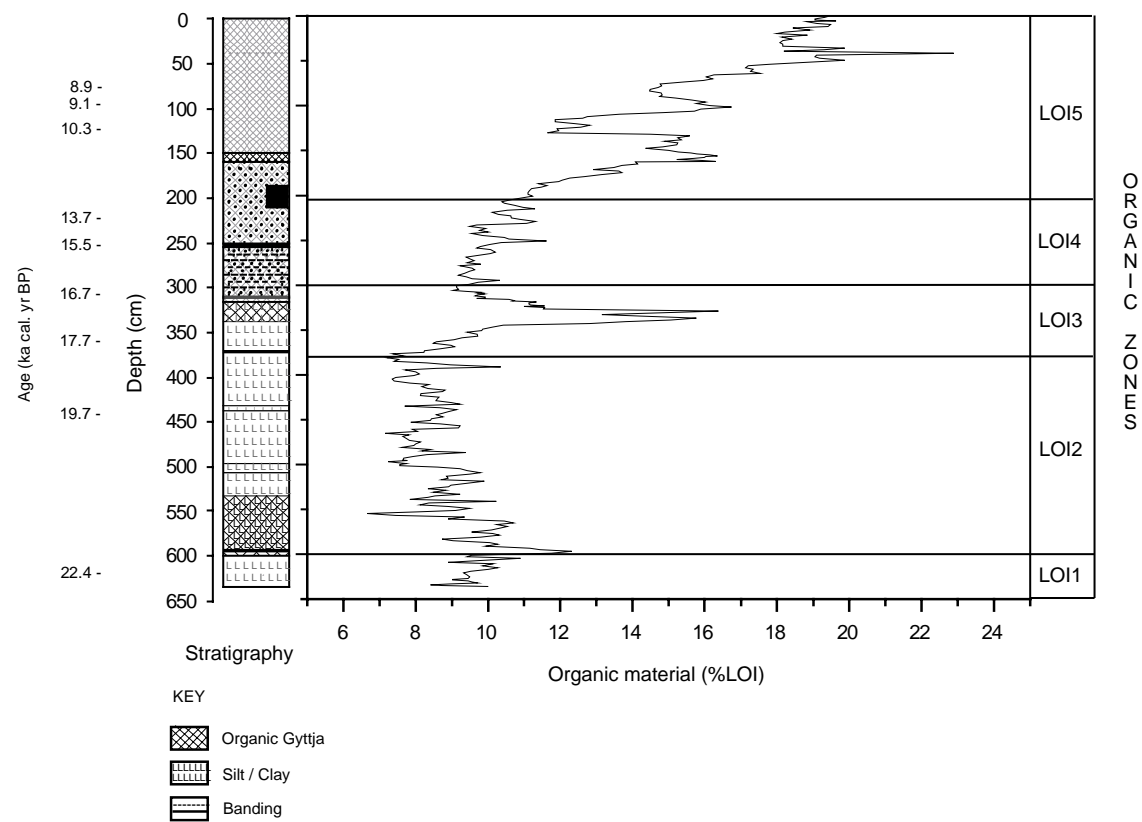


Figure 4-32: 06SD Loss on Ignition (%LOI) organic material.

The 06SD core stratigraphy, calibrated AMS ^{14}C radiocarbon dates and loss on ignition zones are shown for reference.

4.5.3 *Total Organic Carbon (%TOC)*

Within 06SD, %TOC varies from <1% to ~10% (Figure 4-33). The %TOC record is broadly similar to the LOI organic record (%TOC should equate to ~40% of %LOI), although there are slight differences at the base of the core. The mean sampling resolution is approximately ~80 years (2 cm intervals). %TOC values in the lower sections of the core are generally low (0.8 - 3.4%). %TOC becomes more variable, increasing sharply from c. 17.3 - 17.1 ka cal. yr BP (340 and 330 cm). Pronounced peaks punctuate subsequent increases in %TOC values. The most prominent of these (9.4%) occurs at c. 11.5 ka cal. yr BP (154 cm). This is followed by a period of instability. An event at c. 17.2 ka cal. yr BP (336 cm) signifies a transition from low, constant levels of %TOC to a regime defined by a gradual incline towards more rapid accumulation of larger amounts of %TOC, starting at ~3.5% at c. 17.1 ka cal. yr BP (328 cm), rising to ~10% near the top of the core. Four primary %TOC zones were determined by eye (TOC 1 - 4).

%TOC values are generally stable but low during Zone TOC1 (c. 22.6 - 18.1 ka cal. yr BP; 635 - 378 cm), averaging ~1%. There is a slight drop in %TOC values at c. 20.5 ka cal. yr BP (~500 cm), although this is not defined as a separate zone because the decrease is relatively small <1%. The shift may also not be as abrupt as suggested by the graph because it occurs in an overlap zone, and may therefore be a function of the composite core construction.

Zone TOC2 (c. 18.1 - 16.6 ka cal. yr BP; 378 - 302 cm), mean values are 2%, but range from 1 - 6% and shift from gradually rising values to more abrupt increases. The primary feature of this zone is the peak in %TOC (~6%) at c. 17.2 ka cal. yr BP (336 cm). Values generally decrease in incremental stages equating to ~2% to between 2 and 3% thereafter. However, %TOC remains relatively low. The profile of this zone is markedly different from the general trends associated with the other zones (i.e. more abrupt, higher magnitude shifts in %TOC compared to stable or gradually increasing values). During Zone TOC3 (c. 16.6 - 13.2 ka cal. yr BP; 302 - 206 cm), %TOC remains low, in the region of 3%, within a range of 1 - 3%. Organic content resumes the trend of gradually increasing values during this zone, with the exception of a drop in %TOC to <2% at c. 15.2 ka cal. yr BP (246 cm). Zone TOC4 (c. 13.2 - 8.9 ka cal. yr BP; 206 - 0 cm), %TOC is much higher than previous zones, averaging 7%, and more variable, ranging from 3 - 10%. At c. 12.9 ka cal. yr BP (198 cm) productivity rates increase (%TOC rises by 4%). %TOC then rises to ~8%, peaking at ~10% at c. 11.5 ka cal. yr BP (154 cm). This peak is the highest value recorded for the 06SD core. %TOC subsequently drops sharply to ~6% at c. 10.7 ka cal. yr BP (131 cm) but then increases, reaching ~9% - 10% at c. 8.9 ka cal. yr BP (49 cm and 2 cm). The increase in %TOC occurs as a series of incremental centennial scale shifts.

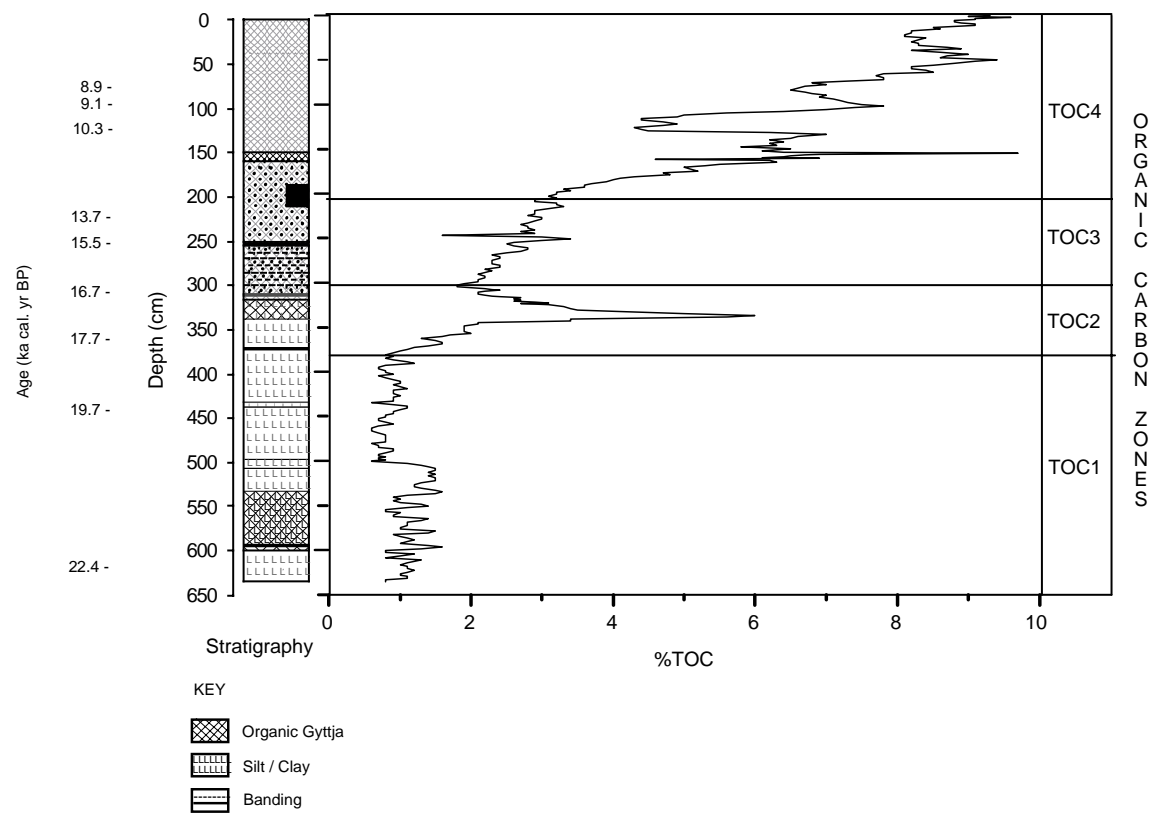


Figure 4-33: 06SD Total Organic Carbon (%TOC) record.

The 06SD core stratigraphy, calibrated AMS ^{14}C radiocarbon dates and total organic carbon zones are shown for reference

4.5.4 Total Nitrogen (%TN)

%TN values are generally low throughout the core (<1%). The mean sampling resolution for is ~80 years (2 cm intervals). Overall, nitrogen content increases and parallels the changes in %TOC. Three primary zones (TN1 - 3) were distinguished by eye (Figure 4-34).

Zone TN1 (c. 22.6 - 17.4 ka cal. yr BP; 635 - 348 cm) is characterised by low, stable nitrogen values averaging ~0.2%, within a range of 0.1 - 0.2%. In Zone TN2 (c. 17.4 - 12.8 ka cal. yr BP; 348 - 194 cm), mean values are ~0.3% but variable. Zone TN3 (c. 12.8 - 8.9 ka cal. yr BP; 194 - 0 cm) is characterised by a marked increase in nitrogen content, manifesting as a series of stepwise shifts. %TN content is ~0.6%, within a range of 0.4 - 0.8%. Nitrogen levels are highest in this section of 06SD.

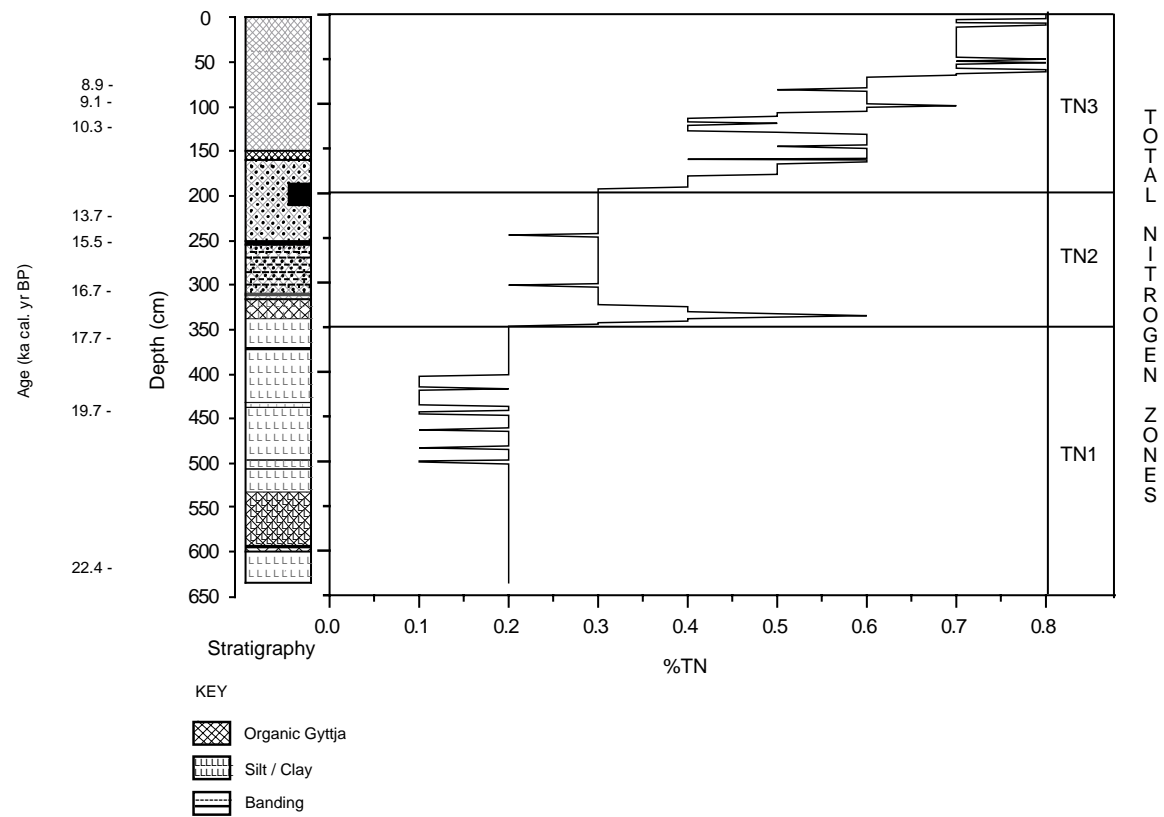


Figure 4-34: 06SD Total Nitrogen (%TN) record.

The 06SD core stratigraphy, calibrated AMS ^{14}C radiocarbon dates and total nitrogen zones are shown for reference.

4.5.5 Carbon and Nitrogen (C/N) ratios

C/N ratios were derived from the %TOC and %TN records. The C/N mean sampling resolution is ~80 years (2 cm intervals). C/N ratios vary from 3 - 13 (Figure 4-35). Ratios are low but stable from c. 22.6 - 18.9 ka cal. yr BP (635 - 410 cm), ranging from ~3 - 7. From c. 18.9 - 16.6 ka cal. yr BP (410 - 300 cm), ratios become much more variable, declining to 3.6 at c. 18.5 ka cal. yr BP (394 cm), before increasing rapidly to 10.7 at c. 17.2 ka cal. yr BP (338 cm) then dropping to ~7 at c. 16.6 ka cal. yr BP (304 cm). From c. 16.6 ka cal. yr BP (300 cm), the general trend is towards increasingly high C/N ratios. However, ratios vary quite widely, on both millennial and sub-millennial timescales. Five C/N zones were defined by eye (CN1 - 5).

Zone CN1 (c. 22.6 - 21.2 ka cal. yr BP; 635 - 544 cm), mean ratios are 5, ranging from 4 - 7 but are generally quite stable. Zone CN2 (c. 21.2 - 20.5 ka cal. yr BP; 544 - 498 cm), the mean ratio is slightly higher, reaching 6, with a range of 4 - 7, although the overall zone trend is towards increasing but low values.

In Zone CN3 (c. 20.5 - 18.6 ka cal. yr BP; 498 - 398 cm), mean values of 5 are observed but range from 4 - 7. Values drop sharply on the boundary between Zones CN2 and 3, and then start to rise quite abruptly, before dropping again at the end of this zone.

In Zone CN4 (c. 18.6 - 16.6 ka cal. yr BP; 398 - 302 cm) mean ratios increase to 8, and range from 4 - 11. C/N ratios peak at >10 from c. 17.2 ka cal. yr BP (338 cm) before declining to ~8 at c. 16.7 ka cal. yr BP (306 cm).

During Zone CN5 (c. 16.6 - 8.9 ka cal. yr BP; 302 - 0 cm), mean ratios are 11, whilst the ratio range is 7 - 13. C/N ratios reached ~9 at c. 15.5 ka cal. yr BP (252 cm), before peaking at ~11 at c. 11.7 ka cal. yr BP (161 cm). Ratios continue to increase in a series of stepwise shifts, reaching 12 at c. 9.8 ka cal. yr BP (103 cm).

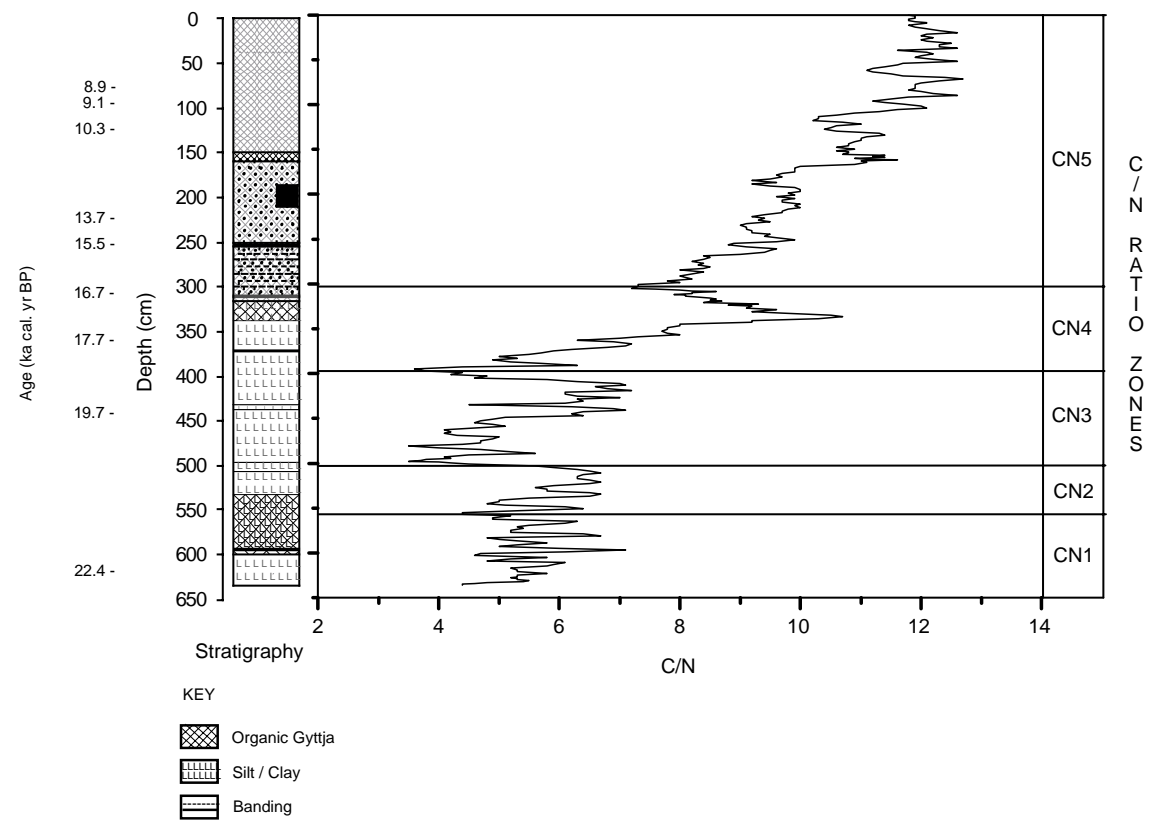


Figure 4-35: 06SD C/N ratios.

The 06SD core stratigraphy, calibrated AMS ^{14}C radiocarbon dates and C/N zones are shown for reference.

4.5.6 $\delta^{13}\text{C}$ analysis

Downcore $\delta^{13}\text{C}$ values range from -24‰ to -28‰ and are generally low, indicating that the sediments are ^{13}C depleted (Figure 4-36). The mean sampling resolution is ~ 80 years (2 cm intervals). Broadly speaking, values in the lower half of the core (c. 22.6 - 17.3 ka cal. yr BP; 635 - 340 cm) are higher (less negative), falling within the range of -26‰ to 24‰ , but trending towards lower (more negative) values. There is an abrupt shift to lower $\delta^{13}\text{C}$ values at -28.2‰ at c. 17.2 ka cal. yr BP (336 cm). From c. 17.1 - 15.6 ka cal. yr BP (330 - 260 cm), $\delta^{13}\text{C}$ values become higher again. However from c. 15.6 ka cal. yr BP (~ 260 cm), $\delta^{13}\text{C}$ values become lower, reaching -28‰ at c. 11.3 ka cal. yr BP (150 cm). Values remain low until c. 9.7 ka cal. yr BP (100 cm), then from c. 9.7 - 8.9 ka cal. yr BP (100 - 0 cm), revert towards higher values, reaching -26‰ at the top of 06SD. Six zones were distinguished by eye (DC1 - 6).

During Zone DC1 (c. 22.6 - 22.0 ka cal. yr BP; 635 - 600 cm), mean values of -24‰ are observed. Values become slightly higher throughout this zone. During Zone DC2 (c. 22.0 - 20.6 ka cal. yr BP; 600 - 508 cm), mean values are -25‰ and the trend towards higher values is reversed. At the start of Zone DC3 (c. 20.6 - 17.6 ka cal. yr BP; 508 - 360 cm), there is an abrupt shift to lower values, with stabilisation occurring at around -26‰ . During Zone DC4 (c. 17.6 - 16.1 ka cal. yr BP; 360 - 282 cm), mean values reach -26‰ . The $\delta^{13}\text{C}$ record indicates a shift towards higher values, from -26‰ to -25‰ at c. 17.6 ka cal. yr BP (358 cm). However, $\delta^{13}\text{C}$ values decline abruptly from -25‰ at 17.6 ka cal. yr BP (358 cm) to -28‰ at c. 17.2 ka cal. yr BP (336 cm). This represents the second lowest $\delta^{13}\text{C}$ reading. Values then rise to -24‰ , shifting back to higher values by the end of this zone.

During Zone DC5 (c. 16.1 - 11.4 ka cal. yr BP; 282 - 153 cm) mean values of -27‰ are reached and the general trend is towards lower $\delta^{13}\text{C}$ values. $\delta^{13}\text{C}$ values gradually become lower, declining from -26‰ to -27‰ at 12.3 ka cal. yr BP (180 cm), before dropping to -28‰ from c. 11.7 ka cal. yr BP (161 cm) to 11.4 ka cal. yr BP (153 cm).

During Zone DC6 (c. 11.4 - 8.9 ka cal. yr BP; 153 - 0 cm), mean values of -27‰ to -28‰ are observed in the $\delta^{13}\text{C}$ record. Initially, $\delta^{13}\text{C}$ values are lower ($> -28\text{‰}$) then become higher at c. 9.6 ka cal. yr BP (99 cm), reaching -26‰ . A temporary return to lower values exceeding -28‰ is observed in the record at 60 cm. The shift to higher $\delta^{13}\text{C}$ values is completed in a series of stepwise millennial to centennial shifts, measured from peak to peak.

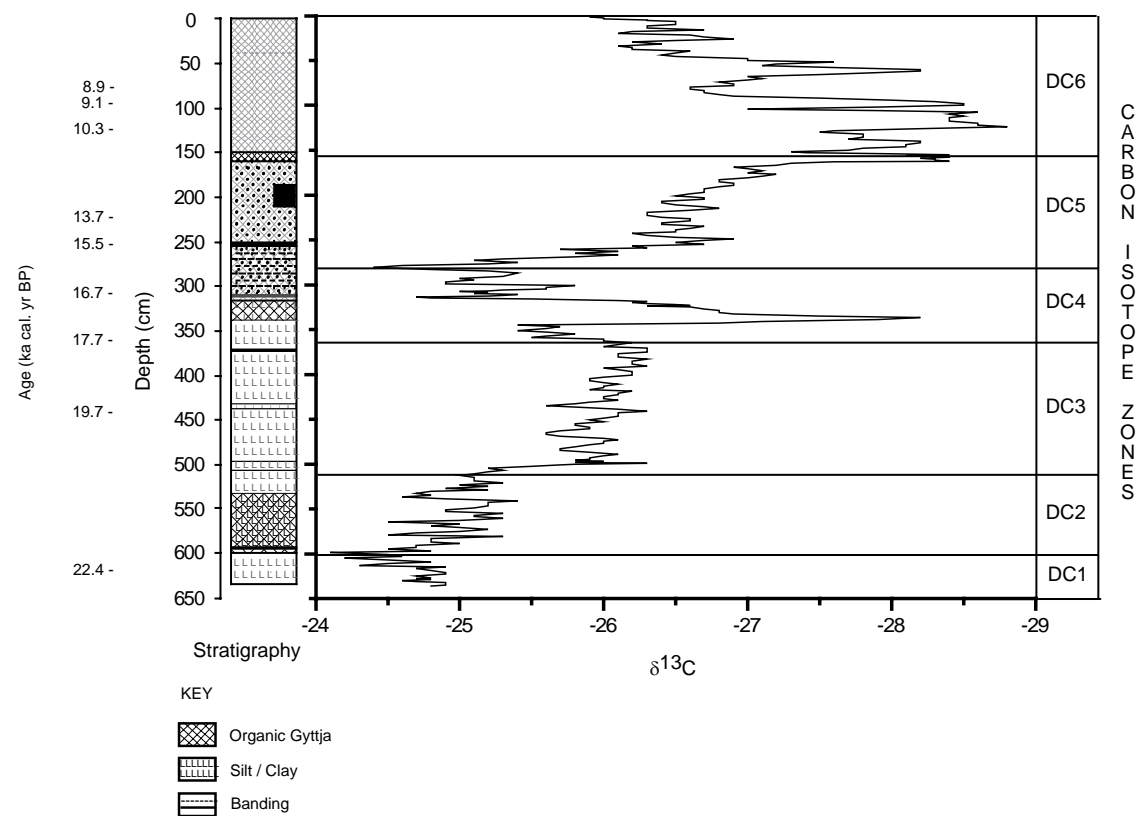


Figure 4-36: 06SD $\delta^{13}\text{C}$ values.

$\delta^{13}\text{C}$ values are quoted in ‰ (per mille). The 06SD core stratigraphy, calibrated AMS ^{14}C radiocarbon dates and $\delta^{13}\text{C}$ zones are shown for reference.

4.5.7 Combined results of C/N and $\delta^{13}\text{C}$ analysis

Cross plotting of the C/N ratios and the $\delta^{13}\text{C}$ values (Figure 4-37) highlighted some interesting trends (Meyers et al., 1999). Approximately 40% of the 06SD samples analysed are primarily composed of lacustrine material. These samples were taken from the bottom half of 06SD (~635 - 340 cm). The remaining samples (located between the primary lacustrine and C_3 plant groupings on the diagram) are most closely aligned to the lacustrine grouping, but contain a mixture of organic material derived from lacustrine and / or C_3 land plant material.

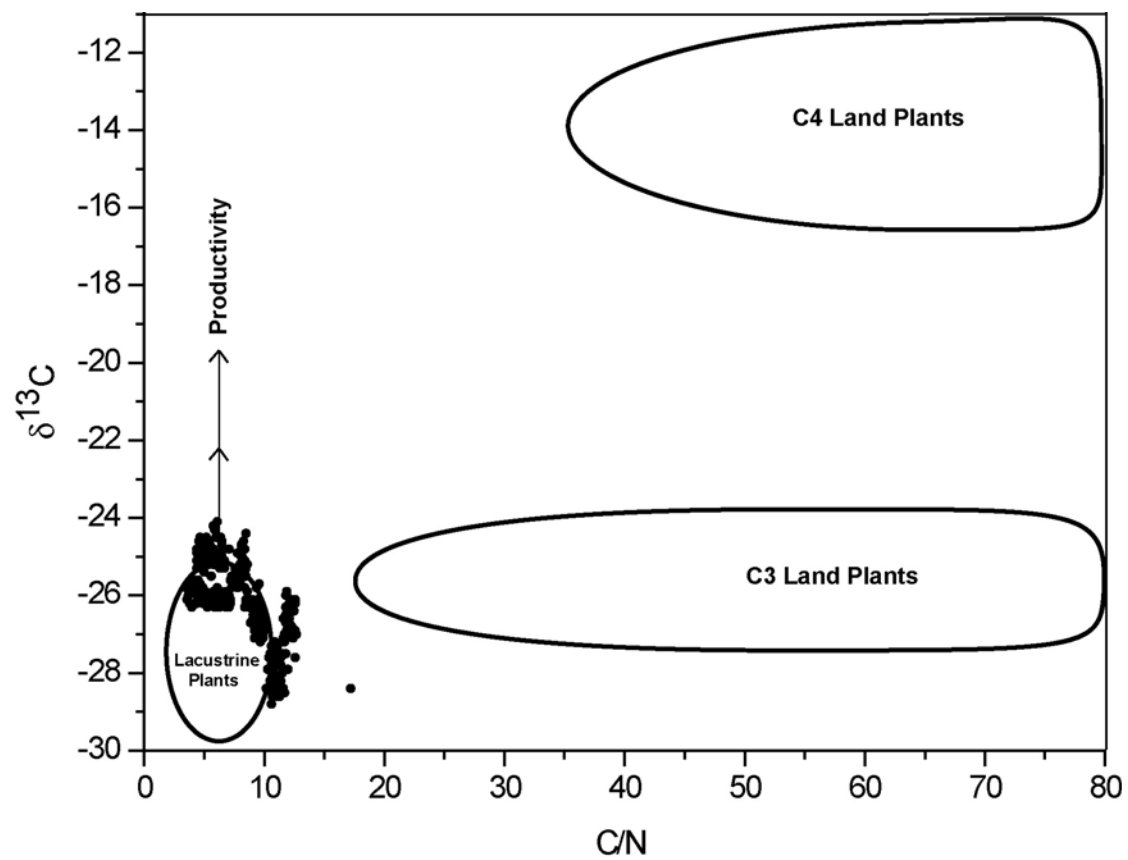


Figure 4-37: 06SD C/N ratios plotted against $\delta^{13}\text{C}$ values.

$\delta^{13}\text{C}$ values are quoted in ‰ (per mille). After Meyers et al. (1999).

4.6 Palaeoecological analysis

The core chronology suggests that the sediments spanning the period of interest to this study (i.e. the Late Pleistocene - Early Holocene transitional phase) are located from ~635 - 144 cm (c. 22.6 - 11.1 ka cal. yr BP). Owing to time constraints and the presence of rare and / or complex pollen present in the core, a targeted analytical approach was adopted in order to maximise the chances of obtaining a high-resolution palaeoecological record for the period under investigation.

Sediments spanning 635 - 144 cm were sampled for pollen and charcoal at 8 cm intervals, whilst the sediments spanning 144 - 0 cm were sampled at 24 cm intervals. This produced a centennial pollen record (~300 - 400 year intervals) for the core spanning 635 - 144 cm, and a millennial scale record (~1000 year intervals) for the core section spanning 144 - 0 cm.

4.6.1 Pollen analysis

Figure 4-38 shows the percentages of arboreal (AP) and non-arboreal pollen (NAP) taxa included in the pollen sum (e.g. trees, shrubs, grasses / sedges and herbs). Ferns, spores and aquatic grain counts not included in the pollen sum are also shown. The inset diagram shows the total percentages for each group. Figure 4-39 shows the pollen concentrations of arboreal taxa, Figure 4-40 shows the concentrations of shrubs, grasses and sedges and Figure 4-41 shows the abundances of herbaceous pollen present in the record. The inset diagrams highlight the total abundances of trees, shrubs, grasses / sedges and herbs.

Pinus pollen features strongly throughout the pollen record. Broadly speaking, the lower half of the record (c. 22.6 - 17.4 ka cal. yr BP; 635 - 350 cm) is dominated by *Pinus*, Poaceae and Cyperaceae with contributions from *Artemisia* and Rosaceae. Conversely, the upper half of the record (c. 17.4 - 8.9 ka cal. yr BP; 350 - 0 cm) is dominated by arboreal taxa including *Pinus*, *Betula* and *Quercus*, with significant contributions from taxa including *Tsuga*, *Abies*, *Picea*, and Rosaceae. Several rare types (<2%) are present in the record, including species of Sapindaceae.

Pollen concentrations are generally very low to moderate (declining to a low of ~6000 grains / g) within the lower half of 06SD and moderate to high (peaking at >1 million grains / g) in the upper sections. The increase is primarily attributed to an increase in *Pinus* and associated changes in sedimentation rates, most notably at c. 17.3 ka cal. yr BP (339 cm), which coincides with an event recorded in the physical and organic proxy records.

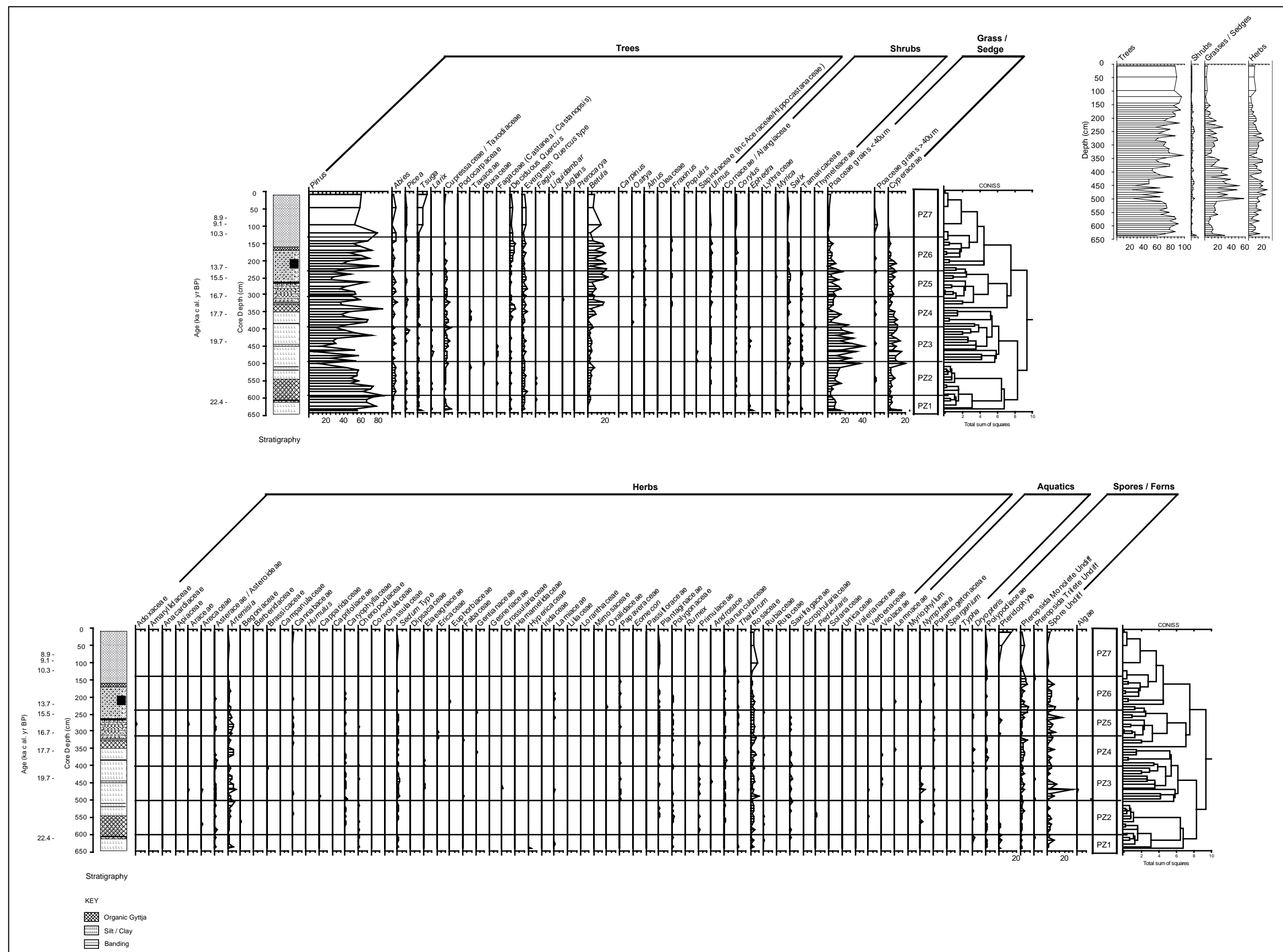


Figure 4-38: 06SD pollen percentage record.

Percentages of arboreal (AP) and non-arboreal pollen (NAP), including trees, shrubs, grass / sedge and herbs are shown. Spores / ferns and aquatic grains not included in the pollen sum are presented as counts. Group totals, pollen zones, CONISS, core stratigraphy and calibrated AMS ^{14}C radiocarbon dates are shown for reference

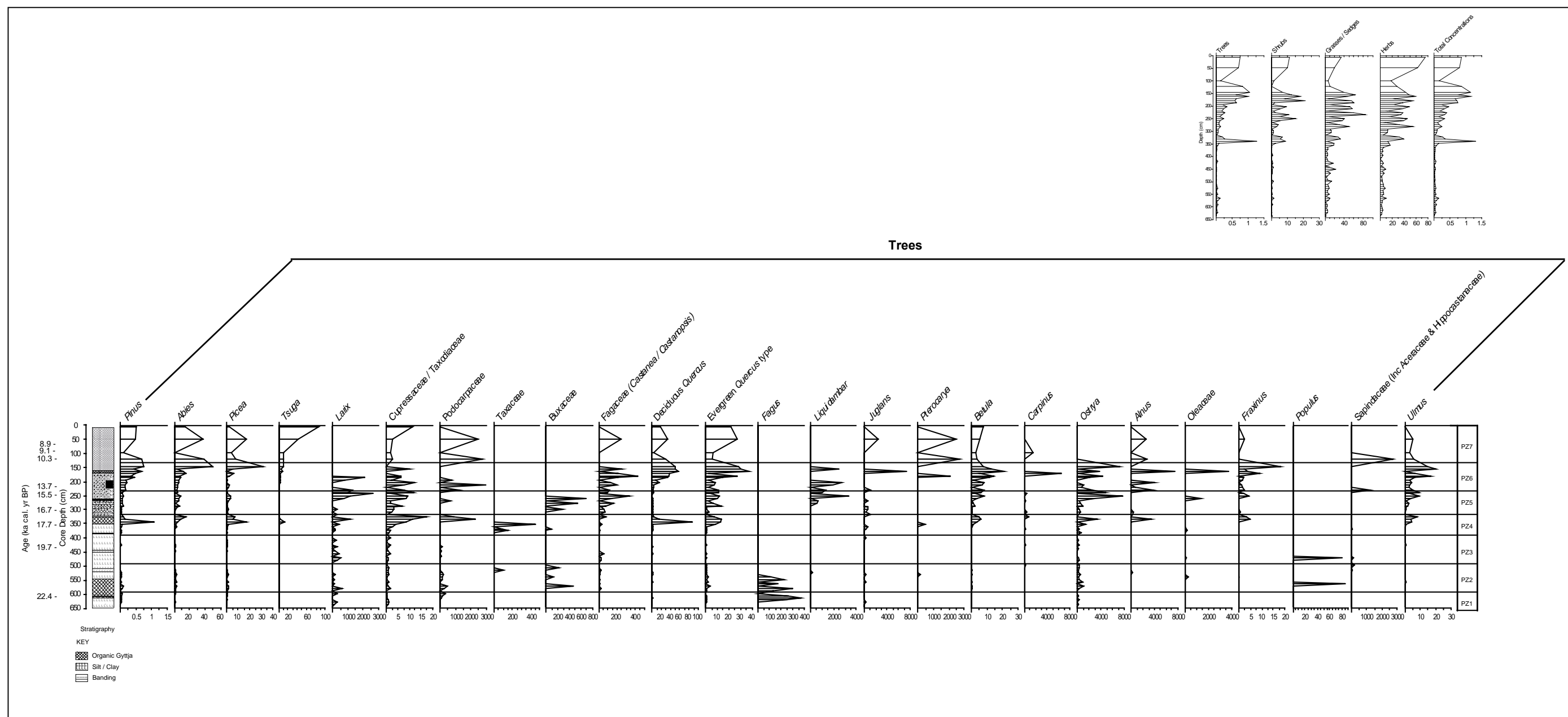


Figure 4-39: 06SD arboreal pollen concentrations.

Pollen concentrations are quoted in grains / g. For taxon which have large abundances, the following notations are used; *Pinus*; 10^6 , *Betula*; 10^5 , *Abies*, *Picea*, *Tsuga*, Cupressaceae / Taxodiaceae, *Quercus*, *Fraxinus* and *Ulmus*; 10^4 . Group totals, pollen zones, core stratigraphy and calibrated AMS ^{14}C radiocarbon dates are shown for reference.

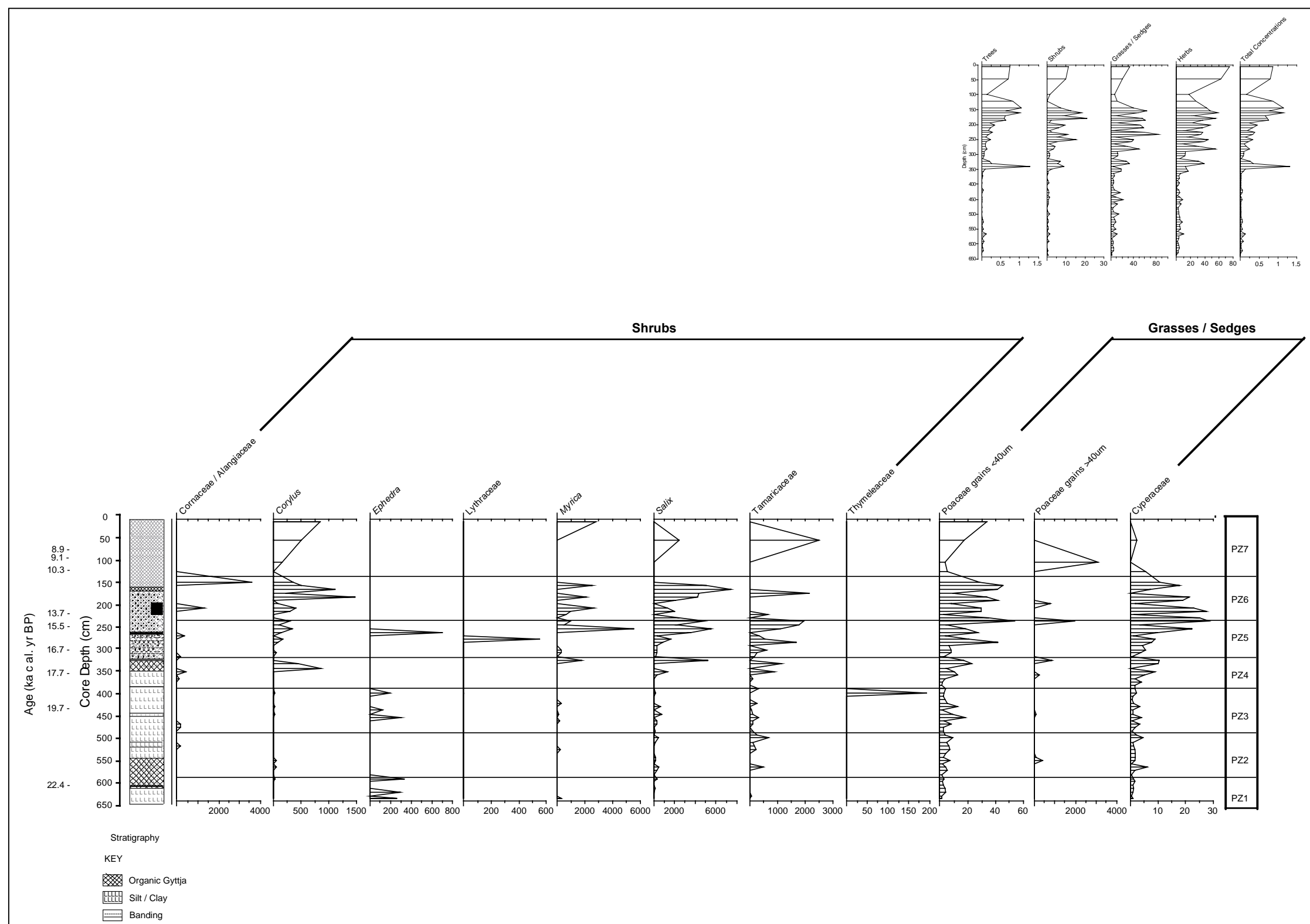


Figure 4-40: 06SD shrub, grass and sedge pollen concentrations.

Pollen concentrations quoted in grains / g. Poaceae <40 μ m and Cyperaceae are quoted as 10^4 . Group totals, pollen zones, core stratigraphy, calibrated AMS ^{14}C radiocarbon dates are shown for reference.

4.6.1.1 Pollen zones

The pollen record is divided into seven pollen zones (PZ1 - 7), defined using CONISS cluster analysis (expressed as the total number of squares) and by eye. CONISS calculations are based on the counts of pollen taxa with abundances of >1%.

Zone PZ1 (c. 22.6 - 21.8 ka cal. yr BP; 635 - 587 cm) is dominated by arboreal pollen (AP) (59 - 91%) and Poaceae / Cyperaceae pollen (~6 - 30%). *Pinus* pollen dominates this phase, accounting for 54 - 85% of the pollen record, whilst Poaceae grains <40 µm comprise 4 - 15% of the record. *Abies* and *Picea* account for ~1 - 2% of the record, and evergreen *Quercus* and *Betula* account for ~1 - 3%. Cyperaceae levels are initially high, accounting for ~15% of the record, but decline to ~2%. Similarly, the contribution of shrubs declines from ~7% to <2%.

Total pollen concentrations are initially ~7000 grains / g, rising to ~75,000 grains / g by c. 21.9 ka cal. yr BP (591 cm). Total arboreal pollen concentrations are initially ~4000 grains / g, rising to ~68,000 grains / g at c. 21.9 ka cal. yr BP (591 cm), with *Pinus* accounting for ~4000 - 64,000 grains / g, making it the most abundant taxon. *Picea* and *Abies* pollen concentrations are <1000 grains / g. Evergreen *Quercus* and *Betula* pollen abundances are typically in the range of 300 - 1000 grains / g, alongside lower levels of deciduous *Quercus* (<400 grains / g). Poaceae / Cyperaceae, shrubs and herb concentrations are <5000 grains / g. *Artemisia*, *Juglans* and Ericaceae abundance rates are <1000 grains / g. Notable shrubs including *Ephedra* also occur in the pollen record, but in very small amounts (~300 grains / g). *Pinus* is the only taxon attaining > 20,000 grains / g.

In Zone PZ2 (c. 21.8 - 20.3 ka cal. yr BP; 587 - 487 cm), AP continues to be the primary contributor to the pollen record, accounting for 25 - 87%. Of this, *Pinus* constitutes 11 - 74% of the AP. Other arboreal taxa present include *Abies*, *Picea*, *Tsuga*, Cupressaceae / Taxodiaceae, deciduous and evergreen *Quercus*. Individually they represent <5% of the pollen record. *Betula* (<7%) is the highest arboreal contributor, after *Pinus*. Poaceae and Cyperaceae accounts for 6 - 57% of the record, trending towards increasing values. Herbs account for 4 - 18% of the record. Herbs such as *Artemisia* and Rosaceous species each contribute up to ~5% of the total pollen percentages. Aquatic counts remain low, but spores / fern counts are quite high.

Total pollen concentrations are quite variable, ranging from ~10,000 - 145,000 grains / g, but are generally low for individual taxon. There is a peak in concentrations at c. 21.5 ka cal. yr BP (565 cm). AP concentrations range from ~6000 - 124,000 grains / g. *Pinus* pollen concentrations account for 5000 - 108,000 grains / g. *Pinus* pollen concentrations exceed 100,000 grains / g for the first time at c. 21.5 ka cal. yr BP (565 cm).

Other non-arboreal taxa that define the pollen assemblage of this zone include Poaceae grains <40 µm and Cyperaceae, representing up to a fifth of the taxa present. Poaceae grains >40 µm appear in the record for the first time at c. 21.2 ka cal. yr BP (549 cm), albeit in very low levels (<500 grains / g). *Artemisia* and Rosaceous pollen concentrations exceed >2000 grains / g during this period. There are marked shifts in the abundance and type of taxa occurring in this zone. Notwithstanding this, pollen levels of the majority of these taxa generally remain low or very low. *Pinus* is the only taxon with pollen concentrations exceeding 20,000 grains / g during this phase.

Zone PZ3 (c. 20.3 - 18.2 ka cal. yr BP; 487 - 385 cm) is characterised by AP values of 23 - 82%. *Pinus* contributions are variable, ranging from 30 - 72%. Notably, Cupressaceae / Taxodiaceae account for ~7% of the record at 19.5 ka cal. yr BP (435 cm) and *Picea* contributes 6% to the record at c. 18.7 ka cal. yr BP (403 cm). However, despite peaking at >80% at c. 19.1 ka cal. yr BP (419 cm), AP percentages generally decrease. Poaceae / Cyperaceae contributes 12 - 51% to the pollen record for Zone PZ3. The contributions of Poaceae / Cyperaceae and Herbs reach >30% and >20% at c. 20.2 ka cal. yr BP (483 cm). Levels of herbaceous pollen rises during this phase, reaching ~21%. Levels of aquatic species are very low, but spore counts remain relatively constant.

Total pollen concentrations for Zone PZ3 range from ~6000 to 57,000 grains / g. AP concentrations range from ~3000 - 47,000 grains / g. Notably, *Pinus* pollen concentrations fall to ~2000 grains / g at c. 19.5 ka cal. yr BP (435 cm), representing just 27% of the pollen record. These are the lowest recorded concentrations for *Pinus* in the 06SD core. This corresponds with a marked decrease in total pollen concentrations. Concentrations of Poaceae grains <40 µm peak at ~13,000 grains / g at c. 19.3 ka cal. yr BP (427 cm). Low Poaceae pollen concentrations persist until the end of Zone PZ3. Taxa with pollen concentrations exceeding 20,000 grains / g include *Pinus*.

During Zone PZ4 (c. 18.2 - 16.8 ka cal. yr BP; 385 - 315 cm), AP remains high, accounting for 57 - 98% of the pollen record. In general, *Pinus* accounts for ~36 - 84% of the record. There are also notable increases in *Betula*, evergreen and deciduous *Quercus* and Cupressaceae / Taxodiaceae. Evergreen *Quercus* accounts for ~7% of the record at c. 17.4 ka cal. yr BP (347 cm). The highest AP percentages (98%) are observed at c. 17.3 ka cal. yr BP (339 cm). The majority of this increase is related to a rise in *Pinus* (84%), although marked increases are evident across the arboreal pollen record during this interval. For example, deciduous *Quercus* represents 6% of the record at c. 17.3 ka cal. yr BP (339 cm). By the end of this zone, *Betula* accounts for 18% and Cupressaceae / Taxodiaceae represents 6% of the record at c. 16.9 ka cal. yr BP (321 cm).

Total Poaceae / Cyperaceae percentages fall from ~20% to <1% from c. 17.9 - 17.3 ka cal. yr BP (370 - 339 cm). Levels of shrubs, herbs, grasses and sedges are very low at c. 17.3 ka cal. yr BP (339cm), each comprising <1% of the pollen record. Notably, *Artemisia* and Rosaceae decrease to negligible levels at c. 17.3 ka cal. yr BP (339cm).

Total pollen concentrations peak at c. 17.3 ka cal. yr BP (339 cm), when total pollen concentrations exceed 1.3 million grains/ gram. This is the highest recorded concentration for the 06SD core. The majority of this is *Pinus* (1.1 million grains / g). This is the highest recorded individual concentration for any taxon within the 06SD record. At the same time, concentrations of deciduous *Quercus* exceed ~86,000 grains / g, whilst *Betula* concentrations reach ~34,000 grains / g. This is the highest value recorded for *Betula*. Poaceae / Cyperaceae and herb concentrations all increase markedly throughout this zone, rising from low levels in the region of ~<4000 grains / g to moderate abundances (>25,000 grains / g). Taxa with concentrations exceeding 20,000 grains / g include *Pinus*, *Betula*, deciduous *Quercus* and Poaceae grains <40 µm.

Zone PZ5 (c. 16.8 - 14.3 ka cal. yr BP; 315 - 230 cm) is characterised by high levels of AP (59 - 86%). 25 - 66% of this is accounted for by *Pinus*. AP peaks at 86% at c. 15.7 ka cal. yr BP (265 cm). At this point, *Pinus* values comprise 66% of the total arboreal pollen percentage. Other taxa featuring in the record in Zone PZ5 include *Betula*, Poaceae grains <40 µm, Cyperaceae and Rosaceae. *Juglans* reaches maximum-recorded levels at the start of this phase (~3%) at c. 16.8 ka cal. yr BP (313 cm). Ericaceae pollen levels rise, reaching maximum core values of ~2% at c. 16.5 ka cal. yr BP (297 cm). Pteridophytes preferring damp, shady conditions increase at c. 15.7 ka cal. yr BP (265 cm).

Total pollen concentrations gradually increase throughout this phase, rising from ~30,000 - 134,000 grains / g. AP concentrations correspondingly rise from 30,000 - 106,000 grains / g. *Pinus* levels increase from ~22,000 to >92,000 grains / g during this phase. Herbs increase from <5000 - >45,000 grains / gram, with contributions of >1000 grains / g from Plantaginaceae, Rosaceae, Gentianaceae, and *Artemisia*. Conversely, Poaceae / Cyperaceae concentrations broadly decline. Taxa with moderate (or higher) concentrations include *Pinus* and *Betula*.

Zone PZ6 (c. 14.3 - 10.6 ka cal. yr BP; 230 - 130 cm) is dominated by AP, which represents 70 - 94% of the pollen record. *Pinus* pollen accounts for 80 - 39%. *Abies* reaches 4% at c. 11.1 ka cal. yr BP (144 cm). Evergreen *Quercus* decreases, but deciduous *Quercus* rises to 6% at c. 12.0 ka cal. yr BP (169 cm). Poaceae grains <40 µm represent ~2 - 17% of the pollen record for this zone. Percentages of herbs, grasses, sedge and shrubs are generally lower, compared to previous zones (<10%).

Total pollen concentrations are markedly higher than previous zones (with the exception of the peak in Zone PZ4), increasing from ~385,000 to over 1.1 million grains / g. This is the second highest total pollen concentration recorded for the 06SD core. AP ranges from ~173,000 to over 1 million grains / g, the majority of which was accounted for by *Pinus*. Relatively high concentrations of *Betula*, *Quercus*, *Abies* and *Picea* all occur at c. 11.1 ka cal. yr BP (144 cm). *Fraxinus*, *Ulmus*, *Tsuga*, *Artemisia* and Rosaceae pollen concentrations also exceed 10,000 grains / g during this interval.

Increased concentrations of shrubs such as *Corylus*, *Salix* and Tamaricaceae are recorded at c. 11.1 ka cal. yr BP (144 cm). Within the herbaceous record, Ericaceae, Primulaceae, Gentianaceae, Ranunculaceae and *Thalictrum* pollen concentrations increase more gradually by c. 11.1 ka cal. yr BP (144 cm). Taxa with pollen moderate concentrations exceeding 20,000 grains / g include *Pinus*, *Betula*, *Quercus*, *Picea* and *Abies* and Poaceae grains <40 µm.

At the start of Zone PZ7 (c. 10.6 - 8.9 ka cal. yr BP; 130 - 0 cm), AP represents ~96% of the record, with *Pinus* accounting for ~80% of this. AP remains at ~80 - 90%. Mean *Pinus* percentages are 50 - 60% for the remainder of this zone. *Betula* pollen accounts for 15% at c. 9.6 ka cal. yr BP (98 cm). *Tsuga* pollen levels continue to rise, reaching a maximum of 10% at the top of the core.

At c. 9.6 ka cal. yr BP (98 cm), herbs represent 10% of the record, with most of this accounted for by Rosaceae, *Artemisia* and Ericaceae. Poaceae / Cyperaceae pollen accounts for up to 5% of the record. Poaceae grains >40 µm reach their highest levels during this phase (~2%). There is a marked rise in the contribution of Spores / Ferns at the top of the core. The contribution of shrubs, which is generally low throughout the core, remains at ~1%.

Total pollen concentrations are ~800,000 grains / g, with the exception of a marked drop to 165,000 grains / g at c. 9.6 ka cal. yr BP (98 cm). Most of this is accounted for by *Pinus*, which rises to ~678,000 grains / g and remains high, with the exception of a drop to ~85,000 grains / g at c. 9.6 ka cal. yr BP (98 cm). *Abies* is absent from the record at c. 9.6 ka cal. yr BP (98 cm), whilst deciduous *Quercus* declines from 30,000 grains / g to just 3000 grains / g. *Picea* and *Tsuga* also decrease at this time. *Fraxinus* is absent from pollen record at c. 10.3 ka cal. yr BP (120 cm), and *Ulmus* pollen declines to ~5000 grains / g, whilst *Alnus* and *Pterocarya* pollen concentrations increase. Conversely, increased abundances of evergreen *Quercus* are observed during this period.

Poaceae grains <40 µm pollen concentrations peak at >30,000 grains / g at the top of the core, which represents the highest recorded level within 06SD. Brassicaceae, Ranunculaceae, Cupressaceae / Taxodiaceae, Podocarpaceae and Sapindaceae pollen concentrations correspondingly increase. Cannabaceae pollen concentrations also increase at the top of the core (6 cm). The pollen record also contains members of the Fagaceae family, including *Carpinus* and *Myrica*. Pteridophytes and Pteropsida monolete spores increase significantly at the top of the core. However, *Artemisia* notably disappears from the record at c. 10.3 ka cal. yr BP (120 cm). Taxa with concentrations exceeding 20,000 grains / g include *Pinus*, *Abies*, *Tsuga*, *Quercus*, *Betula* and Rosaceae.

4.6.2 Charcoal analysis

Broadscale analysis of charcoal fragments present in the core indicates that charcoal levels are generally low throughout the core. From c. 22.6 - 11.1 ka cal. yr BP (635 - 144 cm), the mean sampling resolution is 300 - 400 years (8 cm intervals) and from c. 11.1 - 8.9 ka cal. yr BP (144 - 0 cm) it is ~1000 years at (24 cm intervals). Five charcoal zones (CH1 - 5) were distinguished by eye.

Zone CH1 (c. 22.6 - 21.5 ka cal. yr BP; 635 - 567 cm) is characterised by low concentrations of charcoal fragments >10 - 100 µm. In Zone CH2 (c. 21.5 - 17.8 ka cal. yr BP; 567 - 368 cm), charcoal counts remain low, although there is a peak in small fragments at c. 19.9 ka cal. yr BP (459 cm).

Zone CH3 (c. 17.8 - 16.6 ka cal. yr BP; 368 - 300 cm) is characterised by higher levels of charcoal fragments. Charcoal counts for Zone CH4 (c. 16.6 - 11.7 ka cal. yr BP; 300 - 160 cm) are slightly lower and more variable. Concentrations of larger fragments increase.

Counts are generally higher and much more variable within Zone CH5 (c. 11.7 - 8.9 ka cal. yr BP; 160 - 0 cm). There are also a number of notable peaks in charcoal. At c. 11.1 ka cal. yr BP (144 cm), there is an increase in both large and small fragments.

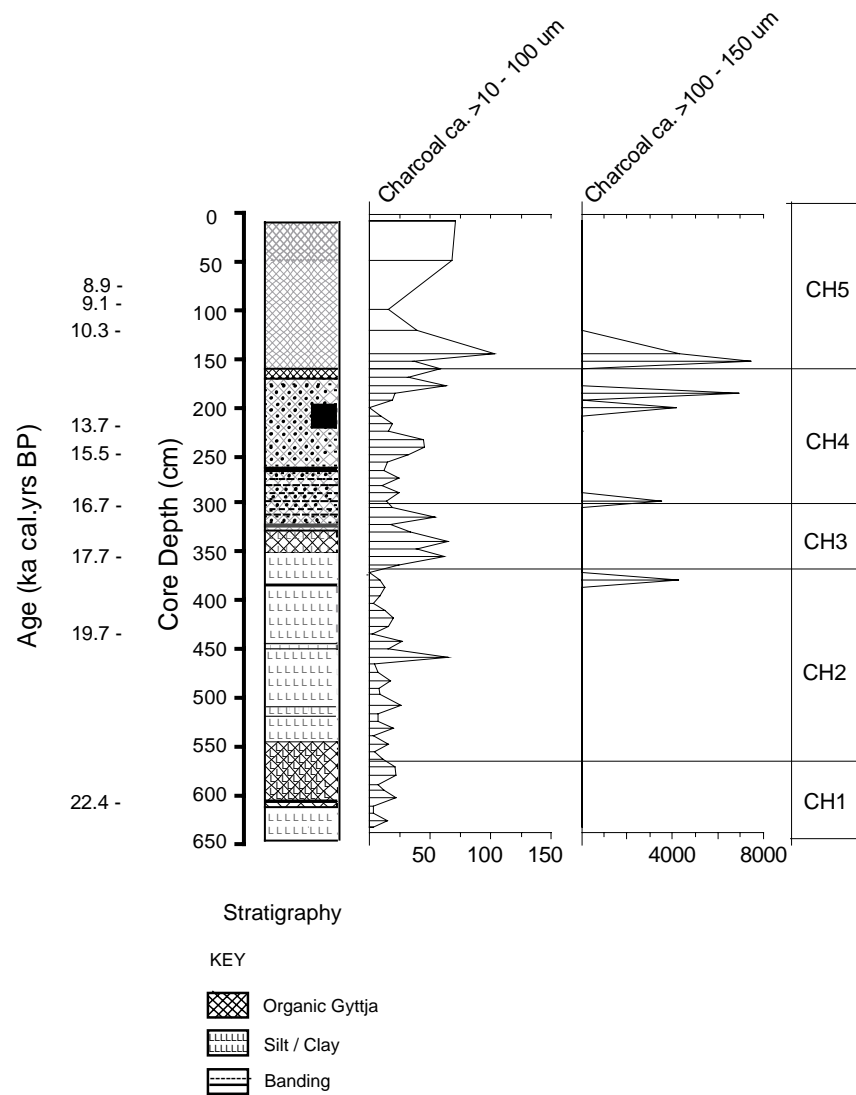


Figure 4-42: 06SD charcoal concentrations.

Concentrations are shown as grains / g. Fragments >10 - 100 μ m are shown in units of 10^4 and 10^5 .

4.7 Construction of 06SD multi-proxy zones

Multi-proxy zone boundaries were determined according to the following criteria. Firstly, the boundaries of individual proxy zones were compared in order to determine any major shifts across the records (Figure 4-43). The three black lines that span all of the proxies indicate where there is agreement on the zonal boundaries across the records. Magnetic susceptibility shows strong agreement in each instance.

Secondly, proxies that display a demonstrable lag between event and response were discounted on the basis that the start boundary of each multi-proxy zone ideally needed to represent the start of a shift or an event. Davis et al. (1991) observed a lag of ~150 years between an event and forest response (see Section 3.5.6). For this reason, the pollen and organic records were therefore discounted.

The physical proxies were examined. The particle size record is lower resolution than the other records, so this was discounted. The visual stratigraphy was also discounted on the basis that it was largely qualitative rather than quantitative. Having discounted all the other proxies, and having noted the close alignment between shifts across the record and individual zones, the magnetic susceptibility zones were therefore chosen to act as the multi-proxy zones, and termed Zones MS-SD1, 2, 3, 4 and 5.

One of the aims of this study was to focus on reconstructing the climate and environment during the Late Pleistocene - Early Holocene Period. The latter part of Zone MS-SD4 and all of MS-SD5 are therefore omitted from further discussion, because they fall outside of the period under investigation. Subsequent chapters therefore focus on the part of the record spanning c. 22.6 - 11.1 ka cal. yr BP (635 - 144 cm), with reference to the calibrated core chronology (cal. yr BP).

4.8 Concluding remarks

This chapter has described the temporal, stratigraphic, physical, organic and palaeoecological properties of the 06SD core. The results indicate that the core is at least c. 22,600 years old. The most prominent feature observed across all of these records is a pronounced event, centred at c. 17.3 ka cal. yr BP (339 cm).

Each multi-proxy zone has distinctive biogeochemical characteristics. The environmental shifts that took place at Lake Shudu are discussed in Chapter 5. Chapter 6, discusses the findings in relation to other regional proxy records introduced in Chapter 2.

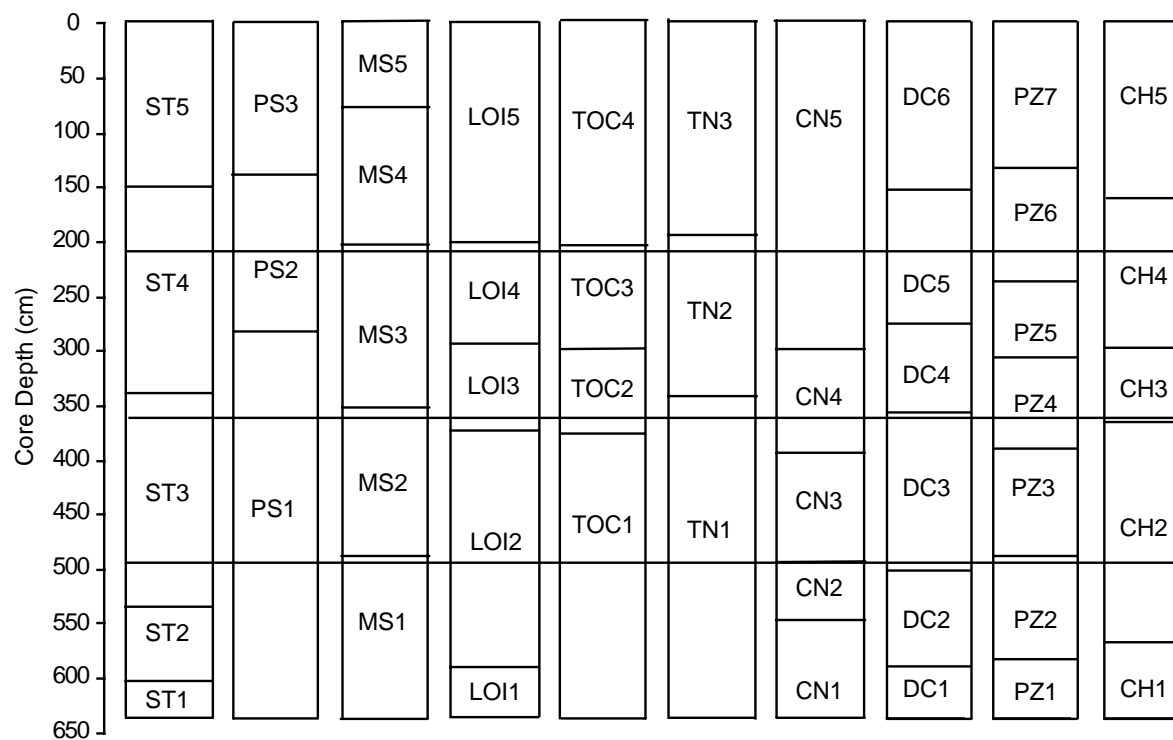


Figure 4-43: Composite diagram showing the zonal boundaries for each 06SD proxy.

The diagram is used to aid comparison of the different zonal boundaries denoting key shifts in each of the proxy records. There are three occasions where there are concurrent zonal shifts in the proxies, denoted by a solid black line running across the diagram. These shifts were used to guide the construction of the 06SD multi-proxy zones.

Key to zones: ST = Core stratigraphy; PS = Particle Size; MS = Magnetic susceptibility; LOI = Loss on Ignition; TOC = Total Organic Carbon; TN = Total Nitrogen; CN = C/N ratios; DC = $\delta^{13}\text{C}$ values; PZ = pollen and CH = Charcoal.

5 Late Pleistocene - Early Holocene environmental changes in southwestern China

5.1 Introduction

The Lake Shudu record provides a rich insight into the environmental changes that occurred in the catchment on millennial to centennial timescales from c. 22.6 - 11.1 ka cal. yr BP. This chapter addresses Aims 1 and 2 and Objective f of this research, and includes an evaluation of multi-proxy zones; MS-SD1 to 4. Subzones highlight the key shifts in the zones.

The primary proxy curves, multi-proxy zones and subzones are shown in Figure 5-1. Figure 5-2 shows the pollen percentages of taxa with abundances of >1% and charcoal fragment counts for the period spanning c. 22.6 - 11.1 ka cal. yr BP. Figure 5-3 shows the pollen percentages excluding *Pinus* from the pollen sum. Changes in the altitude of the upper treeline over time are inferred from the combined percentages of *Abies* and *Picea* shown in Figure 5-4. Table 5-1 summarises the environmental and climatic characteristics of each multi-proxy zone inferred from the Lake Shudu proxies.

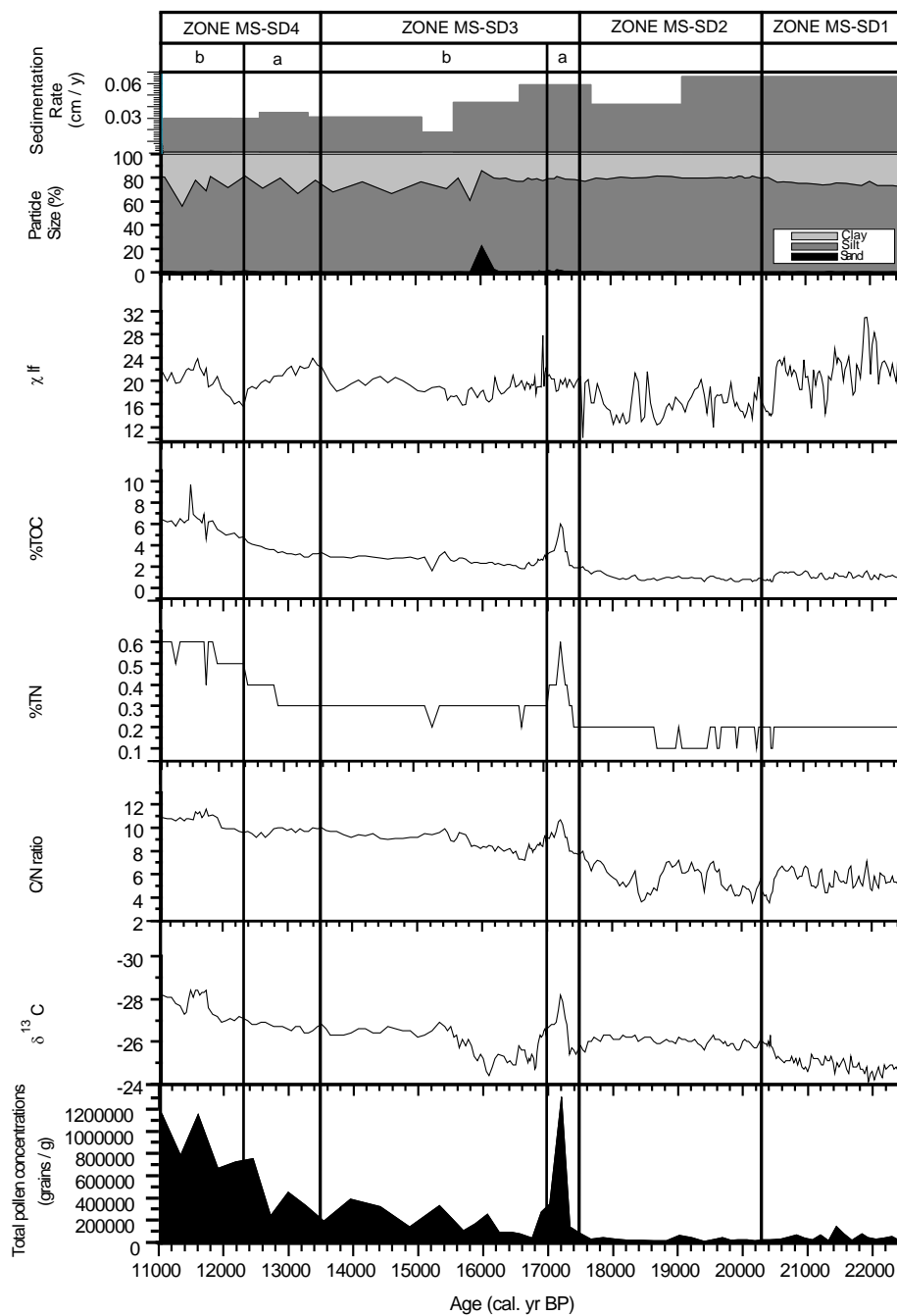


Figure 5-1: Lake Shudu multi-proxy zones.

Primary zones are labelled MS-SD1 to 4 and subzones are labelled a and b.

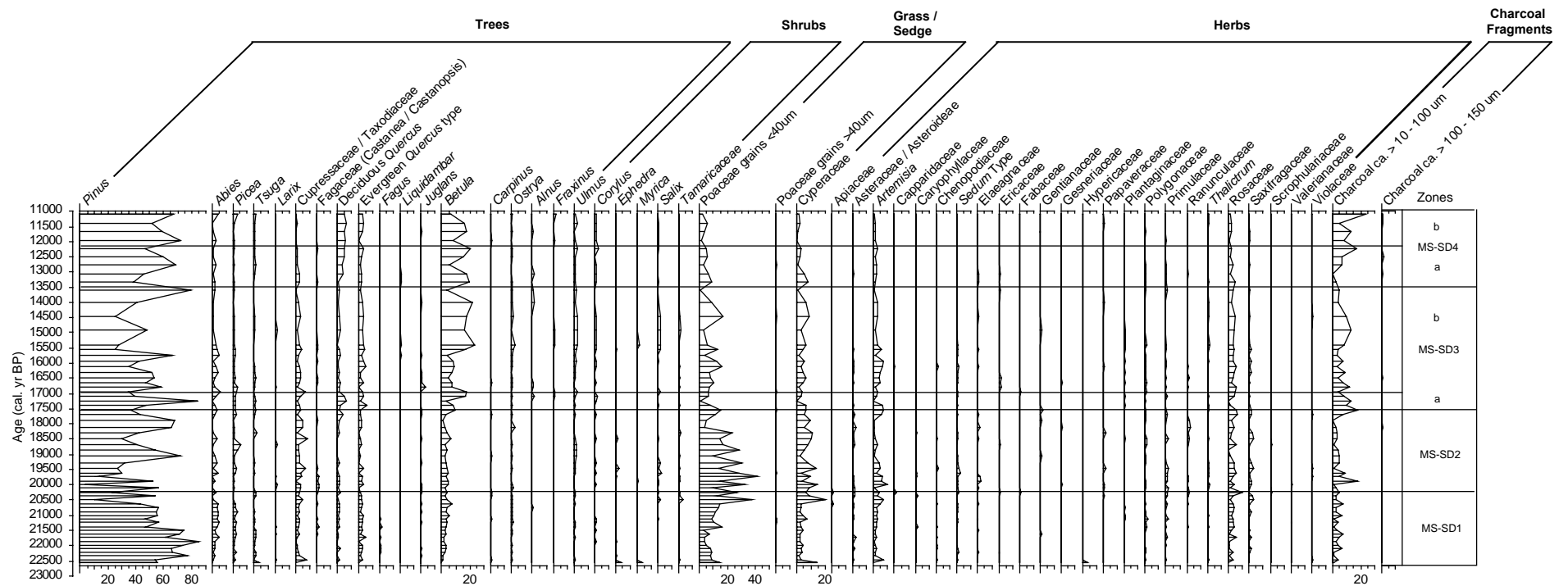


Figure 5-2: Lake Shudu summary pollen percentage diagram.

Taxa with abundances of >1% is shown. Multi-proxy zones MS-SD1 to 4, subzones labelled a and b and charcoal counts are shown for reference.

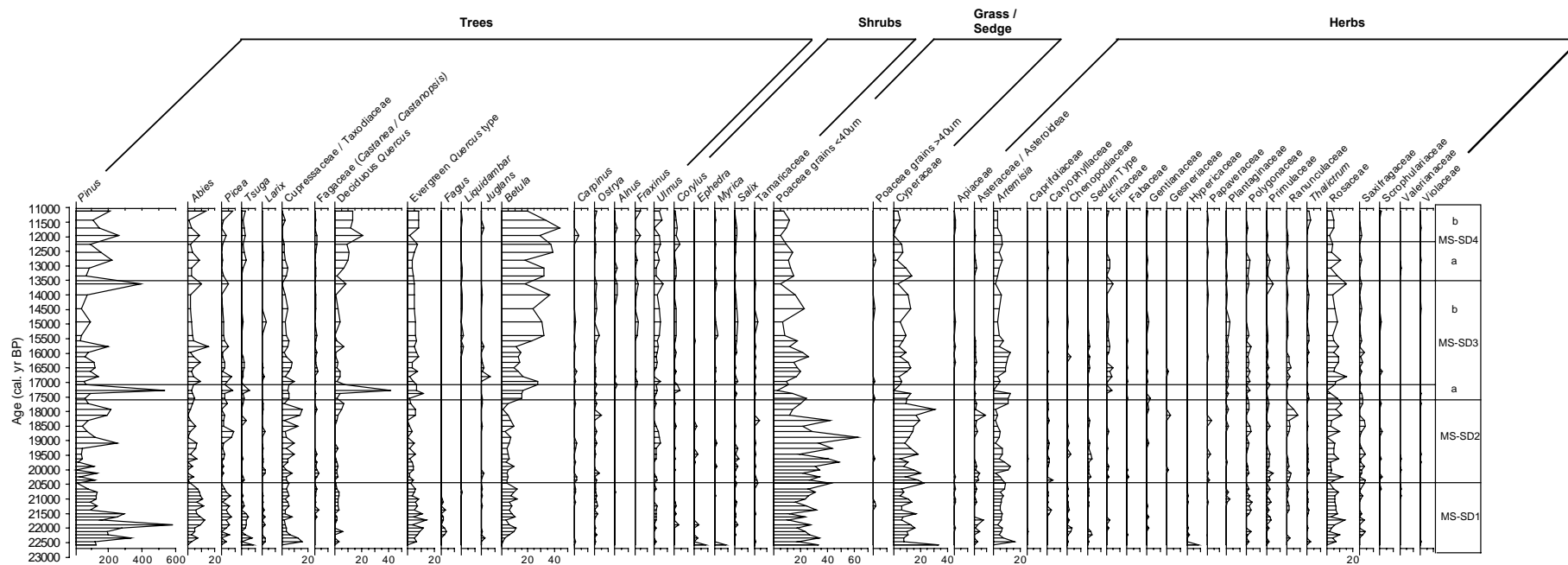


Figure 5-3: Lake Shudu summary pollen percentage diagram excluding *Pinus* from the pollen sum.

Taxa with abundances of >1% is shown. Multi-proxy zones MS-SD1 to 4 and subzones labelled a and b are shown for reference.

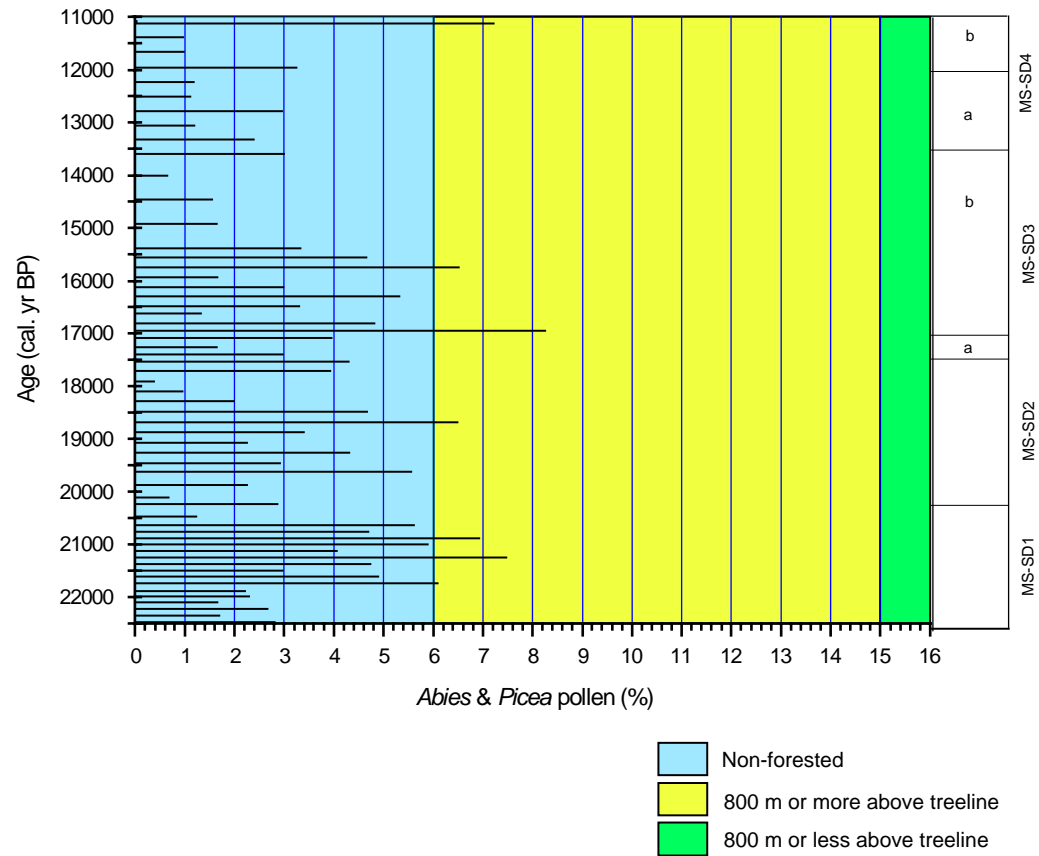


Figure 5-4: Combined percentages of *Picea* / *Abies* in the Lake Shudu pollen record.

Values are used to infer the position of the upper treeline in relation to the lake and the presence of regional forest cover. After Lu et al. (2008).

	Environmental Inferences			
Zone	MS-SD1	MS-SD2	MS-SD3	MS-SD4
Proxy / Age	c. 22.6 - 20.3 ka cal. yr BP	c. 20.3 - 17.5 ka cal. yr BP	c. 17.5 - 13.5 ka cal. yr BP	c. 13.5 - 11.1 ka cal. yr BP
Stratigraphy	<ul style="list-style-type: none"> Silty clay and sediment banding indicating a low energy environment but periods of enhanced activity 	<ul style="list-style-type: none"> Silty clay Low energy environment 	<ul style="list-style-type: none"> Increased organic matter and banding, indicating a more dynamic environment and increased influx of organic material 	<ul style="list-style-type: none"> Shift to organic gyttja pointing to increased influx of organic material into the lake
Particle Size	<ul style="list-style-type: none"> Fine particles Low energy lake flows over millennial timescales 	<ul style="list-style-type: none"> Fine particles Low energy lake flows over millennial timescales 	<ul style="list-style-type: none"> Sub-millennial scale increases in sand deposition indicating short term variability in lake energy, particularly at c. 16 ka cal. yr BP. 	<ul style="list-style-type: none"> Fine particles Low energy lake flows over millennial timescales
Magnetic Susceptibility	<ul style="list-style-type: none"> Variable, indicating changing sediment sources on sub-millennial timescales 	<ul style="list-style-type: none"> Variable but also reduced magnetic susceptibility, indicating a broadscale shift in sediment source 	<ul style="list-style-type: none"> Higher and more stable readings on millennial timescales pointing to stabilisation of sediment sources supplying the lake Peak at c. 16.9 ka cal. yr BP, indicating a short term shift in sediment source 	<ul style="list-style-type: none"> Increased magnetic susceptibility to higher but broadly stable values indicating stabilising of processes supplying minerogenic sediments to the lake
%TOC	<ul style="list-style-type: none"> Low levels of organic productivity 	<ul style="list-style-type: none"> Reduced levels of organic productivity 	<ul style="list-style-type: none"> Low but increasing levels of organic productivity An abrupt increase in organic influx and / or productivity at c. 17.2 ka cal. yr BP 	<ul style="list-style-type: none"> Gradually increasing organic productivity over millennial timescales Centennial scale shifts in organic material entering the lake after c. 12 ka cal. yr BP, implying a change in organic influx and / or productivity
%TN	<ul style="list-style-type: none"> Low levels of organic productivity 	<ul style="list-style-type: none"> Low levels of organic productivity 	<ul style="list-style-type: none"> Low but increasing levels of organic productivity An abrupt increase in organic influx and / or productivity at c. 17.2 ka cal. yr BP 	<ul style="list-style-type: none"> Gradually increasing organic productivity over millennial timescales Centennial scale shifts in organic material entering the lake after c. 12 ka cal. yr BP, implying a change in organic influx and / or productivity
C/N Ratios	<ul style="list-style-type: none"> Low levels of lacustrine productivity Variable on sub-millennial timescales 	<ul style="list-style-type: none"> Low levels of lacustrine productivity Variable rates 	<ul style="list-style-type: none"> Increased lacustrine productivity A shift towards an increased contribution of terrestrial organic carbon, and inferred catchment productivity 	<ul style="list-style-type: none"> Presence of organic material derived from aquatic and terrestrial sources suggesting a change in the balance of organic productivity within the catchment
$\delta^{13}\text{C}_{\text{palaeo}}$	<ul style="list-style-type: none"> Productivity driven by lacustrine plants Reliance upon atmospheric sources of carbon 	<ul style="list-style-type: none"> Productivity driven by lacustrine plants Reliance upon atmospheric sources of carbon Possible increase in soil-derived carbon material entering the lake 	<ul style="list-style-type: none"> Highly variable, particularly at c. 17.2 ka cal. yr BP, indicating changes in the sources of carbon supplying the lake 	<ul style="list-style-type: none"> Increasing but relatively stable $\delta^{13}\text{C}$ values pointing to increased soil development and supply of terrestrial carbon to the lake Marked shifts after c. 12 ka cal. yr BP
Pollen	<ul style="list-style-type: none"> Low pollen abundances indicating sparse grassland growing in the catchment A treeless environment Very cold and / or dry conditions 	<ul style="list-style-type: none"> Low pollen abundances indicating sparse vegetation growing in the catchment A treeless environment Cold and / or dry conditions Tundra conditions 	<ul style="list-style-type: none"> Increases in herbaceous pollen at c. 17.5 ka cal. yr BP, suggesting an increase in vegetation cover An increase in cold, mixed forest <i>Pinus</i> stands in or near to the catchment Still relatively cold but becoming warmer and / or wetter Abrupt shifts in vegetation and / or influx rates at c. 17.3 ka cal. yr BP 	<ul style="list-style-type: none"> Expansion of vegetation associated with alpine meadow, cold / cool mixed forest and shrublands Broadly warmer and wetter seasonal conditions
Charcoal	<ul style="list-style-type: none"> Low levels of secondary charcoal 	<ul style="list-style-type: none"> Low levels of secondary charcoal 	<ul style="list-style-type: none"> Low levels of secondary charcoal 	<ul style="list-style-type: none"> Low levels of secondary charcoal

Table 5-1: Lake Shudu proxies, zones and environmental inferences.

5.2 Zone MS-SD1 (c. 22.6 - 20.3 ka cal. yr BP)

This zone spans ~2200 years (Figure 5-5). The physical proxy records (particle size and magnetic susceptibility) provide an insight into changes in the lake sediment supply (Wang et al., 2005). The clastic sediments in this zone are primarily composed of fine silty clay (Leeder, 1992). Large angular sand or gravel particles are absent from the basal sediments (Figure 5-1 and Figure 5-5), suggesting that they do not contain supra or subglacial till formed by glacial activity (Benn et al., 2002; Leeder, 1992). Similar sediments obtained from Lake Qilu, Yunnan Province comprised of fine silty sediments, with low organic content are classed as glacial clay (Hodell et al., 1999), formed following the retreat of a glacier.

The dominance of fine silty clay is significant for the following reasons. Firstly, fine silt / clay particles require lower flow velocities to be transported and deposited compared to larger sand particles (Knighton, 1984). High levels of silty clay particles therefore imply that low velocity flows were in operation. This implies that Lake Shudu was a low energy depositional environment.

Secondly, the presence of fine-grained clastic particles in the Lake Shudu record implies that there was a water body in the catchment at c. 22.6 ka cal. yr BP. There is limited evidence to suggest that other basins in the region contained water-filled lakes as far back as c. 19 ka cal. yr BP. For example, Lake Ximencuo, which is located on the eastern edge of the Tibetan Plateau, was considered to be relatively deep at this time, inferred from the presence of fine-grained particles in the sedimentary record (Zhang et al., 2009).

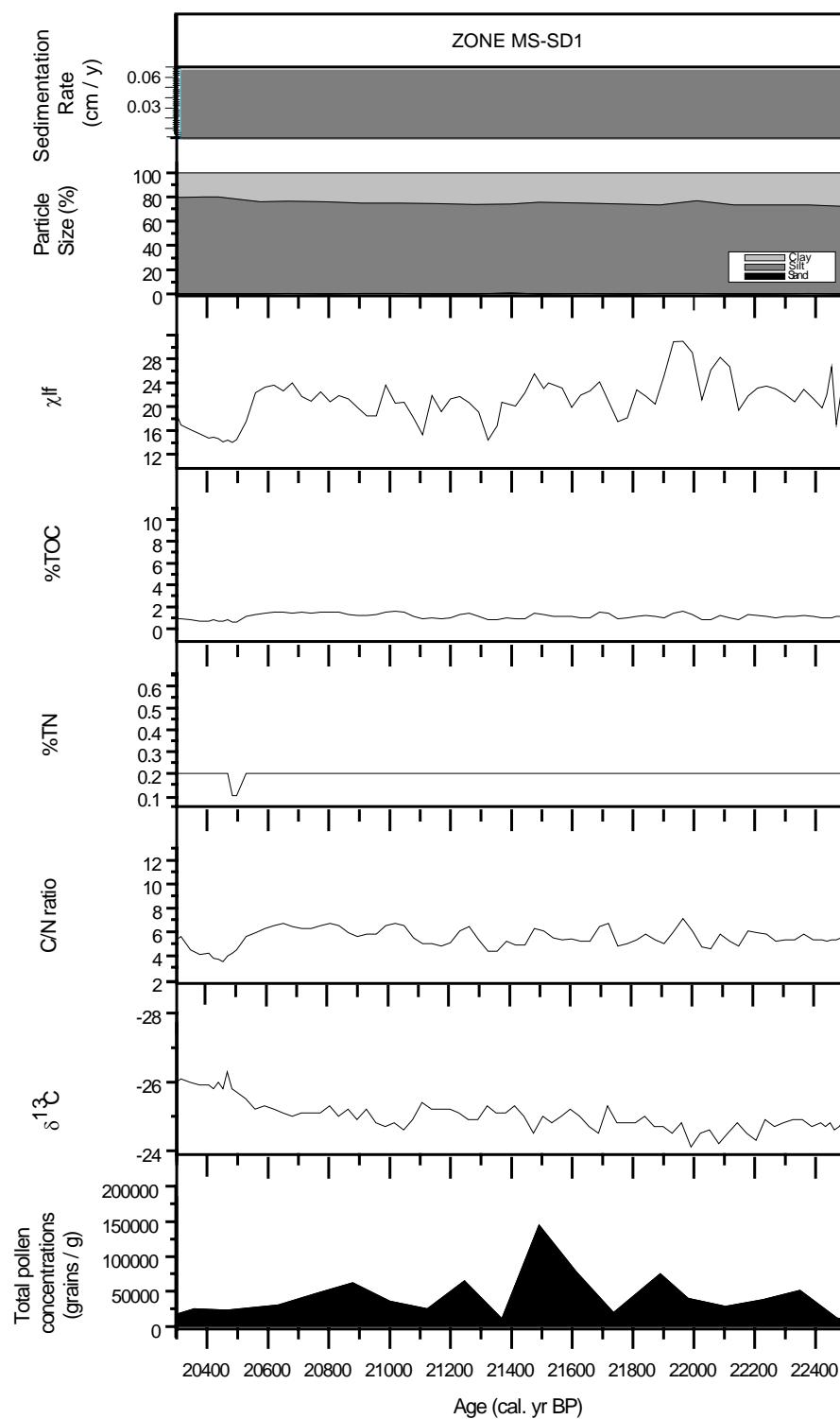


Figure 5-5: Lake Shudu proxy record, Zone MS-SD1 (c. 22.5 - 20.3 ka cal. yr BP).

Magnetic susceptibility readings are weakly magnetic (positive), remaining below $30 \times 10^{-6} \text{ m}^3 \text{ kg}^{-1}$ (Figure 5-5). Broadly speaking, sediments containing lower levels of minerogenic material (e.g. organic-rich sediments) produce lower readings, whereas sediments containing higher levels of magnetic detritus tend to produce higher readings (Walden et al., 1999). Changes in the type and / or sources of minerogenic sediments feeding into the lake are therefore reflected in changing magnetic susceptibility.

Magnetic susceptibility is variable throughout this zone, demonstrating long-term shifts in the sources of minerogenic sediments supplying the lake. On sub-millennial timescales, magnetic susceptibility is highly variable, indicating fluctuations in sediment sources, and sedimentological instability. In previous studies, low frequency magnetic susceptibility has been used as an indirect proxy for catchment instability (Shen et al., 2005a). Observed fluctuations in χ_{lf} values therefore also imply that environmental conditions at Lake Shudu were unstable on centennial timescales (Last et al., 2001), manifesting as short-term fluctuations in the influx of minerogenic materials into the lake. Fine particle sizes coupled with low but variable magnetic susceptibility are associated with sediments produced under periglacial conditions (Jones, pers comm.).

The physical proxies collectively suggest that from c. 22.6 ka cal. yr BP, the lake was largely ice-free; and that there was a water body in the basin. However, remnant ice patches may have been present in the lake and / or wider catchment. Evidence of glacial activity within the catchment, including glacial deposits preserved in sedimentary sequences adjacent to the present lake shoreline, and end and lateral moraines, suggest that a glacier covered the lake at least once before c. 22.6 ka cal. yr BP. This theory is supported by geomorphological evidence from the Hengduan Mountains (presented in Chapter 2), which indicates that glaciers were present at higher altitudes in southwestern China during this period (e.g. Yang et al., 2006).

Glacial meltwaters probably supplied the catchment with water. There is some evidence for meltwater pulses in the Lake Shudu record after c. 22.6 ka cal. yr BP. For example, short term fluctuations in magnetic susceptibility observed during this zone may have been triggered by rapid glacier melting and short-term pulses of sediment delivery coupled with redeposition of sediments previously accumulated on the lake-basin slopes (Zhang et al., 2009). At Lake Ximencuo, which is located on the eastern edge of the Tibetan Plateau, abrupt changes in magnetic susceptibility was used as evidence that conditions during the summer were warm enough to trigger rapid melting and sediment delivery to the lake.

Furthermore, increased concentrations of *Salix* pollen inferred from the pollen record at c. 21.5 ka cal. yr BP is possibly evidence of meltwater pulses (Hakala et al., 2004). *Salix* pollen is locally dominant in modern high elevation environments, which receive meltwater from snow throughout the summer (Hakala et al., 2004). Fluctuations in glacial meltwaters feeding the lake may therefore have been an important influence upon lake dynamics. However, it is not possible to determine whether meltwaters originated from local or regional sources.

Sedimentation rates are higher during Zone MS-SD1 relative to subsequent zones (Figure 5-1). The availability and supply of clastic and biogenic sediments to the lake primarily control sedimentation rates. Decreasing sedimentation rates therefore suggests that sediment influx into the lake reduced over time, possibly in response to a reduction in glacially derived sediments supplying the lake and / or an increase in vegetation cover. On balance, the physical evidence suggests that the sediments in the Lake Shudu record were deposited during the last deglaciation.

The organic and palaeoecological proxies (%TOC, %TN, C/N ratios, $\delta^{13}\text{C}$, pollen and charcoal) provide an insight into vegetation growth and related effective moisture (Wang et al., 2005). The %TOC and %TN records indicate that the sediments contained little organic material, which suggests that either organic productivity was low, or organic material was poorly preserved. Diagenetic processes can alter the elemental (carbon and nitrogen) compositions of organic material. However, lake sediments containing low organic carbon concentrations do not usually exhibit diagenetic effects (Wolfe et al., 1999). Furthermore, the nitrogen record is in concert with the carbon record and does not show any signs of dissimilarity or unusually elevated values. It is therefore likely that the organic proxies accurately reflect changes in organic productivity. Topsoil and subsoil production is likely to have been low (reflected in higher $\delta^{13}\text{C}$ values), and hence pedogenesis is unlikely to have been a major source of minerogenic sediment to the lake. Bedrock and / or glacial deposits must therefore be the primary source of magnetic minerals (Last et al., 2001).

Excluding diagenetic effects upon the organic proxies, light and nutrient availability, water and pH are therefore the primary controls on carbon and nitrogen levels and inferred organic productivity and vegetation changes (Meyers, 1997). It is therefore likely that one or more of these variables were limited during this period. Carbon and nitrogen values of ~2% and 0.2% have been recorded for tundra zones in Russia (Wolfe et al., 1999). Similar values are recorded for this zone for Lake Shudu, implying that tundra conditions were in force, characterised by sparse vegetation cover.

Modern C/N ratios are used as an analogue for interpreting the C/N and $\delta^{13}\text{C}$ palaeorecords. C/N_{modern} ratios obtained from terrestrial sources in the Lake Shudu catchment range from 14 - 58, confirming the relationship proposed by Meyers (1997). However, the ratios of macrophytes are much more variable, ranging from 9 - 75. Consequently, it is difficult to distinguish macrophytes from land plants in the $\delta^{13}\text{C}_{\text{modern}}$ record (Herzschuh et al., 2005).

The high C/N ratios associated with the macrophyte samples are normally associated with terrestrially derived organic matter (Leng et al., 2005). Grazing of domestic animals is common within the modern catchment. It is therefore likely that the high C/N_{modern} ratios reflect contamination from sewage waste rich in ammonium and / or nitrates (Leng, 2006).

$\delta^{13}\text{C}$ values obtained from Lake Shudu are primarily aligned to C₃ land plants and / or lacustrine sources (Section 4.5.6; Leng et al., 2005). Similar $\delta^{13}\text{C}$ values have been reported for sites on the Tibetan Plateau (Herzschuh et al., 2005). Other studies have reported a similar lack of modern C₄ plants from high altitude sites in China (e.g. Li et al., 2006; Xie et al., 2004). Based on modern pCO₂, the C₄ pathway is favoured in locations where daytime growing season temperatures are above approximately 20°C (Fuhrmann et al., 2003). Hence, C₄ plants are often found growing in the tropics in environments such as savannas, suggesting that the lack of C₄ plants in the Lake Shudu record may be related to its location at high altitude, and associated lower temperature gradients (Fan et al., 2009).

Li et al. (2006) studied the photosynthetic pathways of plants at three high altitude sites located on the eastern edge of the Tibetan Plateau at a similar altitude to Lake Shudu. The results revealed that all of the species studied were C₃ plants. Most of these plants were perennial, and therefore able to utilise water more effectively than C₄ plants, and were more able to cope with extreme conditions. The absence of plants utilising the C₄ photosynthetic pathway was attributed to very low temperatures coupled with the high altitude, where climatic extremes are likely, resulting in the preferential growth of C₃ plants.

Rates of variation in $\delta^{13}\text{C}$ with altitude have been examined in previous research (e.g. Zheng et al., 2007; Guo et al., 2006). For example, Guo et al. (2006) concludes that above 3500 m asl, $\delta^{13}\text{C}$ increases with altitude. Guo et al. (2006) compared a number of studies exploring the rate of increase and found that estimates varied from 1.37‰ / km to 1.31‰ / km. Lake Shudu is located at 3630 m asl, 100 m above the threshold, thus $\delta^{13}\text{C}$ values are likely to be slightly elevated, by 0.137 - 0.13‰. Altitudinal effects upon $\delta^{13}\text{C}$ values are therefore likely to be relatively small. However, there is currently little consensus in the literature regarding the reasons for this relationship, or the precise increases involved (Guo et al., 2006).

Catto (2006) investigated the relationship between modern $\delta^{13}\text{C}$ values and altitude based on C_3 plant leaves obtained from sites in the northern and southern Tibetan Plateau. Samples from both areas indicate a positive relationship between $\delta^{13}\text{C}$ and altitude. However, isotopic shifts are attributable to changes in precipitation rather than temperature. In Northern Tibet, $\delta^{13}\text{C}$ values increase by 0.46‰ with an increase of 100 mm in precipitation, while on the southern Tibetan Plateau $\delta^{13}\text{C}$ values decrease by 1.82‰ with an increase of 100 mm in precipitation. It appears that plants / $\delta^{13}\text{C}$ in the northern and southern zones of the Tibetan Plateau respond differently to precipitation. However, at present there is insufficient evidence to confirm the nature and extent of this inferred relationship.

If the abovementioned sites serve as a modern analogue demonstrating the relationship between altitude and C_4 plant distribution, then it can be concluded that since the Late Pleistocene, conditions at Lake Shudu are characterised by low temperatures (indicated by the lack of C_4 plants) and low but gradually increasing levels of precipitation accompanied by seasonal fluctuations in precipitation. However, these relationships are complex and have not yet been fully resolved, therefore it is not possible to further distinguish the relative influences of temperature, precipitation and altitude upon $\delta^{13}\text{C}$ values (Guo et al., 2006).

C/N ratios within Zone MS-SD1 are <10 , indicating that organic material is likely to be derived from lacustrine sources. Ratios of >10 indicates mixed sources, whilst higher ratios indicates the presence of material primarily derived from terrestrial sources (Meyers, 1997). This suggests that organic material in the sediments is mostly autochthonous. The Lake Shudu $\delta^{13}\text{C}$ record is therefore tentatively used as an indicator of past changes in aquatic carbon cycling and within-lake processes (Leng et al., 2005). The pollen record indicates that levels of aquatic taxa (e.g. macrophytes) are low. Consequently, lacustrine material is likely to have originated from phytoplankton containing very little carbon.

Where C/N ratios do not indicate changing plant types being incorporated into lake sediment, biological productivity is the most influential variable upon $\delta^{13}\text{C}$. (Menking et al., 1997). The C/N record confirms that there were no significant changes in plant type (i.e. from aquatic to terrestrial) during this period. Hence, when interpreting the $\delta^{13}\text{C}$ record in terms of lacustrine productivity, the balance between photosynthesis and respiration is assumed to be the dominant signal preserved in the record (Wolfe et al., 1999).

The carbon isotope composition of aquatic cellulose is primarily determined by the $\delta^{13}\text{C}$ of lake water dissolved inorganic carbon (DIC) and CO_2 . This is controlled by a number of interconnecting factors including the isotopic exchange with atmospheric CO_2 , input of DIC from the catchment, the preferential uptake of ^{12}C by phytoplankton during photosynthesis and recycling of ^{13}C depleted carbon from the decay of organic matter in the water column and bottom sediments (Wolfe et al., 1999).

$\delta^{13}\text{C}$ values gradually become lower over the course of this zone and beyond (Figure 5-1 and Figure 5-5). Lowering $\delta^{13}\text{C}$ values may have been triggered by gradual rises in the amounts of $\delta^{13}\text{C}$ -depleted CO_2 (aq) generated by soil development processes being deposited into the lake (Wolfe et al., 1999). The shift in values may therefore have reflected a subtle increase in vegetation cover and soil development. However, organic productivity remains low, and there is no change in the source of organic material, suggesting that terrestrial processes do not have a significant influence upon the sedimentary record. It is notable that in comparison to subsequent zones, $\delta^{13}\text{C}$ values are relatively high, perhaps suggesting that atmospheric CO_2 , which has higher $\delta^{13}\text{C}$ values, was the dominant source of carbon supplying the lake. Changing $\delta^{13}\text{C}$ values may therefore reflect changes in atmospheric sources of carbon and lacustrine productivity (Wolfe et al., 1999).

Very low pollen concentrations characterise Zone MS-SD1. Samples with low total pollen concentrations were checked for sample loss by comparing the abundances of added *Lycopodium* grains with those in samples with high pollen concentrations. Key samples were also re-prepped and counted a second time. The results confirm that the low pollen concentrations were unlikely to be caused by sample loss during processing. Moreover, pollens grains in the small samples did not show signs of significant degradation. It is therefore likely that the low concentrations reflect very low vegetation growth at this time.

Vegetation cover primarily consisted of Poaceae, Cyperaceae and herbaceous taxa including *Artemisia* (Figure 5-2). These taxa are associated with tundra vegetation and cold, dry conditions (Yu et al., 2000a). The dominant taxa in alpine meadows on the Tibetan Plateau today are Cyperaceae, Poaceae and *Artemisia*. Alpine meadow assemblages are commonly comprised of >20% Cyperaceae, 5 - 15% Poaceae and >10% *Artemisia* (Zhao et al., 2009). Both Cyperaceae and *Artemisia* abundances are significantly lower than this. However, Cyperaceae values of >10% occur where areas of treeless vegetation is present (Zhao et al., 2009), as is the case at the start of this zone. Conversely, Poaceae percentages are broadly in line with levels of pollen associated with alpine meadow (5 - 15%). Grasses are generally associated with cool conditions in alpine environments and are often found growing in open ground (Herzschuh, 2007).

Pinus pollen was the primary contributor to the pollen record. *Pinus* is an alpine, coniferous, evergreen species. It is a hardy species with conical needles, enabling the tree to survive in environments where water availability is low (Thomas et al., 2007). *Pinus* is also frost-tolerant and capable of withstanding temperature minimums as low as -40°C (Woodward, 1996). The dominance of *Pinus* in the pollen record therefore implies that conditions were cold and dry.

Pinus is a good disperser rather than an abundant pollen producer (Bradshaw et al., 1985). Large air sacs enable grains to be dispersed long distances via wind and water conduits before being deposited in lakes, bogs etc. Consequently, *Pinus* pollen is often over-represented in pollen percentage diagrams (Van Campo et al., 1993). This effect can be examined by comparing Figure 5-2 and Figure 5-3, which illustrate the difference in the pollen sum when *Pinus* is included and excluded. The diagrams clearly highlight that the contributions of other taxa including Poaceae, Cyperaceae and selected herbs is masked by the inclusion of *Pinus* in the pollen sum.

High percentages coupled with low *Pinus* concentrations occurs when there is a *Pinus* pollen influx from parent trees growing in areas further away, rather than just from local sources (Shen et al., 2005b). *Pinus* percentages generally exceeded 50%, indicating high percentages relative to other taxa. However, *Pinus* pollen concentrations were relatively low up to c. 11.1 ka cal. yr BP. This suggested that the *Pinus* pollen came from areas outside the catchment.

During periods of low regional pollen production, for example during cold / dry periods, non-local pollen grains are particularly well represented in the pollen record (Van Campo et al., 1993). Moreover, the effects of long-distance pollen such as *Pinus* may be enhanced in environments containing sparse vegetation, where local pollen production is low (Gobet et al., 2005). For example, on the Tibetan Plateau, arboreal pollen (particularly *Pinus*) has been found in pollen spectra collected from treeless environments (Herzschuh, 2007).

Furthermore, during periods of low regional pollen production, arboreal pollen is well represented (Van Campo et al., 1993). In addition, arboreal pollen percentages (AP%) within pollen samples appear to increase with lake size. AP% are raised by 1 - 2% in large alpine lakes $>0.25\text{ km}^2$ compared to small alpine lakes $<0.25\text{ km}^2$ (Zhao et al., 2009). Lake Shudu is a medium sized lake, therefore AP% are likely to be partly a function of the lake size. Consequently, the AP% component was possibly over-represented in the record, providing further support for the hypothesis that forest cover was significantly reduced during this period. In the Northern Hemisphere, forest ceases to grow when average temperatures fall below 10°C (Thomas et al., 2007), therefore the lack of forest cover is equated with a climate generally defined by low temperatures.

Low total pollen concentrations coupled with low concentrations of Poaceae and Cyperaceae, coupled with a high influx of *Pinus* pollen suggest that catchment vegetation cover was extremely sparse and primarily composed of grassland. Furthermore, the dominance of *Pinus* pollen concentrations may therefore indicate that pollen abundances and associated vegetation cover was even sparser in the catchment than inferred from the pollen record (Birks et al., 1980).

Picea and *Abies* pollen is poorly dispersed and therefore used to detect changes in the local vegetation (Bunting et al., 2004; Sugita, 1993). *Abies* and *Picea* are evergreen strategists that do not drop their needles regularly and tend to grow in harsh environments, where the growing season is short, or where conditions are extreme all year round (Thomas et al., 2007). Today in northwestern Yunnan Province, sub-alpine coniferous stands comprising of *Abies* and *Picea* is the dominant forest type and forms most of the alpine treeline (Lu et al., 2008).

Percentages of *Abies* were higher than *Picea*. At higher altitudes (~3500 - 4200 m asl), *Abies* out competes *Picea*, because it is able to grow in more extreme conditions and has a wider altitudinal range (McGinley, 2007; Wong, 2005; Shen et al., 2005a). *Abies* can tolerate periods of reduced water availability better than *Picea*; therefore the difference in abundances may be attributable to reduced water availability (Lu et al., 2008). Hence the higher levels of *Abies* pollen compared to *Picea* pollen appears to confirm that conditions were much colder and / or drier than today.

Combined percentages of *Abies* and *Picea* Figure 5-4 indicate that the treeline was located below Lake Shudu at this time. Furthermore, combined percentages of *Abies* and *Picea* were <6%, implying that Lake Shudu was unforested. Hence, arboreal pollen including *Pinus*, *Abies* and *Picea* was probably transported on strong up-blowing winds from lower down the mountain (Lu et al., 2008).

Today, the upper treeline is located ~600 m above Lake Shudu. The upper limit of tree growth is controlled primarily by temperature, whereas the lower limit is restricted by precipitation (Beer et al., 2007), suggesting that conditions were colder at Lake Shudu compared to the present. It is not possible to precisely estimate the altitude of the treeline or temperature at this time owing to the lack of high-resolution records above and below Lake Shudu spanning this period. However, it is possible to conclude that conditions must have been much colder and drier compared the present in order to for the treeline to be located at a lower altitude relative to its present day position at ~4000 m asl (Lu et al., 2008).

Levels of other arboreal taxa are low. For example, *Betula* percentages do not exceed 10% during Zone MS-SD1, suggesting that *Betula* pollen preserved in the record originated from sources outside of the catchment (Huntley et al., 1984). *Betula* is a deciduous alpine pioneer species, which can tolerate minimum temperatures of -40°C , equalling that of boreal conifers (Woodward, 1996). Chinese species of *Betula* tend to grow in temperate mixed broadleaved forests. Low levels of extralocal *Betula* therefore indicate that conditions were extremely cold. Furthermore, *Betula* is associated with stage 1 of forest succession (stand re-initiation) and tends to colonise grassland areas (Martin et al., 1996). Variations in *Betula* in the pollen record therefore point to subtle changes in successional patterns. Charcoal fragments are small and abundances are generally low throughout the whole record, suggesting the presence of secondary charcoal, resulting from natural fluctuations in charcoal accumulation rates (Beer et al., 2007; Last et al., 2001).

In summary, evaluation of the zonal pollen record as a whole suggested that the catchment was treeless, and vegetation consisted primarily of sparse grassland. Very low AP% levels, dominated by *Pinus* transported from the wider environment indicated that the treeline was located well below Lake Shudu. These factors, coupled with low organic productivity, a low energy depositional environment and subtle fluctuations in the sediment sources supplying the lake are elements of a classic periglacial landscape.

5.2.1 Zone MS-SD1 summary

Collectively the proxies suggest the following environmental and climatic conditions;

- a low energy lake regime;
- low lacustrine productivity;
- a largely ice-free lake fed by glacial meltwaters;
- a treeless catchment suggesting that Lake Shudu was located well above the treeline;
- catchment vegetation aligned to alpine grassland / tundra;
- a very cold and dry climate.

5.3 Zone MS-SD2 (c. 20.3 - 17.5 ka cal. yr BP)

This zone spans ~2700 years of environmental change at Lake Shudu (Figure 5-6). Deposition of fine particles and light grey clay suggest that lake energy remained low (Wolfe et al., 1999; Lister et al., 1991). However, there are periods of increased activity captured in the record. For example, at c. 19.5 ka cal. yr BP, mixed laminations of darker and lighter silt indicate a period of enhanced bottom-current activity and / or enhanced sediment inwash (Lister et al., 1991). Levels of silt are highest in this zone.

Magnetic susceptibility readings are generally lower over millennial timescales, but variable on centennial timescales. In particular, there are notable fluctuations after c. 19 ka cal. yr BP, suggesting short term shifts in the sediment sources supplying the lake. At the end of this zone, magnetic susceptibility drops sharply between c. 17.6 and 17.5 ka cal. yr BP, representing the lowest reading for the whole record. This indicates a change in the types and / or sources of minerogenic sediments deposited in the lake. At Lake Ximencuo, also located on the southeastern edge of the Tibetan Plateau, minimum magnetic susceptibility values were equated to a reduction in the delivery of glacially derived material and the decreasing influence of glacial activity which had previously driven sediment dynamics in the catchment (Zhang et al., 2009).

The long term trends in the physical proxies point to a reduction in lake energy and a shift in sediment sources supplying the lake (Lister et al., 1991). Sedimentation rates are lower, pointing to a reduction in sediment availability and / or supply and lower catchment energy. Low total concentrations in the pollen record suggests a sparse vegetation cover, indicating that the reduced sedimentation rates are attributable to factors other than increased catchment stability triggered by denser vegetation cover (Knighton, 1984).

%TOC and %TN remain low, indicating low levels of organic productivity. However, %TN is slightly more variable than the previous zone, suggesting a decrease in the amounts of nitrogen supplying the lake, nitrogen cycling and / or the metabolic rates of dominant taxa (Wolfe et al., 1999).

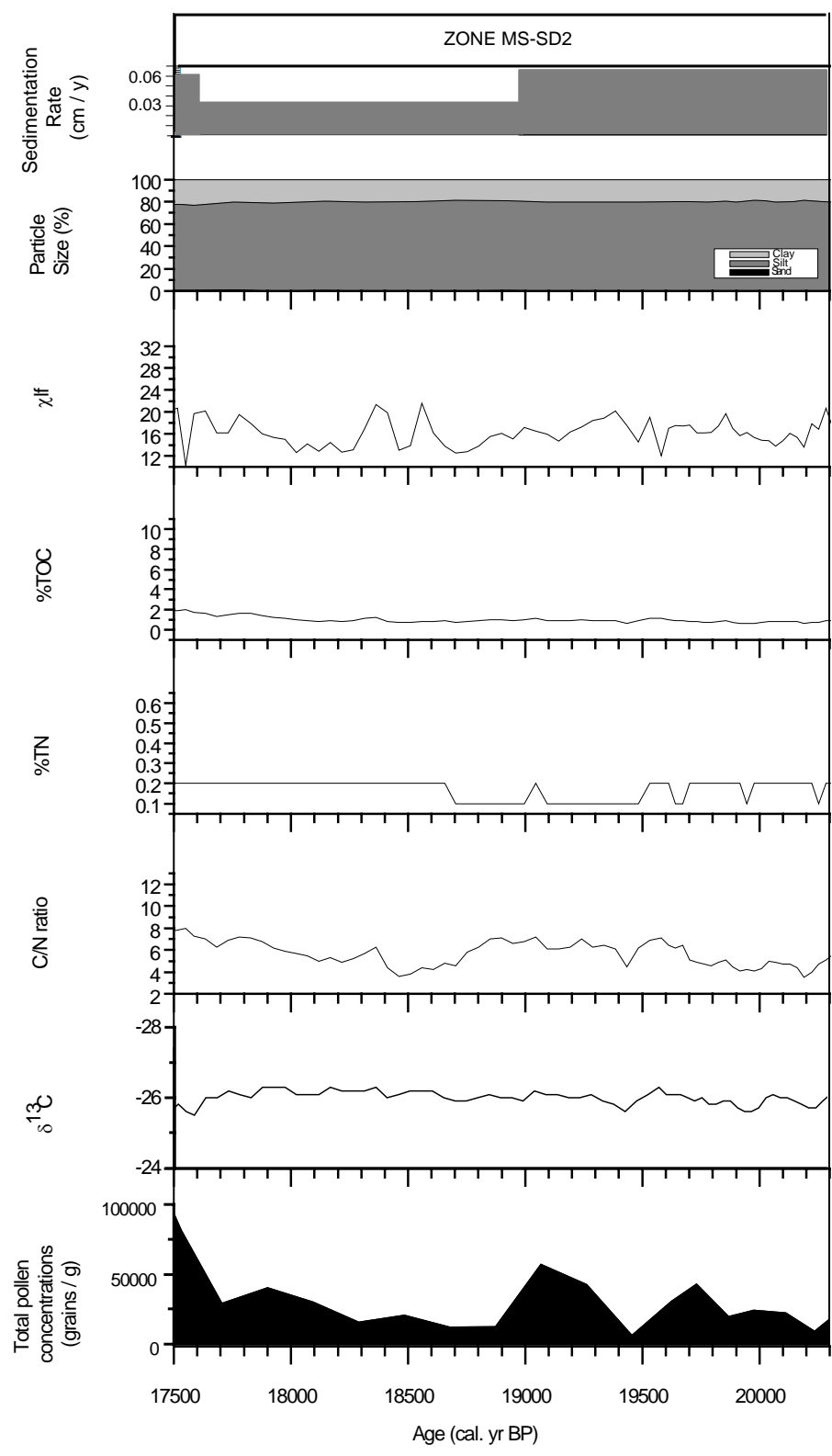


Figure 5-6: Lake Shudu proxy record, Zone MS-SD2 (c. 20.3 - 17.5 ka cal. yr BP).

Zonal C/N ratios remain low (<10), indicating that the organic material contained in the sediments is primarily derived from aquatic plants. However, there are marked fluctuations in the C/N record on sub-millennial timescales. $\delta^{13}\text{C}$ values are slightly lower compared to the previous zone. C/N ratios and $\delta^{13}\text{C}$ values indicate that organic material is primarily autochthonous, suggesting that within-lake processes are more influential than catchment processes (Meyers et al., 1999). Levels of aquatic pollen are low suggesting that phytoplankton were driving within-lake productivity. The shift of $\delta^{13}\text{C}$ values to lower values but with no marked increase in lake productivity or plant type changes implies that soils could have been developing in the catchment, providing a supply of soil-derived material with lower $\delta^{13}\text{C}$ values (Leng et al., 2005).

Similarly to Zone MS-SD1, total pollen concentrations are low and variable on shorter timescales. Key taxa included Poaceae, Cyperaceae and *Pinus* pollen. Minimal amounts of other types of arboreal pollen are present in the pollen record. These include *Abies*, *Picea*, evergreen *Quercus* and pioneer taxa including *Betula* and species of Cupressaceae / Taxodiaceae (Figure 5-2). The low percentage of these taxa implies that they were growing outside of the catchment and that wider forest cover was low. The presence of pioneer species also implies that vegetation assemblages were in the early stages of succession (Martin et al., 1996; Huntley et al., 1984). Combined percentages of *Abies* and *Picea* were $<6\%$ (Figure 5-4) imply that the treeline remained well below Lake Shudu (Lu et al., 2008). Deciduous arboreal taxa are poorly represented in the pollen record, providing further evidence of uniformly cold conditions all year round, and a lack of seasonality (Shen et al., 2005a).

However, at c.19.6 ka cal. yr BP, total pollen concentrations increase, with notable rises in non-arboreal pollen. There are also notable shifts in the abundances of specific taxon at this time. For example, abundances of *Pinus* pollen and *Quercus* pollen decrease, whilst concentrations of other coniferous pollen (including *Picea*, *Abies*, *Tsuga*, Cupressaceae / Taxodiaceae and *Larix* increased. Abundances of *Betula* also increased. However, individual percentages of these taxa are low, confirming that they were probably not growing in the catchment at this time (Herzschuh, 2007; Huntley et al., 1984).

Increased amounts of *Betula* pollen intimates that successional changes continued to drive vegetation changes, possibly including the establishment of coniferous forest patches in the wider environment (Thomas et al., 2007). However, the growth of hardy *Betula* trees coupled with an increase in coniferous taxa suggested that conditions were still very cold and somewhat dry (Woodward, 1996). Levels of herbs associated with more moist conditions such as *Artemisia* remains low, suggesting that effective moisture was correspondingly low (Herzschuh, 2007).

Pollen concentrations fall at c. 19.5 ka cal. yr BP, representing the lowest recorded concentrations for the whole core (Figure 5-6). Arboreal pollen percentages are low (~50%), driven by a reduction in *Pinus* pollen concentrations, which reaches the lowest levels for the whole core. This indicates a further reduction in vegetation at a point in time when land cover was already very sparse. At c. 19.3 ka cal. yr BP, Poaceae and Cyperaceae dominated grasslands began to be re-established following the decline in vegetation cover at c. 19.5 ka cal. yr BP. Cover remained sparse but increasing in density (Van Campo et al., 1993). Other taxa remain minimal. Catchment vegetation was largely comprised of treeless tundra vegetation (Huntley et al., 1984).

From c. 18.9 - 18.7 ka cal. yr BP, levels of non-arboreal pollen decrease. There is a concurrent marked decline in arboreal pollen abundances, including *Pinus* pollen. Low levels of Poaceae dominate the pollen record during this period, indicating the continued influence of grassland / tundra assemblages. At c. 18.5 ka cal. yr BP, total pollen concentrations increase, although abundances of *Pinus* pollen remain relatively low. Cupressaceae / Taxodiaceae, Poaceae, Cyperaceae and *Betula* showed marked increases. A slight increase in herbs including Saxifragaceae also occurs. However, by c. 18.3 ka cal. yr BP, levels of *Pinus* and Poaceae pollen concentrations increase, but there is an overall decrease in the abundances of other taxa. At c. 17.9 ka cal. yr BP, the pollen record indicates increased abundances of *Pinus*, pioneer species of Cupressaceae / Taxodiaceae and Cyperaceae pollen and marginal increases in Poaceae, suggesting that climatic conditions became favourable enough for trees to start colonising open ground (Martin et al., 1996; Woodward, 1996). Pollen concentrations remain low overall, suggesting that cold, dry conditions continued. However, shifts in arboreal / non arboreal pollen abundances, coupled with discernible rises in %TOC, C/N ratios and inferred organic productivity suggest that conditions were perhaps becoming warmer and / or wetter.

5.3.1 Zone MS-SD2 summary

Collectively the proxies pointed to the following environmental and climatic conditions;

- low levels of within-lake productivity;
- a treeless catchment suggesting that the lake was located above the treeline;
- catchment vegetation initially consisting of taxa associated with the tundra biome;
- very cold / dry conditions, becoming warmer and / or wetter from c. 18 ka cal. yr BP.

5.4 Zone MS-SD3 (c. 17.5 - 13.5 ka cal. yr BP)

This zone spans ~4000 years and includes pronounced shifts from c. 17.5 - 17.2 ka cal. yr BP, which are the most prominent feature of the Lake Shudu record (Figure 5-7). In general, there are marked shifts in both the organic and palaeoecological proxies, which suggest that there were fundamental changes taking place in the catchment during this phase. Two subzones distinguish the shifts associated with this event from the rest of the zone. The first subzone spans c. 17.5 - 17.0 ka cal. yr BP, and the second subzone spans c. 17.0 - 13.5 ka cal. yr BP.

5.4.1 Subzone MS-SD3a (c. 17.5 - 17.0 ka cal. yr BP)

At c. 17.5 ka cal. yr BP, total pollen concentrations increase significantly, primarily defined by rises in *Pinus* and Poaceae, coupled with notable increases in *Betula*, Cyperaceae, *Artemisia* and other herbs including Gentianaceae, Ranunculaceae, Rosaceae and Saxifragaceae. It is therefore likely that there was an increase in vegetation cover during this phase. However, there are no stomata visible in the pollen samples, indicating that they were not being inwashed into the lake in high levels, suggesting that trees were not growing in the catchment. Furthermore, incidences of subtropical pollen, including *Ulmus* increase. *Ulmus* tends to grow at lower altitudes, which suggests that pollen grains associated with these taxa were being transported to the lake via up blowing winds (Cour et al., 1999) and / or transported long distances via the stratosphere. Consequently, arboreal pollen grains were probably transported to the lake from other sites.

From c. 17.4 - 17.3 ka cal. yr BP, %TOC, %TN and C/N ratios began to rise and $\delta^{13}\text{C}$ values start to become much lower, perhaps suggesting increased organic productivity and the development of soils, and supplying soil-respired CO_2 to the lake, resulting in the production of organic material with lighter (^{13}C depleted) $\delta^{13}\text{C}$ values. Percentages of evergreen *Quercus* increase quite markedly. Equally, *Salix*, Cyperaceae and *Artemisia* abundances all increase. Conversely, levels of *Pinus* pollen are quite low (<50%). From c. 17.3 - 17.2 ka cal. yr BP, a number of concurrent shifts occur across the proxies. Firstly, the stratigraphy changes from light clay to dark coloured organic gyttja / silt. This is coupled with a marked rise in %TOC and %TN, indicating an increase in levels of organic material being deposited in the lake.

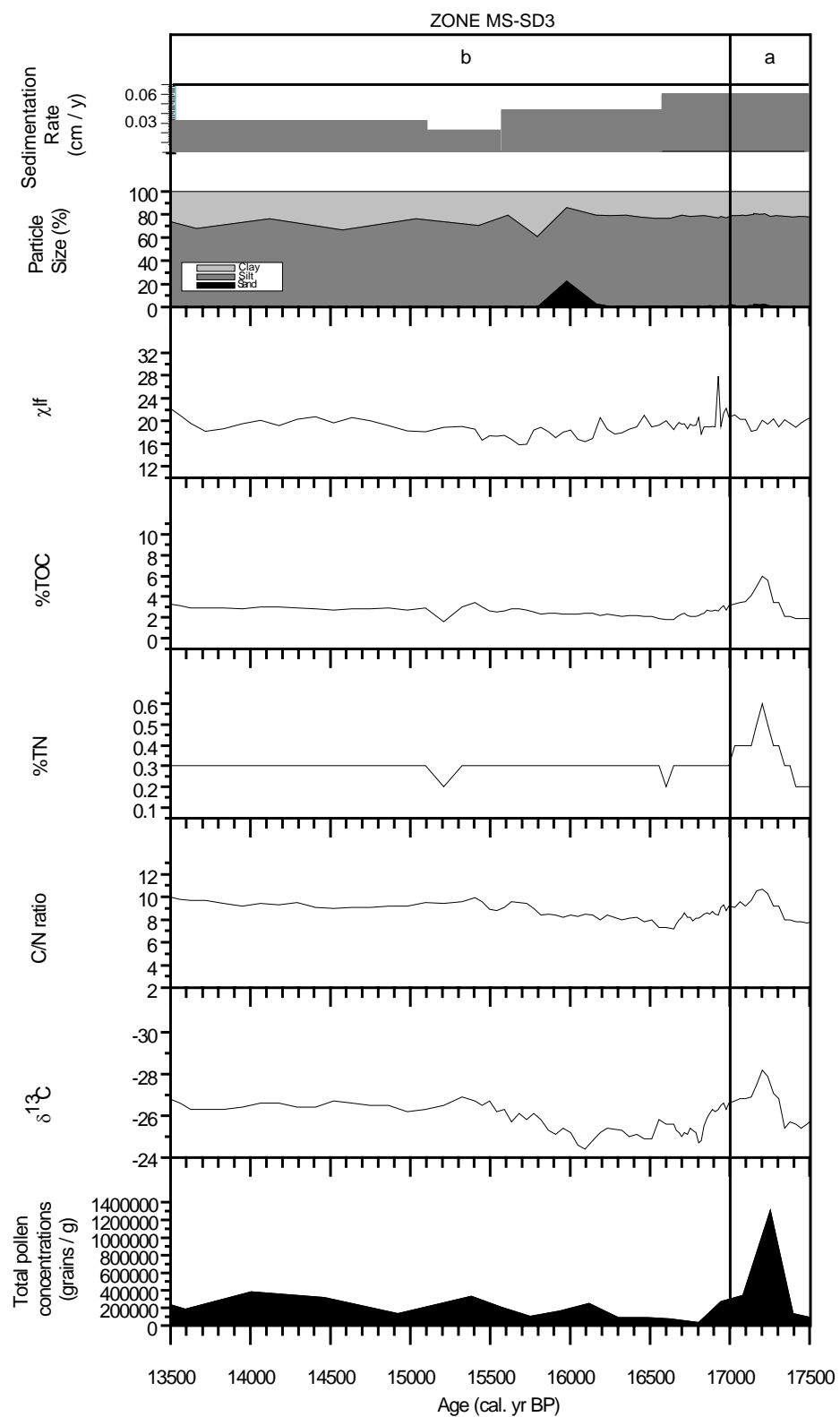


Figure 5-7: Lake Shudu proxy record, Zone MS-SD3 (c. 17.5 - 13.5 ka cal. yr BP).

Secondly, the C/N record indicates that the sources of organic material preserved in the sediments shifts from being derived from purely aquatic sources to a mixture of aquatic and terrestrial C₃ land plant sources. It is difficult to determine whether terrestrial or aquatic productivity was dominant at this time, owing to the mixed provenance of the organic material (Herzschuh et al., 2005). Furthermore, the presence of mixed sources of organic carbon in the C/N record indicate that factors other than biological productivity, such as changes in plant type may have been driving changes in the $\delta^{13}\text{C}$ record during this period. $\delta^{13}\text{C}$ values become much lower, indicating increased levels of soil development supplying soil-respired CO₂ to the lake and implying a shift in nutrient supply from atmospheric to terrestrial sources.

Thirdly, there are pronounced shifts in the pollen record, including a peak in *Pinus* pollen, deciduous *Quercus* and *Betula*. Total pollen concentrations exceed >1.3 million grains / gram. Most of this rise is accounted for by *Pinus* pollen, which represents >80% of the pollen record (>1 million grains / gram). Overall, arboreal pollen represents 98% of the pollen record.

However, combined percentages of *Picea* and *Abies* are <6%, suggesting that the treeline was still located below the lake. Conversely, the presence of stomata in the pollen sample pertaining to this interval suggests that trees (perhaps hardy species of *Pinus*) were growing in or near to the catchment, implying that the treeline was located quite near to Lake Shudu (Vescovi et al., 2007). Notably, grasses, sedges and herb taxa which were rising in abundance prior to this phase, including Poaceae, Cyperaceae, *Artemisia* and Rosaceae are negligible or absent from the record at c. 17.3 ka cal. yr BP.

It should be noted that there are anomalies in the AMS ¹⁴C radiocarbon dates associated with events at c. 17.3 - 17.2 ka cal. yr BP. In particular, the dates obtained for these intervals are significantly younger than the adjacent dates. In deglacial sequences, dating uncertainties may be caused by an influx of meltwaters carrying glacial clay containing older carbon sources (Leng et al., 2005). However, this is unlikely to be a factor in the present study, because the dates in question are younger rather than older. Furthermore, elemental analysis indicates that the sediments contain very low levels of CaCO₃.

The lateral advection (percolation) of humic acids and / or other organic residues produced during the development of the soil profile may result in the production of pre-aged dates (up to ~3000 years too young) obtained from sediments lower down the core (Bol et al., 1996), especially if the sediments are fine-grained (Mollenhauer et al., 2008). Based on available evidence, it is not possible to determine whether this was the cause of the younger dates, although it would seem to be a plausible explanation. However, it is not clear why only this section of the core is affected, but other sections appear to be unaffected. Hence, this issue remains open to debate.

Following the events at c. 17.5 - 17.2 ka cal. yr BP, sedimentation rates decline, suggesting a decrease in sediment availability and / or supply. However, levels of sand particles increase, suggesting a rise in lake energy. Together these factors imply a reduction in sediment transported to the lake but an increase in flow strength. Magnetic susceptibility increases, suggesting a change in sediment source supplying the lake. %TOC and C/N ratios remains relatively high until c. 17.1 ka cal. yr BP, then start to decrease. At the same time, $\delta^{13}\text{C}$ values revert to higher values, suggesting a shift from terrestrial sources (denoted by low $\delta^{13}\text{C}$ values) to atmospheric sources (having high $\delta^{13}\text{C}$ values) of carbon supplying the lake. The organic proxies therefore indicate that organic productivity decreased following events at c. 17.3 ka cal. yr BP, possibly pointing to a return to relatively cooler and / or drier conditions. However, the proxies indicated that organic productivity was higher compared to levels prior to c. 17.5 ka cal. yr BP, implying that conditions were perhaps not as cold and dry as before.

From c. 17.1 ka cal. yr BP, levels of coniferous arboreal taxa (including *Abies* and Cupressaceae / Taxodiaceae) and also *Betula* and evergreen *Quercus* (but not deciduous *Quercus*) increase. Other shrubs, herbs (including Rosaceae) and grass / sedge also increase. Conversely, *Pinus* pollen concentrations decline markedly. Levels of *Pinus* pollen remain at ~50%. These changes point to a shift in the relative abundances of arboreal vegetation.

Overall, the proxies record significant differences between the lake and catchment regime before and after the events at c. 17.5 - 17.2 ka cal. yr BP. On centennial to decadal timescales, changes in vegetation (including treeline advance or retreat) and / or changes in water, ice and sediment regimes are driven by climatic changes, biospheric changes (including landslides or avalanches), changes in greenhouse gases, oceanic circulation or volcanic activity (Pant, 2003). Based on evidence in the Lake Shudu record, it is not possible to comment specifically on the potential influences of changes in greenhouse gases, oceanic circulation or volcanic activity. However, the proxies provide an insight into the potential role of climatic and / or biospheric drivers in effecting changes in the catchment.

The observed increase in moist herbaceous vegetation cover, followed by increased organic productivity, stratigraphic changes and a shift in land cover from meadow to *Pinus* woodland and an advancing treeline are consistent with successional changes triggered by a phase of warmer and / or wetter conditions (Zhao et al., 2009; Hakala et al., 2004; Huntley et al., 1984). However, the extent to which conditions became warmer and / or wetter is debateable. For example, other palynological studies focusing on the palaeovegetation of Yunnan Province at c. 17 - 15 ka cal. yr BP appear to confirm that in high altitude regions, montane conifer forests were dominant, whereas in lowland areas forest covered consisted of a mixture of *Pinus* and evergreen sclerophyllous *Quercus* forest (Lin et al., 1986).

Minimum winter temperature tends to determine the form of trees (i.e. whether shrubby or fully grown) (Ohsawa, 1993). Evergreen *Quercus* tends to be sclerophyllous and exhibit xerophytic characteristics in cold, dry environments, because this makes them more drought and frost resistant (Thomas et al., 2007; Tang, 2006). The presence of evergreen *Quercus* at lower altitudes therefore implies that climatic conditions remained relatively cold and dry at during this period.

Biospheric changes including landslides and avalanches can trigger marked changes in catchment vegetation and sedimentary processes. Because of the issues associated with equifinality (i.e. some ecosystem disturbances produce the same effects), it is difficult to distinguish between types of event based on available evidence (Conedera et al., 2009). Biospheric changes are therefore discussed collectively as inwash events.

Firstly, it is proposed that the events centred at c. 17.3 ka cal. yr BP took place during the last deglaciation. Glacier recession alters the hydrology and rates of sediment transfer within these glaciated and adjacent catchments, and increases the likelihood of glacier lake outburst floods and other types of inwash events (Benn et al., 2002). If this were the case, then there should be a corresponding shift in the particle size record to include a higher component of coarser particles (i.e. sand) at c. 17.3 ka cal. yr BP (Lin et al., 1986), reflecting an increase in lake energy; however, there is no discernible increase in particle size. However, it is possible that the rise occurred but is not recorded at the chosen resolution (~40 years for this section of the record). Secondly, the shifts recorded in the Lake Shudu record possibly occurred over centennial timescales, whereas inwash events occur on much shorter timescale. Hence, these factors suggest that an inwash event was not the primary cause of these shifts. On balance, the evidence in the proxies tentatively supports the theory that climatic conditions were ameliorating, triggering marked increases in pollen abundances and organic productivity and a shift in the position of the treeline.

5.4.2 Subzone MS-SD3b (c. 17.0 - 13.5 ka cal. yr BP)

Magnetic susceptibility peaks at c. 16.9 ka cal. yr BP indicating a short term change in sediment source to sources more rich in magnetic minerals. C/N ratios decrease to <10, suggesting that within-lake rather than terrestrial processes were once again driving organic productivity (Meyers, 1997). $\delta^{13}\text{C}$ values also become slightly higher, which when coupled with low C/N ratios suggests greater within-lake productivity. Combined percentages of *Abies* and *Picea* exceed ~6%, suggesting that the lake catchment was located >800 m above the upper treeline (Figure 5-4). Conversely, Cupressaceae / Taxodiaceae and *Betula* abundances also increase. Evergreen and deciduous *Quercus* both decrease. Herbs generally diversify.

The core stratigraphy indicates a shift from silty clay to finely banded organic gyttja at c. 16.8 ka cal. yr BP, confirmed by the particle size record and fluctuations in %TOC, possibly linked to fluctuating catchment processes following events at c. 17.5 - 17.2 ka cal. yr BP. From c. 16.8 - 16.7 ka cal. yr BP, thick grey green organic gyttja dominate the core stratigraphy, which was banded from c. 16.7 ka cal. yr BP, suggesting a shift in the sediment composition to include higher levels of organic material. At the same time, *Pinus* exceeds 50%. Pioneer species of *Betula* and Cupressaceae / Taxodiaceae percentages decrease and *Picea* increase, pointing to a change in forest composition outside of the catchment. Herbs including Ericaceae and Ranunculaceae increase. However, total pollen concentrations markedly decline. $\delta^{13}\text{C}$ values are variable, indicating subtle shifts in the supply of organic carbon to the lake. C/N ratios decline to <10 until c. 16.6 ka cal. yr BP before beginning to rise once more, suggesting that within-lake productivity initially decreased, then increased. Overall, the proxies suggest that the lake catchment was in a state of flux following the events at c. 17.5 - 17.2 ka cal. yr BP.

However, from c. 16.6 ka cal. yr BP, conditions began to stabilise. Levels of arboreal pollen decrease, but Poaceae increases, pointing to an expansion of grassland. Total pollen concentrations rise gradually, reaching ~100,000 grains / gram at c. 15.7 ka cal. yr BP. At c. 16.5 ka cal. yr BP, levels of coniferous arboreal pollen, spores and ferns increase, indicating an increase in effective moisture. At c. 16.3 ka cal. yr BP, *Abies*, deciduous *Quercus* and *Betula* increase, signifying the expansion of forest and confirming a shift towards warmer, wetter conditions able to support forest growth. After c. 16.1 ka cal. yr BP, $\delta^{13}\text{C}$ values become much lower. Given the evidence for increased vegetation cover, lower $\delta^{13}\text{C}$ values may have been caused by a marked increase in the amounts of $\delta^{13}\text{C}$ -depleted CO_2 (aq) generated by soil development processes being deposited into the lake (Wolfe et al., 1999). The shift in values may therefore reflect a corresponding increase in vegetation cover and pedogenesis.

The particle size record shows that from c. 16.1 - 15.9 ka cal. yr BP, there is a temporary, but marked increase in sand, which supports the theory for increased deposition of material into the lake during this period (Figure 5-1 and Figure 5-7). Dark laminated layers associated with periods of increased catchment energy reflected in rapid deposition of sediment particles also occurred in the stratigraphy (Hakala et al., 2004). Bed load transport of larger particles at c. 16 ka cal. yr BP is likely to reflect increased fluvial activity and / or stronger currents (Leeder, 1992). Increased deposition of sand to the lake therefore denotes a shift to slightly higher velocity conditions and increased current activity, suggesting a change to a slightly more dynamic lake regime (Hakala et al., 2004; Lin et al., 1986). However, sub-centennial sand influx / deposition of sand in the centre of the lake, followed by a rise in silt implies enhanced catchment energy. Higher sand levels may therefore represent an event or phase of enhanced water flows resulting from an event, such as a flood (Pant, 2003).

A Lateglacial stratigraphic sequence from Lake Qinghai contains similar patterns (Lister et al., 1991), consisting of layers of flat bedded fine-grained sediments overlaying sand sediments, interpreted as an abrupt and permanent expansion of the lake. Following Lister et al. (1991), it is therefore possible that the sequence of events recorded in the Lake Shudu proxies is evidence of a lake transgression. However, sand may also appear in a core taken from the centre of a lake when the lake recedes, causing the position of the lake margin to move towards the present day centre (Hakanson et al., 1983). The presence of sand can therefore sometimes reflect periods of a reduction in lake levels. Nevertheless, the pollen record indicates a broad increase in vegetation cover, including an increase in arboreal taxa, which supports the theory of enhanced effective moisture rather than lake recession over millennial timescales (Zhao et al., 2009; Van Campo et al., 1993). However, based on the available evidence it is difficult to determine the exact nature of this event.

From c. 15.7 ka cal. yr BP, coniferous arboreal pollen and *Quercus* increase. Shrubs also increase, but herbs and grass decrease. A shift towards vegetation assemblages containing higher levels of shrubs suggests that the open grassland areas were being colonised by sclerophyllous species of evergreen *Quercus* and shrubs. At c. 15.6 ka cal. yr BP, magnetic susceptibility decreases, signifying a reduction in the amounts of minerogenic material entering the lake. After this, readings become much less variable, indicating a stabilisation of the sediment sources supplying the lake. Light banding of the organic sediments persisted until c. 15.4 ka cal. yr BP, followed by darker banding until c. 15.4 ka cal. yr BP, indicating that steady deposition of material continued, but that the levels of sediment being deposited into the lake were reducing, which is seemingly confirmed by gradually reducing sedimentation rates.

From c. 15.4 - 13.5 ka cal. yr BP, alternating light/ dark green bands in the core stratigraphy suggests subtle variations in the amounts of material deposited into the lake. At c. 15 ka cal. yr BP, C/N ratios, %TOC and %TN rise then fall, whilst $\delta^{13}\text{C}$ values decline, suggesting increased deposition of CO_2 - depleted material into the lake. A temporary decrease in lacustrine organic productivity coupled with lower $\delta^{13}\text{C}$ values may point to dilution of nutrients in the lake triggered by an influx of water (Menking et al., 1997).

Overall, the proxies show marked signs of stability and recovery after c. 15 ka cal. yr BP, suggesting a stabilisation in catchment organic and hydrological processes. %TOC and %TN values rise above 2% and 0.2%, suggesting a shift away from sparse tundra vegetation and low organic productivity associated with and cold, dry conditions, to more dense vegetation associated with warmer and / or wetter conditions (Wolfe et al., 1999). C/N ratios are stable but $\delta^{13}\text{C}$ values are lower, suggesting an increase in the amounts of soil-derived CO_2 entering the lake and increasing soil development and within-lake productivity.

From c. 14.9 ka cal. yr BP, *Pinus* decreases, along with all other arboreal pollen except evergreen *Quercus* and *Betula*, suggesting a wider increase in cold mixed forest consisting of taxa including *Pinus*, *Picea*, *Abies*, *Betula*, *Salix* and *Ulmus* (Yu et al., 2000a). At c. 13.6 ka cal. yr BP, AP% exceeds 90%. *Pinus* pollen increases markedly. *Abies*, *Picea* and deciduous *Quercus* also increase, whilst evergreen *Quercus* and *Betula* decrease. However, combined percentages of *Abies* and *Picea* remain low, suggesting that the treeline was located below the lake. Hence, forest expansion was taking place outside, rather than within the catchment (Figure 5-4). Evergreen tree strategists out-compete deciduous strategists when conditions are uniformly harsh all year round (Thomas et al., 2007). The increased presence of deciduous *Quercus* therefore indicates that conditions were perhaps becoming more seasonal. Furthermore, deciduous strategists may grow in zones near to the timberline, because the winter tends to be severe and trees use less energy growing a new set of leaves annually during the warmer months rather than attempting to maintain leaf growth all year round (Thomas et al., 2007). Liu et al. (2007) suggest that trees become deciduous in response to prolonged dry periods. The presence of deciduous *Quercus* may therefore indicate a more seasonal climate, possibly including drier winters (Dearing et al., 2008).

Shrubs including *Salix* and Tamaricaceae increase, suggesting an expansion in shrubland. Clay particles increase markedly at c. 14.5 ka cal. yr BP, suggesting a decrease in flow strength and deposition of sediments in a lower energy environment. After this, there are fluctuations in the relative proportions of silt and clay. Overall, following an initial period of instability, including at least one lake transgression, the proxies indicate that lacustrine and terrestrial processes began to stabilise.

5.4.3 Zone MS-SD3 summary

The proxies indicate the following;

- an abrupt event centred at c. 17.3 ka cal. yr BP that appeared to trigger the expansion of vegetation cover, increased soil development and increased within-lake and terrestrial productivity, pointing to warmer and / or wetter conditions, followed by marked catchment instability and a shift to cooler, drier conditions thereafter;
- denser catchment vegetation particularly from c. 16.5 ka cal. yr BP, pointing to ameliorating climatic conditions;
- evidence of a possible inwash event occurring between c. 16.1 and 16.0 ka cal. yr BP;
- more stable catchment conditions from c. 15.6 ka cal. yr BP.

5.5 Zone MS-SD4 (c. 13.5 - 11.1 ka cal. yr BP)

This zone spans ~2400 years (Figure 5-8). Key features of this zone include subtle variations in magnetic susceptibility and greater variation in the particle size record, indicating broadscale fluctuations in sediment sources, flow strengths and inferred effective moisture levels (Last et al., 2001; Leeder, 1992).

The organic proxies indicate initially gradual increases in terrestrial and / or lacustrine productivity (Figure 5-1 and Figure 5-8). The increased presence and diversity of coniferous and deciduous species and enhanced colonisation rates by pioneer species such as *Betula* suggests that boreal *Pinus* forest was being replaced by cold / cool mixed forest (consisting of *Pinus*, *Abies*, *Picea* and *Ulmus*) (Yu et al., 2000a). Increased amounts of *Picea*, coupled with increased silt were used as indicators of a rise in effective moisture and fluvial flow at Zhuye Lake, NW China, from c. 13 ka cal. yr BP (Li et al., 2009). However, the treeline was located below Lake Shudu (Figure 5-4), suggesting that the shifts in arboreal pollen are related to changes outside of the catchment.

Shrubs including *Salix* and Cornaceae increase (Figure 5-2). Poaceae grains <40 µm and moisture-loving Cyperaceae also increase, although levels remain below 25%, which suggests that the region was not wholly open grassland, but rather covered by patches of grass and shrubland (Zhao et al., 2009). Herbs also increase and diversify. *Artemisia*, which is associated with relatively moist conditions, remains relatively stable during this period (Herzschuh, 2007). *Sedum* type, Gentianaceae, Saxifragaceae, Violaceae and Plantaginaceae all showed small but increased abundances. *Sedum* grows in dry grassland or rocky areas (Wu et al., 2008). Gentianaceae is associated with grassland or meadows. Saxifragaceae is a grassland family (Wu et al., 2008). Plantaginaceae pollen has a cosmopolitan distribution and is associated with alpine assemblages (Huntley et al., 1984). Moist steppe vegetation includes these herbaceous taxa (Yu et al., 2000a). Spores / ferns also increased markedly, reaching levels comparable to those at the top of the core. These tend to proliferate in wet and shady conditions, such as the understorey of forests, suggesting a rise in vegetation cover and effective moisture.

There are notable shifts in the proxies from c. 12.3 ka cal. yr BP. Consequently this zone is divided into Subzones MS-SD4a, which spans c. 13.5 - 12.3 ka cal. yr BP and MS-SD4b, which spans c. 12.3 - 11.1 ka cal. yr BP.

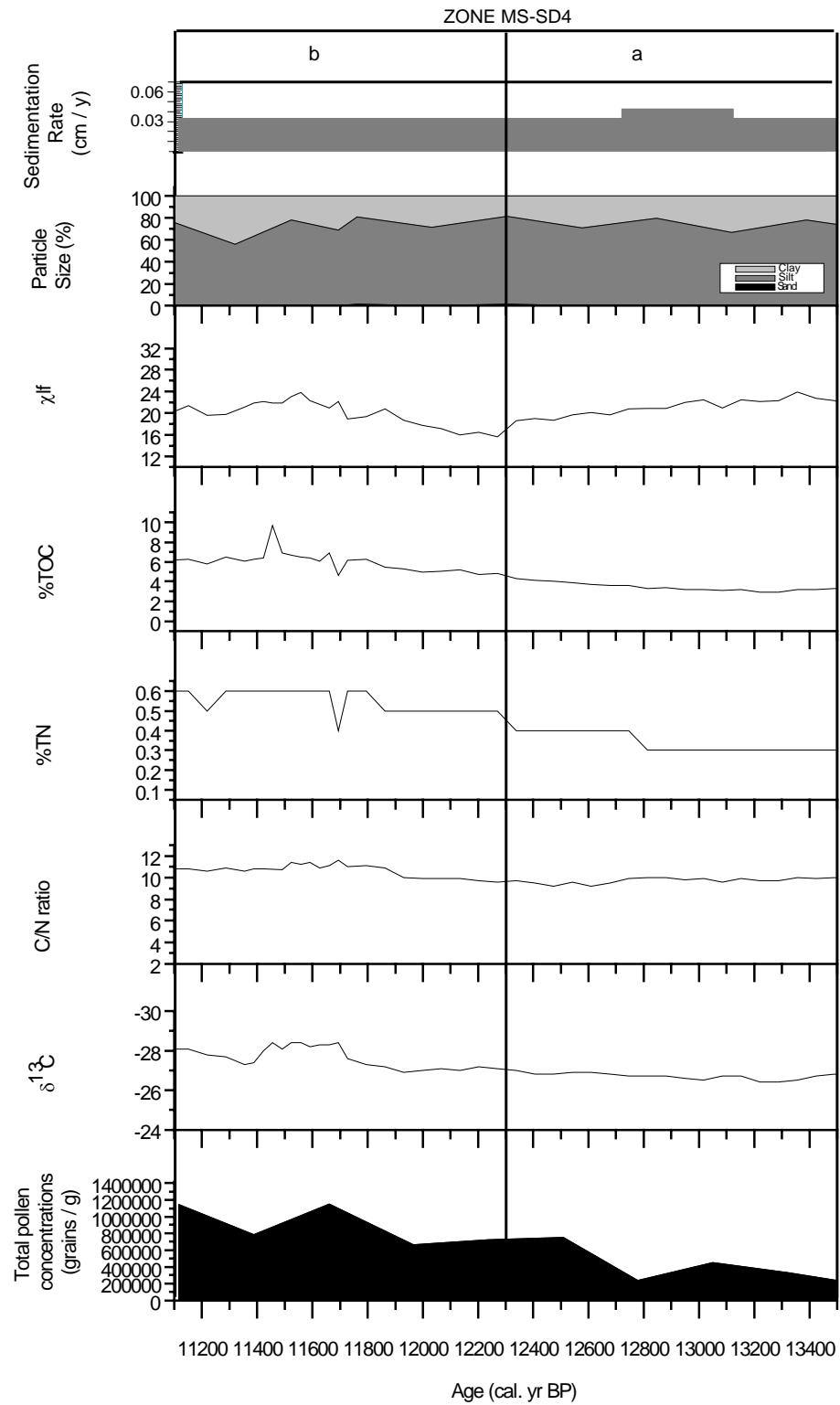


Figure 5-8: Lake Shudu proxy record, Zone MS-SD4 (c. 13.5 - 11.1 ka cal. yr BP).

5.5.1 Subzone MS-SD4a (c. 13.5 - 12.3 ka cal. yr BP)

Overall, the proxies are generally much more stable throughout this subzone compared to previous zones, with the exception of particle size, which continues to alternate between silt and clay; although silt remains predominant. Magnetic susceptibility rises gradually to a peak at c. 13.4 ka cal. yr BP, before commencing an equally gradual descent to lower values (Figure 5-1 and Figure 5-8). %TOC and %TN increase gradually from c. 12.8 ka cal. yr BP. C/N ratios indicate that organic material was derived from mixed sources, and $\delta^{13}\text{C}$ values become lower, pointing to rising levels of terrestrially derived organic carbon entering the lake.

Total pollen concentrations continue to rise (Figure 5-8). The pollen record indicates that meadow herbs diversified markedly to include higher levels of taxa such as Rosaceae, Asteraceae, Primulaceae and Polygonaceae. An similar increase in meadow taxa, including *Artemisia* from is observed in pollen sequences obtained from at Tso Kar, northwestern India from c. 12.9 - 12.5 ka cal. yr BP (Demske et al., 2009).

Reducing magnetic susceptibility suggests that there were subtle changes in sediment sources supplying the lake over millennial timescales. Lower $\delta^{13}\text{C}$ values coupled with rising %TOC and %TN support this hypothesis, indicating that there was a shift in the balance of the relationship between sediment and / or water influx (and nutrient supply) and lacustrine productivity. Reduced magnetic susceptibility coupled with increased vegetation density also points to increased vegetation cover and stabilisation of the slopes surrounding the lake. Overall, the proxies intimate sub-millennial scale variations in sediment supply but also a shift towards more stable conditions prompted by a millennial scale shift to warmer and wetter conditions.

5.5.2 Subzone MS-SD4b (c. 12.3 - 11.1 ka cal. yr BP)

Marked shifts occur across the proxies from c. 12 ka cal. yr BP, attaining peak values from c. 11.7 - 11.5 ka cal. yr BP (Figure 5-1 and Figure 5-8). Firstly, magnetic susceptibility began to rise. This is accompanied by rises in %TOC, %TN. Levels of organic carbon and nitrogen are comparable with levels associated with forested regions of Russia during the Lateglacial (Wolfe et al., 1999). C/N ratios exceed 10, indicating the presence of terrestrially and aquatically derived material. Much lower $\delta^{13}\text{C}$ values are attributed to a greater influx of soil-derived CO_2 , which occurs during wetter periods (Figure 5-1 and Figure 5-8) (Leng et al., 2005).

Within the pollen record, the recorded shifts are more gradual and occurred over a longer timescales. These changes are characterised by rising total pollen concentrations (Figure 5-8) and include increases across all of the major plant groups pointing to increased inferred catchment productivity, vegetation cover and soil development. There are notable increases in *Pinus*, pioneer species of *Betula* and an increase in herbs. Conversely, there is a reduction in shrubs and grass / sedge (Figure 5-2). These factors point to a shift in vegetation cover from grassland and shrubland to a more dense herbaceous vegetation cover. Recorded percentages of herbs such as *Artemisia* and deciduous *Quercus* suggested that they were locally present in the catchment (Huntley et al., 1984). Poaceae grains <40 µm, Polypodiaceae and Spores also increase during this phase. These taxa collectively provide further evidence that conditions were becoming wetter.

Shortly afterwards, the proxies indicate a return to previous values, suggesting that this event was relatively short-lived. On balance, the evidence in the proxies points towards increased catchment productivity, and the onset of conditions more favourable for plant growth, associated with increasingly warmer and / or wetter climatic conditions.

5.5.3 Zone MS-SD4 summary

The proxies collectively point to the following environmental and climatic shifts during this zone;

- millennial scale increases in vegetation and productivity driven by an increasingly warm and wet climate, particularly from c. 11.7 ka cal. yr BP;
- marked changes in vegetation cover and organic productivity from c. 11.7 - 11.5 ka cal. yr BP, possibly associated with an ameliorating climate.

5.6 Concluding remarks

The Lake Shudu record provides an environmental and climatic history of events during the Late Pleistocene - Early Holocene Period. From c. 22.6 - 20.3 ka cal. yr BP, periglacial conditions were dominant. Catchment and lacustrine processes were generally low on millennial timescales, but quite variable on centennial timescales. Catchment vegetation was sparse and consisted of tundra vegetation. Overall, the proxies indicate that climatic conditions were cold and dry. These trends largely continued until c. 17.5 ka cal. yr BP.

From c. 17.5 - 13.5 ka cal. yr BP, organic productivity and herbaceous vegetation cover both increased and soils started to develop, pointing to a shift to warmer, wetter conditions. An event centred at c. 17.3 ka cal. yr BP possibly triggered a temporary advance in the treeline and fundamentally altered lacustrine and wider catchment dynamics operating at Lake Shudu. The precise cause of this event remains unconfirmed, but it is characterised by significant fluctuations in the environmental processes operating at Lake Shudu, possibly associated with an ameliorating climate. Afterwards, conditions became slightly cooler and / or drier. However, there is clear evidence of a shift to denser vegetation and much warmer and / or wetter conditions from c. 16 ka cal. yr BP onwards.

From c. 13.5 - 11.1 ka cal. yr BP, vegetation and soil cover broadly increased. Outside of the catchment, cold - cool mixed forests expanded, suggesting a shift to warmer, wetter conditions. On centennial to decadal timescales, there are notable shifts in the proxies between c. 11.7 and 11.5 ka cal. yr BP, which appear to be triggered by fluctuations in sediment delivery and changes in nutrient and water availability.

Having outlined the environmental shifts in the Lake Shudu record and their broad climatic implications, the trends are examined in more depth in Chapter 6 in relation to the climatic trends recorded in other regional proxy records. The dynamics of glacial - interglacial boundary conditions, solar insolation and the Asian palaeomonsoon variability are considered in the light of the evidence captured in the Lake Shudu record.

6 Late Pleistocene - Early Holocene glacial dynamics and Asian palaeomonsoon variability in southwestern China

6.1 Introduction

The Lake Shudu record spans c. 22.6 - 11.1 ka cal. yr BP, and provides a unique opportunity to explore the dynamics between the Asian monsoon, solar insolation and ice cover during the transition from glacial to interglacial conditions. The findings are compared with other regional proxy records. This chapter addresses Aims 2 and 3, and Objective g of this research project.

6.2 The timing of the LGM

The timing of the LGM in southwestern China remains a contested issue in the literature (see Chapter 2, Section 2.5.3 and Figure 6-1). For example, Zhou et al. (2008) compared speleothem records from different regions of China and concluded that the LGM occurred between ~20 - 18 ka. In contrast, Zhang et al. (2009) place the LGM at c. 21 ka cal. yr BP, based on evidence obtained from a lake located on the eastern edge of the Tibetan Plateau. However, the primary barrier to constraining the onset of LGM conditions in southwestern China is the lack of high-resolution records extending back far enough into the Pleistocene (Herzschuh, 2006b).

A basal date of c. 22.6 ka cal. yr BP, coupled with the lack of glacial till in the Lake Shudu record places the end of the LGM at least one to two millennia earlier than other published records for southwestern China suggest (e.g. Zhou et al., 2008). A number of studies suggest that the end of the LGM is likely to have occurred at different times in different locations (e.g. Owen et al., 2005). Consequently, the possibility that the end of the LGM occurred earlier than previously reported is feasible.

However, solar insolation levels only began to rise at c. 23 - 22 ka BP (Berger et al., 1991), as illustrated by (Figure 6-1). Consequently, it is likely that the end of the LGM occurred sometime after this. The basal date of c. 22.6 ka cal. yr BP coupled with a lack of basal till implies either that deglaciation commenced before solar insolation began to rise and / or that the LGM was completed in <500 years; or alternatively, that rising solar insolation and deglaciation were synchronous. These possibilities are at odds with evidence provided by other studies described here and in Chapter 2. The basal date should therefore be treated with caution. Chronological inconsistencies are inevitable when comparing chronologies derived from different records, and having different temporal resolutions. Further dating and examination of evidence from other proxy records located near to Lake Shudu (e.g. Bita Hai) is required to resolve this issue.

6.3 Post-LGM climatic conditions

On millennial timescales, climatic changes are driven by global scale changes in ice volume and / or sun-earth geometry (Pant, 2003 and Figure 6-1). Herzschuh (2006b) identified trends in pollen, isotopic and lithological records obtained from Tibet and Northern China, which suggest that millennial scale trends broadly correspond with solar insolation changes for 30°N in June (Figure 6-1). Rising solar insolation is thought to have triggered an increase in summer monsoon intensity, which in turn triggered environmental changes, including higher lake levels. However, rising solar insolation can also trigger higher moisture levels, which may initially cause glacial accumulation and cooler conditions, helping to buffer against the onset of warmer conditions. Consequently, the changes captured in the Lake Shudu record may be a product of rising insolation, increasing summer monsoon intensity and glacial dynamics, and the shifting influence of each of these drivers during the transition from glacial to interglacial conditions.

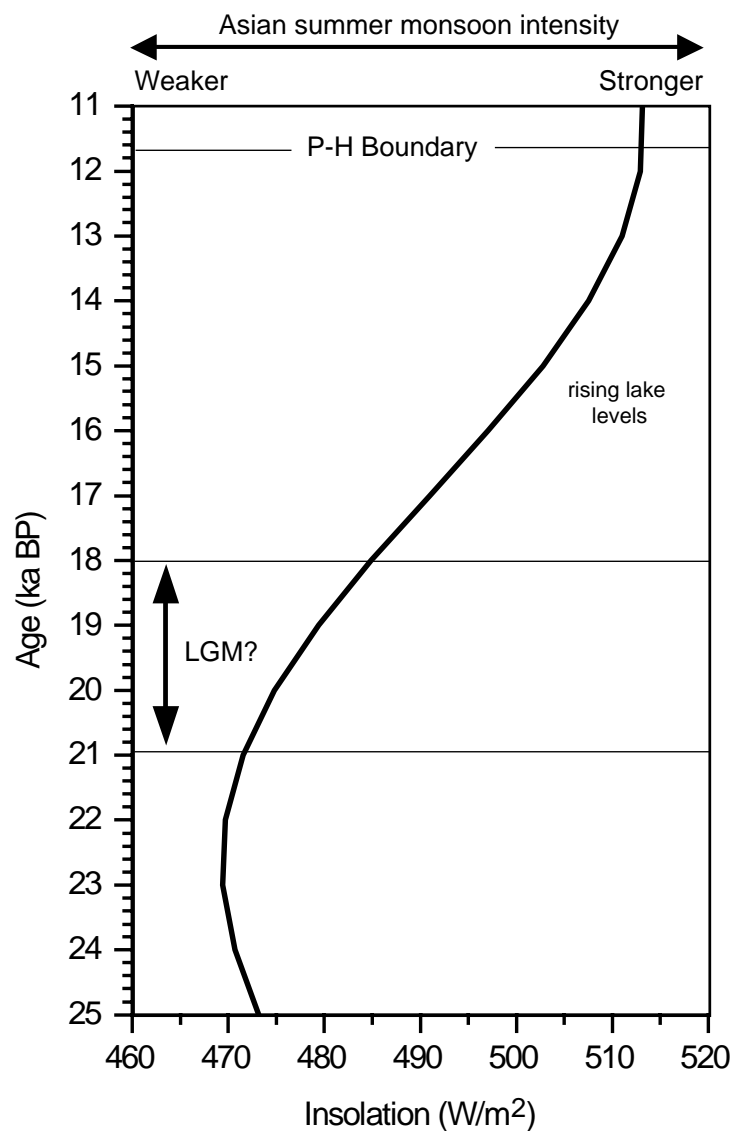


Figure 6-1: Solar insolation during June at 30°N spanning the last ~25 ka BP.

The diagram shows the relationship between changing insolation levels and Asian summer monsoon intensity operating over millennial (or longer) timescales, and the approximate timings of key climatic events / phases inferred from the Lake Shudu record and other regional records (e.g. Walker et al., 2009; Herzschuh, 2006b; Fang, 1991; Walker, 1986).

After Thompson et al. (2006) and Berger et al., 1991.

Yu et al. (2000a) produced a model of palaeovegetation cover based on analysis and modelling of modern pollen datasets derived from locations across China. At c. 18,000 ¹⁴C yrs BP, steppe and in some places desert vegetation were the dominant land cover, extending into eastern China to 125°E (Sun et al., 1998), suggesting that the impact of the LGM lasted several millennia. Furthermore, previous studies have indicated that conditions during the LGM were cold and dry (Shi (2002); Zheng et al., 1998), providing further support for the theory that vegetation cover was sparse in China during the Late Pleistocene Period.

Tang (2006) obtained six millennial scale pollen records from Tibetan lakes and concluded that the LGM climate of the Tibetan Plateau vegetation (including *Artemisia* and *Poaceae*) was allied to the desert-steppe biome, indicating a cold and dry plateau climate. Enhanced magnetic susceptibility is also observed in the Qilu Hu record for from c. 30 - 18 ka cal. yr BP (Hodell et al., 1999). After the LGM, sparse grassland / tundra vegetation was the primary assemblage growing at Lake Shudu. This was coupled with low energy lake conditions inferred from the physical proxies and low organic productivity inferred from the carbon and nitrogen proxies. AP/NAP ratios indicate that the catchment vegetation cover was open (Figure 6-2). Higher up in the Himalayan Mountains, permafrost desert conditions appear to have existed in the unglaciated regions after the LGM, consisting of 70% polar desert and 30% dry montane tundra (Adams et al., 1998). Records from sites outside the region reflect similar conditions. For example, Schlutz et al. (2004) analysed palynological and pedological records from a lake sediment core from Gorkal Himal, Nepal, located at 3500 m asl. Dry steppe-like vegetation occurred in the catchment area. The high mountain forests were opened up and replaced species of *Poaceae*, *Caryophyllaceae* and *Rosaceae* and weeds, including *Chenopodiaceae*, *Bupleurum*-type, *Dipsacus*, *Aconitum* and *Erodium*.

In China, forest cover was significantly reduced and had retreated southward to lower altitudes (Otto-Bliesner et al., 2005). Treelines in mountainous areas in both northern and southern China were ~1700 m lower than at present (An et al., 1991). This hypothesis is broadly supported by the Lake Shudu pollen record, which indicates that the treeline was located at least ~800 m below the catchment. Adams et al. (1998) conclude that open pine forests were located in Western China, evidenced by the presence of low concentrations of *Pinus* pollen at c. 18 ka BP in a pollen record obtained from the upland plateau region of the upper Yangtze (Sun (1990), [translated by Adams et al., 1998]). The dominance of *Pinus* pollen in the Lake Shudu record up to c. 17.5 ka cal. yr BP would appear to support the hypothesis that the dominant forest type growing regionally was patchy boreal *Pinus* forest. The inferred vegetation trends in the Lake Shudu record and these studies provide strong evidence for cold and dry post-LGM conditions. These conditions were attributable to the continuing influence of ice cover in the Northern Hemisphere, which allowed cold streams into the mid latitudes via Siberian High, inducing a strong winter monsoon and / or increasing local aridity (Demske et al., 2009; Yu et al., 2000a).

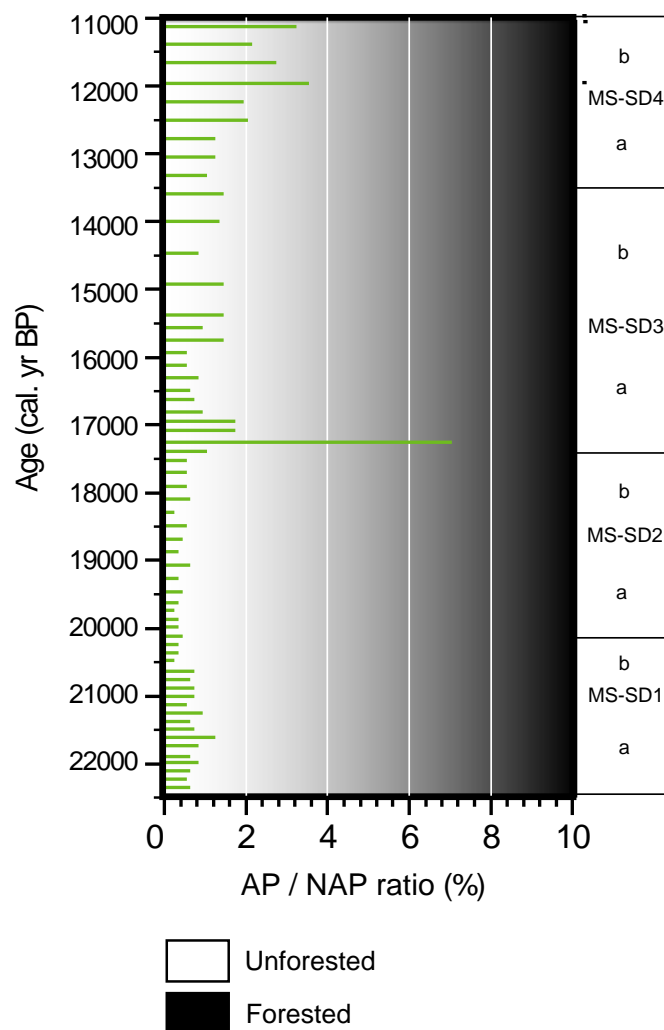


Figure 6-2: AP/NAP ratios in the Lake Shudu pollen record.

The ratios of arboreal pollen percentages (AP) to non-arboreal pollen (NAP) are used as an indicative vegetation density index. The colour gradient represents increasing vegetation density from sparse (white) to dense (black) land cover. Ratios of >8.5 reflect closed, dense forest. Woodland ratios are >4 , open grassland ratios are >2.5 and wholly open conditions have a ratio of <0.2 . The diagram indicates that with the exception of the assemblage at c. 17.3 ka cal. yr BP, the Late Pleistocene - Early Holocene vegetation cover at Lake Shudu was largely open, sparse and unforested.

After Herzschuh, 2007.

Vegetation changes captured in the Lake Shudu pollen record were examined in detail using the statistical methods outlined in Chapter 3 and A.3.1., Appendix A.3. All pollen taxa with abundances of >2% were included in the analyses. Samples are plotted to highlight any significant differences in the composition of pollen samples, possibly denoting periods during which there were marked changes in vegetation assemblages. Figure 6-3 is a PCA scattergraph showing the samples in the Lake Shudu pollen dataset. Five outlying samples are evident including the basal sample dated c. 22.6 ka cal. yr BP, three intervals clustered together, dated c. 20.5, 20.0 and 19.7 ka cal. yr BP and the c. 17.3 ka cal. yr BP interval.

The basal sample contains very low levels of *Pinus* pollen (<100 grains), so is probably not statistically significant, although the low pollen concentrations may imply that trees were growing a long distance away from the catchment. However, the other outliers are statistically significant and are likely to reflect differences in vegetation during these periods relative to other intervals.

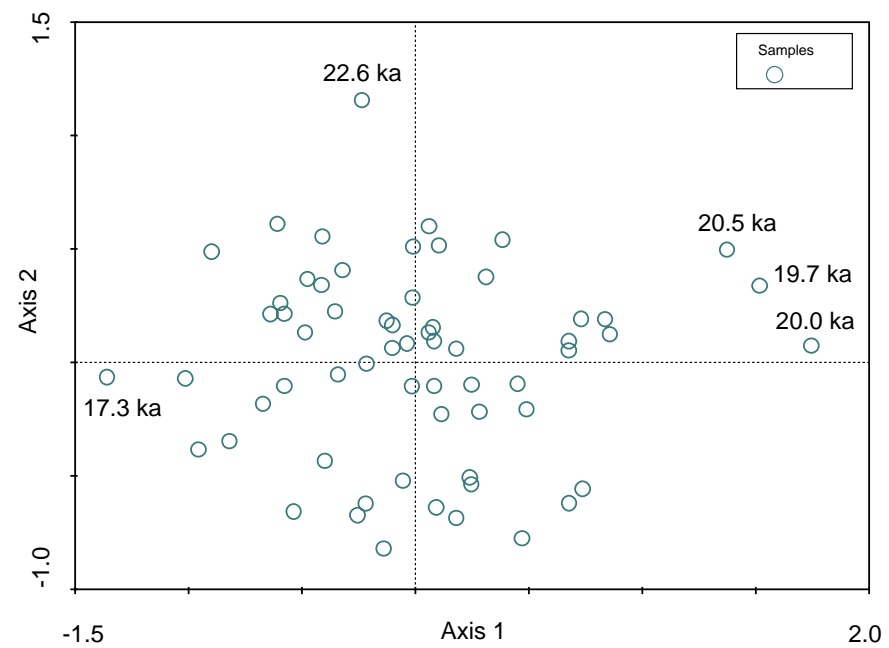


Figure 6-3: PCA scattergraph showing outlier samples.

Outlier samples contain vegetation assemblages dissimilar to the other samples in the Lake Shudu pollen dataset. Outlier ages are quoted in cal. yr BP.

The first subtle signs of vegetation change therefore occurred at c. 20.5 ka cal. yr BP, reflected in a pollen record as a shift from grassland to alpine meadow including *Artemisia*. Liu et al., (1986) suggested that up to c. 20 ka BP, Yunnan Province was subject to increased winter humidity and rainfall. The spread of meadow may therefore reflect an increase in winter precipitation associated with the westerly winds, and / or an intensification of glacial melt perhaps triggered by rising solar insolation (Demske et al., 2009).

A/C ratios increase markedly c. 20.0 ka cal. yr, indicating that there was a pronounced rise in effective moisture (set within the context of generally dry conditions indicated by sparse vegetation cover and low AP/NAP ratios) (Figure 6.4). Evidence from lake level studies indicates that post-LGM conditions in western China were wetter relative to conditions in eastern China (e.g. Herzschuh, 2006b; Yu et al., 2000b). The A/C ratios provide semi-quantitative evidence that there were periods when regional conditions were markedly wetter following the LGM, triggering marked shifts in vegetation. However, the changes in A/Cy ratios are less marked, suggesting that conditions generally remained cold.

The difference in moisture levels between western and eastern China is attributable to the existence of a strong glacial anticyclone and areas of permafrost to the north, which may have blocked the eastward extension of the Asian monsoon, resulting in drier conditions in the east, and enhancing precipitation in the west. Alternatively continental cooling may have produced evaporation conditions much lower than today, leading to positive P-E in Western China (Fang, 1991). Either way, this implies that both glacial and monsoon activity played a role in post-LGM climate dynamics. However, at present, the relative contributions of local glacial melting versus increased monsoon precipitation remain difficult to distinguish (Herzschuh, 2006b).

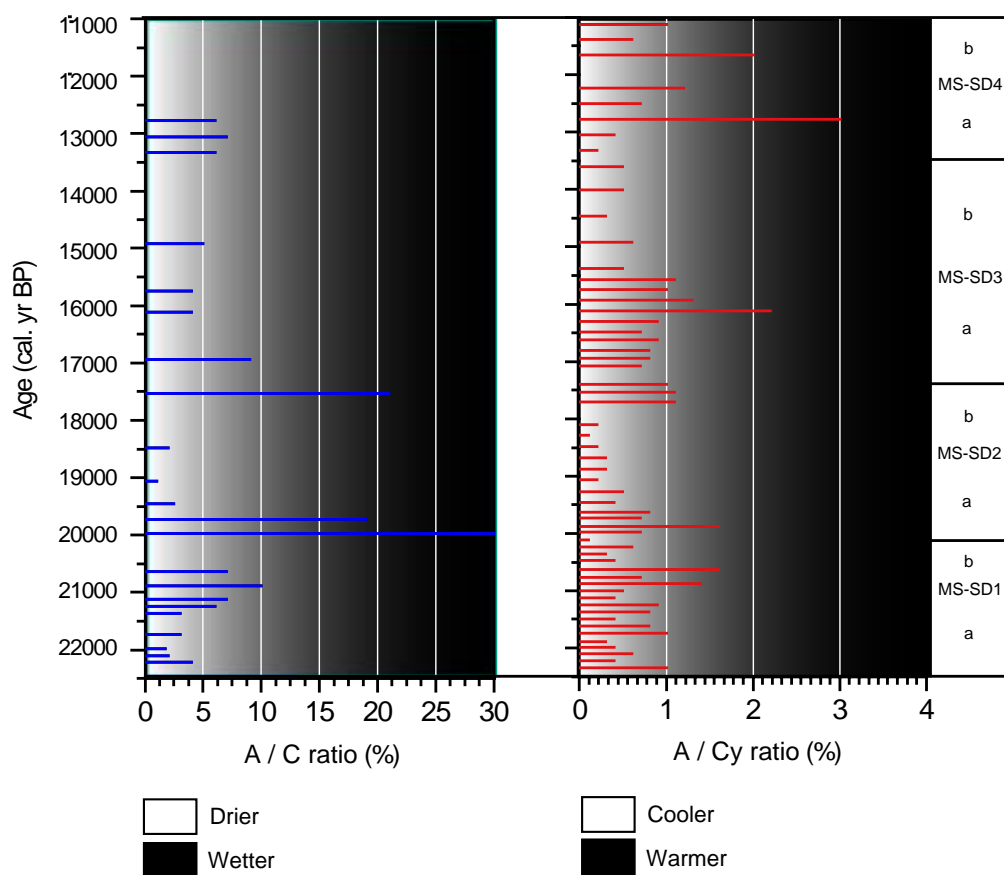


Figure 6-4: A/C and A/Cy ratios in the Lake Shudu pollen record.

A/C and A/Cy ratios are used when AP/NAP ratios indicate that vegetation assemblages are primarily aligned to the non-forested biomes (e.g. steppe, desert, tundra), therefore the forested interval at c. 17.3 ka cal. yr BP and zero values (denoting the absence of one or more of the indicator species) are excluded. A/C ratios denote the ratio of *Artemisia* to Chenopodiaceae. Low ratios (<1) correlate with drier (desert) conditions. Higher ratios (>33) equate to more moist (steppe) conditions. Intermediate ratios correspond to tundra. A/Cy ratios denote the ratio of *Artemisia* to Cyperaceae. Low ratios (<1) equate to cooler (tundra) conditions, whereas higher ratios (>1) are correlated with warmer (steppe) conditions. The ratios collectively indicate that vegetation is primarily aligned to the dry, cool tundra biome.

After Zhao et al. (2009).

6.3.1 Evidence for an abrupt climate amelioration from c. 17.5 - 17.2 ka cal. yr BP

Samples were plotted in order to highlight any changes in vegetation over time. Figure 6-5 is a PCA sample scattergraph. The samples containing similar taxa are clustered together. Within the main group of samples, two clusters are distinguished (labelled A and B). Cluster A contains the majority of samples pertaining to the period c. 22.6 - 17.5 ka cal. yr BP. Cluster B contains samples spanning the period c. 17.5 - 11.1 ka cal. yr BP. This indicates firstly, that there are significant differences in the vegetation composition of the samples in Group A relative to those in Group B, and secondly, that there were marked and sustained changes in the vegetation composition of the samples on the boundary between the two clusters, at c. 17.5 ka cal. yr BP.

The PCA species biplot in Figure 6-6 shows the correlations between taxa, which provides insight into the primary types of vegetation assemblages that were dominant in the pollen record. Four assemblages are distinguished; boreal (*Pinus*) forest (top left quadrant), cool - cold mixed forest (bottom left quadrant), steppe / tundra shrubs and herbs (bottom right quadrant) and desert / tundra vegetation (top right quadrant). Inter-species correlations are particularly high between desert / tundra taxa denoted by the blue square.

The length of the species arrow in Figure 6-6 represents the multiple correlations of individual taxa with the axes (Smilauer, 2003). In particular, *Pinus* is highly correlated with Axis 2. Conversely, *Betula* and *Artemisia* are highly correlated with Axis 1. Poaceae and Cyperaceae are positively correlated with both axes.

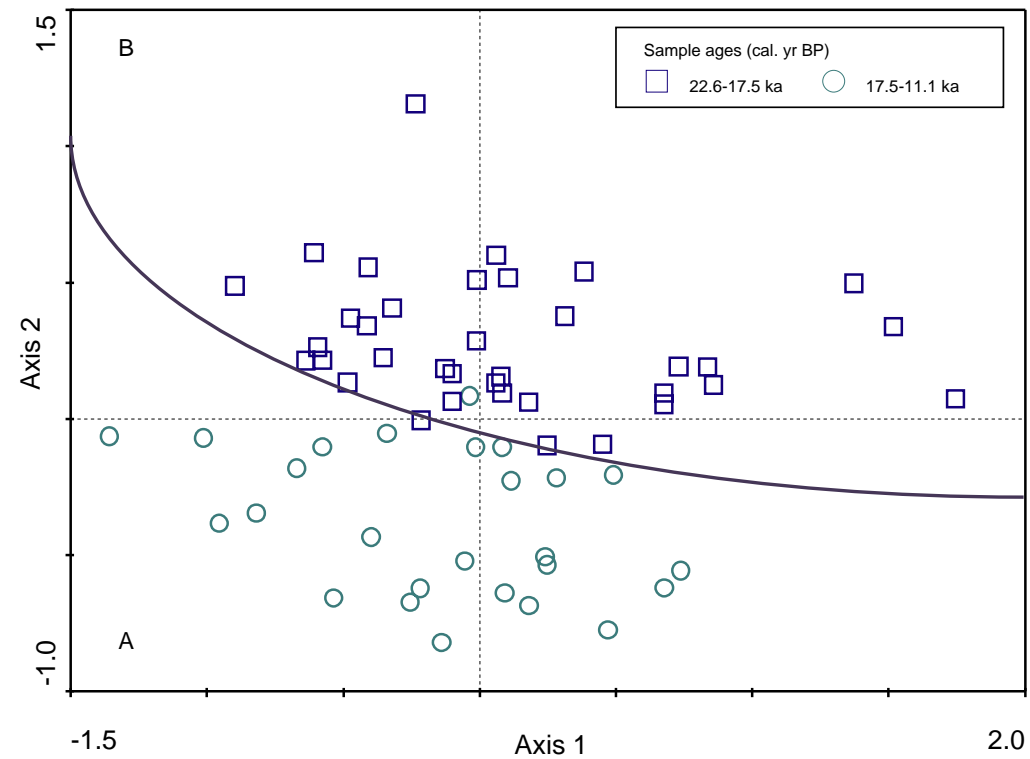


Figure 6-5: PCA scattergraph showing the clustering of samples in the Lake Shudu pollen record.

The samples are split into two clusters labelled A and B (illustrated by the black line). There is a clear division between samples older and younger than c. 17.5 ka cal. yr BP.

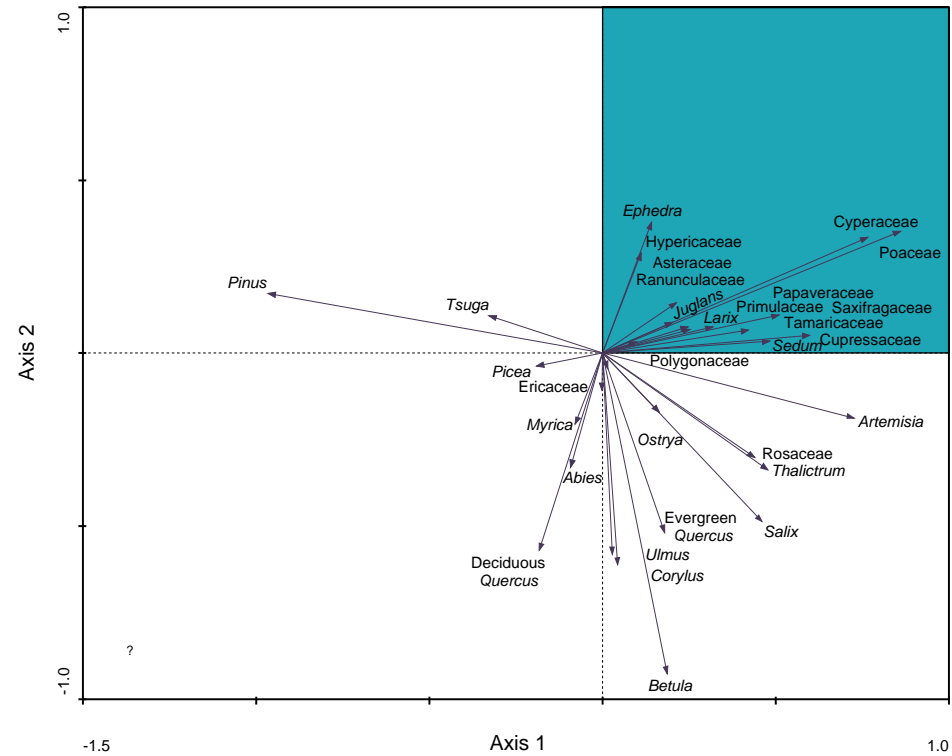


Figure 6-6: PCA species biplot showing inter-species correlations between Lake Shudu pollen taxa.

The angles between the arrows illustrate the degree of correlation between individual taxa. The blue square denotes taxa that are highly correlated with one another, and with both axes. The length of the species arrow represents the multiple correlations of individual taxa with the axes (Smilauer, 2003).

Cross plotting of the samples against species shows how the primary assemblages in (Figure 6-6) align to sample groups A and B (Figure 6-5), thus highlighting how vegetation changed over time (Figure 6-7). Prior to c. 17.5 ka cal. yr BP, the primary vegetation assemblage consisted of grassland and dry desert / tundra taxa. Outside of the catchment, boreal *Pinus* forest was likely to have been the dominant forest type. After c. 17.5 ka cal. yr BP, vegetation shifts to include a higher component of alpine meadow / steppe taxa and cold - cool mixed forest taxa.

The inferred changes in vegetation over time enabled inferences to be made about how climatic conditions correspondingly changed over time. The first principal component (Axis 1) captured 35% of the total variance in the dataset, whilst the second principal component (Axis 2) captured 17% of the total variance in the dataset.

Figure 6-7 indicates that Axis 1 separates xerophytic steppe / tundra vegetation including (e.g. Poaceae) from taxa preferring more moist conditions, including deciduous (e.g. *Ulmus* and *Corylus*) and mesophilous vegetation (e.g. *Tsuga* and *Picea*). Axis 2 separates cold-tolerant alpine / tundra herbs (e.g. Saxifragaceae) and boreal *Pinus* forest from shrubs and thermophilous trees (e.g. *Ulmus*, *Ostrya*). However, some taxa do not conform to these patterns. Firstly, *Pinus* is drought-resistant but is not grouped with the other xerophytic taxa. Secondly, *Betula*, which can withstand very low temperatures, is not grouped with the cold-tolerant taxa. This may be attributable to their wide ecological tolerances (i.e. an ability to tolerate broad temperature / moisture conditions) relative to other taxon in the pollen record and is reflected by the fact that *Pinus* and *Betula* are not strongly correlated with other species / samples in the pollen record, which reflects their over-arching influence upon the whole record. Thirdly, Cyperaceae is hygrophilous but is grouped with the xerophytic taxa. Cyperaceae is a significant component of non-forested assemblages, and can withstand dry conditions relative to arboreal taxa, which may explain why it is grouped with the alpine herbs.

Taking into account the ecological affinities of the taxa outlined above and in Zhao et al. (2009), Yu et al. (2000a) and Li et al. (1986), and inferred correlations between individual taxa, broadly speaking, Axis 1 represents effective moisture and Axis 2 represents summer temperature. Consequently, the eigenvalues imply that most of the variance in the pollen dataset was accounted for by changes in effective moisture (35%), followed by changes in summer temperature (17%).

Cold, dry tolerant taxa are primarily aligned to samples older than c. 17.5 ka cal. yr BP (Figure 6-7). In contrast, taxa preferring warmer, wetter conditions are aligned to samples younger than c. 17.5 ka cal. yr BP. Consequently, it would appear that conditions became markedly wetter and warmer after c. 17.5 ka cal. yr BP. A/C ratios (Figure 6-4) support the view that conditions became markedly wetter from c. 17.5 ka cal. yr BP.

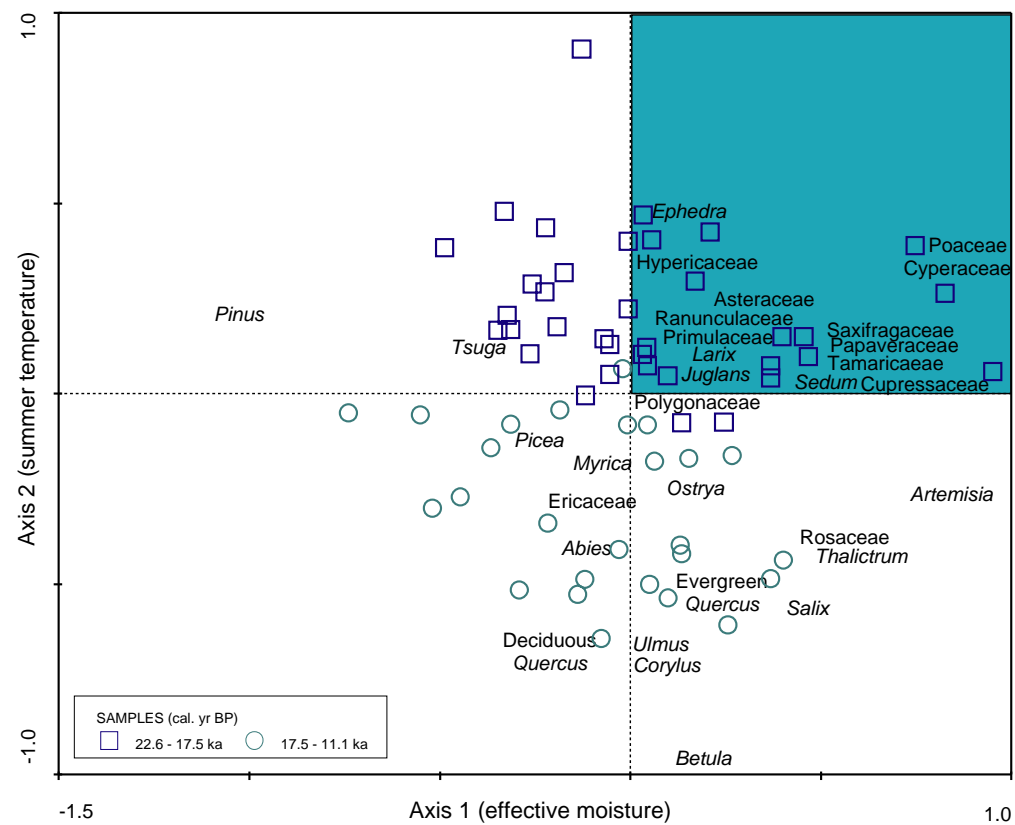


Figure 6-7: PCA species / samples scattergraph derived from the Lake Shudu pollen record.

The scattergraph highlights the correlations between taxa and samples, showing how the composition of the Lake Shudu pollen record changed over time. The blue box denotes taxa associated with cold, dry climatic conditions.

Following events at c. 17.5 ka cal. yr BP, there were marked environmental changes at c. 17.3 ka cal. yr BP (Figure 6-3), denoted by high pollen concentrations, and a shift in vegetation cover from alpine meadow to a mixture of alpine meadow and *Pinus* woodland. This shift is highlighted in combined *Abies* and *Picea* percentages and the presence of stomata discussed in Chapter 5, suggesting that the treeline had advanced to a higher elevation, coupled with much higher AP/NAP ratios (Figure 6-2), increased soil development and rising catchment productivity inferred from the organic proxies.

There is evidence of comparable shifts in records obtained from other sites in southwestern China. For example, Adams et al. (1998) propose that warm temperate forest grew locally in the southwestern quadrant of Yunnan Province at c. 17 ka cal. yr BP. In addition, semi-humid conditions were inferred from the presence of montane conifers and sclerophyllous *Quercus* forest taxa at c. 17 - 15 ka BP in pollen records obtained from southern Yunnan (Lin et al., 1986). Higher levels of precipitation were inferred from higher levels of aquatic taxa in a pollen record obtained from Kunming spanning the last c. 16 ka BP (Sun et al., 1986). These trends are attributable to increasing solar insolation triggering higher temperatures and a strengthening summer monsoon.

Analysis of key arboreal indicator species reveals some interesting trends (Figure 6-8). Levels of evergreen *Quercus* are used as a proxy for dry (late) winters. Graph A shows that abundances slightly increased over time, pointing to increasingly seasonal conditions, particularly from c. 18 - 17 ka cal. yr BP. However, the linear trend line indicates that the increase was quite subtle. Graph B shows the combined percentages of deciduous *Quercus* and *Betula*, which are used as a proxy for cold, dry winters. There is a marked increase in these taxa, further confirming the increased establishment of seasonal conditions, particularly from c. 18 - 17 ka cal. yr BP. In summary, statistical analysis of the Lake Shudu pollen record indicates that the changes recorded at c. 17.5 - 17.2 ka cal. yr BP represent a phase of warmer and / or wetter conditions.

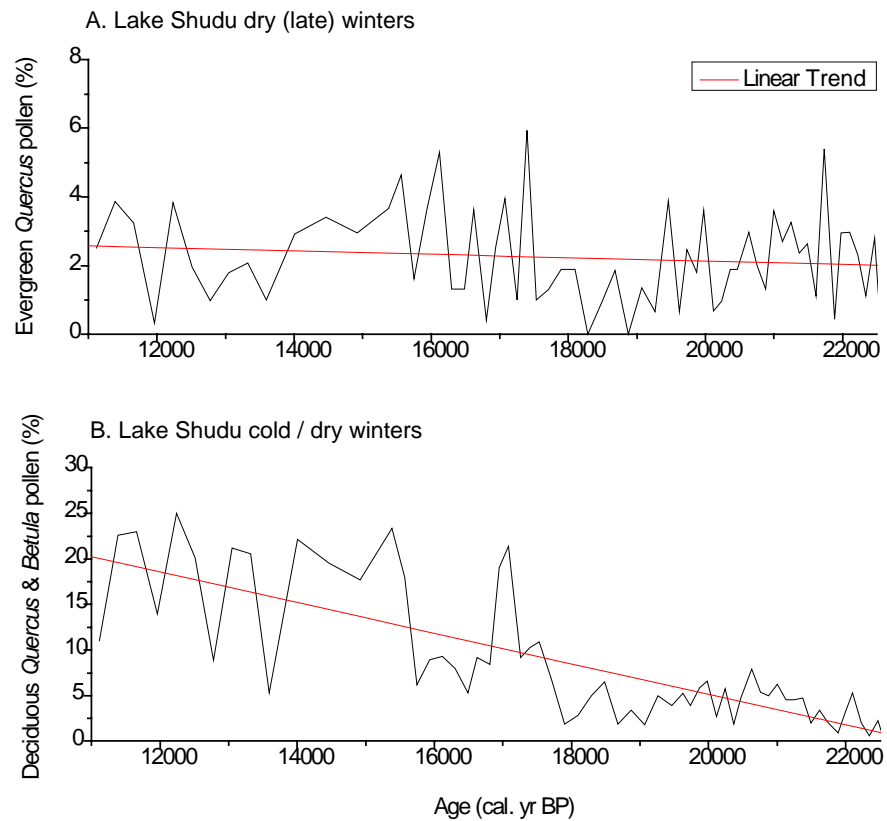


Figure 6-8: Percentages of *Quercus* and *Betula* in the Lake Shudu pollen record.

Individual taxa are used indicatively only, because other factors such as species competition and succession may also influence the abundances of specific taxa. Indicators should therefore be used with reference to the full pollen record.

After Dearing et al. (2008) and Shen et al. (2005a).

6.3.2 Evidence for rising lake levels at c. 16 ka cal. yr BP

From c. 17 - 12 ka cal. yr BP, the Lake Shudu arboreal pollen record indicates that the treeline descended to a lower altitude, indicating that conditions became colder and / or drier relative to conditions during the abrupt warming phase centred at c. 17.3 ka cal. yr BP. However, the proxies provide evidence for gradually increasing vegetation cover including a shift to a mixture of alpine meadow / shrubland, gently rising organic productivity and increased soil development which implies that conditions were warmer and / or wetter compared to conditions prior to the abrupt warming phase.

In particular, there was evidence of a lake transgression in the physical proxies at c. 16 ka cal. yr BP, denoted by laminated grey-green sediments from c. 16.5 - 15 ka cal. yr BP and an increase in sand at c. 16.1 - 16 ka cal. yr BP, consistent with increased deposition of material and increased lake energy (Lister et al., 1991). Furthermore, there is an increase in A/Cy ratios at c. 16.1 ka cal. yr BP (Figure 6-4), which coincides with these shifts and suggests that climatic conditions were ameliorating.

High lake levels were possibly triggered by rising solar insolation and associated positive feedbacks, leading to glacier accumulation and increased meltwater supply (Figure 6-1). Evidence of lake transgressions during this period has been found at other lakes in southwestern China. For example, Fang (1991) concluded that on the Tibetan Plateau, the highest lake levels were achieved at either c. 15 or 12 ka BP, evidenced by the deposition of thick sequences of freshwater lacustrine mud. The same trend was observed in high alpine lakes in southwestern China, including Lake Dianchi and Fuxian, which reached their maximum extent at c. 12 ka BP. Lake Fuxian was estimated to be 30 to 40 m higher at that time. Evidence from Lake Shudu suggests that the lake expanded at c. 16 ka cal. yr BP, which is relatively early, but still in broad agreement with other regional lake levels records.

Lin et al. (1986) reported climatic fluctuations, increased warming and intense periods of seasonality based on a pollen record from Er Yuan spanning c. 15 - 10 ka BP. Rising temperatures have been linked to increases in solar insolation and a strengthening summer monsoon (e.g. Wang et al., 2001). Further changes occurred in the Lake Shudu record from c. 13 ka cal. yr BP, including gradual rises in vegetation cover, organic productivity and soil development inferred from the pollen and organic proxies. A/Cy ratios also increased markedly at c. 12.8 ka cal. yr BP, suggesting a shift to warmer conditions.

6.4 The Pleistocene - Holocene Transition

Based on evidence in the Lake Shudu record, it is probable that the environmental shifts that took place from c. 11.7 - 11.5 ka cal. yr BP correlate with climatic shifts (i.e. increased vegetation cover and expansion of forests in response to summer monsoon strengthening and increasing solar insolation) that occurred during the Pleistocene - Holocene Transition. Thompson et al., 1989 place the start of the P-H Transition at 11,950 yrs BP, based on an ice core record obtained from the Qinghai - Tibet Plateau. The Transition took place in <100 years. However, the Lake Shudu record does not provide strong evidence for an abrupt transition. Sites higher up on the Tibetan Plateau may be more sensitive to changes in solar insolation, which may explain why this event is not captured in the Lake Shudu record. Alternatively, it is possible that the associated shifts in vegetation were not captured at the chosen sampling resolution, given the short duration of this event. Further high-resolution analysis of the Lake Shudu pollen record is required to constrain the timing and duration of the P-H Transition.

6.5 The Pleistocene - Holocene Boundary

The Pleistocene - Holocene (P-H) Boundary is formally defined as 11,700 cal. yr b2k (Walker et al., 2009; Figure 6-1). At Lake Shudu, there is marked increase in arboreal pollen concentrations at c. 11.7 ka cal. yr BP, signifying the expansion of forest cover outside of the catchment. Furthermore, there are marked rises in deciduous *Quercus* and *Betula* pollen abundances, which are correlated with the onset of warmer, wetter Holocene conditions in other pollen records from Yunnan Province (e.g. Dearing et al., 2008). The increasing presence of temperate deciduous trees in the Lake Shudu record, including *Ulmus* which is able to withstand prolonged dry periods also suggests increasing seasonality, probably characterised by long dry winters and warm wet summers (Shen et al., 2005a). These factors point to increasing summer monsoon intensity and the onset of Holocene conditions. During this period, mean winter temperatures in Southwest China were in the order of -10°C , whilst mean annual precipitation was ~500 - 600 mm.

The marked vegetation shifts in the Lake Shudu record at c. 11.7 ka cal. yr BP are in good agreement with the formal definition of the P-H Boundary proposed by Walker et al., 2009 and associated environmental conditions highlighted in other studies. The shifts in the Lake Shudu pollen record at c. 11.7 ka cal. yr BP could therefore signify the P-H Boundary. If correct, this implies that the P-H Boundary for southwestern China is synchronous with other regions. However, further high-resolution analysis of the Lake Shudu proxies is required to confirm or refute this hypothesis.

In addition, the formal definition of the P-H Boundary is based on a highly resolved ice core record. Walker et al. (2009) acknowledge that there are ongoing issues associated with defining the P-H Boundary in lake sediment records, including dating uncertainties and debates over what constitutes the defining features of the boundary in palynological and other records. In addition, the timing of the P-H Boundary in southwestern China is contested, with estimates ranging from c. 12.8 ka cal. yr BP (Hodell et al., 1999), c. 11.5 ka BP (Herzschuh, 2006b) and 10.5 ka BP (Walker, 1986). These issues need to be resolved before a formal definition of the base of the Holocene can be determined and applied to lacustrine records.

6.6 Comparisons with events in other regional proxy records

In the Lake Shudu record, the first marked signs of warming occur at c. 17.5 - 17.2 ka cal. yr BP. However, a comparable climatic shift is not recorded in the speleothem records spanning this period (e.g. Hulu and Songjia Caves (Zhou et al., 2008; Wang et al., 2001). This suggests that this event may have been regional in extent and reflecting Lake Shudu's position on the Tibetan Plateau. On the southeastern edge of the Tibetan Plateau today, the climate is characterised by relatively warm summers and cold but mild winters compared to other parts of the Tibetan Plateau at similar altitudes (Zhao et al., 2009). Enhanced summer temperatures are attributable to the increased levels of annual solar radiation reaching the Tibetan Plateau. Furthermore, the blocking effect of the mountains to the north prevents cold Siberian air masses from reaching the Plateau (Fang et al., 1988), helping to maintain higher than expected temperatures. Enhanced levels of solar radiation leading to higher temperatures may therefore explain why Lake Shudu was more sensitive to changing climatic conditions at this time.

It is noticeable that whilst the Lake Shudu record is sensitive to the centennial scale warmings at c. 17.3 ka cal. yr BP, parallel events in the Chinese speleothem records (correlated with H1, the BA and the YD) do not appear to have been recorded. It is possible that these events were not captured at the chosen resolution. Alternatively, there may have been site-specific reasons why these changes were not captured. Firstly, the palaeorecord indicates that Late Pleistocene conditions were uniformly cold. According to Dykoski et al. (2005), only the largest climatic events trigger an observable response in the proxy records, because of the influence of snow cover on the Tibetan Plateau. Consequently, some events may not be captured. Secondly, *Pinus* and *Poaceae* dominate the Lake Shudu pollen record. Both taxa have wide ecological tolerances, meaning that they would have been somewhat buffered against changes in temperature and precipitation. These factors in combination may have acted as a buffer, meaning that vegetation changes may have been effected only in response to the highest magnitude climatic changes, which may explain why some of these events are not recorded.

6.7 The influence of glacial - interglacial boundary conditions upon palaeomonsoon intensity during the deglacial period

The Lake Shudu records point to a millennial scale shifts in non-arboreal and arboreal vegetation cover (Figure 6-9) coupled with increased organic productivity and lake energy. The shifts were most likely triggered by a long term shift from cold, dry conditions dominated by lower solar insolation levels, glacial conditions and a strong winter monsoon, to warmer and wetter conditions, driven by rising solar insolation levels and summer monsoon strengthening. This accords with the findings of other studies which record rising temperatures over this period, including the Chinese speleothem records obtained from the Dongge, Hulu and Songjia Caves which recorded millennial scale changes in $\delta^{18}\text{O}$ values during the Lateglacial (Zhou et al., 2008; Dykoski et al., 2005; Wang et al., 2001).

Superimposed on this long term trend were periods of markedly increased vegetation cover, organic productivity and lake energy, which pointed to periods of enhanced warming and effective moisture driven by a stepwise strengthening of the Asian summer monsoon, most notably from c. 17.5 - 17.2 ka cal. yr BP and c. 11.7 - 11.5 ka cal. yr BP. The abrupt nature and timing of these events suggest that the relationship between Asian monsoon intensity and solar insolation levels was non-linear. This climate trajectory is conceptualised in Figure 6-10.

During the transition from glacial to interglacial conditions, slow solar forcing coupled with the continuing influence of ice cover are thought to have resulted in climate instability, triggering a non-linear response in the Asian monsoon (Hodell et al., 1999; Zonneveld et al., 1997). In the Lake Shudu palaeorecord, this manifests as centennial scale shifts in vegetation and organic productivity as critical ecological thresholds were exceeded (Maslin et al., 2001), providing compelling evidence in support of this theory.

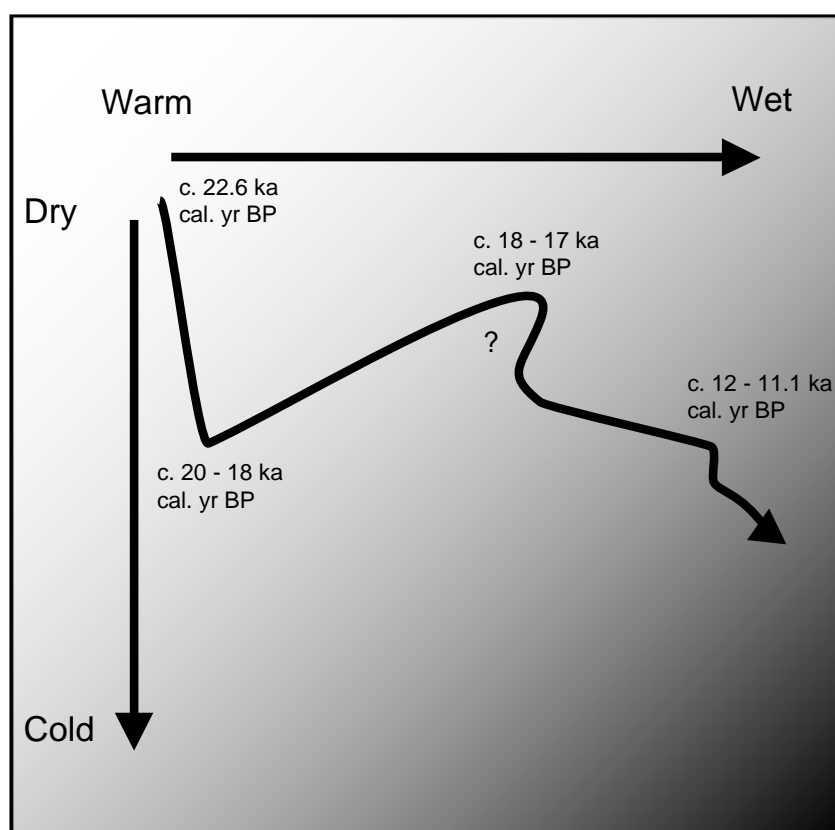


Figure 6-10: Conceptualised climate trajectory.

Conditions inferred from the Lake Shudu pollen and auxiliary records;
c. 22.6 - 11.1 ka cal. yr BP.

6.8 Concluding remarks

Based on the evidence contained in the Lake Shudu record and correlations with other regional proxy records, the following conclusions can be drawn;

1. The LGM occurred one to two millennia earlier than previous studies suggest.
2. Late Pleistocene - Early Holocene climatic conditions in southwestern China were very cold and dry, but became warmer and much wetter after c. 18 ka cal. yr BP.
3. Both solar forcing and local and / or regional glacial dynamics were important influences driving Asian palaeomonsoon variability during the Late Pleistocene.
4. There was a discernible long-term strengthening in the Asian summer monsoon from c. 16 ka cal. yr BP.
5. Millennial scale warming was punctuated by two marked warming phases at c. 17.5 - 17.2 ka cal. yr BP and c. 11.7 - 11.5 ka cal. yr BP, suggesting a non-linear relationship between solar insolation and monsoon intensity.
6. There was evidence in the Lake Shudu record pointing to enhanced effective moisture levels, particularly from c. 17.5 ka cal. yr BP, contributing to growing evidence for wetter regional conditions relative to the rest of China after the LGM.
7. The timing of the Pleistocene - Holocene Boundary appears to be located at c. 11.7 ka cal. yr BP in the Lake Shudu pollen record, which broadly agrees with evidence derived from other records.

7 Main conclusions and suggestions for further work

7.1 Main conclusions

The Lake Shudu record is one of the longest high-resolution Late Pleistocene - Early Holocene climate records available for southwestern China, extending back to c. 22.6 ka cal. yr BP. It provides a unique insight into the environmental and climatic changes that took place following the LGM, and captures the shift from Pleistocene to Holocene climatic conditions.

The primary goal of this research was to examine the hypothesis that Late Pleistocene - Early Holocene millennial to centennial scale climatic and environmental and climatic changes in southwestern China were driven by changes in solar insolation and / or glacial - interglacial boundary conditions, characterised by stepwise increases in palaeomonsoon intensity.

The main conclusions arising from this study are;

- The LGM possibly occurred earlier in southwestern China than previously thought;
- Late Pleistocene - Early Holocene climatic and environmental changes in southwestern China were driven by changes in glacial and solar activity, which triggered changes in palaeomonsoon intensity;
- The relationship between the Asian palaeomonsoon and solar insolation was non-linear, resulting in abrupt centennial scale Asian summer monsoon intensifications, particularly from c. 17.5 - 17.2 ka cal. yr BP;
- The P-H Boundary is possibly located at c. 11.7 ka cal. yr BP in southwestern China.

These findings broadly accord with evidence from other regional proxy records.

7.2 Suggestions for further work

The findings of this research raise several issues worthy of further investigation;

7.2.1 *The timing of the LGM*

The precise timing of the LGM in southwestern China remains an outstanding issue. Further high-resolution multi-proxy analysis of lakes in this region, incorporating pollen modelling and oxygen isotope analysis to determine temperature / precipitation changes over time, coupled with a full assessment and dating of glacial landforms present in the catchment would provide further insight into this issue. Further investigation / dating of the basal layers of the Lake Shudu record may also provide further insight into this issue. Determining the timing of the LGM in this region would also facilitate comparisons with the timing in other regions, and would establish whether the LGM was globally synchronous or asynchronous.

7.2.2 *The timing of the response to warming*

The findings of this research indicate that there were differences in the timings in the regional proxy records of marked warmings following a rise in solar insolation. Further high-resolution analysis and dating of the Lake Shudu pollen record, coupled with analysis of other regional pollen records including Bitu Hai, would help to more precisely determine the timing of these events.

7.2.3 *Abrupt shifts from c. 17.5 - 17.2 ka cal. yr BP*

These events potentially represent a marked warming phase. However, as discussed, there are a number of outstanding questions relating to the nature, timing and significance of these events. Further high-resolution analysis of the pollen record and dating of this event would help to clarify this issue and facilitate better comparisons between the Lake Shudu record and other regional records.

7.2.4 *Quantification of the forest ecosystem response to climate change*

This research has highlighted that the ecosystems in this region are highly sensitive to climatic change. These changes are particularly evident in changes in the position of the treeline. However, owing to the lack of sites above and below Lake Shudu, it is currently not possible to precisely determine the position of the treeline at any given point in time. High-resolution analysis of regional pollen records obtained from lakes forming an altitudinal transect would provide insight into the precise location of the treeline over time.

The results could be compared to modern treeline positions and associated temperature gradients. A pollen transfer function could also be applied to the pollen records in order to quantify the treeline shifts in terms of temperature and precipitation changes. The analysis would facilitate enable quantitative estimations of the temperature change required to prompt a change in the treeline, and would provide an insight into how future climate change may affect the sensitive ecosystems of southwestern China, many of which are biodiversity hotspots.

7.2.5 *The P-H Transition and Boundary*

The findings of this study suggest that the P-H Boundary occurred from c. 11.7 ka cal. yr BP. However, the precise timing of the P-H Boundary and the P-H Transition remain unclear. Higher resolution (sub-centennial) analysis of the pollen record (including rises in *Quercus* and *Betula*) and other proxies, coupled with a more detailed core chronology spanning this event would help to clarify this issue.

7.2.6 *Human - landscape - climate interactions*

This research focused upon climatic changes during the Late Pleistocene - Early Holocene Period. However, the Lake Shudu record extends into the Holocene. Humans were active in southwestern China from the Early Holocene (Dearing et al., 2008). Further work focusing on the younger sections of the record would enable key issues to be explored, including the timing of the onset of human activities in this region, the impact of anthropogenic activity upon the landscape and ecosystem dynamics and the impact of climate change upon human occupation of high altitude sites in southwestern China.

Appendices

Appendix A.1: Additional information for Chapter 3 (Methods)

A.1.1. Assignments of pollen taxa from China to selected Plant Functional Types (PFTs).

From (Yu et al., 2000a).

*This image has been removed by the author of this thesis/dissertation for
copyright reasons.*

A.1.2. Vegetation types, Yunnan Province, China. After Li et al. (1986).

Type	Dominant plant type	Constituent families	Distribution	Ecological Preferences	Subdivisions	Comments
Tropical Evergreen Forest (TEF)	Trees, shrubs, herbs. Abundant epiphytes (commonly orchids and ferns). Abundant woody vines and mosses. Strangler figs.	Annonaceae, Burseraceae, Combretaceae, Crypteroniaceae, Dipterocarpaceae, Euphorbiaceae, Guttiferae, Lauraceae, Lecythidaceae, Meliaceae, Moraceae, Myristicaceae, Papilionaceae, Arecaceae, Polygalaceae, Rubiaceae, Sapindaceae, Sapotaceae, Samydaceae, Sterculiaceae	South, up to 1800 m asl.	Hot and humid. Sensitive to small environmental changes. Represents the northern tip of the SE Asian Rainforest, so very sensitive to environmental perturbations	Humid Tropical Evergreen Forest	Occurs only in SE Yunnan valleys below 700 m asl. Shares species with SE Asian rainforest including <i>Dipterocarpus</i> , <i>Hopea</i> and <i>Cryptomeria</i> . Trees, shrubs and vines are common elements.
					Seasonal Tropical Rainforest	Also called Chinese Rainforest, widely distributed across southern Yunnan in valleys below 1000 m asl. Cool temperatures in early winter and low rainfall in late winter. Four types typified by presence of; <ul style="list-style-type: none">- <i>Terminalia myriocarpa-Pomelia tomentosa-Pterospermum lanceaefolium</i> forest- <i>Antiaris toxicaria-Pouteria grandifolia-Canarium album</i> forest- <i>Shorea assamica</i> forest- <i>Parashorea chinensis</i> forest
					Montane Tropical Evergreen Forest	Found in the mountains of south Yunnan, 800-1000 m asl. Tolerates lower temperatures but higher humidities than Seasonal TEF. Key species include <i>Castanopsis</i> , <i>Garcinia</i> and dominant tropical species including <i>Semecarpus</i> , <i>Calophyllum</i> and <i>Psychotria</i> . Epiphytes and large woody vines are common.
Tropical Semi-Evergreen (monsoon) Forest (TS - EF)	Trees, shrubs and herbs Few epiphytes and woody vines	Moraceae, Meliaceae, Sapindaceae, Tiliaceae, Bignoniaceae, Euphorbiaceae, Ulmaceae, Berseraceae, Annonaceae, Guttiferae, Tetramelaceae, Sapotaceae, Anacardiaceae, Bombacaceae, Sterculiaceae, Papilionaceae. Includes several endemic species such as <i>Garuga forestii</i> .	Valleys below 1000 m asl	Thrives in areas with a marked seasonal climate. Shares affinities with Indian Monsoon rainforest.	Deciduous Monsoon Rainforest	Grows in dry valleys and basins. Often commercially managed. Species include <i>Salix</i> , <i>Pterocarya</i> and <i>Bombax</i> . Sparse shrub layer.
					Semi-evergreen Monsoon Forest	Found in wet basins below 1000 m asl.
					Limestone Monsoon Forest	Southern Yunnan, below 700 m asl. Ulmaceae characterise this forest type. Few herbs, epiphytes and vines.
Subtropical Evergreen Broadleaved Forest (SEBF)	Mainly evergreen trees.	Fagaceae, Theaceae, Lauraceae and Magnoliaceae.	Dominates zones between 1000 - 2000 m asl in central Yunnan.	Widespread, along with SCF.	Semi-humid evergreen broadleaved forest	Grows in the hills, 1500 - 2500 m asl. Prefers subtropical, strongly seasonal climate. Dominant species include <i>Castanopsis</i> , <i>Cyclobalanopsis</i> , <i>Lithocarpus</i> , <i>Keteleeria</i> , <i>Pinus</i> , <i>Cupressus</i> and <i>Quercus</i> . After severe disturbance, this forest is often replaced by <i>Pinus yunnanensis</i> .
					Monsoon evergreen broadleaved forest	South tropical evergreen fagaceous forest, growing at altitudes of 1100 - 1500 m asl. Prefers a warmer and wetter climate compared to semi-humid forest. Species include <i>Castanopsis</i> , <i>Lithocarpus</i> , <i>Schima</i> and <i>Annesia</i> .
					Montane humid evergreen broadleaved forest	Montane forest grows 1800 - 2500 m asl (near cloudline), higher altitudes, further north. Dominant species in this mossy forest include Fagaceae, Magnoliaceae, Lauraceae, Theaceae, Hamamelidaceae, Styracaceae, Elaeocarpaceae, Aquifoliaceae, Araliaceae and Oleaceae. Bamboo and ferns including Acanthaceae, Liliaceae and Urticaceae and mossy epiphytes are abundant.

Subtropical evergreen sclerophyllous forest (SESF)	Trees, shrubs, herbs. Few vines and epiphytes.	Evergreen <i>Quercus</i> , <i>Sorbus</i> and <i>Rhododendron</i> , <i>Thalictrum</i> , <i>Polygonum</i> , <i>Viola</i> .	Jinsha Valley	Suited to locations with dry and cold winters. Plants are predominantly xeromorphic and cold resistant.	Montane sclerophyllous Quercus forest	Found at ~2600 m asl in the Jinsha Valley where annual rainfall is low and frost / snow are common in winter. Several varieties of forest exist; each dominated by a different species of evergreen <i>Quercus</i> including <i>Q. Aquifollioides</i> . Accompanying species include <i>Sorbus</i> , <i>Rhododendron</i> , <i>Spiraea</i> , <i>Lonicera</i> , <i>Chrysosplenium</i> , <i>Thalictrum</i> , <i>Polygonum</i> and <i>Viola</i> .
					Valley sclerophyllous Quercus forest	1000 - 2000 m asl where rainfall is low but temperatures are less extreme. Three types of forest exist, dominated by <i>Q. cocciferoides</i> , <i>Q. franchetti</i> , <i>Q. rehderiana</i> - <i>Cyclobalanopsis glaucoides</i> . The understorey is rich in shrubs including <i>Myrsine</i> , <i>Campylotropsis</i> and <i>Desmodium</i> . Few epiphytes and vines.
Subtropical deciduous broadleaved forest (SDBF)	Trees, shrubs and herbs. Abundant lichens, mosses and epiphytes.	Four variants identified by dominant species present in each assemblage.	High altitude zones	Sparsely distributed. Secondary forest.	Subtropical deciduous Quercus forest	800 - 2300 m asl. includes <i>Quercus acutissima</i> , <i>Keteleeria</i> , <i>Pinus</i> , <i>Viburnum</i> , <i>Potentilla</i> and <i>Pteridium</i> .
					Quercus variabilis forest	Primary or secondary forest found 700 - 2500 m asl, growing on sunny slopes across Yunnan except in the northwest and southwest. Sometimes grows as a mixed stand with <i>Pinus yunnanensis</i> .
					Subtropical deciduous Betula forest	Found growing in cold, humid but sunny locations 3200 - 3500 m asl in northwest Yunnan. This is secondary forest, which grows on sites previously occupied by MonCF. Dominant species include <i>Betula</i> , <i>Picea</i> , <i>Larix</i> , <i>Abies</i> , <i>Prunus</i> , and <i>Rhododendron</i> . 25% shrubs including <i>Rosa</i> , <i>Berberis</i> , <i>Lonicera</i> and <i>Aconitum</i> .
					Subtropical deciduous Alnus forest	Valleys 1800 - 3150 m asl. Prefers warmer, humid climate compared to <i>Betula</i> and <i>Alnus</i> forests. Dominant species is <i>Alnus</i> , but <i>Liquidambar</i> , <i>Betula</i> and <i>Rhus</i> . Few shrubs, but abundant herbs including <i>Polygonum</i> , <i>Mischanthus</i> and <i>Pteridium</i> .
Subtropical Mixed deciduous-evergreen Broadleaved Forest (SMBF)	Trees, shrubs and herbs. Many vines present	<i>Cyclobalanopsis</i> , <i>Lithocarpus</i> , <i>Cinnamomum</i> , <i>Dendropanax</i> , <i>Platycarya</i> , <i>Carpinus</i> , <i>Ulmus</i> , <i>Celtis</i> , <i>Carex</i> , <i>Viburnum</i> , <i>Polygonatum</i> , <i>Asplenium</i> , <i>Clematis</i>	Restricted local presence	No data	No data	No data
Subtropical conifer forest (SCF)	Trees, shrubs and herbs.	Five variants identified by dominant species present in each assemblage.	Found in patches below 2700 m asl.	Primary or secondary forest. Replaces SEBF following disturbance	Pinus armandii forest	Montane, 2500-3000 m asl in northwest Yunnan on shady slopes where temperatures are low but humidity is moderate. Species in the northwest stands include <i>Pinus</i> , <i>Cupressus</i> , <i>Quercus</i> , <i>Rhododendron</i> , <i>Lyonia</i> and <i>Cotoneaster</i> .
					Pinus yunnanensis forest	Central Yunnan between 600 - 3500 m asl. Prefers to grow where there are only small seasonal differences in temperature, a wet summer / autumn and dry winter / spring. Three variants exist; - <i>Pinus yunnanensis</i> - <i>Cyclobalanopsis delavayi</i> (inc species of <i>Quercus</i> , <i>Lithocarpus</i> , <i>Castanopsis</i> , <i>Keteleeria</i> , <i>Alnus</i>) - <i>Pinus yunnanensis</i> -sclerophyllus <i>Quercus</i> - <i>Pinus yunnanensis</i> - <i>Schima</i> (inc species of <i>Betula</i> , <i>Lithocarpus</i> , <i>Ficus</i> , <i>Castanopsis</i>)
					Pinus kesiya forest	Growth restricted to zones of South / central Yunnan 1000 -1900 m asl where there is low winter rainfall. Dominant species include <i>Pinus</i> , <i>Castanopsis</i> , <i>Lithocarpus</i> and shrubs including <i>Wendlandia</i> and <i>Aporosa</i> .
					Keteleeria evelyniana forest	Warm sunny zones 1800 - 2300 m asl. Species include <i>Castanopsis</i> , <i>Cyclobalanopsis</i> , <i>Pinus</i> , <i>Quercus</i> , <i>Viburnum</i> , <i>Lyonia</i> and <i>Rhododendron</i> .
					Cupressus duclouxiana forest	Grows on limestone, 2000 - 3000 m asl. Few shrubs including <i>Myrsine</i> , <i>Berberis</i> , <i>Rhamnus</i> , <i>Leptodermis</i> and <i>Rosa</i> and the herbs <i>Miscanthus</i> and <i>Imperata</i> .

Subtropical evergreen shrubland (SESh)	Primarily shrubs	Five types defined by dominant species in assemblage.	Widespread	Found in a wide range of climates	Homonia - riparia	Grows along riverbanks in subtropical and tropical Yunnan. Other shrubs include <i>Litsea</i> , <i>Ficus</i> and <i>Phyllanthus</i> .
					Opuntia monacantha - Euphorbia royleana	Prefers the dry zones of the Jinsha Valley. Other shrubs include <i>Acacia</i> , <i>Solanum</i> and <i>Erythrina</i> .
					Viburnum - Zanthoxylum - Bauhina	Grows on limestone in southeastern Yunnan, 400 - 800 m asl. Dominant shrubs include <i>Viburnum</i> , <i>Zanthoxylum</i> and <i>Alchornea</i> . Abundant vines and epiphytes.
					Pistacia weinmannfolia - Engelhardia roxburghiana	Grows on limestone in southeastern Yunnan, 1000-1500 m asl. Dominant shrubs include <i>Rhus</i> , <i>Coriaria</i> and <i>Viburnum</i> . Herbs include <i>Imperata</i> , <i>Leontopodium</i> and <i>Pteridium</i> .
					Myrsine africana -- Berberis wilsonae	Central and eastern limestone regions. Most of the woody plants are xeromorphic. Dominant species include <i>Cotoneaster</i> , <i>Zanthoxylum</i> , <i>Rosa</i> , <i>Indigofera</i> , <i>Leptodermis</i> and <i>Rhamnus</i> . Herbs and grasses are also abundant. Shrubby vines and ferns are also present.
					Macaranga denticulata - Microcos paniculata	Widespread distribution. Secondary shrubland, which grows after cutting or burning of tropical and subtropical forests. Dominated by <i>Croton</i> . Many vines present.
Subtropical mixed deciduous-evergreen shrubland (SMSh)	Primarily shrubs	Five different types defined by the dominant species present in each assemblage.	Restricted to extreme or disturbed zones	In areas with an extreme climate or areas subjected to intense human disturbance	Phyllanthus embelica	Grows in hot dry valleys with little or no biomass. Includes shrubs such as <i>Pistacia</i> , <i>Campylotropia</i> , and <i>Dodonea</i> .
					Vitex negundo	Subtropical montane region and valleys. <i>Negundo</i> is a xerophyte. Other shrubs include <i>Terminalia</i> , <i>Phyllanthus</i> and <i>Bombax</i> . Selected herbs and vines also present.
					Coriaria nepalensis	Subtropical slopes 600 - 1000 m asl. Includes <i>Evonymus</i> , <i>Pyracantha</i> , <i>Rhamnus</i> and <i>Rhus</i> and herbs such as <i>Imperata</i> , <i>Themeda</i> and <i>Carex</i> .
					Sophora viciifolia	Occurs as secondary land cover following destruction of forests in very dry habitats of the Plateau and valleys. Shrubs include <i>Pyrus</i> , <i>Cotoneaster</i> , <i>Pyracanthus</i> , <i>Rosa</i> , <i>Prinsepia</i> , <i>Rubus</i> and <i>Berberis</i> .
Montane Conifer Forest (MonCF)	Trees and shrubs	Six subtypes are defined by dominant species in each assemblage.	Widespread	Only grows above 2700 m asl in northwest Yunnan	Montane Pinus densata forest	3000 - 3400 m asl in Hengduanshan. Subalpine species, thermophilous and drought tolerant. Occasionally mixed with <i>Picea</i> , <i>Betula</i> , <i>Populus</i> and <i>Acer</i> in transitional zones. Abundant shrubs including <i>Rhododendron</i> , <i>Lyonia</i> and herbs including <i>Drynaria</i> and <i>Drosera</i> .
	Tsuga dumosa forest				2700 - 3100 m asl. Associated with moist temperate climate. Thrives in the northwest and often found mixed with <i>Abies</i> , <i>Picea</i> , <i>Pinus</i> , <i>Betula</i> , <i>Quercus</i> , <i>Lindera</i> , <i>Taxus</i> and <i>Acanthopanax</i> . Shrubs include <i>Rhododendron</i> and <i>Sinarundinaria</i> .	
	Larix forest				Occurs as secondary forest following the destruction of subalpine <i>Abies</i> or <i>Picea</i> forest. Occurs with <i>Betula</i> , <i>Abies</i> , <i>Picea</i> , <i>Pinus</i> , <i>Quercus</i> , <i>Rhododendron</i> , <i>Spiraea</i> , <i>Lonicera</i> and <i>Ribes</i> . Few herbs including <i>Polygonum</i> , <i>Kobresia</i> and <i>Anaphalis</i> .	
	Picea forest				3100 - 3800 m asl, alpine or subalpine climate, but has a wide ecological tolerance. Two types of forest; <i>Picea likiangensis</i> forest (including <i>Salix</i> and <i>Betula</i> with Bamboo and <i>Rhododendron</i> , <i>Rosa</i> , <i>Spiraea</i> , <i>Lonicera</i> , <i>Ribes</i> and <i>Berberis</i> . Herbs include <i>Dryopteris</i> , <i>Pedicularis</i> , <i>Fragaria</i> and <i>Rubus</i> . Mosses also present. <i>Picea brachytyla</i> forest (including <i>Tsuga</i> , <i>Acer</i> , <i>Betula</i> , shrubs including <i>Rhododendron</i> , <i>Sorbus</i> , <i>Lonicera</i> , <i>Ilex</i> and herbs including <i>Oxalis</i> , <i>Galium</i> , <i>Fragaria</i> and <i>Sedum</i> .	

					Abies forest <p>Mountain environments more extreme than those occupied by <i>Picea</i> forests.</p> <p>Two variants;</p> <p><i>Abies georgei</i> grows at 3500 - 4300 m asl accompanied by <i>Picea</i>, <i>Quercus</i>, <i>Rhododendron</i> and sparse herbs such as <i>Dryopteris</i>, <i>Saxifraga</i>, <i>Viola</i>, <i>Oxalis</i> and <i>Circaea</i>. Grasses and mosses are abundant.</p> <p><i>Abies delavayi</i> forest is restricted to sandy slopes in Dali County, 3400 - 3800 m asl, where the climate is humid. Moss and lichen cover the trees. <i>Rhododendron</i> and <i>Sorbus</i> are abundant, along with <i>Viburnum</i>, <i>Lonicera</i>, <i>Ribes</i> and <i>Sabina</i>.</p>	
					Sabina forest <p>Discontinuous stands on sunny slopes from 2400 - 4000 m asl. Accompanied by <i>Abies</i>, <i>Picea</i> and <i>Larix</i>. <i>Sabina</i> is a heliophyte and can tolerate cold, drought and high winds.</p> <p>Three types;</p> <ul style="list-style-type: none"> - <i>Sabina saltuaria</i> forest accompanied by dense shrubs and herbs including <i>Rhododendron</i>, <i>Spiraea</i>, <i>Rosa</i>, <i>Lonicera</i>, <i>Berberis</i> and <i>Cotoneaster</i>. - <i>Sabina pingii</i> forest is restricted to 3000 - 3500 m asl. Dense shrub layer includes <i>Rhododendron</i>, <i>Lonicera</i> and <i>Rosa</i>. Few herbs present. - <i>Sabina recurva</i> forest occurs only at 2900 - 3200 m asl in western Yunnan. Includes <i>Abies</i>, <i>Tsuga</i>, <i>Magnolia</i>, <i>Betula</i> and thick moss coverage. Very few herbs present. 	
Montane shrubland (MonSh)	Shrubs and few herbs	<i>Sabina</i> , <i>Rhododendron</i> , <i>Salix</i> , <i>Quercus</i> , <i>Cotoneaster</i> , <i>Berberis</i> , <i>Primula</i> , <i>Pedicularis</i> , <i>Carex</i> .	~4000 m asl, above the forest limit.	Widespread.	N/A	N/A
Alpine Meadow (Mon Mea)	Herbs	<i>Kobresia</i> , <i>Caltha</i> , <i>Sanguisorba</i> , <i>Polygonum</i> , <i>Potentilla</i>	~4000 m asl, above the forest limit.	Many variants. Grows in a mosaic with MonSh	Roscoea alpina meadow	Widespread in northern Yunnan on slopes 3200 - 3700 m asl. Dominant species includes <i>Polygonum</i> , <i>Cyananthus</i> , <i>Fragaria</i> , <i>Anenome</i> and <i>Potentilla</i> .
Savannah (Sav)	Shrubs	Widely dispersed shrubs rarely <1m high including <i>Heteropogon contortus</i> .	Below 1200 m asl.	Southern Yunnan hot dry valleys with strong seasonal climate, low annual rainfall. Succeeds TS - EF.	N/A	N/A

A.1.3. Pollen preparation method for Chinese sediment samples.

All pollen preparations were carried out in a clean room using appropriate health and safety precautions. Samples were freeze-dried beforehand.

The process was as follows;

1. Addition of exotic *Lycopodium* tablets x2
2. Sieving of samples using 10 and 150 μm sieves
3. Hydrofluoric Acid Digestion to remove silicates x2
4. Acetolysis to remove organic material x2
5. Suspension of pollen samples in silicon oil

A.1.4: Canoco DCA / PCA metadata.

The metadata was generated during statistical analysis of the Lake Shudu pollen dataset including taxa with abundances of >2%.

Program CANOCO Version 4.52 October 2003 - written by Cajo J.F. Ter Braak

Stage 1: DCA

Species data: 06SD2%

Number of segments = 26

Rescaling threshold = 0.00

Number of axes in biplot = 2

Diagnostics = 2

File: 06SD2%

Number of samples: 62

Number of species: 31

Number of occurrences: 1192

Options: Squareroot-transformation of species data; no species-weights specified; no sample-weights specified; downweighting of rare species.

Final species weights applied (weight*downweight)

1.000 1.000 1.000 1.000 1.000 1.000 1.000 1.000 1.000 1.000 1.000 1.000 1.000 0.493 1.000
1.000 1.000 1.000 1.000 1.000

1.000 1.000 1.000 0.652 1.000 1.000 1.000 1.000 1.000 1.000 1.000

Axes are rescaled

No. of active samples: 62

No. of passive samples: 0

No. of active species: 31

Sum of all eigenvalues of CA = 0.44966

**** Summary ****

Axes	1	2	3	4	Total inertia
------	---	---	---	---	---------------

Eigenvalues : 0.066 0.048 0.032 0.023 0.450

Lengths of gradient : 1.449 1.735 0.919 0.682

Cumulative percentage variance

of species data : 14.7 25.4 32.5 37.6

Sum of all eigenvalues 0.450

Type of analysis:

Model	Gradient analysis		
	indirect	direct	hybrid
linear	1 = PCA	2 = RDA	3
unimodal	4 = CA	5 = CCA	6
„	7 = DCA	8 = DCCA	9
	10= non-standard analysis		

Recommended type of analysis = 1 (PCA)

Stage 2: PCA

Species data: 06SD2%

Scaling of ordination scores = 2

Diagnostics = 1

File: 06SD2%

Number of samples: 62

Number of species: 31

Number of occurrences: 1192

Options: Squareroot-transformation of species data; no species-weights specified; no sample-weights specified.

Centering/standardization by species = 1

Centering/standardization by samples = 0

No. of active samples: 62

No. of passive samples: 0

No. of active species: 31

Total sum of squares in species data = 755.093

Total standard deviation in species data TAU = 0.626792

**** Summary ****

Axes	1	2	3	4	Total variance
------	---	---	---	---	----------------

Eigenvalues	:	0.351	0.170	0.071	0.049	1.000
-------------	---	-------	-------	-------	-------	-------

Cumulative percentage variance

of species data	:	35.1	52.1	59.2	64.1
-----------------	---	------	------	------	------

Sum of all eigenvalues						1.000
------------------------	--	--	--	--	--	-------

CANOCO call succeeded

A.2: Additional information for Chapter 4 (Results)

A.2.1. ^{14}C AMS radiocarbon dating of coniferous pollen concentrations: extraction method

NB: Stages 1-5 are undertaken in a clean room / fume cupboard.

1. Chemical Treatment

- 10% solution of NaOH (to remove humic acids)
- 10% solution of HCl (to remove carbonates)
- 48% Hf (to remove silicates)
- 10% solution of HCl (to remove carbonates)
- 10% solution of Nitric Acid (to remove organic detritus)

NB samples are placed in a hot water bath, centrifuged and decanted, then washed with distilled water between treatments.

2. Sieving

Samples are sieved (to remove larger and smaller particles from the estimated pollen fractions), washed and then placed in cold storage to minimise biological activity.

3. Microscopy

View each vial to determine pollen content. The purest / largest samples are taken forward to the next stage.

4. Density Separation

This method is adapted from Newnham et al. (2006) and Vandergoes et al. (2003). SMT is added to each sample at the required density. Samples are then agitated and left to stand until a clear band forms between the heavier material at the bottom from the lighter (pollen) fraction at the top. A fresh solution is used for each separation.

Once separated, the supernatant is sieved, rinsed and transferred to a clean tube ready for the next separation. The precipitate (the separated fraction) is then sieved, rinsed and transferred to storage vial. Repeat this process until the sample is separated into fractions.

5. Microscopy

Undertake a pollen percentage count to determine the amount of pollen versus organic material to assess the purity of each sample.

References

- Adams, J., Maslin, M. and Thomas, E. (1999) Sudden climate transitions during the Quaternary. *Progress in Physical Geography* **23** (1): 1-36.
- Adams, J. M. and Faure, H. (1998) *Global atlas of palaeovegetation since the Last Glacial Maximum*. Quaternary Environments Network (QEN) Retrieved 28/04/09, from <http://www.esd.ornl.gov/projects/gen>.
- An, Z. (2000) The history and variability of the East Asian palaeomonsoon climate. *Quaternary Science Reviews* **19**: 171 - 187.
- An, Z. S., Wu, X. H., Wang, P. X., Wang, S. M., Dong, G. R., Sun, X. J., Zhang, D. E., Lu, Y. C., Zheng, S. H. and Zhao, S. L. (1991) Paleomonsoons of China over the last 130,000 years - paleomonsoon variation. *Science in China Series B - Chemistry, Life Sciences and Earth Sciences* **34** (8): 1016-1024.
- Anonymous (2009) *The Global Historical Climatology Network (GHCN) v.2 Beta (1939 - 1988)*, National Climatic Data Center and the Carbon Dioxide Information Analysis Center, Oak Ridge National Laboratory.
- Anonymous. (2004) *China facts and figures (2004)*. Retrieved 12/08/08, from <http://www.china.org.cn/english/en-shuzi2004/index.htm>.
- Barry, R. G. and Chorley, R. J. (1995) *Atmosphere, weather and climate*. London, Routledge.
- Beer, R., Heiri, O. and Tinner, W. (2007) Vegetation history, fire history and lake development recorded for 6300 years by pollen, charcoal, loss on ignition and chironomids at a small lake in southern Kyrgyzstan (Alay Range, Central Asia). *The Holocene* **17** (7): 977-985.
- Benn, D. I. and Owen, L. A. (2002) Himalayan glacial sedimentary environments: a framework for reconstructing and dating the former extent of glaciers in high mountains. *Quaternary International* **97-98**: 3-25.
- Benn, D. I. and Owen, L. A. (1998) The role of the Indian summer monsoon and the mid-latitude westerlies in Himalayan glaciation: review and speculative discussion. *Journal of the Geological Society*.

- Berger, A. and Loutre, M. F. (1991) Insolation values for the climate of the last 10 million years. *Quaternary Sciences Reviews* **10** (4): 297-317.
- Beug, H.-J. (2004) *Leitfaden der Pollenbestimmung*. Munchen, Dr Friedrich Pfeil.
- Birks, H. H. and Birks, H. J. B. (2000) Future uses of pollen analysis must include plant Macrofossils. *Journal of Biogeography* **Millennium guest editorial number 6**. (27): 31-35.
- Birks, H. J. B. and Birks, H. H. (1980) *Quaternary Palaeoecology*. London, Edward Arnold.
- Birks, J. B. (2007) *Quantitative palaeoecology (Powerpoint lecture)*.
- Birks, J. B. (2006) *Introduction to Palaeoecology (Powerpoint Lecture)*.
- Bol, R., Huang, Y., Meredith, J. A., Eglinton, G., Harkness, D. D. and Ineson, P. (1996) The ¹⁴C age and residence time of organic matter and its lipid constituents in a stagnohumic gley soil.
- Bond, G. C. and Lotti, R. (1995) Iceberg discharges into the North Atlantic on millennial timescales during the last glaciation. *Science* **267** (5200): 1005-1010.
- Boyle, J., Yun, D., Baoyin, H. and Handong, Y. (2000) *Unpublished site investigation for Lake Shudu, Yunnan Province, China*.
- Bradley, R. S. (1999) *Paleoclimatology: Reconstructing climates of the Quaternary*. London, Harcourt Academic Press.
- Bradshaw, R. H. W. and Webb, T. (1985) Relationships between contemporary pollen and vegetation data from Wisconsin and Michigan, USA. *Ecology* **66** (3): 721-737.
- Bronk-Ramsey, C. (2001) Development of the radiocarbon calibration programme. *Radiocarbon* **43** (2A): 355-363.
- Bronk-Ramsey, C. (1995) Radiocarbon calibration and analysis of stratigraphy: The OxCal Program. *Radiocarbon* **37** (2): 425-430.
- Bronk-Ramsey, C., Higham, T. F. G. and Leach, P. (2004) Towards high precision AMS: progress and limitations. *Radiocarbon* **46** (1): 17-24.

- Brown, T. A., Farwell, G. W., Grootes, P. and Schmidt, F. H. (1992) Radiocarbon AMS dating of pollen extracted from peat samples. *Radiocarbon* **34** (3): 550-556.
- Brown, T. A., Nelson, D. E., Mathewes, R. W., Vogel, J. S. and Southon, J. R. (1989) Radiocarbon dating of pollen by accelerator mass spectrometry. *Quaternary Research* **32**: 205-212.
- Bunting, M. J. (2008) A role for palaeoecology in anticipating future climate change in mountain regions? *Palaeoecology, Palaeoclimatology, Palaeoecology* **259**: 1-5.
- Bunting, M. J., Gaillard, S., Sugita, S., Middleton, R. and Brostrom, A. (2004) Vegetation structure and pollen source area. *The Holocene* **14**: 651-660.
- Cao, M. (2007) *Plant diversity, forest ecosystems and influence forecasts of disturbance in Yunnan, SW China*, Chinese Academy of Sciences.
- Catto, N. (2006) Precipitation: Its influence on Quaternary events in eastern Asia (Editorial). *Quaternary International* **144**: 1-3.
- Chen, F.-H., Cheng, B., Zhao, Y., Zhu, Y. and Madsen, D. B. (2006) Holocene environmental change inferred from a high resolution pollen record, Lake Zhuyeze, arid China. *The Holocene* **16**: 675-684.
- Chen, F. H., Bloemendal, J., Zhang, P. Z. and Liu, G. X. (1999) An 800 ky proxy record of climate from lake sediments of the Zioge Basin, eastern Tibetan Plateau. *Palaeogeography, palaeoclimatology, palaeoecology* **151**: 307-320.
- Conedera, M., Tinner, W., Neff, C., Meurer, M., Dickens, A. F. and Krebs, P. (2009) Reconstructing past fire regimes: methods, applications and relevance to fire management and conservation. *Quaternary Science Reviews* **28**: 555-576.
- Cour, P., Zheng, Z., Duzer, D., Calleja, M. and Yao, Z. (1999) Vegetational and climatic significance of modern pollen rain in northwestern Tibet. *Review of Palaeobotany and Palynology* **104**: 183-204.
- Dalan, R. (2008) *MS2 Magnetic Susceptibility System*, Bartington Instruments Ltd: Marketing brochure.

Davis, M. B., Schwartz, M. W. and Woods, K. (1991) Detecting a species limit from pollen in sediments. *Journal of Biogeography* **18** (6): 653-668.

Dearing, J., Jones, R. T., Shen, J., Yang, X., Boyle, J. F., Foster, G. C., Crook, D. S. and Elvin, M. J. D. (2008) Using multiple archives to understand past and present climate-human-environment interactions: Lake Erhai catchment, Yunnan Province, China. *Journal of Paleolimnology* **40**: 3-31.

Dearing, J. A. (2008) Landscape change and resilience theory: a palaeoenvironmental assessment from Yunnan, SW China. *The Holocene* **18**: 117-127.

Dee, M. and Bronk-Ramsey, C. (2000) *Refinement of graphite target production at ORAU*. Proceedings of 8th AMS Conference, Vienna, Elsevier.

Demske, D., Tarasov, P., Wunnemann, B. and Riedel, F. (2009) Late glacial and Holocene vegetation, Indian Monsoon and westerly circulation in the Trans-Himalaya recorded in the lacustrine pollen sequence from Tso Kar, Ladakh, NW India. *Palaeoecology, Palaeoclimatology, Palaeoecology* **279**: 172-185.

Ding, Y. and Sikka, D. R. (2006) Synoptic systems and weather. In: Wang, B. *The Asian Monsoon*. Berlin, Springer: pp131-193.

Dykoski, C. A., Edwards, R. L., Cheng, H., Yuan, D. X., Cai, Y. J., Zhang, M. L., Lin, Y. S., Qing, J. M., An, Z. S. and Revenaugh, J. (2005) A high-resolution, absolute dated Holocene and deglacial Asian monsoon record from Dongge Cave, China. *Earth and Planetary Science Letters* **233** (1-2): 71-86.

E-Floras (2006) *Flora of China*, Flora of China Editorial Committee.

Evans, M. E. and Heller, F. (2003) *Environmental magnetism: principles and applications of enviromagnetics*. Amsterdam, Boston Academic Press.

Faegri, K. and Iversen, J. (1981) *Textbook of pollen analysis*. Chichester, John Wiley & sons.

Fan, Z. X., Brauning, A., Yang, B. and Cao, K. F. (2009) Tree ring density-based summer temperature reconstruction for the central Hengduan Mountains in southern China. *Global and Planetary Change* **65**: 1-11.

- Fang, J.-Q. (1991) Lake evolution during the past 30,000 years in China, and its implications for environmental change. *Quaternary Research* **36**: 37-60.
- Fang, J.-Q. and Yoda, K. (1988) Climate and vegetation in China (I): changes in the altitudinal lapse rate of temperature and distribution of sea level temperature. *Ecological Research* **3**: 37-51.
- Frey, D. and Deevey, E. S. (1998) Numerical tools in palaeolimnology - progress, potentialities and problems. *Journal of Paleolimnology* **20**: 307-332.
- Fritz, P. and Fontes, J. C., Eds (1986) *The Terrestrial Environment, B. Handbook of environmental isotope geochemistry*. Amsterdam, Elsevier.
- Fuhrmann, A., Mingram, J., Lucke, A., Lu, H., Horsfield, B., Liu, J., Negendank, J. F. W., Schleser, G. H. and Wilkes, H. (2003) Variations in organic matter compositions in sediments from Lake Huguang Maar (Huguangyan), south China during the last 68ka: implications for environmental and climatic change. *Organic Geochemistry* **34**: 1497-1515.
- Fujiki, T., Zhou, Z. and Yasuda, Y. (2005) *The pollen flora of Yunnan, China*. Singapore, Roli Books Pvt. Ltd.
- Galy, V., Francois, L., France-Lanord, C., Faure, P., Kudrass, H., Palhol, F. and Singh, S. K. (2008) C4 plants decline in Himalayan Basin since the Last Glacial Maximum. *Quaternary Science Reviews* **27**: 1396-1409.
- Gasse, F., Arnold, M., Fontes, J. C., Fort, M., Gibert, E., Huc, A., Li, B., Li, Y. F., Lju, Q., Melieres, F., Van Campo, E., Wang, F. B. and Zhang, Q. S. (1991) A 13,000 year climate record from Western Tibet. *Nature* **353** (6346): 742-745.
- Genty, D., Blamart, D., Ghaleb, B., Plagnes, V., Causse, C., Bakalowicz, M., Zouari, K., Chkir, N., Hellstrom, J., Wainer, K. and Bourges, F. (2006) Timing and dynamics of the last glaciation from European and North African $\delta^{13}C$ stalagmite profiles - comparison with Chinese and Southern Hemisphere stalagmites. *Quaternary Science Reviews* **25**: 2118-2142.
- Gobet, E., Tinner, W., Bigler, C., Hochuli, P. A. and Ammann, B. (2005) Early-Holocene afforestation processes in the lower subalpine belt of the Central Swiss Alps as inferred from macrofossil and pollen records. *The Holocene* **15**: 672-686.
- Google (2008) *Elevation profile, Yunnan Province, China*, Generated using Google Earth.

- Grimm, E. C. (2004) *TILIA and TILIA.GRAPH v.2.0.2*. Springfield, USA, Illinois State Museum.
- Guo, G. and Xie, G. (2006) The relationship between plant stable isotope composition, precipitation and satellite data, Tibet Plateau, China. *Quaternary International* **144**: 68-71.
- Hakala, K. J. and Adam, D. P. (2004) Late Pleistocene vegetation and climate in the southern Cascade Range and the Modoc Plateau region. *Journal of Paleolimnology* **31**: 189-215.
- Hakanson, L. and Jansson, M. (1983) *Principles of lake sedimentology*. Berlin, Springer-Verlag.
- Harris, N. (2006) The elevation history of the Tibetan Plateau and its implications for the Asian Monsoon. *Palaeogeography, palaeoclimatology and palaeoecology* **241**: 4-15.
- Hedges, R. E. M. (1991) AMS dating: present status and potential applications. *Conference Proceedings - Radiocarbon dating: recent applications and future potential* **1**: 5-9.
- Herzschuh, U. (2007) Reliability of pollen ratios for environmental reconstructions on the Tibetan Plateau. *Journal of Biogeography* **34**: 1265-1273.
- Herzschuh, U. (2006a) Late Quaternary climate history of the monsoon in Central Asia. *Quaternary Science Reviews* **25** (1-2): 163-178.
- Herzschuh, U. (2006b) Paleo-moisture evolution in monsoonal Central Asia during the last 50,000 years. *Quaternary Science Reviews* **25** (1-2): 163-178.
- Herzschuh, U., Zhang, C. J., Mischke, S., Herzschuh, R., Mohammadi, F., Mingram, B., Kurschner, H. and Riedel, F. (2005) A Late Quaternary lake record from the Qilian Mountains (NW China): evolution of the primary production and the water depth reconstructed from macrofossil, pollen, biomarker, and isotope data. *Global and Planetary Change* **46** (1-4): 361-379.
- Hodell, D. A., Brenner, M., Kanfoush, S. L., Curtis, J. H., Stoner, J. S., Song, X., Wu, J. and Whitmore, T. (1999) Paleoclimate of Southwestern China for the Past 50,000 yr Inferred from Lake Sediment Records. *Quaternary Research* **52**: 369-380.

- Hu, S., Goddu, S. R., Appel, E., Verosub, K., Yang, X. and Wang, S. (2005) Paleoclimatic changes over the past 1 million years derived from lacustrine sediments of Heqing Basin (Yunnan, China). *Quaternary International* **136**: 123-129.
- Huang, R., Huang, G. and Wei, Z. (2004) Climate variations of the summer monsoon over China. In: Chang, C.-P. *East Asian Monsoon*. New Jersey, World Scientific Publishing: pp213-268.
- Huntley, B. and Birks, H. J. B. (1984) *An atlas of past and present pollen maps for Europe: 0-13,000 years ago*. Cambridge, Cambridge University Press.
- IPCC (2007a) *Climate Change 2007: The Physical Science Basis. Contribution of Working Group I to the Fourth Assessment Report of the Intergovernmental Panel on Climate Change*. Solomon, S., Qin, D., Manning, M., Chen, Z., Marquis, M., Averyt, K., Tignor, M. and Miller, H. L. (eds) Cambridge University Press, Cambridge.
- IPCC (2007b) *Climate Change 2007: Impacts, Adaptation and Vulnerability. Contribution of Working Group II to the Fourth Assessment Report of the Intergovernmental Panel on Climate Change*. Parry, M. L., Canziani, O. F., Palutikof, J. P., van der Linden, P. J. and Hanson, C. E. (eds) Cambridge University Press, Cambridge.
- Jacobson, G. L. and Bradshaw, R. H. W. (1981) The selection of sites for palaeovegetational studies. *Quaternary Research* **16**: 80-96.
- Jarvis, D. I., Leopold, E. B. and Liu, Y. (1992) Distinguishing the pollen of deciduous oaks, evergreen oaks, and certain rosaceous species of southwestern Sichuan Province, China. *Review of Palaeobotany and Palynology* **75**: 259-271.
- Knighton, D. (1984) *Fluvial forms and processes*. London, Edward Arnold.
- Korner, C. and Paulsen, J. (2004) A world-wide study of high altitude treeline temperatures. *Journal of Biogeography* **31**: 713-732.
- Kuang, M. (1997) Quaternary glaciation series and glacial landform in Gongwang Mountains in Northeast part of Yunnan Province, China. *Chinese Geographical Science* **7** (2): 180-190.
- Kutzbach, J. E. (1981) Monsoon climate of the early Holocene: climate experiment with Earth's orbital parameters for 9000 years ago. *Science* **214**: 59-61.

Lamb, A. L., Leng, M. J., Mohammed, M. U. and Lamb, H. F. (2004) Holocene climate and vegetation change in the Main Ethiopian Rift Valley, inferred from the composition (C/N and $\delta^{13}\text{C}$) of lacustrine organic matter. *Quaternary Science Reviews* **23**: 881-891.

Last, W. M. and Smol, J. P., Eds (2001) *Tracking environmental change using lake sediments: Physical and geochemical methods*. Developments in paleoenvironmental research series, Kluwer Academic Publishers.

Leeder, M. R. (1992) *Sedimentology*. London, Chapman & Hall.

Leefers, K. (2005) *The Impacts of the Natural Forest Protection Program on Rural Livelihoods in Yunnan, China*. Michigan, Michigan State University: 25p.

Leng, M. J., Ed. (2006) *Isotopes in Palaeoenvironmental Research*. Developments in Palaeoenvironmental Research. Netherlands, Springer.

Leng, M. J. and Barker, P. A. (2006) *A review of the oxygen isotope composition of lacustrine diatom silica for palaeoclimate reconstruction*. Earth Science Reviews, BGS, Keyworth.

Leng, M. J., Lamb, A. L., Marshall, J. D., Wolfe, B. B., Jones, M. D., Holmes, J. A. and Arrowsmith, C. (2005) Isotopes in Lake Sediments. In: Leng, M. J. *Isotopes in palaeoenvironmental research*. Dordrecht, The Netherlands, Springer: pp148-184.

Leng, M. J. and Marshall, J. D. (2004) Palaeoclimate interpretation of stable isotope data from lake sediment archives. *Quaternary Science Reviews* **23**: 811 - 831.

Li, M. C., Liu, H. Y., Yi, X. F. and Li, L. X. (2006) Characterization of photosynthetic pathway of plant species growing in the eastern Tibetan Plateau using stable isotope carbon composition. *Photosynthetica* **44** (1): 102-108.

Li, X., Liu, S., Shanguan, D. and Lu, A. (2008) Progresses in the ice formation of glaciers in China. *Frontiers in Earth Science of China* **2** (3): 346-355.

Li, X. and Walker, D. (1986) The plant geography of Yunnan Province, southwest China. *Journal of Biogeography* **13** (5): 367-397.

Li, Y., Wang, N., Morrill, C., Cheng, H., Long, H. and Zhao, Q. (2009) Environmental change implied by the relationship between pollen assemblages and grain size in NW

Chinese lake sediments since the Late Glacial. *Review of Palaeobotany and Palynology* **154**: 54 - 64.

Lin, S., Qiao, Y. and Walker, D. (1986) Late Pleistocene and Holocene vegetation history at Xi Hu, Er Yuan, Yunnan Province, southwest China. *Journal of Biogeography* **13** (5): 419 - 440.

Lister, G. S., Kelts, K. R., Chen, K. Z., Yu, J. Q. and Niessen, F. (1991) Lake Qinghai, China: closed-basin lake levels and the oxygen isotope record for ostracoda since the latest Pleistocene. *Palaeogeography, palaeoclimatology and palaeoecology* **84**: 141 - 162.

Liu, J., Tang, L., Qiao, Y., Head, M. J. and Walker, D. (1986) Late Quaternary vegetation history at Menghai, Yunnan Province, southwest China. *Journal of Biogeography* **13**: 399-418.

Liu, Y.-S., Zetter, R., Ferguson, D. K. and Mohr, B. A. R. (2007) Discriminating fossil evergreen and deciduous *Quercus* pollen: A case study from the Miocene of eastern China. *Review of Palaeobotany and Palynology* **145**: 289-303.

Liu, Z., Bartlein, P., Lynch-Stielitz, J. and Otto-Bliesner, B. L. (2009) *Science Session PP07: Reconstruction and modelling of the transient climate evolution of the last 21 ka*. AGU Fall Meeting, San Francisco.

Lowe, J. J. and Walker, M. J. C. (1997) *Reconstructing Quaternary Environments*. Harlow, Longman.

Lu, H. Y., Wu, N. Q., Yang, X. D., Shen, C. M., Zhu, L. P., Wang, L., Li, Q., Xu, D. K., Tong, G. B. and Sun, X. J. (2008) Spatial patterns of *Abies* and *Picea* surface pollen distribution along the elevation gradient in the Qinghai-Tibetan Plateau and Xinjiang, China. *Boreas* **37**: 254-262.

Maher, B. A. (2008) Holocene variability of the East Asian summer monsoon from Chinese cave records: a re-assessment. *The Holocene* **18**: 861-866.

Mansfield, S. (2001) *China: Yunnan Province*. London, Bradt Travel Guides.

Martin, J. and Gower, T. (1996) *Forest succession*. Forestry Facts no.78. Department of forest ecology and management, University of Wisconsin, Madison.

Maslin, M., Seidov, D. and Lowe, J. (2001) *Synthesis of the nature and causes of rapid climate transitions during the Quaternary*, American Geophysical Union.

Mayewski, P. A., Rohling, E. E., Stager, J. C., Karlen, W., Maasch, K. A., Meeker, L. D., Meyerson, E. A., Gasse, F., van Kreveld, S., Holmgren, K., Lee-Thorp, J., Rosqvist, G., Rack, F., Staubwasser, M., Schneider, R. R. and Steig, E. J. (2004) Holocene climate variability. *Quaternary Research* **62**: 243 - 255.

McGinley, M. (2007) *Hengduan Mountains subalpine conifer forests*. Retrieved 01/12/2008, from [www.eoearth.org/article/Hengduan Mountains subalpine conifer forests](http://www.eoearth.org/article/Hengduan_Mountains_subalpine_conifer_forests).

Menitsky, Y. L. (2005) *Oaks of Asia*. Plymouth, Science Publishers.

Menking, K. M., Bischoff, J. L., Fitzpatrick, J. A., Burdette, J. W. and Rye, R. O. (1997) Climatic/Hydrologic Oscillations since 155,000 yr B.P. at Owens Lake, California, Reflected in Abundance and Stable Isotope Composition of Sediment Carbonate. *Quaternary Research* **48**: 58-68.

Mensing, S. A. and Southon, J. R. (1999) A simple method to separate pollen for AMS radiocarbon dating and its application to lacustrine marine sediments. *Radiocarbon* **41** (1): 1-8.

Meyers, P. A. (1997) Organic geochemical properties of paleoceanographic, paleolimnological and paleoclimatic processes. *Organic Geochemistry* **27** (5/6): 213-250.

Meyers, P. A. and Lallier-Verges, E. (1999) Lacustrine sedimentary organic matter records of Late Quaternary paleoclimates. *Journal of Paleolimnology* **21**: 345-372.

Meyers, P. A. and Takemura, K. (1997) Quaternary changes in delivery and accumulation of organic matter in sediments of Lake Biwa, Japan. *Journal of Paleolimnology* **18**: 211-218.

Mollenhauer, G., Kretschmer, S., Kusch, S., Mix, A. C. and Eglinton, G. (2008) *Contributions from compound-specific radiocarbon and size fraction specific Th-230 excess data towards understanding of sediment redeposition processes in the Panama Basin*. AGU conference paper.

Moore, P. D., Webb, J. A. and Collinson, M. E., Eds (1991) *Pollen Analysis*. Oxford, Blackwell Science.

- Newnham, R. M., Vandergoes, M. J., Garnett, M. H., Lowe, D. J., Prior, C. A. and Almond, P. C. (2006) Test of AMS ¹⁴C dating of pollen concentrates using tephrochronology. *Journal of Quaternary Science* **21**: 1-5.
- Ohsawa, M. (1993) Latitudinal patterns of mountain vegetation zonation in southern and eastern Asia. *Journal of Vegetation Science* **4** (1): 13-18.
- Otto-Bliesner, B. L., Brady, E. C., Clauzet, G., Tomas, R., Levis, S. and Kothavala, Z. (2005) Last Glacial Maximum and Holocene climate in CCSM3. *Journal of Climate* **19**: 2526-2544.
- Owen, L. A. and Benn, D. I. (2005) Equilibrium line altitudes for the Last Glacial Maximum for the Himalaya and Tibet: an assessment and evaluation of results. *Quaternary International* **138-139**: 55-78.
- Owen, L. A., Finkel, R. C., Haizhou, M. and Barnard, P. L. (2006) Late Quaternary landscape evolution in the Kunlun Mountains and Qaidam Basin, Northern Tibet: A framework for examining the links between glaciation, lake level changes and alluvial fan formation. *Quaternary International* **154-155**: 73-86.
- Pant, G. B. (2003) Long-term climate variability and change over monsoon Asia. *Journal of Indian Geophysics Union* **7** (3): 125-134.
- Pendall, E., Markgraf, V., White, J. W. C., Dreier, M. and Kenny, R. (2001) Multiproxy record of late Pleistocene-Holocene climate and vegetation changes from a peat bog in Patagonia. *Quaternary Research* **55**: 168-178.
- Peng, B., Pu, L., Bao, H. and Higgitt, D. L. (1997) Vertical zonation of landscape characteristics in the Namjagbarwa Massif of Tibet, China. *Mountain Research and Development* **17** (1): 43-48.
- Population Reference Bureau. (2010) *World population data*. Retrieved 20/01/10, from <http://www.prb.org/>.
- Punt, W., Hoen, P. P., Blackmore, S., Nilsson, S. and Le Thomas, A. (2007) Glossary of pollen and spore terminology. *Review of Palaeobotany and Palynology* **143**: 1-81.
- Qiao, B. (2004) *Color atlas of air-borne pollens and plants in China*, Peking Union Medical College Press.

- Regnell, J. (1992) Preparing pollen concentrates for AMS dating - a methodological study from a hard-water lake in Southern Sweden. *Boreas* **21**: 373-378.
- Reimer, P. J., Baillie, M. G. L., Bard, E., Bayliss, A., Beck, J. W., Bertrand, C. J. H., Blackwell, P. G., Buck, C. E., Burr, G. S., Cutler, K. B., Damon, P. E., Edwards, R. L., Fairbanks, R. G., Friedrich, M., Guilderson, T. P., Hogg, A. G., Hughen, K. A., Kromer, B., McCormac, G., Manning, S., Bronk-Ramsey, C., Reimer, R. W., Remmele, S., Southon, J. R., Stuiver, M., Talamo, S., Taylor, F. W., van der Plicht, J. and Weyhenmeyer, C. E. (2004) INTCAL04 terrestrial radiocarbon age calibration, 0-26 kyr BP. *Radiocarbon* **46** (3): 1029-1058.
- Ren, G. (2007) Changes in forest cover in China during the Holocene. *Vegetation History and Archaeobotany* **16**: 119-126.
- Ren, G. (2000) Decline of the mid to late Holocene forests in China: climatic change or human impact? *Journal of Quaternary Science* **15** (3): 273-281.
- Ruddiman, W. F. (2001) *Earth's climate: past and future*. New York, W.H. Freeman and Company.
- Santisteban, J. I., Mediavilla, R., Lopez-Pamo, E., Dabrio, C. R., Zapata, M. B. R., Garcia, M. J. G., Castano, S. and Martinez-Alfaro, P. E. (2004) Loss on ignition: a qualitative or quantitative method for organic matter and carbonate mineral content in sediments? *Journal of Paleolimnology* **32**: 287-299.
- Schlutz, F. and Zech, W. (2004) Palynological investigations on vegetation and climate change in the Late Quaternary of Lake Rukche area, Gorkal Himal, Central Nepal. *Vegetation History and Archaeobotany* **13**: 81-90.
- Sejrup, H. P., Nygard, A., Hall, A. M. and Haflidason, H. (2009) Middle and Late Weichselian (Devensian) glaciation history of south-western Norway, North Sea and eastern UK. *Quaternary Science Reviews* **28**: 370-380.
- Shen, J., Jones, R. T., Yang, X., Dearing, J. A. and Wang, S. (2005a) The Holocene vegetation history of Lake Erhai, Yunnan Province, southwestern China: the role of climate and human forcings. *The Holocene* **16** (2): 265-276.
- Shen, J., Liu, X., Wang, S. and Ryo, M. (2005b) Palaeoclimatic changes in the Qinghai Lake area during the last 18,000 years. *Quaternary International* **136**: 131-140.

- Sherman, R., Mullen, R., Li, H., Fang, Z. and Wang, Y. (2008) Spatial patterns of plant diversity and communities in Alpine ecosystems of the Hengduan Mountains, northwest Yunnan, China. *Journal of Plant Ecology* **1** (2): 117-136.
- Shi, Y. (2002) Characteristics of late Quaternary monsoonal glaciation on the Tibetan Plateau and in East Asia. *Quaternary International* **97-98**: 79-91.
- Shi, Y. and Wang, J. (1979) *The fluctuations of climate, glaciers and sea level since late Pleistocene in China*. Sea level, ice and climatic change, Proceedings of the Canberra Symposium. *131*: 281-293.
- Short, N. M. (2008) *Atmospheric circulation: weather systems*. Retrieved 15/10/08, from http://rst.gsfc.nasa.gov/Sect14/Sect14_1c.html.
- Shukla, J. (2007) Monsoon Mysteries. *Science* **318**: 204-205.
- Sirocko, F., Garbe-Schonberg, D., McIntyre, A. and Molfino, B. (1996) Teleconnections between the subtropical monsoons and high latitude climates during the last deglaciation. *Science* **272** (5261): 526-529.
- Smilauer, P. (2003) *CanocoDraw for Windows v.4.12*.
- Smol, J. P., Birks, H. J. and Last, W. M., Eds (2001a) *Tracking environmental change using lake sediments: Terrestrial, algal and siliceous indicators*. Developments in palaeoenvironmental research series, Kluwer Academic Publishers.
- Smol, J. P. and Last, W. M., Eds (2001b) *Tracking environmental change using lake sediments: Basin analysis, coring, and chronological techniques*. Developments in palaeoenvironmental research series, Kluwer Academic Publishers.
- Song, X.-Y., Blackmore, S., Bera, S. and Li, C.-S. (2007) Pollen analysis of spider webs from Yunnan, China. *Review of Palaeobotany and Palynology* **145**: 325-333.
- Stockmarr, T. (1971) Tablets with spores used in absolute pollen analysis. *Pollen et spores* **13**: 615-621.
- Strahler, A. H. and Strahler, A. N. (1992) *Modern Physical Geography*. London, John Wiley & sons.

- Stull, R. B. (2000) *Meteorology for scientists and engineers*, Brooks / Cole Thomson Learning.
- Stuvier, M., Grootes, P. M. and Braziunas, T. F. (1995) The GISP2 delta O-18 climate record of the past 16,500 years and the role of the sun, ocean and volcanoes. *Quaternary Research* **44** (3): 341-354.
- Sugita, S. (1993) A model of pollen source area for an entire lake surface. *Quaternary Research* **39**: 239-244.
- Sun, J., Ding, Z. and Liu, T. (1998) Desert distributions during the glacial maximum and climatic optimum: Example of China. *Episodes* **21** (1): 28-30.
- Sun, X., Wu, Y. and Walker, D. (1986) Late Pleistocene and Holocene vegetation history at Kunming, Yunnan Province, southwest China. *Journal of Biogeography* **13** (5): 441-476.
- Tang, C. Q. (2006) Evergreen sclerophyllous *Quercus* forests in northwestern Yunnan, China as compared to the Mediterranean evergreen *Quercus* forests in California, USA and northeastern Spain. *Web Ecology* **6**: 88-101.
- ter Braak, C. J. F. and Smilauer, P. (2003) *Canoco for Windows v.4.52*. Wageningen, The Netherlands, Biometris.
- Thomas, P. A. and Packham, J. R. (2007) *Ecology of woodlands and forests: Description, dynamics and diversity*. Cambridge, Cambridge University Press.
- Thompson, L. G., Mosley-Thompson, E., Davis, M. E., Bolzan, J. F., Dai, J., Yao, T., Gundestrup, X., Wu, X., Klein, L. and Xie, Z. (1989) Holocene-Late Pleistocene climatic ice core records from Qinghai-Tibetan Plateau. *Science* **246** (4929): 474-477.
- Thompson, L. G., Mosley-Thompson, E., Davis, M. E., Mashiotto, T. A., Henderson, K. A., Lin, P.-N. and Tandong, Y. (2006) Ice core evidence for asynchronous glaciation on the Tibetan Plateau. *Quaternary International* **154-155**: 3-10.
- Tinner, W. and Kaltenreider, P. (2005) Rapid responses of high mountain vegetation to early Holocene environmental changes in the Swiss Alps. *Journal of Ecology* **93**: 936-947.

Trenberth, K. E., Hurrell, J. W. and Stepaniak, D. P. (2006) The Asian monsoon: Global perspectives. In: Wang, B. *The Asian Monsoon*. Berlin, Springer: pp67-87.

Van Campo, E. and Gasse, F. (1993) Pollen and diatom inferred climatic and hydrological changes in Sumxi Co Basin (Western Tibet) since 13,000 yr B.P. *Quaternary Research* **39**: 300-313.

Vandergoes, M. J. and Prior, C. A. (2003) AMS dating of pollen concentrates - a methodological study of late Quaternary sediments from South Westland, New Zealand. *Radiocarbon* **45** (3): 479-491.

Vescovi, E., Ravazzi, C., Arpent, E., Finsinger, W., Pini, R., Valsecchi, V., Wick, L., Ammann, B. and Tinner, W. (2007) Interactions between climate and vegetation during the Lateglacial period as recorded by lake and mire sediment archives in Northern Italy and Southern Switzerland. *Quaternary Science Reviews* **26**: 1650-1669.

Walden, J., Oldfield, F. and Smith, J., Eds (1999) *Environmental magnetism: a practical guide*. Technical Guide No. 6. London, Quaternary Research Association.

Walker, D. (1986) Late Pleistocene-early Holocene vegetational and climatic changes on Yunnan Province, southwest China. *Journal of Biogeography* **13**: 477-486.

Walker, M., Johnsen, S., Rasmussen, S. O., Popp, T., Steffensen, J.-P., Gibbard, P., Hoek, W., Lowe, J., Andrews, J., Björck, S., Cwynar, L. C., Hughen, K. A., Kershaw, P., Kromer, B., Litt, T., Lowe, D. J., Nakagawa, T., Newnham, R. and Schwander, J. (2009) Formal definition and dating of the GSSP (Global Stratotype Section and Point) for the base of the Holocene using the Greenland NGRIP ice core, and selected auxiliary records. *Journal of Quaternary Science* **24** (1): 3-17.

Wang, B. (2006) *The Asian Monsoon*. Berlin, Springer.

Wang, B., Clemens, S. and Liu, P. (2003) Contrasting the Indian and East Asian monsoons: implications on geologic timescales. *Marine Geology* **201**: 5-21.

Wang, L., Sarnthein, M., Erlenkeuser, H., Grimalt, J., Grootes, P., Heilig, S., Ivanova, E., Kienast, M., Pelejero, C. and Pflaumann, U. (1999) East Asian monsoon climate during the Late Pleistocene: high resolution sediment records from the South China Sea. *Marine Geology* **156**: 245-284.

- Wang, P., Clemens, S., Beaufort, L., Braconnot, P., Ganssen, G., Jian, Z., Kershaw, P. and Sarnthein, M. (2005) Evolution and variability of the Asian Monsoon system: state of the art and outstanding issues. *Quaternary Science Reviews* **24**: 595-629.
- Wang, S. M., Yang, X. D., Ma, Y., Pan, H. X., Tong, G. B. and Wu, X. H. (1996) Environmental change of Gucheng Lake of Jiangsu in the past 15ka and its relation to palaeomonsoon. *Science in China Series D - Earth Sciences* **39** (2): 144-151.
- Wang, Y. J., Cheng, H., Edwards, R. L., An, Z. S., Wu, J. Y., Shen, C.-C. and Dorale, J. A. (2001) A high-resolution absolute date Late Pleistocene Monsoon record from Hulu Cave China. *Science* **294**: 2345-2348.
- Webb, T. (1980) The reconstruction of climatic sequences from botanical data. *Journal of Interdisciplinary History* **10** (4): 749-772.
- Webster, P. J. (2006) The coupled monsoon system. In: Wang, B. *The Asian Monsoon*. Berlin, Springer: pp3-65.
- Wetzel, R. G. (2001) *Limnology: lake and river ecosystems*. London, Academic Press.
- Wigley, T. M. L., Ingram, M. J. and Farmer, G., Eds (1981) *Climate and history: studies in past climate and their impact on man*. Cambridge, Cambridge University Press.
- Winkler, M. G. and Wang, P. K. (1997) *The Late Quaternary vegetation and climate of China*.
- Wohlfarth, B. (1996) The chronology of the Last Termination: a review of radiocarbon-dated, high resolution terrestrial stratigraphies. *Quaternary Science Reviews* **15**: 267-284.
- Wolfe, B. B., Edwards, T. W. D. and Aravena, R. (1999) Changes in carbon and nitrogen cycling during treeline retreat recorded in the isotopic content of lacustrine organic matter, western Taimyr, Peninsula, Russia. *The Holocene* **9** (2): 215-222.
- Wong, K. K. (2005) Diverse botanical communities in Yunnan and the Yangtze River shelter forest system. *Geography* **90** (3): 288-293.
- Woodward, F. I. (1996) *Climate and plant distribution*. Cambridge, Cambridge University Press.

- Wu, Z. and Raven, P. H. (2008) *Flora of China*, Flora of China Editorial Committee.
- Xie, S., Guo, J., Huang, J., Chen, F., Wang, H. and Farrimond, P. (2004) Restricted utility of $\delta^{13}\text{C}$ of bulk organic matter as a record of palaeovegetation in some loess - paleosol sequences in the Chinese Loess Plateau. *Quaternary Research* **62**: 96-93.
- Xu, J.-X., Ferguson, D. K., Li, C.-S., Wang, Y.-F. and Du, N.-Q. (2004) Climatic and ecological implications of Late Pliocene palynoflora from Longling, Yunnan, China. *Quaternary International* **117**: 91-103.
- Yanai, M. and Wu, G.-X. (2006) Effects of the Tibetan Plateau. In: Wang, B. *The Asian Monsoon*. Berlin, Springer: pp513-549.
- Yang, J., Zhang, W., Cui, Z., Yi, C., Lui, K., Ju, Y. and Zhang, X. (2006) Late Pleistocene glaciation of the Diancang and Gongwang Mountains, southeast margin of the Tibetan Plateau. *Quaternary International* **154-155**: 52-62.
- Yihui, D. and Chan, J. C. L. (2005) The East Asian Summer Monsoon: an overview. *Meteorology and Atmospheric Physics* **89**: 117-142.
- Yu, G., Chen, X. and Ni, J. (2000a) Palaeovegetation of China: a pollen data-based synthesis for the Mid Holocene and the last glacial maximum. *Journal of Biogeography* **27**: 635-664.
- Yu, G., Xue, B., Wang, S. and Liu, J. (2000b) Lake records and LGM climate in China. *Chinese Science Bulletin* **45** (13): 1158-1164.
- Yu, L., Cao, M. and Li, K. (2006) Climate-induced changes in the vegetation pattern of China in the 21st century. *Journal of Ecological Research* **21** (6).
- Zhang, B., Wu, H., Xiao, F., Xu, J. and Zhu, Y. (2006a) Integration of data on Chinese mountains into a digital altitudinal belt system. *Mountain Research and Development* **26** (2): 163-171.
- Zhang, C. and Mischke, S. (2009) A Lateglacial and Holocene lake record from the Nianbaoyeze Mountains and inferences of lake, glacier and climate evolution on the eastern Tibetan Plateau. *Quaternary Science Reviews* **28**: 1970-1983.

Zhang, Q. S. (1992) Late Quaternary environmental changes in the antarctic and their correlation with global change. *Recent progress in Antarctic earth science*: 781-785.

Zhang, W., Cui, Z., Feng, J., Yi, C. and Yang, J. (2005) Late Pleistocene glaciation of the Hulifang Massif of Gongwang Mountains in Yunnan Province. *Journal of Geographical Sciences* **15** (4): 448-458.

Zhang, W., Cui, Z. and Li, Y. (2006b) Review of the timing and extent of glaciers during the last glacial cycle in the bordering mountains of Tibet and in East Asia. *Quaternary International* **154-155**: 32-43.

Zhao, S. (1986) *Physical geography of China*. New York, John Wiley and Sons Inc.

Zhao, Y. and Herzsuh, U. (2009) Modern pollen representation of source vegetation in the Qaidam Basin and surrounding mountains, north-eastern Tibetan Plateau. *Vegetation History and Archaeobotany* **18**: 245-260.

Zheng, S. and Shangguan, Z. (2007) Spatial patterns of foliar stable carbon isotope compositions of C3 plant species in the Loess Plateau of China. *Ecological Research* **22**: 342-353.

Zheng, Z., Yuan, B. and Petit-Maire, N. (1998) Palaeoenvironments during the Last Glacial Maximum and the Holocene Optimum. *Episodes* **21** (3): 152-158.

Zhou, H., Zhao, J., Feng, Y., Gagan, M. K., Zhou, G. and Yan, J. (2008) Distinct climate change synchronous with Heinrich event one, recorded by stable oxygen and carbon isotope compositions in stalagmites from China. *Quaternary Research* **69**: 306-315.

Zhou, J., Wang, S., Yang, G. and Xiao, H. (2007) Younger Dryas event and cold events in Early - Mid Holocene: record from the sediment of Erhai lake. *Advances in Climate Change Research* **3** (Suppl): 41-44.

Zonneveld, K., Ganssen, G., Troelstra, S., Versteegh, G. J. M. and Visscher, H. (1997) Mechanisms forcing abrupt fluctuations of the Indian Ocean summer monsoon during the last deglaciation. *Quaternary Science Reviews* **16**: 187-201.